Final Research Report
Agreement T2695, Task 53
Bridge Rapid Construction

Design of Precast Concrete Piers for Rapid Bridge Construction in Seismic Regions

by

Jonathan M. Wacker
Graduate Research Assistant

David G. Hieber
Graduate Research Assistant

John F. Stanton
Professor

Marc O. Eberhard
Professor

Department of Civil and Environmental Engineering
University of Washington
Seattle, Washington 98195

Washington State Transportation Center (TRAC)
University of Washington, Box 354802
1107 NE 45th Street, Suite 535
Seattle, Washington 98105-4631

Washington State Department of Transportation Technical Monitor
Jugesh Kapur
Bridge Design Engineer, Bridge and Structures Office

Prepared for

Washington State Transportation Commission
Department of Transportation
and in cooperation with
U.S. Department of Transportation
Federal Highway Administration

December 2005

TECHNICAL REPORT STANDARD TITLE PAGE

1. REPORT NO.	2. GOVERNMENT ACCESSION NO.	3. RECIPIENT'S CATALOG NO.
WA-RD 629.1		

4. TITLE AND SUBTITLE	5. REPORT DATE
DESIGN OF PRECAST CONCRETE PIERS FOR RAPID BRIDGE CONSTRUCTION IN SEISMIC REGIONS	December 2005
	6. PERFORMING ORGANIZATION CODE

7. AUTHOR(S)	8. PERFORMING ORGANIZATION REPORT NO.
Jonathan M. Wacker, David G. Hieber, John F. Stanton, Marc O. Eberhard	

9. PERFORMING ORGANIZATION NAME AND ADDRESS	10. WORK UNIT NO.
Washington State Transportation Center (TRAC) University of Washington, Box 354802 University District Building; 1107 NE 45th Street, Suite 535 Seattle, Washington 98105-4631	11. CONTRACT OR GRANT NO. Agreement T2695, Task 53

12. SPONSORING AGENCY NAME AND ADDRESS	13. TYPE OF REPORT AND PERIOD COVERED
Research Office Washington State Department of Transportation Transportation Building, MS 47370 Olympia, Washington 98504-7370 Kim Willoughby, Project Manager, 360-705-7978	Draft Research Report
	14. SPONSORING AGENCY CODE

15. SUPPLEMENTARY NOTES

This study was conducted in cooperation with the U.S. Department of Transportation, Federal Highway Administration.

16. ABSTRACT

Incorporating precast concrete components in bridge piers has the potential to accelerate bridge construction and reduce the negative impacts that construction operations have on traffic flow. As part of this project, methodologies were developed to design economical and safe bridge piers out of precast concrete components. This research developed force-based and displacement-based procedures for the design of both cast-in-place emulation and hybrid precast concrete piers. The design procedures were developed so that they require no nonlinear analysis making them practical for use in a design office.

The expected level of damage to piers designed using the proposed procedures was estimated. The evaluation considered three types of damage to the columns of a pier: cover concrete spalling, longitudinal reinforcing bar buckling, and fracture of the longitudinal reinforcing bars. Both the force-based and displacement-based design procedures were found to produce bridges designs expected to experience an acceptable amount of damage in a design-level earthquake.

17. KEY WORDS	18. DISTRIBUTION STATEMENT
Rapid construction, design procedures, hybrid, bridge	No restrictions. This document is available to the public through the National Technical Information Service, Springfield, VA 22616

19. SECURITY CLASSIF. (of this report)	20. SECURITY CLASSIF. (of this page)	21. NO. OF PAGES	22. PRICE
None	None		

DISCLAIMER

The contents of this report reflect the views of the authors, who are responsible for the facts and the accuracy of the data presented herein. The contents do not necessarily reflect the official views or policies of the Washington State Transportation Commission, Department of Transportation, or the Federal Highway Administration. This report does not constitute a standard, specification, or regulation.

CONTENTS

LIST OF FIGURES

LIST OF TABLES

LIST OF SYMBOLS

A Acceleration coefficient (AASHTO LRFD Article 3.10.2)

A_{bar} Area of a mild steel reinforcing bar [in.^{2}]

A_g Gross cross-sectional area of column [in.^{2}]

A_{loop} Area of hysteretic loop on load-deflection plot [k-in.]

A_p Area of unbonded post-tensioning steel in column [in.^{2}]

A_{rect} Area of rectangle circumscribing hysteretic loop of pier response [k-in.]

A_s Area of mild steel reinforcement in column [in.^{2}]

a Depth of uniform stress distribution depicting compressive stress in column [in.]

a_0 Peak ground motion acceleration [in./sec^2]

$a_g(t)$ Ground acceleration as a function of time [in./sec^2]

C_1, C_2 Numerical coefficients in equation-based method for estimating equivalent viscous damping

c Distance from extreme compressive face to neutral axis of column cross-section, also referred to as the depth of the neutral axis [in.]

c_0 Depth of neutral axis when considering recentering properties of pier [in.]

c_{eq} Equivalent viscous damping coefficient of equivalent linear system

D_c Column diameter [in.]

d_b Diameter of mild steel reinforcing bar [in.]

d_c Center-to-center spacing of exterior pier columns [in.]

d_{Fc} Distance from resultant compressive force in concrete to extreme compressive face of column cross-section [in.]

$d_{ms,i}$ Distance from the ith reinforcing bar to the extreme compression face of the column [in.]

E_c $=0.033(1000\omega_c)^{1.5}\sqrt{1000\,f_c'}$; Elastic modulus of concrete [ksi]

E_{eq} Energy dissipated by equivalent linear system in one displacement cycle [k-in.]

E_{hyst} Energy dissipated by inelastic pier in one displacement cycle [k-in.]

E_p Elastic modulus of unbonded post-tensioning steel [ksi]

E_s Elastic modulus of mild steel reinforcing bars [ksi]

EI Flexural rigidity of column [k-in.^{2}]

EI_{cr} Flexural rigidity of cracked pier column [k-in.^{2}]

EI_{eff} Effective flexural rigidity of columns in hybrid pier at first yield [k-in.^{2}]

EI_g Flexural rigidity of uncracked pier column [k-in.^{2}]

F Lateral force [kips]

$F_{0.004}$ Lateral force on pier causing extreme concrete compression fiber to reach a strain of 0.004 [kips]

F_c Compressive force in concrete of column cross-section [kips]

F_{c0} Compressive force in concrete when considering recentering [kips]

F_{cap} Lateral force resisting capacity of pier [kips]

$F_{cap,nla}$ Lateral force capacity of pier determined using nonlinear analysis [kips]

$F_{cap,sa}$ Lateral force capacity of pier determined using sectional analysis [kips]

F_d Design force for pier [kips]

F_{eq} Equivalent lateral force on pier [kips]

$F_{eq,i}$ Equivalent lateral force on pier for ith mode of vibration [kips]

$F_{\max}$ Lateral force on pier at maximum displacement during earthquake [kips]

F_{ms} Net force in the mild steel reinforcement in column cross-section [kips]

$F_{ms,i}$ Force in the ith mild steel reinforcing bar [kips]

F_{ms0} Net resisting force in mild reinforcement when considering recentering [kips]

$F_{ms0,i}$ Resisting force provided by the ith mild steel reinforcing bar when considering recentering [kips]

F_p Force in post-tensioning tendons when pier is displaced to Δ_t [kips]

F_{p0} Force in post-tensioning tendons when pier is undeformed [kips]

F_s Force capacity of pier with mild steel reinforcement alone [kips]

F_t Lateral force on pier at target displacement [kips]

F_w Force capacity of pier with axial load alone [kips]

$F_y^{'}$ Lateral force on pier causing first reinforcing bar to yield [kips]

$\overline{F}_{\max}$ Lateral force on pier when displaced to $\overline{\Delta}_{\max}$ [kips]

$f_c^{'}$ Compressive strength of unconfined concrete [ksi]

$f_{cc}^{'}$ Compressive strength of confined concrete [ksi]

$f_{cu}^{'}$ Ultimate compressive strength of confined concrete [ksi]

f_D Damping force on equivalent linear system [kips]

f_I Inertial force on equivalent linear system [kips]

f_K Spring force on equivalent linear system [kips]

$f_{ms,i}$ Stress in the i^{th} mild steel reinforcing bar [ksi]

f_p Stress in post-tensioning tendon at Δ_t [ksi]

f_{p0} Stress in post-tensioning, after losses, of undeformed pier [ksi]

f_{pi} Maximum allowable stress in post-tensioning after initial losses [ksi]

f_{pu} Ultimate strength of unbonded post-tensioning reinforcement [ksi]

f_{py} Yield strength of unbonded post-tensioning reinforcement [ksi]

f_s Stress in mild steel reinforcing bar [ksi]

f_{su} Ultimate strength of mild steel reinforcement [ksi]

$f_t^{'}$ Tensile strength of concrete [ksi]

f_y Yield strength of mild steel reinforcement [ksi]

f_{yt} Yield strength of transverse reinforcement [ksi]

g Gravitational constant = 386.4 in./sec^2

I_{cr} Cracked moment of inertia of column [in.^{4}]

I_g Gross (uncracked) moment of inertia of column [in.^{4}]

j Distance from neutral axis to extreme tensile reinforcing bar in CIP emulation pier column at first yield divided by D_c

K Stiffness of pier [k/in.]

K_{eq} Stiffness of equivalent linear system [k/in.]

K_p Lateral stiffness of pier [k/in.]

k $=\frac{1}{2}(1-\frac{M_{cr}}{M_y^{'}})$

L_c Height of columns, measured from top of foundation to bottom of cap beam [in.]

L_{pu} Unbonded length of post-tensioning tendons [in.]

L_{unb} Unbonded length of mild steel reinforcement in interface region [in.]

M Moment demand on column [k-in.]

M_c Moment capacity contribution from compressive force in concrete [k-in.]

M_{c0} Restoring moment from compressive force in concrete when considering recentering [k-in.]

M_{cap} Moment capacity of a pier column [k-in.]

M_{cr} Cracking moment of column [k-in.]

M_D Moment capacity contribution of axial dead load to column capacity [k-in.]

M_{D0} Restoring moment provided by axial load on pier when considering recentering [k-in.]

M_{ms} Net resisting moment contribution from mild steel reinforcing bars to column capacity [k-in.]

$M_{ms,i}$ Moment capacity contribution from i^{th} mild steel reinforcing bar [k-in.]

M_{ms0} Net resisting moment contribution from mild steel reinforcing bars to column capacity when considering recentering [k-in.]

$M_{ms0,i}$ Moment capacity contribution from i^{th} mild steel reinforcing bar when considering recentering [k-in.]

M_p Moment capacity contribution from post-tensioning tendons [k-in.]

M_{p0} Restoring moment caused by post-tensioning tendons when considering recentering [k-in.]

M_{resist} Net resisting moment on pier when considering recentering [k-in.]

$M_{restore}$ Net restoring moment on pier when considering recentering [k-in.]

M_s Moment capacity of pier columns with mild steel reinforcement alone [k-in.]

$M_y^{'}$ Moment on column causing first reinforcing bar to yield [k-in.]

m_0 Initial slope of parabola used to represent compressive portion of unconfined concrete stress-strain relationship [ksi]

m_i Seismic mass associated with the ith mode of vibration [kip-in.^{2}/sec]

m_p Total seismic mass on pier [kip-in.^{2}/sec]

n_c Number of columns in pier

P Axial load on rigid rocking block

P_{bb} Probability of buckling of longitudinal reinforcing bars

P_c Gravity load per column from weight of superstructure [kips]

P_{spall} Probability of onset of concrete cover spalling

R Response modification factor

S Site coefficient (AASHTO LRFD Article 3.10.5)

S_a Spectral absolute acceleration [in./sec^2]

$S_{a,i}$ Spectral acceleration for the ith mode of vibration [in./sec^2]

S_d Spectral relative displacement [in.]

$S_{d-5\%}$ Spectral displacement given 5% viscous damping [in.]

$S_{d-\xi}$ Spectral displacement given ξ viscous damping [in.]

$S_{d-\hat{\xi}_{eq}}$ Spectral displacement given $\hat{\xi}_{eq}$ viscous damping [in.]

T Period of vibration [sec]

T_i Period of ith mode of vibration [sec]

T_{eq} Period of vibration of equivalent linear system [sec]

T_n Natural period of vibration [sec]

t Time [sec]

$u(t)$ Relative displacement of pier as a function of time [in.]

$\dot{u}(t)$ Relative velocity of pier as a function of time [in./sec]

$\ddot{u}(t)$ Relative acceleration of pier as a function of time [in./sec^2]

W Self-weight of rigid rocking block [kips]

α Proportion of mild steel reinforcement assumed to yield in interface of hybrid column at first yield

β Damping modification factor for equivalent viscous damping

β_1 Depth of uniform stress distribution in concrete divided by c

β_{da} Value of β determined for a particular pier using nonlinear analysis

Δ Displacement [in.]

Δ_{bb} Displacement at which longitudinal reinforcing bars buckle [in.]

$\Delta_{bb,cal}$ Estimated displacement at which longitudinal reinforcing bars buckle [in.]

$\Delta_{\max}$ Maximum displacement of pier subjected to an earthquake [in.]

Δ_{spall} Displacement at onset of concrete cover spalling [in.]

$\Delta_{sp,calc}$ Estimated displacement at onset of cover concrete spalling [in.]

Δ_t Target displacement [in.]

Δ_y Yield displacement of pier [in.]

$\Delta_{y,bar}$ Yield displacement of a mild steel reinforcing bar [in.]

Δ_y' Displacement of pier when first reinforcing bar yields [in.]

$\Delta_{y,c}'$ Displacement of CIP emulation pier when first reinforcing bar yields due to flexural deformation of the column [in.]

$\Delta_{y,\text{int}}'$ Displacement of pier when first reinforcing bar yields due to deformation of the interface region [in.]

$\Delta_{y,sp}'$ Displacement of CIP emulation pier when first reinforcing bar yields due to deformation caused by strain penetration [in.]

$\Delta^{*}_{y,c}$ Displacement due to elastic deformation of column when first reinforcing bar yields [in.]

Δf_p Change in stress in post-tensioning tendons when pier is displaced to Δ_t

ΔP Additional axial load in columns of pier due to overturning [kips]

$\overline{\Delta}_{\max}$ Average maximum displacement of pier subject to five earthquakes [in.]

$\delta_{ms,i}$ Deformation of the ith mild steel reinforcing bar [in.]

δ_p Deformation of post-tensioning tendons at Δ_t [in.]

δ_{sp} Elongation of reinforcing bar due to strain penetration [in.]

ε_{c0} Strain at $f_c^{'}$ of unconfined concrete [in./in.]

ε_{cc} Strain at $f_{cc}^{'}$ of confined concrete [in./in.]

$\varepsilon_{con,c}$ Strain in extreme compressive concrete fibers of column [in./in.]

ε_{cu} Ultimate strain of confined concrete [in./in.]

$\varepsilon_{\max}$ Maximum strain in extreme tensile reinforcing bar [in./in.]

$\varepsilon_{ms,i}$ Strain in ith mild steel reinforcing bar [in./in.]

ε_{sh} Ultimate strain of unconfined concrete [in./in.]

$\varepsilon_{stl,t}$ Strain in extreme tensile reinforcing bar of column [in./in.]

ε_{su} Ultimate strain of mild steel reinforcement [in./in.]

ε_y Yield strain of a mild steel reinforcing bar [in./in.]

$\overline{\varepsilon}_{\max}$ Average maximum strain in extreme tensile reinforcing bar [in./in.]

Φ Cumulative density function for a normal distribution

ϕ Curvature in column [rad/in.]

ϕ_{cf} Resistance factor for reinforced concrete member subject to compression and flexure in seismic applications

$\phi_y^{'}$ Curvature of column cross-section at first yield [rad/in.]

φ Distance between tensile steel and resultant compressive force in hybrid column at first yield divided by D_c

γ Distance from neutral axis to extreme tensile reinforcing bar in strain penetration region of CIP emulation pier column at first yield divided by D_c

γ_1 Angle defining compression region of circular column

η Distance from neutral axis to extreme tensile reinforcing bar at first yield in the interface region of hybrid column divided by D_c

κ Distance from resultant compressive concrete force to force representing reinforcing bars in column of pier with mild steel reinforcement alone divided by D_c

λ $= \frac{EI_{cr}}{EI_g}$

μ_Δ Displacement ductility

θ Rotation of hybrid column relative to footing and cap beam when pier is displaced to Δ_t [rad]

θ_{int} Rotation due to deformation of the interface region at first yield [rad]

θ_{sp} Rotation due to strain penetration at first yield [rad]

ρ_{eff} Effective confinement ratio

ρ_{eq} $= \frac{1}{f_y}(\rho_s f_y + \rho_p f_{py})$; Equivalent reinforcing ratio

ρ_p $= \frac{A_p}{A_g}$; Post-tensioning steel reinforcing ratio

ρ_s $= \frac{A_s}{A_g}$; Mild steel reinforcing ratio

ρ_t Volumetric transverse reinforcing ratio

τ_e Elastic bond strength between concrete and mild steel reinforcement [ksi]

τ_i Inelastic bond strength between concrete and mild steel reinforcement [ksi]

ω_c Unit weight of concrete [kcf]

ω_n Natural frequency of vibration of equivalent linear system [1/sec]

ξ Viscous damping

ξ_{eq} Viscous damping of equivalent linear system measured from hysteretic behavior of pier

$\xi_{eq,eb}$ Equivalent viscous damping estimated using equation-based method

$\xi_{eq,emp}$ Equivalent viscous damping estimated using empirical method

$\xi_{eq,nla}$ Equivalent viscous damping estimated using nonlinear analysis method

$\hat{\xi}_{eq}$ Effective viscous damping of equivalent linear system

ψ Distance between vertical forces acting on column with axial load alone divided by D_c

EXECUTIVE SUMMARY

Bridge construction can cause significant traffic delays on already congested highways in many metropolitan areas. The incorporation of precast concrete elements, which can be fabricated off-site in advance of construction, in bridges can reduce the negative impacts of construction on traffic flow by shortening construction schedules and reducing the number of construction operations performed at the bridge site. Precast concrete pier elements have been used rarely in seismic regions because of the difficulty associated with making connections between the precast elements that not only can withstand the force and deformation demands during an earthquake but that can also be constructed easily. This report describes research that developed and evaluated practical methodologies for the seismic design of precast bridge piers. Such methods are needed for bridge engineers to design economical and safe precast bridges.

Two precast concrete pier systems, a cast-in-place (CIP) emulation system and a hybrid system, were developed for use in seismically active regions to facilitate the rapid construction of bridges. The CIP emulation system contains only mild steel reinforcement and is an emulation of conventional cast-in-place concrete construction. The hybrid system is reinforced with a combination of mild steel and vertical, unbonded post-tensioning.

In order to use the CIP emulation and hybrid systems, procedures are needed to develop economical designs that are not overly conservative, nor prone to excessive amounts of damage in an earthquake. Two design procedures were examined in this research: an equivalent lateral force design (ELFD) procedure and a direct displacement-based design (DDBD) procedure.

The ELFD procedure determines the inertial force on the bridge pier by using elastic structural dynamics and then reduces the elastic inertial force by an empirical response modification factor to establish the design force for the pier. A range of response modification factors (R) commonly specified in bridge design (AASHTO 2002; AASHTO 2004) were considered in this study. The ELFD procedure is easy to implement, requires no iteration, and is widely used in current practice. One main drawback of the ELFD procedure is that it is unclear how much damage piers designed for a particular response reduction factor will experience in a design-level earthquake.

In the DDBD procedure, the designer selects a target displacement and then determines the required strength and stiffness of the pier so that the maximum displacement in a design-level earthquake is approximately equal to the target displacement. The target displacement can be selected on the basis of the desired performance of the pier in a design-level earthquake, so the designer has a clear idea of the expected damage. The DDBD procedure is more complex than the ELFD procedure and requires iteration, but simple computer programs can be developed to design piers with either the ELFD or DDBD procedure, making the effort required to use either procedure similar.

To evaluate the ELFD and DDBD procedures, the expected damage was determined for a population of piers designed with both procedures for a design-level earthquake. Three types of damage were considered: concrete cover spalling, longitudinal reinforcing bar buckling, and longitudinal reinforcing bar fracture.

The piers designed with the ELFD procedure had an average probability of spalling ranging between 5 percent (R=1.5) and 35 percent (R=5.0) for CIP emulation piers and 2 percent (R=1.5) and 37 percent (R=5.0) for hybrid piers, depending on the response modification factor used. The average probability of bar buckling ranged between 0.1 percent (R=1.5) and 3 percent (R=5.0) for CIP emulation piers and 0.1 percent (R=1.5) and 4 percent (R=5.0) for hybrid piers. Significant variation in the amount of damage experienced by each pier was predicted because of the variation in the response of the pier to different ground motions.

The DDBD procedure was used to design the piers for three target probabilities of cover concrete spalling: 5 percent, 15 percent, and 35 percent. The target displacement was determined on the basis of the target probability of spalling. Although this research considered the probability of spalling, other types of damage or ductility limits could be used to develop target displacement values. The average probability of spalling was close to the target values for both the CIP emulation and hybrid piers. There was still considerable scatter in the amount of damage experienced by individual piers because of variation in the response of the individual piers to ground motions.

Both the ELFD and DDBD procedures produced acceptable designs of CIP emulation and hybrid pier systems that were not prone to excessive damage. The DDBD

procedure has the advantage that the expected amount of damage is predicted in design; however, relationships between the response reduction factor and expected amount of damage for a particular level of seismic risk could be developed for the ELFD procedure to provide similar estimates.

This research suggests that the CIP emulation and hybrid piers should experience similar amounts of damage during earthquakes. However, the models used to estimate the seismic response of the piers and the damage models for the hybrid piers were not calibrated with experimental results. Future calibration of the design procedures using experimental test results is necessary to ensure that the design procedures are accurate. Additional work is also required to expand the design procedures to consider multiple-degree-of-freedom bridge systems and soil-structure interaction.

CHAPTER 1
INTRODUCTION

Bridge construction in the Puget Sound region and other metropolitan areas can severely exacerbate traffic congestion, resulting in costly delays to motorists and freight. Bridge types that can be constructed and/or reconstructed rapidly are needed to reduce these delays. The use of precast concrete components in bridges presents a potential solution, because the components can be fabricated off-site in advance of construction, reducing the amount of time required to complete the bridge and the number of construction tasks that must be completed on-site.

Precast, prestressed concrete girders are currently used widely; however, the use of precast components for other portions of a bridge has been limited. Precast components for bridge substructures have been used mainly in non-seismic regions because difficulties creating moment connections between precast components have hindered their use in seismic regions.

Two precast concrete bridge pier systems developed for use in the seismically active portion of Washington State are presented in this report. In order to use these systems, design procedures are required to ensure that the precast pier systems will exhibit acceptable performance in earthquakes and not experience excessive damage. This report focuses on the development and evaluation of these design procedures.

1.1 MOTIVATION FOR RAPID CONSTRUCTION

Disruption of highway traffic flow due to bridge construction is becoming less tolerable as the amount of congestion in metropolitan areas increases. The direct costs (traffic control, barricades, etc.) and indirect costs (delays to motorists) from partial or full closure of a roadway to accommodate bridge construction can be staggering. A recent study in Houston found that the indirect costs associated with closing a highway bridge near the city center were over $100,000 a day (Jones and Vogel 2001). Bridge designs that can be constructed rapidly are needed to reduce these costs and better serve motorists.

Rapid construction can be considered in two contexts. Optimal rapid construction solutions should meet both of these needs.

1. **Reduced Construction Time.** Rapid construction can significantly reduce the amount of time required to construct a bridge, allowing traffic to return to its normal patterns sooner. This is particularly important where a convenient detour is not available, such as in rural areas, or in regions, such as the Puget Sound, where most highways are already operating near or over their intended capacities, leaving nowhere for additional traffic to go.
2. **Reduced Impact on Traffic Flow.** Construction methods that allow portions of the bridge to be built off-site and then erected quickly on-site can significantly reduce the negative impacts of on-site construction. In many cases, prefabricating elements allows the on-site work to be completed during night and weekend hours, when traffic volumes are lower. This consideration is critical in urban areas.

Bridge designs that can be constructed rapidly are particularly useful when a bridge is unexpectedly put out of service because of a vehicular collision, earthquake, or other disaster. This was illustrated by the I-65 Bridge over I-59 in Birmingham, Alabama (Barkley and Strasburg 2002). In 2002, a gasoline tanker collided with one of the piers of the I-65 Bridge. The impact and ensuing fire damaged the bridge beyond repair. With user costs from the closed bridge estimated at over $100,000 a day, the Alabama Department of Transportation implemented a rapid construction solution that replaced the bridge in only 53 days (Barkley and Strasburg 2002). Less than three years later, a similar accident occurred less than one-half mile from the I-65 bridge, and the replacement bridge was designed, fabricated, and constructed in 26 days (Endicott 2005).

Cast-in-place concrete bridges have been used extensively in Washington State. Bridges constructed with cast-in-place concrete substructures, prestressed concrete girders, and cast-in-place concrete decks have a good service record in terms of durability and seismic performance; however, these bridges require lengthy construction periods. Multiple concrete pours are required, and each pour must be allowed to cure before construction can proceed. Construction activities associated with cast-in-place concrete,

including the construction of falsework, placement of formwork, tying of reinforcing steel, and removal of formwork, also increase construction time and must be completed on-site where traffic patterns may be disrupted. This project aims to develop alternative bridge designs that can be constructed rapidly while preserving the durability and seismic performance exhibited by cast-in-place bridges.

1.2 PRECAST CONCRETE COMPONENTS: A POTENTIAL SOLUTION

Bridge designs incorporating precast concrete components are a potential solution for providing rapid construction. Precast concrete components are reinforced concrete members that are fabricated off-site, either in a fabrication plant or staging area, and then brought on-site and connected together. The number of on-site construction tasks is significantly reduced when precast concrete is used because the building of formwork, tying of reinforcing steel, and pouring and curing of concrete for many of the components can be completed off-site. Reducing the amount of work that must be done on-site reduces traffic disruption, especially because the precast components can usually be erected and connected at night. The overall construction time on-site can be reduced by using precast concrete components because the components can be fabricated in advance, eliminating the time spent waiting for concrete to cure.

Incorporating precast components into bridge designs can also provide several secondary benefits. They include the following:

- improved worker safety because the on-site construction time, during which workers are potentially exposed to high-speed traffic, is reduced
- higher quality members with better durability because of stringent quality control at fabrication plants
- components that are smaller and lighter because prestressing is incorporated in the design
- reduced environmental impacts, especially when bridges are constructed over waterways.
- components that are more uniform because of the use of high-quality formwork.

The design and construction of connections between precast bridge components are critical for good performance. The connections significantly affect the performance of the

bridge in an earthquake, and connection failure can lead to structural collapse. Previous applications have also shown that connections are especially prone to durability problems and can limit the life span of a bridge (Hieber et al. 2005a).

1.3 PRECAST CONCRETE APPLICATIONS FOR BRIDGES IN WASHINGTON STATE

An initial step toward using precast concrete components to facilitate rapid construction is determining which components of bridges in Washington State could be replaced with precast concrete. Previously, the authors published a state-of-the-art report on the use of precast concrete components for rapid bridge construction for Washington State Department of Transportation (WSDOT) (Hieber et al. 2005a). The report covered the use of precast components for both superstructures and substructures. The majority of previous applications of precast concrete have been for bridge superstructures in non-seismic areas. The superstructure of a bridge is intended to remain elastic during an earthquake, and seismic superstructure designs are similar to non-seismic designs. Therefore, the precast concrete superstructure designs developed for non-seismic areas can be implemented in the seismically active western portion of Washington State with little modification.

Precast concrete components have only been used for bridge substructures in the last 15 years, and the majority of applications have been in non-seismic regions. Unlike the superstructure, the substructure can experience large inelastic deformations during an earthquake, and special designs are required in seismic areas. For this reason, the substructure systems that have been used in non-seismic areas cannot be used in Western Washington without significant adaptation.

The current research initiative focuses on the development of precast concrete bridge piers for use in the seismically active regions of Washington State. A pier from a typical highway overpass bridge is shown in Figure 1.1. The feasibility of replacing the columns and cross beam, the bottom portion of the cap beam, with precast concrete components was investigated. The research examined the expected seismic performance of the piers, assessed their potential for rapid construction, and developed preliminary details for the connections between precast components (Hieber et al. 2005b). Procedures

for designing precast concrete bridge piers were also developed. These design procedures are the focus of this report.

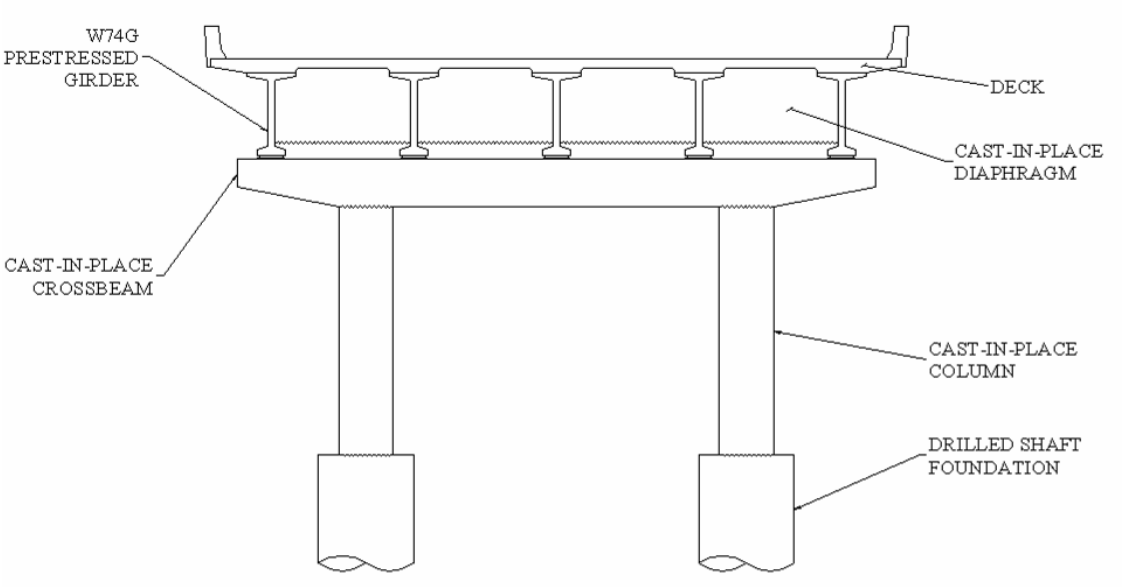

Figure 1.1: Cast-in-Place Reinforced Concrete Bridge Pier

1.4 PROPOSED PRECAST CONCRETE PIER SYSTEMS

Two types of precast concrete pier systems were developed in this research. The first system is an emulation of current cast-in-place reinforced concrete pier designs, hereafter referred to as the cast-in-place (CIP) emulation pier system. The second system uses a combination of vertical, unbonded post-tensioning tendons and bonded mild steel reinforcing bars to reinforce the pier, hereafter referred to as the hybrid pier system. Descriptions of the two systems and their expected behavior during an earthquake are presented below.

The columns and cross beam in a CIP emulation pier are fabricated out of precast concrete and connected in the field to facilitate rapid construction. The proposed CIP emulation pier system is shown in Figure 1.2. The foundations and diaphragm of the pier are constructed out of cast-in-place concrete. The columns are reinforced with mild steel reinforcement. The cross beam can be pretensioned to reduce the congestion of the reinforcement and improve the capacity of the cross beam to withstand transportation and erection loads. The connections are facilitated by extending the reinforcing bars out of both ends of the columns. The bars extending from the bottom of the column are

embedded into the top portion of the cast-in-place foundation. The reinforcing bars extending from the top of the column fit into openings in the cross beam, which are filled with grout to complete the connection. Hieber et al. (2005b) presented several potential details for the column-to-footing and column-to-cross beam connections.

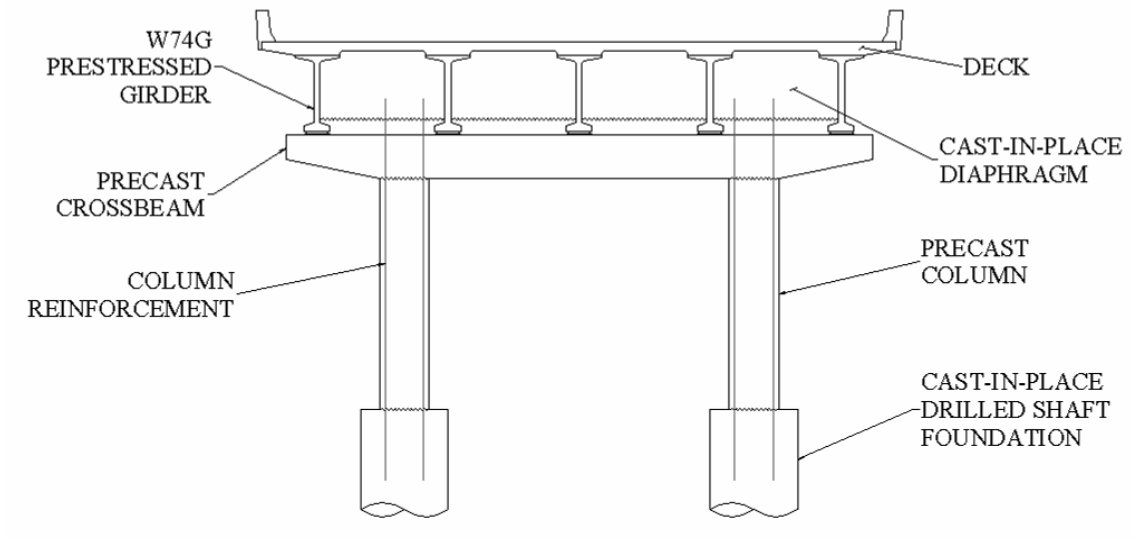

Figure 1.2: Cast-in-Place (CIP) Emulation Precast Pier System

The connections of the precast columns to the foundation and the columns to the cross beam are designed to be stronger than the columns. Therefore, plastic hinges are expected to form at the ends of the columns during an earthquake, as shown in Figure 1.3. Confining the inelastic deformations to these regions will result in satisfactory performance, provided that the columns are appropriately confined so that they exhibit little strength degradation at large deformation demands. Because the columns are weakest, they will yield first, and the other components of the pier will remain elastic and relatively undamaged during an earthquake. This practice is commonly referred to as capacity design.

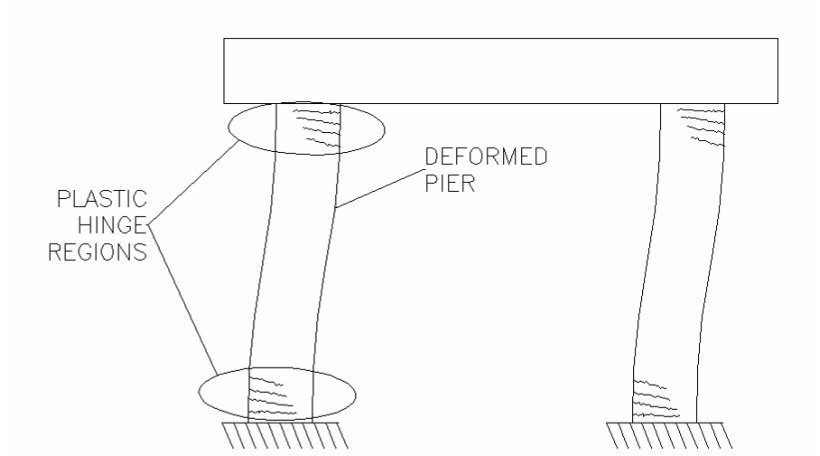

Figure 1.3: Expected Seismic Behavior of a CIP Emulation Pier

The hybrid precast pier system is reinforced with a combination of mild steel reinforcement and unbonded post-tensioning. A schematic of the proposed hybrid system is shown in Figure 1.4. As with CIP emulation piers, the columns and cross beam of the pier are precast concrete, while the foundations and diaphragm are cast-in-place concrete. The precast components are similar to those used in the CIP emulation system, except that a duct is installed in the center of the column for the post-tensioning tendons. A corresponding opening is fabricated in the cross beam. The post-tensioning contributes to the moment capacity of the columns, allowing the required number of mild steel reinforcing bars to be decreased. This decrease reduces congestion of the column-to-cap beam connection, making the components easier to fabricate and to erect. The anchors for the post-tensioning are located in the cast-in-place concrete of the foundations and diaphragm. For typical column lengths, furnishing the post-tensioning tendons without requiring splices should not be a problem. Hieber et al. (2005b) presented potential details for the column-to-footing and column-to-crossbeam connections.

Corrosion of the post-tensioning tendons is a concern in the design of hybrid piers. A corrosion protection system is envisioned consisting of a combination of epoxy coated strand, plastic sheathing, and/or grease. Future work would be required to finalize the corrosion protection system and develop methods for inspecting the post-tensioning.

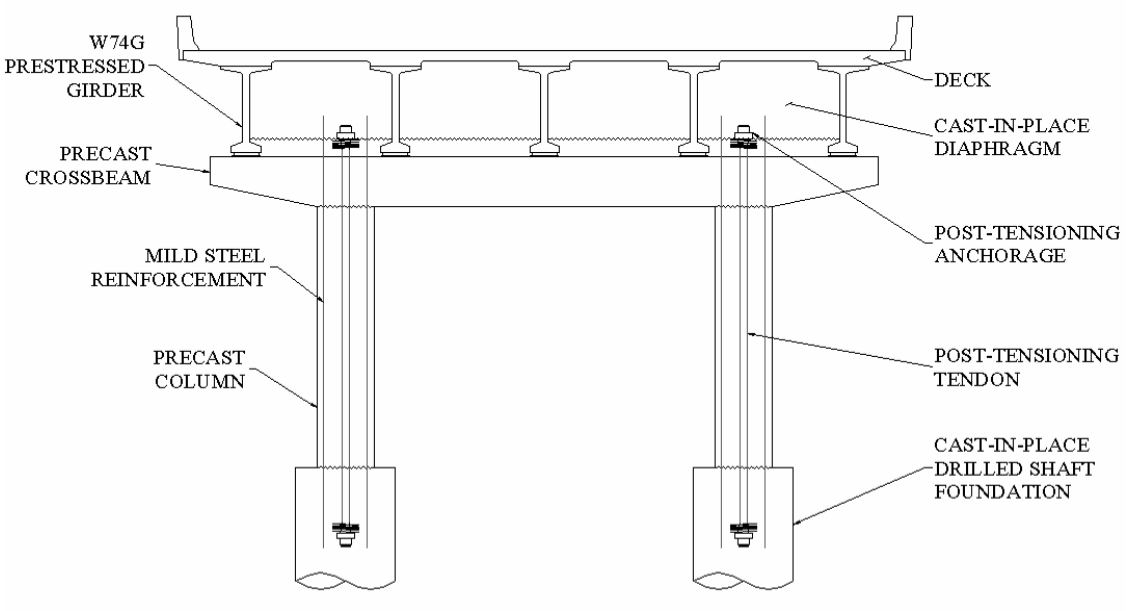

Figure 1.4: Hybrid Precast Concrete Pier System

The hybrid piers are expected to perform differently than CIP emulation and cast-in-place reinforced concrete piers during an earthquake. Only a portion of the mild steel reinforcement in the precast columns of a hybrid pier extends into the footing and cross beam. This causes the interfaces between the column and footing, and column and cross beam to be the weakest portion of the pier. Consequently, the majority of deformation during an earthquake will be concentrated at these interfaces. The deformation is expected to be dominated by one large crack at the top and bottom of the columns, and the overall behavior of the pier is expected to be similar to rocking blocks, as shown in Figure 1.5. With deformation concentrated at the interfaces, little cracking is expected to occur in the precast components and plastic hinges should not form.

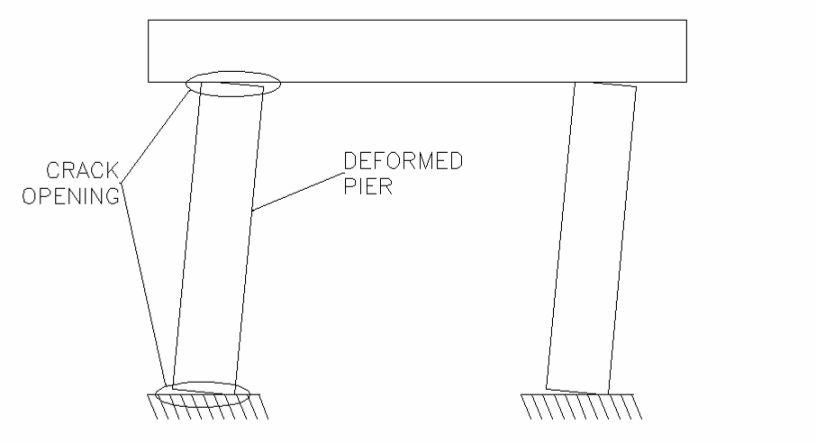

Figure 1.5: Expected Seismic Behavior of a Hybrid Pier

The interface regions of the piers must be detailed to withstand large deformations. For example, the mild steel reinforcement is unbonded in the interface region to reduce the peak strains and prevent the bars from fracturing. The ends of the columns are also heavily confined to reduce damage to the columns caused by high local compressive stresses.

The post-tensioning in the columns is designed to remain elastic during an earthquake. After an earthquake, the post-tensioning will provide a recentering force and reduce residual displacements. The mild steel is intended to yield and to dissipate energy, reducing the maximum deflection. The proportion of post-tensioning reinforcement to mild steel reinforcement can be adjusted to balance the maximum and residual displacements.

1.5 DESIGN PROCEDURES FOR PRECAST CONCRETE PIERS

Design procedures are needed to proportion the reinforcement of the columns and cap beam of precast concrete bridge piers to ensure economical piers with acceptable seismic performance. It is uneconomical to design bridge piers with enough capacity to remain elastic during an earthquake because the induced forces would be extremely large. Therefore, the seismic design philosophy typically implemented in the United States allows the piers to deform inelastically during an earthquake. This strategy significantly reduces the forces for which the pier must be designed, but it results in damage to the pier during a major earthquake. Damage to reinforced concrete structures, such as bridge

piers, is most closely related to the displacement demands (Priestley et al. 1996). Accordingly, suitable design procedures should limit the inelastic deformations of the pier during an earthquake to a level that does not exceed the deformation capacity of the pier.

Procedures for the seismic design of bridge piers based on two methodologies are presented in this report. An equivalent lateral force design (ELFD) method is presented in Chapter 2. In the ELFD procedure, the demands placed on the pier by an earthquake are represented by equivalent lateral forces. The elastic equivalent lateral force is determined on the basis of the spectral acceleration of the pier and its weight, and it is then reduced by an empirical response modification factor. Designing the pier for this reduced force implies that the pier will deform inelastically in a design-level earthquake. Larger reduction factors result in smaller design forces and increased inelastic deformation. The value of the reduction factor is chosen so that the amount of inelastic deformation will not exceed the deformation capacity of the pier. Ductile structures with large deformation capacities are assigned large reduction factors, and brittle structures with little deformation capacity are assigned small reduction factors. The ELFD is a common methodology for designing bridges in the United States (AASHTO 2002; AASHTO 2004).

A direct displacement-based design (DDBD) method is presented in Chapter 3. In the DDBD procedure, the designer chooses a maximum allowable displacement on the basis of a performance objective, such as the maximum amount of damage allowed in an earthquake, and determines the strength and stiffness of the bridge pier so that this target displacement is not exceeded in a design-level earthquake. Larger target displacement values can be selected for ductile systems, and smaller target displacements are selected for brittle structures, according to their deformation capacity. The DDBD procedure, in the form presented in this report, has yet to become widely used for designing bridge piers.

It would be preferable to design both the CIP emulation and hybrid precast pier systems with the same design method. This would simplify the design process and ensure that comparable designs were used for both types of piers. Cast-in-place reinforced concrete piers are typically designed with the ELFD method. Because CIP emulation

piers behave similarly to cast-in-place reinforced concrete piers, the ELFD procedure is seen as the logical choice for design. Hybrid moment frames in buildings have typically been designed with the DDBD method because it allows the designer more flexibility in balancing the maximum and residual displacements. This implies that the DDBD procedure may be best suited for hybrid piers. Furthermore, few provisions have been developed for designing hybrid structures with the ELFD method, largely because consensus has yet to be reached on the response reduction factor (R) to be used.

In this study, both types of structures were designed with both design methods, and the suitability of the two methods was evaluated for both pier types.

1.6 RESEARCH OBJECTIVES

The objective of this research was to develop guidelines for the seismic design of the precast concrete pier systems presented in Section 1.4. The following steps were required to meet this objective:

- Develop procedures according to both the ELFD and DDBD approaches.
- Develop methods for determining the values required in the design procedures, such as the yield displacement of a pier.
- Verify that piers designed with the DDBD procedure will be displaced to approximately the target displacement during a design-level earthquake.
- Predict the damage likely to occur to the piers.
- Compare the results obtained with the two design procedures.
- Compare the level of damage expected for CIP emulation and hybrid piers in a design-level earthquake.

1.7 SUMMARY OF REPORT CONTENTS

Background information and design procedures for the ELFD and DDBD procedures are presented in chapters 2 and 3. Chapter 4 presents several methods for estimating the yield displacement of the piers, which is required in the DDBD procedure. Methods for estimating the equivalent viscous damping in the DDBD procedure for idealized conditions are presented in Chapter 5, followed by the development of an empirical damping modification factor in Chapter 6 to account for real earthquake loading. Methods for determining the capacity of the pier systems are presented in

Chapter 7. Validation of the displacement predictions of the DDBD procedures is presented in Chapter 8. Evaluations of the expected damage to piers designed with the ELFD and DDBD procedures are presented in chapters 9 and 10, respectively. Conclusions and recommendations are presented in Chapter 11.

The analytical models used to assess the performance of the piers during an earthquake are presented in Appendix A. Appendix B documents the development of ground-motion acceleration records used in this research to represent design-level earthquakes. Examples of the CIP emulation and hybrid piers designed with the ELFD and DDBD methods are presented in appendices C and D, respectively. Example calculations for determining the capacity of the CIP emulation and hybrid piers are included in Appendix E. The five ground motion acceleration records considered in this research are documented in Appendix F. The computer scripts used for modeling pier behavior and designing piers with the different procedures presented in this report are presented by Wacker (2005).

CHAPTER 2
EQUIVALENT LATERAL FORCE DESIGN METHOD

This chapter provides background information on the equivalent lateral force design (ELFD) method and its implementation for precast concrete bridge piers.

2.1 BACKGROUND

Seismic provisions based on the ELFD method were first developed for designing buildings and then adapted to bridges. The first building design specifications to use the ELFD method appeared at the beginning of the 20th century in the building specifications for localities, such as the City of San Francisco. These specifications required buildings to be designed for equivalent lateral forces equal to a portion of the building's weight (Hamburger 2003).

The first regional building specification to include the ELFD method was the 1927 Uniform Building Code (UBC). The 1927 UBC recommended that buildings be designed for equivalent lateral forces on each floor equal to 10 percent of the floor weight if the building rested on soft soil and 3 percent of the floor weight if the building rested on firm soil. The Riley Act and Field Act implemented in California after the 1933 Long Beach earthquake made seismic design mandatory for certain structures. The concept of determining the equivalent lateral force by using dynamic analysis was first adopted into building specifications in the 1950s, including the 1958 UBC (Hamburger 2003). A design acceleration response spectrum was specified in the 1958 UBC that could be used to find the equivalent lateral force, given the fundamental period of vibration of the structure and weight of the floors.

The general concept of the ELFD method has not changed much since the 1950s. Improvements have been made to the design response spectra, seismic hazard maps, and soil type modification factors used in the ELFD method. The main effect of these changes has been an increase in the equivalent lateral forces for which the structures must be designed.

The ELFD method currently used for bridges is included in the American Association of State Highway and Transportation Officials (AASHTO) specifications

(AASHTO 2002; AASHTO 2004) and was adapted from the ATC-6 report (ATC 1981) jointly published by the Applied Technology Council (ATC) and the Federal Highway Administration (FHWA) in 1981. The ELFD provisions in the ATC-6 report were similar to the seismic design provisions included in the ATC-3-06 report for buildings (ATC 1978). The provisions of ATC-3-06 were adopted into the 1988 UBC.

The ATC-6 provisions were adopted as AASHTO interim specifications in 1983 and incorporated into the 15th edition of the AASHTO Standard Specifications for Highway Bridges in 1992 (AASHTO 1992). The AASHTO Load and Resistance Factor (LRFD) Bridge Design Specifications were first published in 1994 (AASHTO 1994) and copied the seismic provisions nearly verbatim from the Standard Specification of the time. An effort is currently under way to update the seismic provisions in the AASHTO specifications (AASHTO 2002; AASHTO 2004). The proposed changes are outlined in NCHRP Report No. 472 (ATC/MCEER 2002).

2.2 PROCEDURE

The following ELFD procedure is proposed for the design of both CIP emulation and hybrid precast pier systems. The procedure was adapted primarily from the AASHTO specifications (AASHTO 2002; AASHTO 2004). In places where the AASHTO specifications are not clear, the development of the procedure is documented in detail. The same procedure can be used to design the two types of piers. The steps of the procedure are summarized in the flowchart shown in Figure 2.1. Design examples for both types of piers are presented in Appendix C.

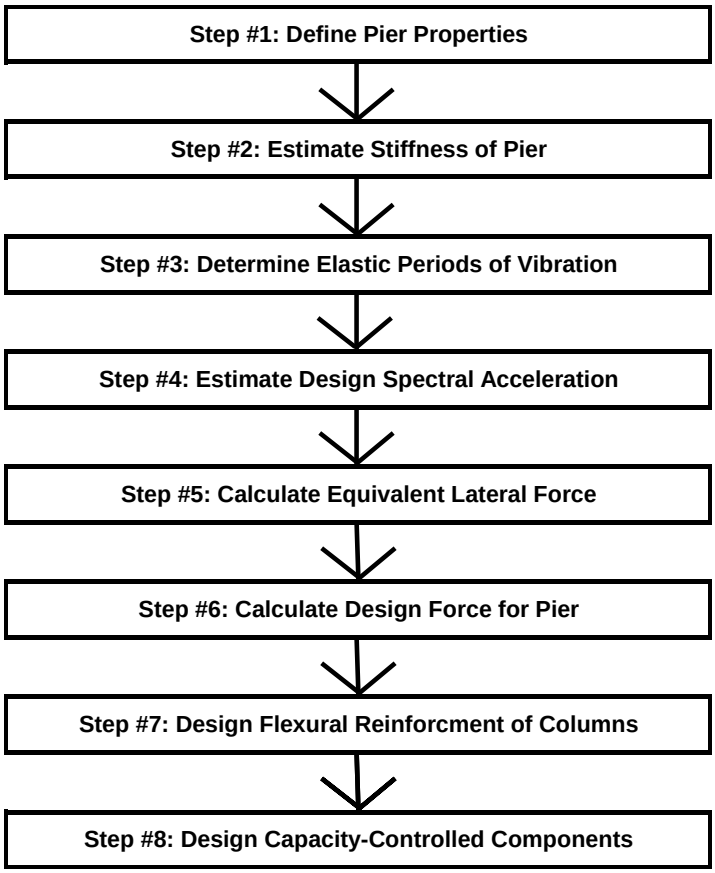

Figure 2.1: Equivalent Lateral Force Design (ELFD) Procedure

Step #1: Define the Pier Properties

Trial values for several pier properties must be selected before seismic design can be performed. These properties include the following:

- column height (L_c)
- column diameter (D_c)
- number of columns in the pier (n_c)
- axial dead load per column due to the weight of the superstructure (P_c)
- material properties of the concrete, mild steel reinforcement, and post-tensioning reinforcement (if any).

If desired, the design procedure can be iterated to determine the optimal values of these variables.

Step #2: Estimate the Stiffness of the Pier

The AASHTO specifications (AASHTO 2002; AASHTO 2004) are not clear as to whether the cross-section of the columns should be considered to be cracked or uncracked for the purpose of determining the stiffness of the pier. An uncracked cross-section has a larger moment of inertia, which increases the pier stiffness and equivalent lateral force on the pier. A cracked cross-section has a smaller moment of inertia, which decreases the stiffness of the pier and equivalent lateral force. Conventional wisdom is that using an uncracked cross-section will increase the amount of reinforcement required in the pier but reduce the amount of damage during an earthquake. Piers designed with the cracked stiffness will require less reinforcing steel but will possibly incur more damage during an earthquake because of larger inelastic deformations. Provided that the columns of the pier have sufficient deformation capacity, the use of either cracked or uncracked properties will result in an acceptable design (WSDOT Design Memorandum, Chuck Ruth, December 22, 1999).

The method that the Washington State Department of Transportation (WSDOT) currently uses to determine the moment of inertia of the columns was adopted for this research. WSDOT uses the cracked column cross-section when determining the moment of inertia. For simplicity, WSDOT assumes that the cracked moment of inertia (I_{cr}) is equal to one-half the gross moment of inertia (I_g) (personal communication, Jugesh Kapur, February 8, 2005). The gross moment of inertia for a circular column is

$$I_g = \frac{\pi D_c^{\,4}}{64} \tag{2.1}$$

The stiffness of the pier can be determined by using linear structural analysis. If the cap beam and foundations are rigid in comparison to the columns, as was assumed in this study, Equation (2.2) can be used to estimate the stiffness of an individual pier (K_p). The implications of these assumptions are discussed in Appendix A.

$$K_p = \frac{12 n_c E_c I_{cr}}{L_c^3} \tag{2.2}$$

In Equation (2.2), E_c is the elastic modulus of concrete.

Although WSDOT does not currently design hybrid piers, the assumption that I_{cr} is equal to one-half of I_g was used for hybrid piers in this research. The additional axial load in the columns of hybrid piers due to the vertical post-tensioning should increase the cracked stiffness of the columns in comparison to columns in CIP emulation piers. This implies that the hybrid piers should have a larger stiffness and, according to the conventional ELFD approach, be designed for a larger equivalent lateral force. However, when properly designed and detailed, hybrid systems have been shown to exhibit deformation capacities that are comparable or superior to reinforced concrete systems (Stone et al. 1995). This observation supports the use of the same equivalent lateral force and stiffness for both hybrid and CIP emulation piers.

Step #3: Determine the Elastic Periods of Vibration

The period of the ith mode of vibration for the structure (T_i) can be determined by using the principles of dynamics. If the pier is assumed to behave as a single degree of freedom (SDOF) oscillator, the natural period of vibration (T_n) can then be calculated as

$$T_n = 2\pi\sqrt{\frac{m_p}{K_p}} \tag{2.3}$$

where m_p is the total mass on the pier due to the weight of the superstructure and self-weight of the pier.

Step #4: Estimate the Design Spectral Acceleration

For each mode of vibration, the design spectral acceleration ($S_{a,i}$) can be determined from the design acceleration response spectrum provided by the AASHTO specifications (AASHTO 2002; AASHTO 2004) and represented by Equation (2.4),

$$S_{a,i} = \frac{1.2ASg}{T_i^{2/3}} < 2.5Ag \tag{2.4}$$

where g is the gravitational constant; A is the acceleration coefficient, which is equal to the peak ground acceleration with units of g, with a 10 percent probability of being

exceeded in 50 years; and S is the site coefficient to account for the effects of local soil conditions.

Step #5: Calculate the Equivalent Lateral Force

The equivalent lateral force on the pier (F_{eq}) used to represent the demands on the pier caused by a design-level earthquake under elastic conditions is determined by combining the inertial forces on the pier for each mode of vibration considered. The inertial force on the pier for the ith mode of vibration ($F_{eq,i}$) is

$$F_{eq,i} = S_{a,i} m_i \tag{2.5}$$

where m_i is the mass on the pier attributed to the ith mode of vibration. The inertial forces for several modes can be combined by using the square-root-of-sum-of-squares rule, complete quadratic combination (CQC) rule, or other appropriate method to determine F_{eq} (Chopra 2001).

If the pier is assumed to be an SDOF oscillator, F_{eq} can be calculated as

$$F_{eq} = S_a m_p \tag{2.6}$$

where S_a is the spectral acceleration from the design spectrum for T_n.

Step #6: Calculate the Design Force for the Pier

The equivalent lateral force (F_{eq}) is reduced by an empirical response modification factor (R) to account for the effects of inelastic behavior on the pier's response when the design force is determined (F_d) for the pier. The design force (F_d) for the pier is

$$F_d = \frac{F_{eq}}{R} \tag{2.7}$$

The AASHTO specifications (AASHTO 2002; AASHTO 2004) provide R values for cast-in-place reinforced concrete piers. The value of R for flexural yielding failure of columns in a multi-column pier varies, depending on the importance of the bridge as follows:

- R = 1.5 for critical bridges

- R = 3.5 for essential bridges
- R = 5.0 for all other bridges.

CIP emulation piers, by definition, behave similarly to cast-in-place reinforced concrete piers, so they may be designed with the R values included in the AASHTO specifications. Selecting appropriate R values for hybrid piers is not a trivial matter. Previous experimental testing of hybrid moment frames has shown that hybrid systems appear to have deformation capacities equal to or greater than similar reinforced concrete systems (Cheok and Lew 1991; Cheok and Lew 1993; Stone et al. 1995). Because larger R values are given to systems with greater deformation capacity, this research assumed that the R values in the AASHTO specifications (AASHTO 2002; AASHTO 2004) for cast-in-place reinforced concrete piers could be used conservatively for hybrid piers. A comparison of CIP emulation and hybrid piers designed with the same R values is provided in Chapter 9.

Step #7: Design the Flexural Reinforcement of Columns

The amount of reinforcement required to withstand F_d should be determined. The sectional analysis method presented in Section 7.4 can be used for both CIP emulation and hybrid piers.

The proportion of mild steel reinforcement to unbonded post-tensioning reinforcement must be specified for hybrid piers. Although any proportion of reinforcement can be used, provided that it results in sufficient force capacity, it is recommended that enough post-tensioning be used to cause the pier to re-center after an earthquake, as described in Section 7.5. The use of additional unbonded post-tensioning may be desirable to reduce the amount of mild steel reinforcement, thereby relieving congestion caused by a large number of bars extending into the cross beam.

Step #8: Design the Capacity-Controlled Components

After the flexural reinforcement of the pier columns has been selected, several other components of the pier still need to be designed. The transverse reinforcement of the columns should be designed to withstand the shear demand and provide adequate confinement to the core concrete so that the pier has acceptable deformation capacity.

The cap beam also needs to be designed and the reinforcement detailed to ensure acceptable embedment lengths.

2.3 ADVANTAGES AND DISADVANTAGES OF THE ELFD PROCEDURE

The main advantage of the ELFD method is that it is widely used, and the majority of bridge engineers who perform seismic design already know how to apply it, primarily because it is included in the AASHTO specifications (AASHTO 2002; AASHTO 2004). The ELFD procedure also requires no iteration and can be completed quickly.

The main disadvantage of the ELFD method is that it is not transparent, making it difficult for a designer to predict the extent of damage to the bridge pier in a design-level earthquake. The designer is required to select an empirical response modification factor (R), but no information is available on the inelastic displacements that will occur or the level of damage that can be expected in a design-level earthquake. The implications of assumptions made in design, such as the method used to determine pier stiffness, are also difficult to ascertain. The development of R values is also quite subjective. The ELFD method leads to larger design forces for systems with greater initial stiffness independent of their deformation capacity. This can result in systems with larger deformation capacity being designed for greater forces than those with less capacity, thereby undermining the seismic design philosophy.

CHAPTER 3
DIRECT DISPLACEMENT-BASED DESIGN METHOD

This chapter presents the development of the direct displacement-based design (DDBD) method and two procedures for implementing the method.

3.1 BACKGROUND

The fundamentals of the DDBD procedure were established approximately 30 years ago. Gulkan and Sozen (1974) developed the substitute-structure method for single-degree-of-freedom (SDOF) systems, and Shibata and Sozen (1976) extended the concepts to multiple-degree-of-freedom (MDOF) systems. In the substitute-structure method, design forces for structural members are established on the basis of a specified target displacement and levels of inelastic deformation. The methodology proposed in this research is most similar to the DDBD method proposed by Kowalsky et al. (1995), and described for hybrid systems by Stanton and Nakaki (2002).

Because the basic premise of the DDBD method is that the structure should be designed to reach a specific peak displacement during a ground motion with a known time-history, a methodology is needed for relating the peak displacement to the structural properties and the ground motion acceleration record. Two approaches have been proposed for accomplishing this: (1) approximating the inelastic behavior by using an equivalent linear system and (2) approximating the inelastic displacement by using inelastic design spectra (Chopra and Goel 2001). The equivalent linear system approach consists of representing the real, inelastic system with an equivalent elastic system whose mass, stiffness, and damping are chosen so that the peak seismic displacements of the two systems are the same. In the inelastic design spectrum approach, the displacement of the system is determined directly using an inelastic design spectrum. At this time, experts disagree over which approach is best for the DDBD procedure (Chopra and Goel 2001).

The representation of the inelastic system subjected to seismic excitation by an equivalent linear system is inherently approximate and will result in some error. The equivalent linear system approach has been shown to overestimate displacement in the short-period range, while providing reasonable estimates for longer periods (Miranda and

Ruiz-Garcia 2002). The inelastic design spectrum approach eliminates some of this error; however, inelastic response spectra depend on the ground motion acceleration record of the earthquake, the maximum ductility that the system reaches, and the hysteretic behavior of the inelastic system. It is impractical to develop design response spectra for every possible ductility level and hysteretic model that could occur, so error is introduced through the use of approximate or averaged inelastic design spectra.

The equivalent linear system approach was used in this research because it can accurately predict displacements when appropriate correction factors are employed, and it avoids the substantial work associated with developing inelastic design spectra.

The equivalent viscous damping and equivalent stiffness of the elastic system need to be determined so that the peak displacement of the equivalent linear system matches the peak displacement of the inelastic system in an earthquake. The concept of equivalent viscous damping was first proposed by Jacobsen (1930). He showed that a nonlinear, damped SDOF oscillator subjected to sinusoidal loading could be represented by an oscillator with an equivalent amount of viscous damping. Following the initial work by Jacobsen (1930), a number of researchers proposed the use of equivalent linear systems to represent the response of yielding SDOF systems subjected to sinusoidal excitation (e.g., Rosenblueth and Herrera, 1964).

Jennings (1968) examined several formulations for the equivalent linear system of an elasto-plastic SDOF structure subjected to both sinusoidal and earthquake excitation. Jennings found that the required amount of equivalent viscous damping depended strongly on the method used for determining the equivalent stiffness of the elastic system and the characteristics of the ground motion acceleration record.

The first application of the equivalent linear system approach to the design of SDOF reinforced concrete structures was proposed by Gulkan and Sozen (1974). They proposed that the equivalent viscous damping and equivalent stiffness are related to the hysteretic behavior of the inelastic reinforced concrete system. They proposed that the equivalent stiffness be taken equal to the secant stiffness at the maximum displacement. This choice results in the equivalent stiffness being not a unique characteristic of the structure but one that also depends on the excitation. Gulkan and Sozen (1974) also proposed that the equivalent viscous damping be calculated such that the energy

dissipated by the equivalent linear system is equal to the hysteretic energy dissipated by the reinforced concrete system. The equivalent viscous damping is modified by a factor to account for the fact that the maximum displacement of the structure is only reached once during an earthquake, and smaller displacement cycles result in less energy dissipation.

3.2 PROCEDURE

There are no provisions for the DDBD method in the American Association of State Highway and Transportation Officials (AASHTO) specifications (AASHTO 2002; AASHTO 2004). The procedures presented below were adapted primarily from the work of Kowalsky et al. (1995), and Stanton and Nakaki (2002). The first procedure uses iteration to determine the best possible design. The second procedure requires no iteration. The accuracy of the two procedures is compared in Chapter 8. Example calculations using both DDBD procedures are provided in Appendix D.

Both of the procedures develop the equivalent linear system by using an approach similar to that followed by Gulkan and Sozen (1974). The equivalent stiffness (K_{eq}) is defined as the secant stiffness of the inelastic pier response at the maximum displacement (Δ_{max}) expected in a design-level earthquake, as shown in Figure 3.1. The equivalent damping is determined to equate the amount of energy dissipated by the equivalent linear system and the inelastic pier. An empirical factor is applied to the damping to account for error and the fact that the majority of cycles have displacements less than the target displacement.

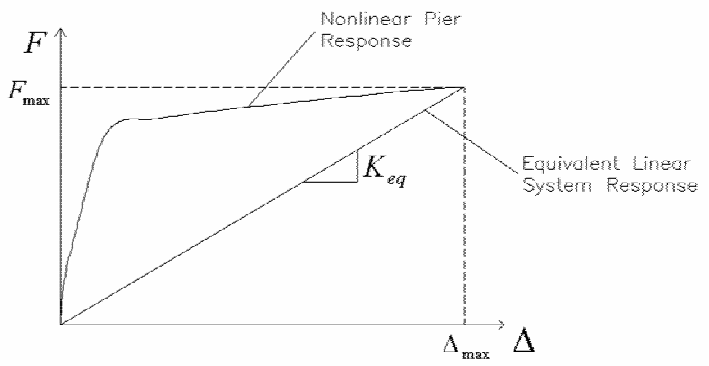

Figure 3.1: Stiffness of Equivalent Linear System

3.2.1 Iterative Procedure

The steps of the iterative DDBD procedure are presented below. The design steps are summarized in the flowchart presented in Figure 3.2. The steps of the procedure are nearly identical for CIP emulation and hybrid pier systems. Differences are mentioned specifically in the text below.

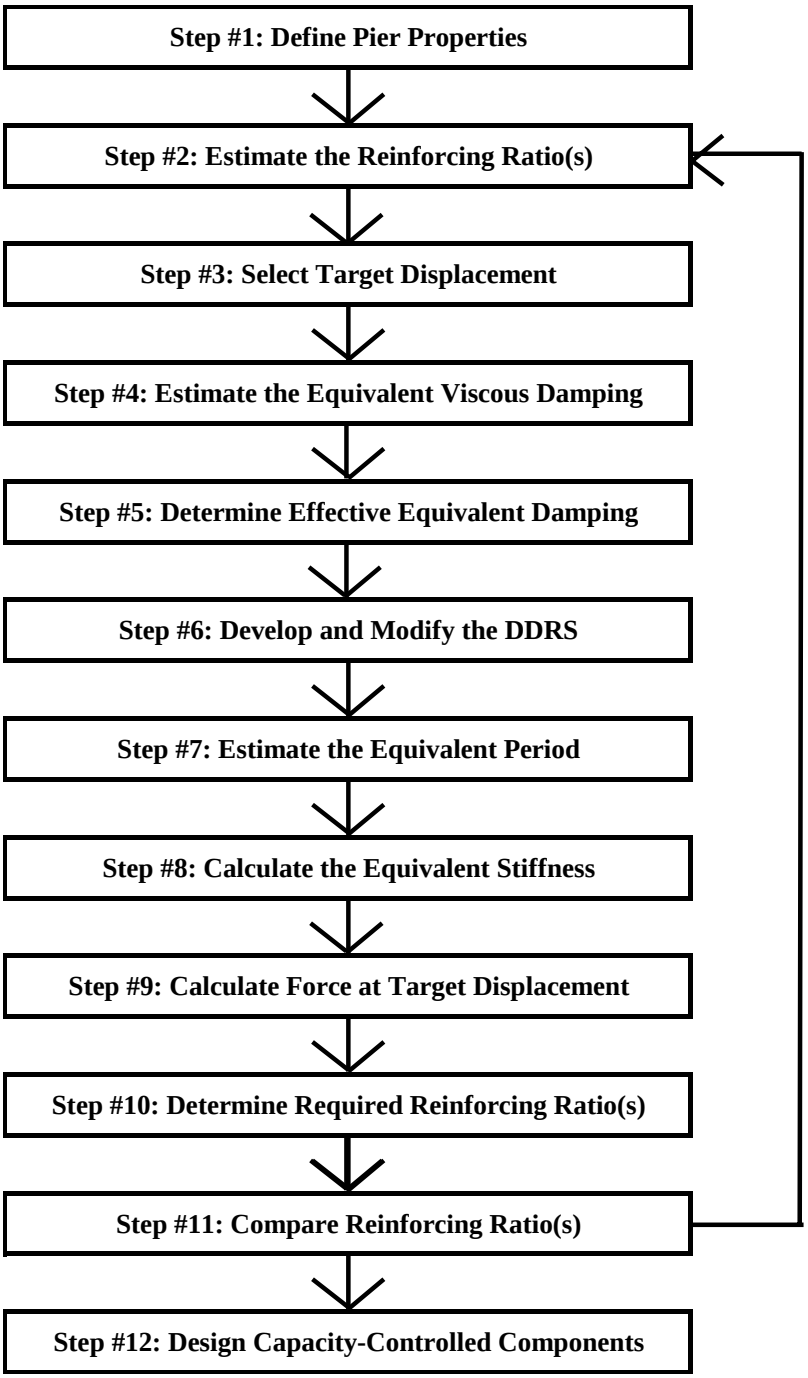

Figure 3.2: Flowchart of Iterative DDBD Procedure

Step #1: Define the Pier Properties

Trial values for several pier properties must be selected before seismic design can be performed. They include the following:

- column height (L_c)
- column diameter (D_c)
- number of columns in the pier (n_c)
- axial dead load per column due to the weight of the superstructure (P_c)
- material properties of the concrete, mild steel reinforcement, and post-tensioning reinforcement.

If desired, the design procedure can be iterated to determine the optimal values of these variables.

Step #2: Estimate the Reinforcing Ratio(s) for the Column

The reinforcing ratio(s) must be estimated before the design can proceed. Iteration will be used to improve the values, so the initial estimate is not critical. For example, an initial estimate for the mild steel reinforcing ratio (ρ_s) of 1 percent could be used for CIP emulation piers.

Hybrid piers require initial estimates for both ρ_s and the post-tensioning reinforcing ratio (ρ_p). For example, initial estimates for ρ_s and ρ_p of 1.0 percent and 0.05percent, respectively, could be used.

Step #3: Select the Target Displacement

The maximum displacement that the pier is desired to reach during a design-level earthquake is chosen by the designer. This displacement is referred to as the target displacement (Δ_t). The designer can select Δ_t to achieve a performance objective, such as limiting the probability of a certain type of damage occurring during an earthquake, or limit Δ_t to a certain fraction of the deformation capacity of the pier to achieve a desired factor of safety. If the method chosen for determining Δ_t is independent of the amount of

reinforcement in the pier, there is no need for iterating the value of Δ_t, and this step can be swapped with Step #2.

The selection of Δ_t depends on a number of factors, including the importance of the bridge and the ease with which the bridge can be repaired after a major earthquake. The California Department of Transportation (CALTRANS) recommends the following displacement ductility (μ_Δ) limits for bridge piers (CALTRANS 2004):

- Single column bents supported on fixed foundation: $\mu_\Delta \leq 4.0$
- Multiple column bents supported on fixed or pinned footings: $\mu_\Delta \leq 5.0$
- Pier walls (weak direction) supported on fixed or pinned footings: $\mu_\Delta \leq 5.0$
- Pier walls (strong direction) supported on fixed or pinned footings: $\mu_\Delta \leq 1.0$

The target displacement can be determined from the displacement ductility by using Equation (3.1), with the yield displacement (Δ_y) estimated by using the procedures presented in Chapter 4.

$$\Delta_t = \mu_\Delta \Delta_y \tag{3.1}$$

Step #4: Estimate the Equivalent Viscous Damping

The viscous damping of the equivalent linear system (ξ_{eq}), commonly referred to as the equivalent viscous damping, must be estimated. The relationship for determining ξ_{eq} from the hysteretic behavior of the pier when displaced to Δ_t can be complex. Methods for estimating ξ_{eq} are presented in Chapter 5. Both the nonlinear analysis method (Section 5.2) and equation-based method (Section 5.3) can be used to estimate ξ_{eq} in the iterative procedure.

Step #5: Determine the Effective Equivalent Viscous Damping

The value of ξ_{eq} estimated in Step #4 is not accurate because the pier only reaches Δ_{max} once during an earthquake. The majority of oscillations reach smaller displacements, which correspond to smaller values of ξ_{eq}. The relative amplitude of the

displacement cycles is affected significantly by the frequency content and other characteristics of the ground motion.

To correct for these issues, ξ_{eq} is multiplied by a damping modification factor (β) that relates ξ_{eq} to the effective equivalent viscous damping ($\hat{\xi}_{eq}$) that would cause the maximum displacement to reach the target displacement of the pier in a design-level earthquake. This step could also be described as finding the modification factor required for the equivalent linear system to match the peak inelastic displacement exactly. This research used an approximate value of β that was determined to match the results of nonlinear analyses on an average basis. The development of the β factors is presented in Chapter 6. Equation (3.2) can be used to estimate $\hat{\xi}_{eq}$.

$$\hat{\xi}_{eq} = \beta \xi_{eq} \tag{3.2}$$

Separate relationships for β were determined for the two types of piers because they behave differently and cannot be represented by using the same equivalent linear system. Despite the use of a modification factor, the design procedure still will not be exact. This disparity can be attributed to the use of an average value for β and the fact that β is sensitive to the frequency content of the earthquake, which is likely to differ from the earthquakes used to determine β.

Step #6: Develop and Modify the Design Displacement Response Spectrum

The design displacement response spectrum (DDRS), developed from the design acceleration response spectrum specified in the AASHTO specifications (AASHTO 2002; AASHTO 2004), can be expressed as

$$S_{d-5\%} = \frac{1.2}{4\pi^2} ASgT^{4/3} \leq \frac{2.5}{4\pi^2} AgT^2 \tag{3.3}$$

In Equation (3.3), $S_{d-5\%}$ is the design spectral displacement for 5 percent viscous damping; g is the gravitational constant; A is the acceleration coefficient, which is equal to the peak ground acceleration with a 10 percent probability of being exceeded in 50 years; and S is the site coefficient to account for the effects of local soil conditions.

The DDRS can be used to relate the period of vibration of the equivalent system (T_{eq}) to Δ_t. Because the DDRS was developed for 5 percent viscous damping, which is not necessarily equal to $\hat{\xi}_{eq}$, the DDRS must be altered to reflect the amount of damping in the equivalent linear system. The AASHTO specifications (AASHTO 2002; AASHTO 2004) provide no guidance for doing this. The following equation relating the spectral displacement for different amounts of viscous damping was taken from EUROCODE 8 (EUROCODE 1994) and was used to modify the DDRS in this study.

$$S_{d-\hat{\xi}_{eq}} = \sqrt{\frac{7}{2+100\hat{\xi}_{eq}}} S_{d-5\%} \tag{3.4}$$

In Equation (3.4), $S_{d-\hat{\xi}_{eq}}$ is the design spectral displacement for $\hat{\xi}_{eq}$. Combining equations (3.3) and (3.4) results in the following modified DDRS.

$$S_{d-\hat{\xi}_{eq}} = \sqrt{\frac{7}{2+100\hat{\xi}_{eq}}} \frac{1.2}{4\pi^2} ASgT^{4/3} \le \sqrt{\frac{7}{2+100\hat{\xi}_{eq}}} \frac{2.5}{4\pi^2} AgT^2 \tag{3.5}$$

Step #7: Estimate the Equivalent Period of Vibration

The period of vibration of the equivalent linear system (T_{eq}) can be estimated from the modified DDRS, expressed in Equation (3.5), by using Δ_t as shown in Figure 3.3.

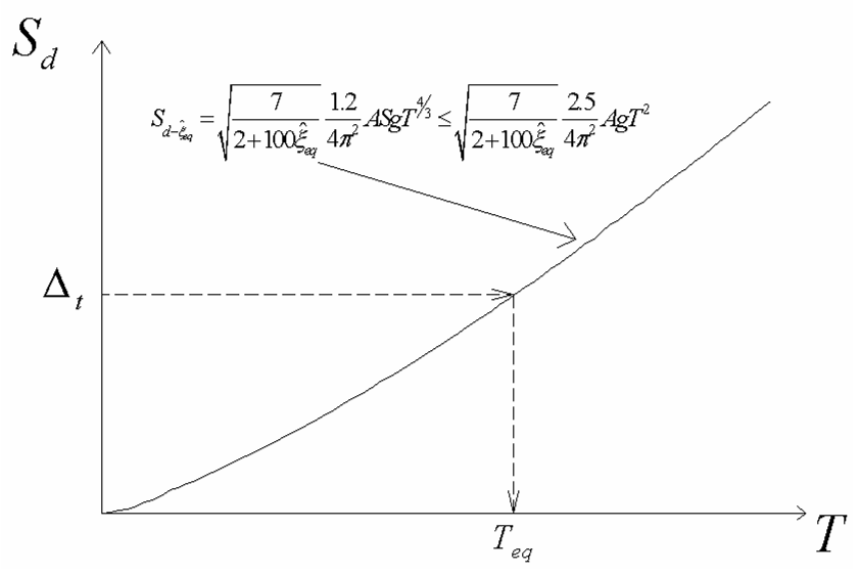

Figure 3.3: Determination of the Equivalent Period of Vibration

Step #8: Calculate the Equivalent Stiffness

Because the equivalent linear system is an elastic SDOF oscillator, the equivalent stiffness (K_{eq}) can be determined as

$$K_{eq} = 4\pi^2 \frac{m_p}{T_{eq}^{\ 2}} \tag{3.6}$$

where m_p is the total mass on the pier, including the weight of the superstructure and self-weight of the pier.

Step #9: Calculate the Force at the Target Displacement

The force at the target displacement (F_t) of the equivalent linear system can be determined by using Equation (3.7).

$$F_t = K_{eq}\Delta_t \tag{3.7}$$

Because of the definition for the equivalent stiffness, this is equal to the force on the inelastic pier at the target displacement. The design force (F_d) of the pier should be taken as F_t to ensure that Δ_t is not exceeded in a design-level earthquake.

Step #10: Determine the Required Reinforcing Ratio(s)

The amount of column reinforcement required so that the pier will reach F_t calculated in Step #9 at Δ_t must be determined. This calculation is complicated by the fact that the capacity of the pier is specified at a given amount of deformation and could be affected by different post-yield behavior. Methods for determining the amount of reinforcement required are provided in Chapter 7 of this report. Either the nonlinear analysis method (Section 7.3) or sectional analysis method (Section 7.4) can be used.

Hybrid piers require determination of both ρ_s and ρ_p . This requires the designer to decide the proportions of the total moment capacity to be provided by the mild steel and the post-tensioning. It is recommended that the amount of post-tensioning provided be at least enough to cause the columns to re-center automatically. A method for achieving this is discussed in Section 7.5. The weight of the superstructure on the pier also provides a recentering force, provided that the lateral displacement is less than the

column diameter. Therefore, for large-diameter columns and small displacements no post-tensioning may be required. Unless there are other constraints, the pier can then be designed as a CIP emulation pier rather than a hybrid pier.

Step #11: Compare the Reinforcing Ratio(s)

Steps #2 through 10 of the design procedure must be repeated until the reinforcing ratio(s) calculated in Step #10 are sufficiently close to the value(s) computed in the previous iteration. The reinforcing ratios will typically converge after only a few iterations.

Step #12: Design the Capacity-Controlled Components

This is identical to Step #8 in the ELFD procedure presented in Section 2.2.

3.2.2 Direct (Non-iterative) Procedure

In the direct procedure, ξ_{eq} is approximated by using an empirical equation. The estimates of ξ_{eq} are not as accurate as the methods that take the amount of reinforcement into consideration; however, the need to iterate is eliminated.

The steps of the direct procedure are the same as the iterative procedure with the following exceptions.

- Step #2 of the iterative procedure, in which the reinforcing ratio(s) are estimated, is removed from the direct procedure.
- The equivalent viscous damping (ξ_{eq}) is estimated with the empirical method (Section 5.4) presented in Chapter 5.

Figure 3.4 shows a flowchart of the non-iterative DDBD procedure.

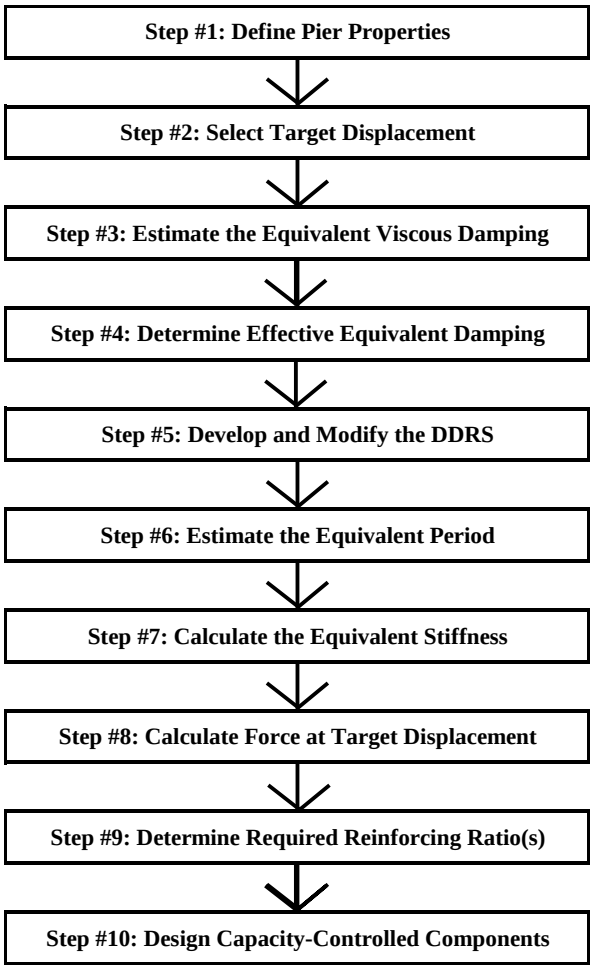

Figure 3.4: Flowchart of Direct (Non-Iterative) DDBD Procedure

3.3 ADVANTAGES AND DISADVANTAGES OF THE DDBD PROCEDURE

The main advantages of the DDBD procedure are that it is more transparent than the ELFD procedure and that it gives the designer more control over the performance of the structure. By choosing an appropriate target displacement, the designer can set the probability of different types of damage and failure, such as bar bucking, cover spalling, and collapse, occurring in a design-level earthquake because all of these quantities are closely related to displacement. Because damage in reinforced concrete structure is more closely related to inelastic displacements than forces (Priestley et al. 1996), designing structures to limit displacements, as is done in the DDBD procedure, inherently makes more sense than designing to limit seismic forces, as is done in the ELFD procedure. Another advantage of the DDBD method is that the inelastic behavior of a typical bridge pier, shown in Figure 3.5, is much less sensitive to changes in displacement than force. It

can be seen in the figure that, in the strain-hardening region, changes to the target displacement result in approximately the same force demand on the pier. On the other hand, a small change in the force on the pier can result in a big change in the displacement demand on the pier.

The primary disadvantages of the DDBD procedure are the need for iteration and additional complexity in comparison to the ELFD procedure.

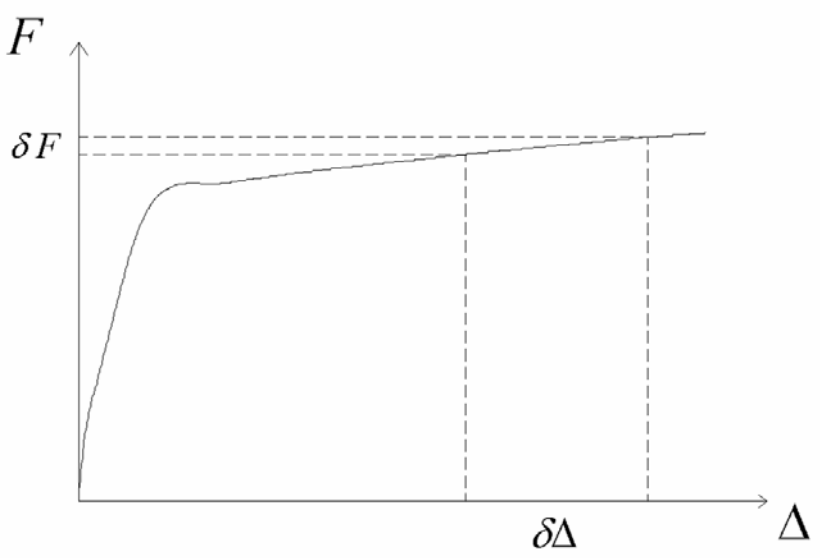

Figure 3.5: Effects of Inelastic Pier Behavior on Changes in Force and Displacement

CHAPTER 4
METHODS FOR ESTIMATING YIELD DISPLACEMENT

The yield displacement (Δ_y)is an important quantity because it is used to determine the displacement ductility (μ_Δ) of a pier, which, in turn, is used to determine the equivalent viscous damping in the DDBD procedure. The yield displacement is also a suitable target displacement value for critical bridges that are intended to remain elastic during an earthquake.

Two methods for estimating Δ_y of CIP emulation and hybrid pier systems are presented in this chapter. The first method uses the results of nonlinear analyses to estimate Δ_y. The second method uses closed-form equations representing the stiffness of the pier to estimate Δ_y. The equations were calibrated by using results from nonlinear analyses, so that the estimates of Δ_y obtained with either method would be similar. The nonlinear analysis method is nearly identical for the CIP emulation and hybrid pier, whereas the equation-based method differs significantly between the two types of bridge systems. These relationships were developed specifically for bridge piers with the modeling constraints presented in Appendix A. Their use should be limited to similar applications.

4.1 NONLINEAR ANALYSIS METHOD

The yield displacement (Δ_y) of a pier can be estimated from the results of a nonlinear pushover analysis. The pushover response does not have a sharply defined yield point because the mild steel reinforcing bars in the columns do not all yield simultaneously. Because the yield point is not well defined, a procedure is required for defining a nominal yield displacement. In this research, the nominal yield displacement was defined as the intersection of the secant stiffness of the pier through the point at which the first reinforcing bar yields and the force required to induce a strain of 0.004 in the extreme compression concrete of the column (Berry and Eberhard 2004). This procedure is shown graphically in Figure 4.1 and can be expressed as

$$\Delta_y = \frac{F_{0.004}\Delta_y^{'}}{F_y^{'}} \tag{4.1}$$

where $\Delta_y^{'}$ is the displacement of the pier at first yield, $F_y^{'}$ is the force acting on the pier at first yield, and $F_{0.004}$ is the force acting on the pier when the extreme compression concrete reaches a strain of 0.004. These values depend on the characteristics of the model and the material models used in analysis, which are presented in Appendix A.

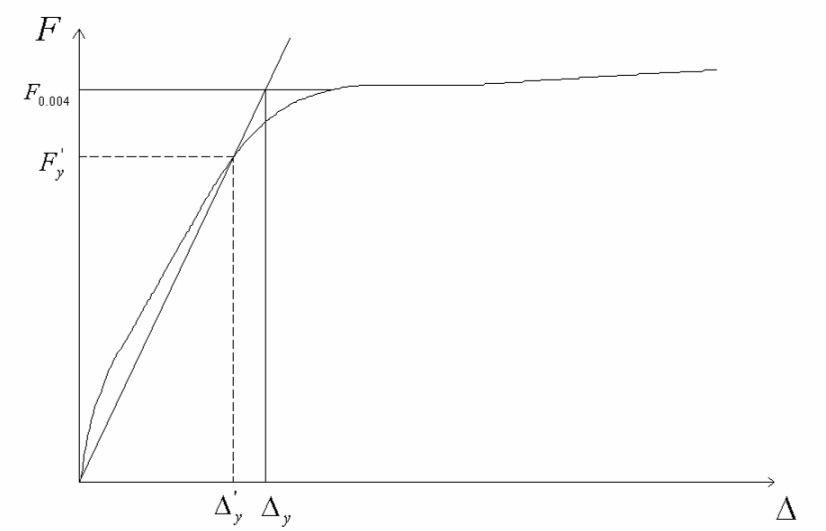

Figure 4.1: Procedure for Estimating the Yield Displacement

The displacement at first yield ($\Delta_y^{'}$) and force at first yield ($F_y^{'}$) can be determined by monitoring the strain in the extreme tensile reinforcing bar of the column ($\varepsilon_{stl,t}$) during a pushover analysis. The displacement of the pier and force on the pier when $\varepsilon_{stl,t}$ reaches the yield strain (ε_y) are $\Delta_y^{'}$ and $F_y^{'}$, respectively. A similar approach can be used to determine $F_{0.004}$ by recording the strain at the extreme compression face of the column ($\varepsilon_{con,c}$) and determining the force required to reach a strain of 0.004 during a pushover analysis.

The location at which strains are monitored differs for the CIP emulation and hybrid piers. In the CIP emulation piers, the majority of inelastic deformation during an earthquake is expected to occur near the ends of the columns, where the seismically

induced moments are largest. Accordingly, the strains are largest at the top and bottom of the columns for the CIP emulation piers.

In the hybrid piers, the majority of inelastic deformation is expected to occur in the interface regions between the column and footing and cap beam. Therefore, the strains are monitored in the interface region for the hybrid piers. If models similar to those presented in Appendix A are used, this corresponds to monitoring the strains at the top and bottom integration points of the beam-column element, representing the column for the CIP emulation pier, and in the zero-length element, representing the interface region for the hybrid pier.

This procedure for estimating the nominal yield displacement by using nonlinear analysis is straightforward but requires the creation of a nonlinear finite-element model of the pier, which can be time consuming. Furthermore, the results depend on the underlying numerical model used. A method for estimating the yield displacement with equations is presented in the following sections.

4.2 PIERS CONSIDERED IN THE CALIBRATION OF EQUATION-BASED METHODS

The equation-based method differs for the CIP emulation and hybrid piers because the responses of the two types of piers during an earthquake are different. The equations were calibrated with results from nonlinear analyses so that the equation-based method would produce results similar to those from the nonlinear analysis method. Consequently, the equation-based yield displacements depend on the model used to represent the piers, the material models considered, and the definition for the location of the yield displacement presented in Section 4.1.

To ensure that the equation-based method is applicable to a wide range of pier characteristics, the equations were calibrated with a large number of piers encompassing the characteristics typically seen in practice. To calibrate the equations, 108 CIP emulation piers were considered consisting of all combinations of the following:

- column diameter (D_c): 36 in., 48 in., and 60 in.
- column aspect ratio (L_c / D_c): 5, 6, and 7
- mild steel reinforcing ratio (ρ_s): 0.005, 0.01, 0.02, and 0.03

- normalized axial dead load ($\frac{P_c}{f_c^{'} A_g}$): 0.05, 0.10, and 0.15

A total of 162 hybrid piers were considered consisting of all combinations of the following:

- column diameter (D_c): 36 in., 48 in., and 60 in.
- column aspect ratio (L_c / D_c): 5, 6, and 7
- mild steel reinforcing ratio (ρ_s): 0.008, 0.012, and 0.016
- post-tensioning reinforcing ratio (ρ_p): 0.0005, 0.0016, and 0.0028
- normalized axial dead load ($\frac{P_c}{f_c^{'} A_g}$): 0.05 and 0.10

Certain equations were calibrated with a slight variation of these sets. In these situations, the alteration to the calibration pier set is discussed.

4.3 EQUATION-BASED METHOD FOR CIP EMULATION PIERS

The deformation of a CIP emulation pier at the nominal yield displacement can be attributed to two main sources: flexural deformation of the columns and strain penetration of the column reinforcing bars extending into the footing and cap beam. All of the mild steel reinforcement in the columns of a CIP emulation pier extends into the footing and cap beam. Because of the continuity of reinforcing bars, the displacement of the pier when the first reinforcing bar yields ($\Delta_y^{'}$) will be the sum of the displacement at first yield due to both the flexural displacement of the column ($\Delta_{y,c}^{'}$) and strain penetration displacement ($\Delta_{y,sp}^{'}$). The strain penetration displacement is defined as the displacement of the column attributable to partial pull-out of the bar from the foundation or cap beam to which it is connected.

$$\Delta_y^{'} = \Delta_{y,c}^{'} + \Delta_{y,sp}^{'} \tag{4.2}$$

If the nominal yield displacement is defined in the same manner as that in the nonlinear analysis method, Equation (4.2) can be combined with Equation (4.1) to determine Δ_y.

$$\Delta_y = \frac{F_{0.004}}{F_y^{'}} (\Delta_{y,c}^{'} + \Delta_{y,sp}^{'}) \tag{4.3}$$

The ratio of the forces on the pier in Equation (4.3) can be related to the ratio of Δ_y to $\Delta_y^{'}$ by using Equation 4.4, which is derived from the geometry of the secant stiffness expressed in Figure 4.1.

$$\frac{F_{0.004}}{F_y^{'}} = \frac{\Delta_y}{\Delta_y^{'}} \tag{4.4}$$

Combining equations (4.3) and (4.4) results in

$$\Delta_y = \frac{\Delta_y}{\Delta_y^{'}}(\Delta_{y,c}^{'} + \Delta_{y,sp}^{'}) \tag{4.5}$$

Expressions for $\Delta_{y,c}^{'}$, $\Delta_{y,sp}^{'}$, and $\Delta_y / \Delta_y^{'}$ were developed separately and are presented in subsequent sections, followed by an examination of the accuracy of the overall method.

4.3.1 Displacement at First Yield Due to Flexural Deformation

The displacement at first yield due to flexural deformation in the columns ($\Delta_{y,c}^{'}$) is shown in Figure 4.2. Because the cap beam was assumed to be rigid in this study, $\Delta_{y,c}^{'}$ is equivalent to the displacement at first yield of a single column with fixed end conditions. The moment distribution along the column, shown in Figure 4.3, can be determined by using statics and symmetry. For columns with large aspect ratios, such as typical bridge columns, under elastic conditions, the moment on the column (M) is related to the curvature (ϕ) by

$$\phi = \frac{M}{EI} \tag{4.6}$$

where EI is the flexural rigidity of the column. Assuming that yielding occurs at the top and bottom of the columns, the total deflection of the column ($\Delta_{y,c}^{'}$) can be found by integrating the curvature along the length of the column twice. For a column with uniform EI, as shown in Figure 4.3,

$$\Delta_{y,c}^{'} = \frac{\phi_y^{'} L_c^2}{6} \tag{4.7}$$

where $\phi_y^{'}$ is the curvature of the column cross-section corresponding to the first reinforcing bar yielding.

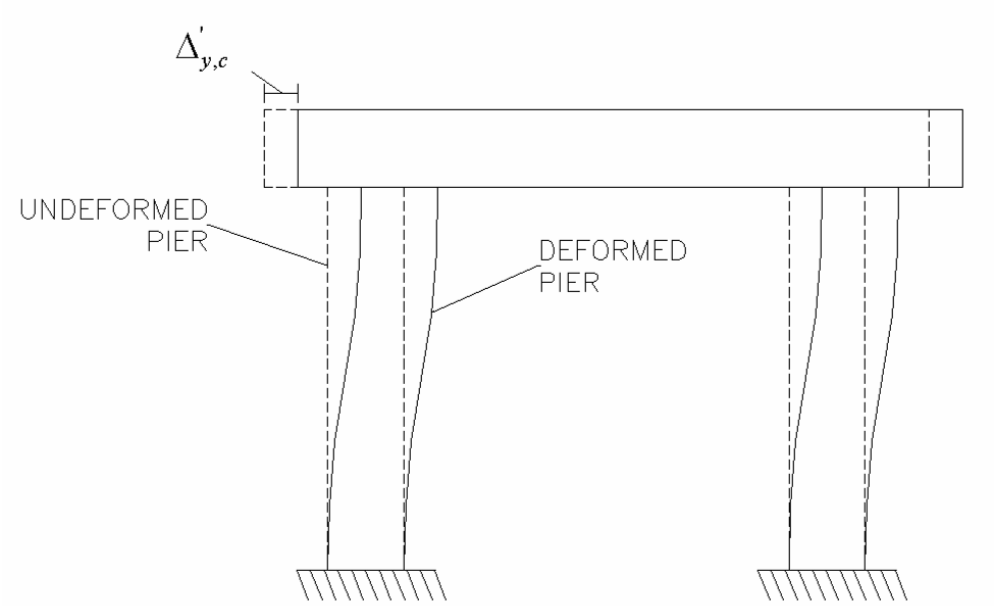

Figure 4.2: Displacement of Pier Due to Flexural Deformation of Columns

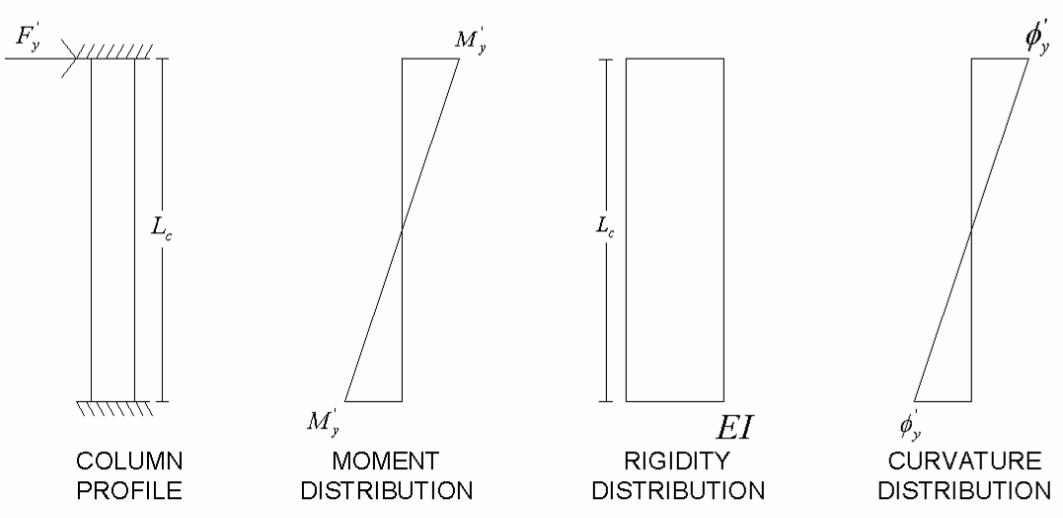

Figure 4.3: Distribution of Moment and Curvature along Column with Uniform Stiffness

In most situations, EI will not be uniform because of cracking at the top and bottom of the column. The cracking will reduce EI and increase the curvature at the ends of the column, as shown in Figure 4.4. The displacement of the column can still be found by integrating the curvature twice along the length of the column. Integrating the curvature distribution shown in Figure 4.4 results in Equation (4.8) for displacement at first yield (Wacker 2005).

$$\Delta'_{y,c} = (\frac{1}{2})\phi_y' L_c^2 \left[\frac{\lambda}{3} + (1-\lambda)(\frac{k^3}{3} - k^2 + k) \right] \tag{4.8}$$

where

$$\lambda = \frac{EI_{cr}}{EI_g} \tag{4.9}$$

$$k = \frac{1}{2}(1 - \frac{M_{cr}}{M_y'}) \tag{4.10}$$

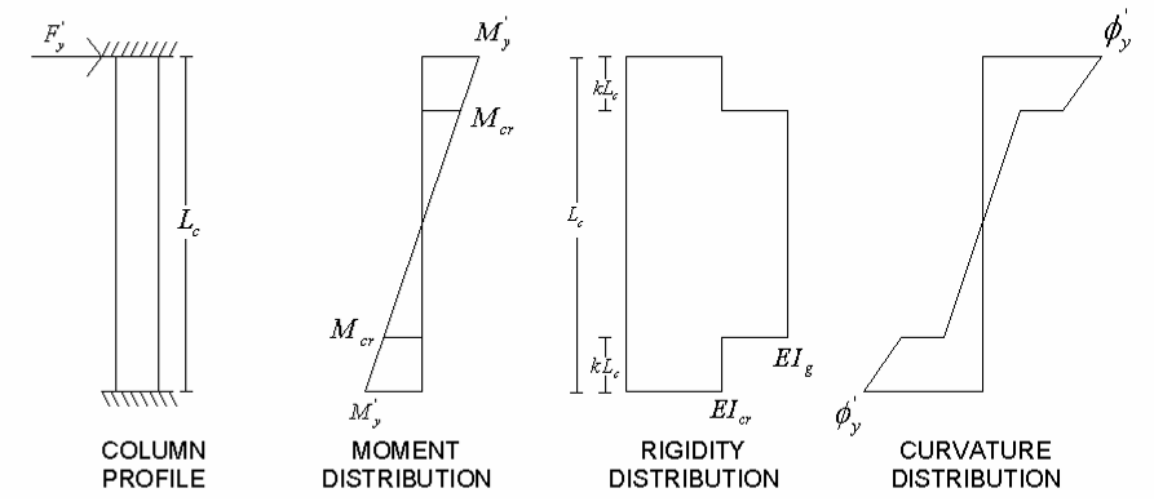

Figure 4.4: Distribution of Moment and Curvature along Column with Non-Uniform Stiffness Due to Cracking

In equations (4.9) and (4.10), EI_g is the flexural rigidity of the uncracked cross-section, EI_{cr} is the flexural rigidity of the cracked cross-section, M_{cr} is the cracking moment of the column, and M'_y is the moment on the column at first yield.

The values of ϕ'_y, λ, and M_{cr}/M'_y can be obtained from moment curvature analysis. As an alternative, approximate expressions for ϕ'_y, λ, and M_{cr}/M'_y have been developed and are presented in this section.

The curvature of a reinforced concrete column at first yield (ϕ'_y) can be determined from the strain distribution across the section. Figure 4.5 depicts the strain distribution across the cross-section of the column at first yield if plane sections are assumed to remain plane as the column deforms. By using small angle approximations

and Equation (4.11), $\phi_y^{'}$ can be related to $\varepsilon_{stl,t}$, which is equal to ε_y, and the distance from the extreme tensile steel to the neutral axis of bending (jD_c).

$$\phi_y^{'} = \frac{\varepsilon_y}{jD_c} \tag{4.11}$$

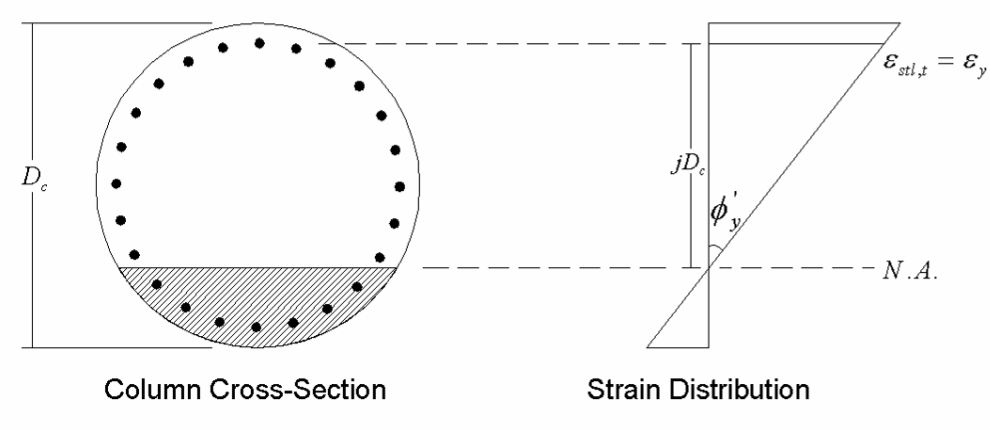

Figure 4.5: Distribution of Strain across Column Cross-Section

The only unknown value in Equation (4.11) is j. An empirical expression for j was determined to match results from nonlinear analyses. Moment curvature analysis, based on the material models presented in Appendix A, was conducted on 36 cross-sections corresponding to all combinations of variables for the CIP emulation piers listed in Section 4.2. The curvature ($\phi_y^{'}$) when $\varepsilon_{stl,t} = \varepsilon_y$ was recorded and used to determine values of j from Equation (4.11).

The values of j determined from the moment-curvature analyses are shown in Figure 4.6. The values of j depend primarily on ρ_s and the normalized axial force in the column. For the CIP emulation piers, the main source of axial load in the columns is the weight of the superstructure, and the normalized axial force is equal to $P_c / f_c^{'} A_g$. The following equation for j, which depends linearly on both ρ_s and $P_c / f_c^{'} A_g$, was fitted to the results of moment-curvature analysis. The coefficients were determined to minimize the sum of the squared difference between the nonlinear analysis results and equation values.

$$j = 0.68 - 2.0\rho_s - 0.80\frac{P_c}{f_c^{'}A_g} \tag{4.12}$$

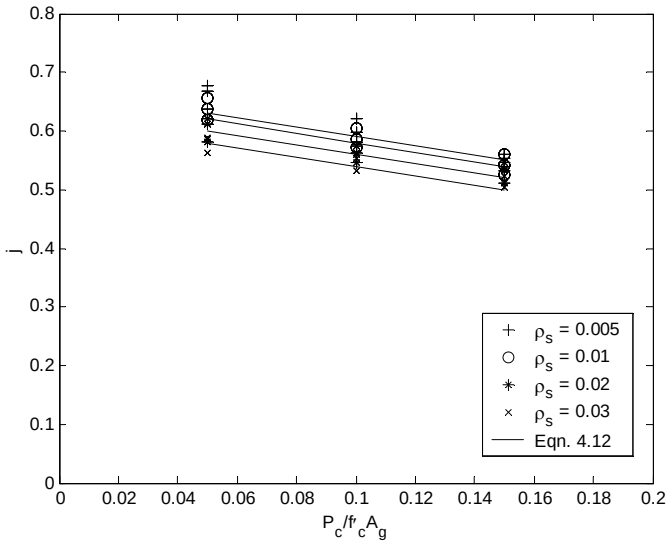

Figure 4.6: Values of j from Moment-Curvature Analyses

The ratio of the cracking moment to the moment at first yield ($M_{cr}/M_y^{'}$) of the pier columns can also be estimated with an empirical equation determined to match the results of nonlinear analyses. Values for $M_{cr}/M_y^{'}$ were determined from the same 36 moment-curvature analyses that were used to develop Equation (4.12). The cracking moment (M_{cr}) was defined to be the moment at which the stress at the extreme tension face of the cross-section reached the concrete tension strength, which was taken as $7.5\sqrt{f_c^{'}}$, where $f_c^{'} = 5ksi$. The yield moment was defined as the moment when $\varepsilon_{stl,t}$ reached ε_y. Figure 4.7 shows that the values for $M_{cr}/M_y^{'}$ also depend on ρ_s and $P_c/f_c^{'}A_g$. The following empirical equation for $M_{cr}/M_y^{'}$ was fit to the results of moment-curvature analyses.

$$\frac{M_{cr}}{M_y^{'}} = 0.46 - 10.0\rho_s + 1.00\frac{P_c}{f_c^{'}A_g} \tag{4.13}$$

This equation would be expected to vary if the concrete strength differs significantly from the assumed value of 5 ksi.

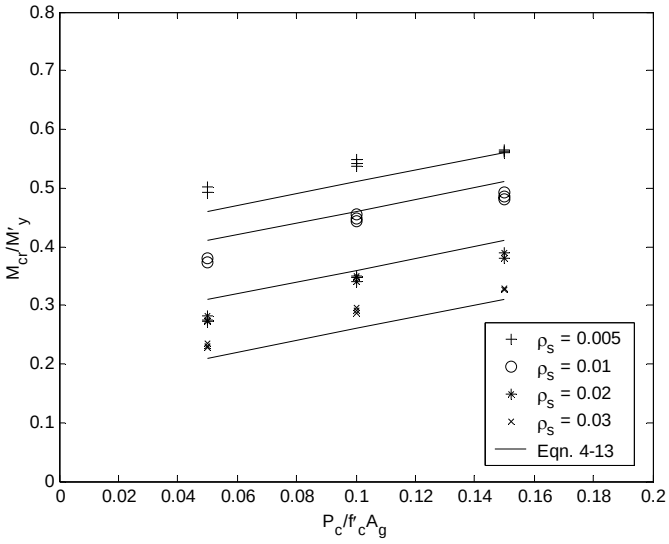

Figure 4.7: Values of $\frac{M_{cr}}{M_y^{'}}$ from Nonlinear Analyses

The ratio of EI_{cr} to EI_g (λ) for the columns was determined in a similar manner. Using the same 36 nonlinear moment curvature analyses EI_g was defined as M_{cr} divided by the corresponding curvature in accordance with Equation (4.6). EI_{cr} was defined as $M_y^{'}$ divided by $\phi_y^{'}$. The values of λ are shown in Figure 4.8. The trends were represented with an empirical equation that depends linearly on ρ_s and $P_c \big/ f_c^{'} A_g$. Fitting the equation to the nonlinear analysis results gave

$$\lambda = 0.33 + 9.0\rho_s - 0.20\frac{P_c}{f_c^{'} A_g} \tag{4.14}$$

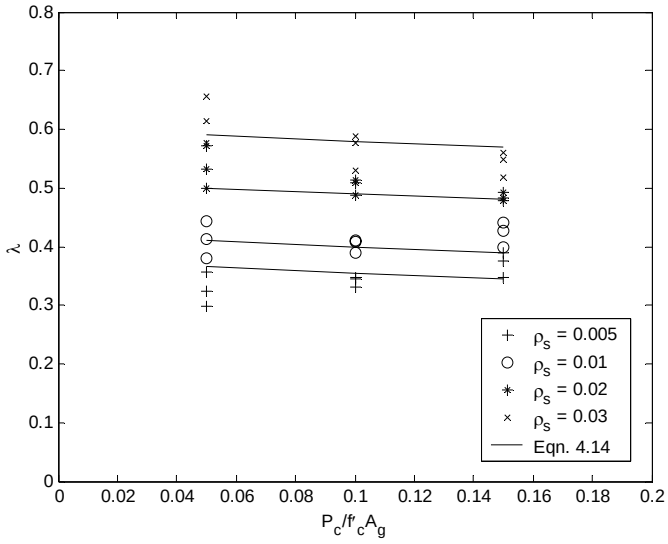

Figure 4.8: Values of λ from Nonlinear Analyses

4.3.2 Displacement of the Pier at First Yield Due to Strain Penetration

Strain penetration of the reinforcing bars into the footing and cap beam increases the flexibility of the pier, resulting in larger displacements at first yield. The increase in displacement can be computed by treating the effects of strain penetration as concentrated rotations at the top and bottom of each column. The pier displacement caused by strain penetration can be estimated by assuming that the columns rotate rigidly, as shown in Figure 4.9. The displacement at first yield due to strain penetration ($\Delta'_{y,sp}$) can be determined from the rotation due to strain penetration at first yield (θ_{sp}) by using Equation (4.15).

$$\Delta'_{y,sp} = \theta_{sp} L_c \tag{4.15}$$

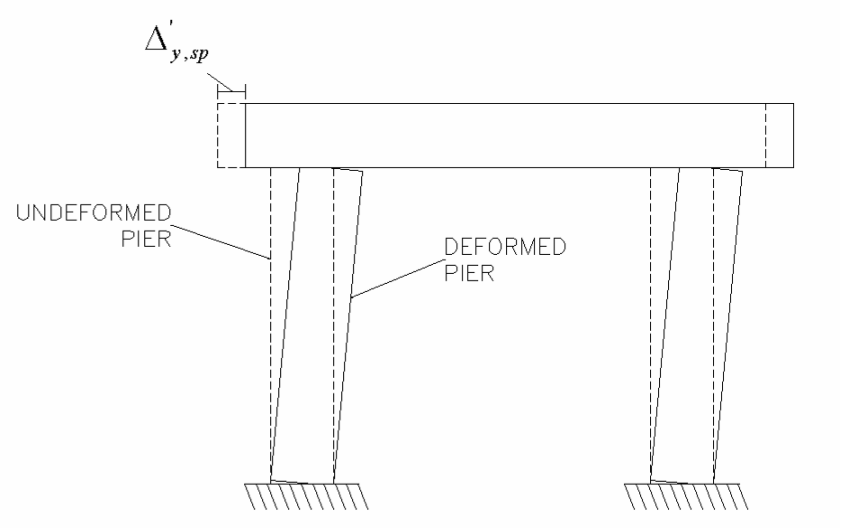

Figure 4.9: Displacement at First Yield Due to Strain Penetration

The rotation due to strain penetration (θ_{sp}) of the column relative to the footing or cap beam at first yield is shown in Figure 4.10. The column is assumed to be fully rigid, as shown. As illustrated in Figure 4.10, θ_{sp} can be determined from the yield elongation in the extreme tensile bar ($\Delta_{y,bar}$) and the distance to the neutral axis (γD_c). By using small angle approximations,

$$\theta_{sp} = \frac{\Delta_{y,bar}}{\gamma D_c} \tag{4.16}$$

The elongation of an embedded reinforcing bar at yield can be estimated by assuming that the bond stress is constant along the bar length until the steel stress drops to zero (Lehman and Moehle 2000). This assumption leads to

$$\Delta_{y,bar} = \frac{1}{8}\frac{f_y{}^2 d_b}{\tau_e E_s} \tag{4.17}$$

In Equation (4.17), f_y is the yield strength of the reinforcing steel, d_b is the diameter of the reinforcing steel bars, and τ_e is the elastic bond strength between the concrete and reinforcing steel, determined from

$$\tau_e = 12\frac{\sqrt{1000 f_c'}}{1000} \tag{4.18}$$

where $f_c^{'}$ and τ_e are in units of ksi (Lehman and Moehle 2002). Combining equations (4.15), (4.16), and (4.17) results in the following expression for $\Delta_{y,sp}^{'}$.

$$\Delta_{y,sp}^{'} = \frac{1}{8}\frac{f_y^{\,2} d_b}{\tau_e E_s}\frac{L_c}{\gamma D_c} \tag{4.19}$$

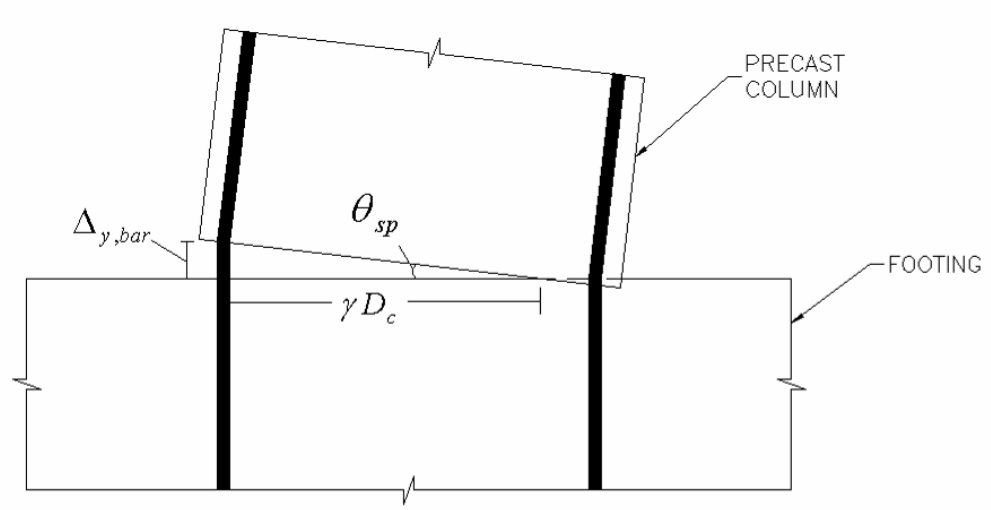

Figure 4.10: Deformation of Column-Footing and Column-Cap Beam Connection Caused by Strain Penetration

The only unknown value in Equation (4.19) is γ. An empirical relationship for γ was determined by using the results of pushover analyses. Pushover analyses of the 108 CIP emulation piers in Section 4.2 were performed, and the rotation of the nonlinear spring representing the effects of strain penetration was recorded when the frame reached the first yield displacement. Values of γ were then determined with Equation ,(4.20) which is derived from equations (4.16) and (4.17).

$$\gamma = \frac{1}{8}\frac{f_y^{\,2} d_b}{\tau_e E_s}\frac{1}{\theta_{sp} D_c} \tag{4.20}$$

The values of γ are shown in Figure 4.11. It can be seen that the values depend primarily on $P_c / f_c^{'} A_g$ and D_c. The following equation was determined for γ to minimize the sum of the squared difference between nonlinear analysis and equation values:

$$\gamma = 0.70 - \frac{3D_c}{1000} - 1.0\frac{P_c}{f_c^{'} A_g} \tag{4.21}$$

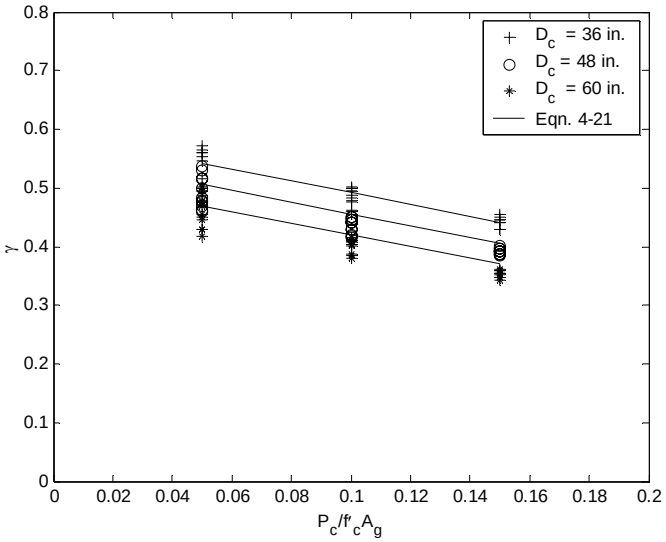

Figure 4.11: Values of γ from Nonlinear Analyses

4.3.3 Ratio of Yield Displacement to Displacement at First Yield

The ratio of the nominal yield displacement to the displacement at first yield ($\Delta_y / \Delta_y^{'}$) was represented by using an empirical equation calibrated to match the results of nonlinear analyses. Pushover analyses of the 108 CIP emulation calibration piers (Section 4.2) were performed, and $\Delta_y^{'}$ was recorded. The nonlinear analysis method presented in Section 4.1 was used to determine Δ_y. The values obtained for $\Delta_y / \Delta_y^{'}$ are shown in Figure 4.12. The values for $\Delta_y / \Delta_y^{'}$ are dependent on both ρ_s and $P_c / f_c^{'} A_g$ and were represented by the following empirical equation fit to the nonlinear analysis results:

$$\frac{\Delta_y}{\Delta_y^{'}} = 1.30 + 5.50\rho_s - 1.25\frac{P_c}{f_c^{'} A_g} \tag{4.22}$$

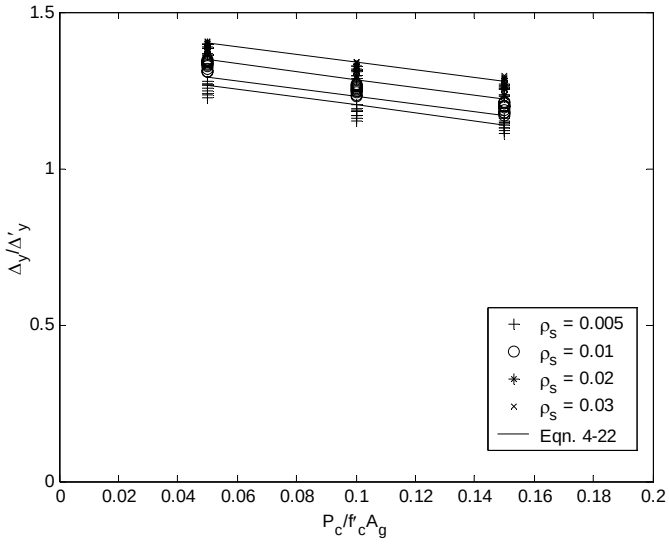

Figure 4.12: Values of $\frac{\Delta_y}{\Delta_y'}$ from Nonlinear Analyses

4.3.4 Accuracy of the Equation-Based Estimates for CIP Emulation Piers

The equations presented in sections 4.3.1, 4.3.2, and 4.3.3 can be used to estimate Δ_y of a CIP emulation pier. The equations are summarized in Figure 4.13. The accuracy of these equations was evaluated by comparing the values they gave for Δ_y with the values of Δ_y determined with the nonlinear analysis method (Section 4.1) for the 108 CIP emulation calibration piers. The ratio of Δ_y from the equation-based method to Δ_y from the nonlinear analysis method (Section 4.1) was computed for each pier and found to have a mean value of 0.96 with a coefficient of variance of 8.4 percent. The distribution of the difference between the estimates is shown in Figure 4.14. Figure 4.14 also shows that for about 75 percent of the piers considered the equation-based method underestimates the yield displacement. However, for over 90 percent of the piers considered, the difference lay between -10 percent and +10 percent of the nonlinear analysis value. This level of accuracy, combined with the time savings provided by eliminating the need for nonlinear analysis, makes use of the equation-based method attractive.

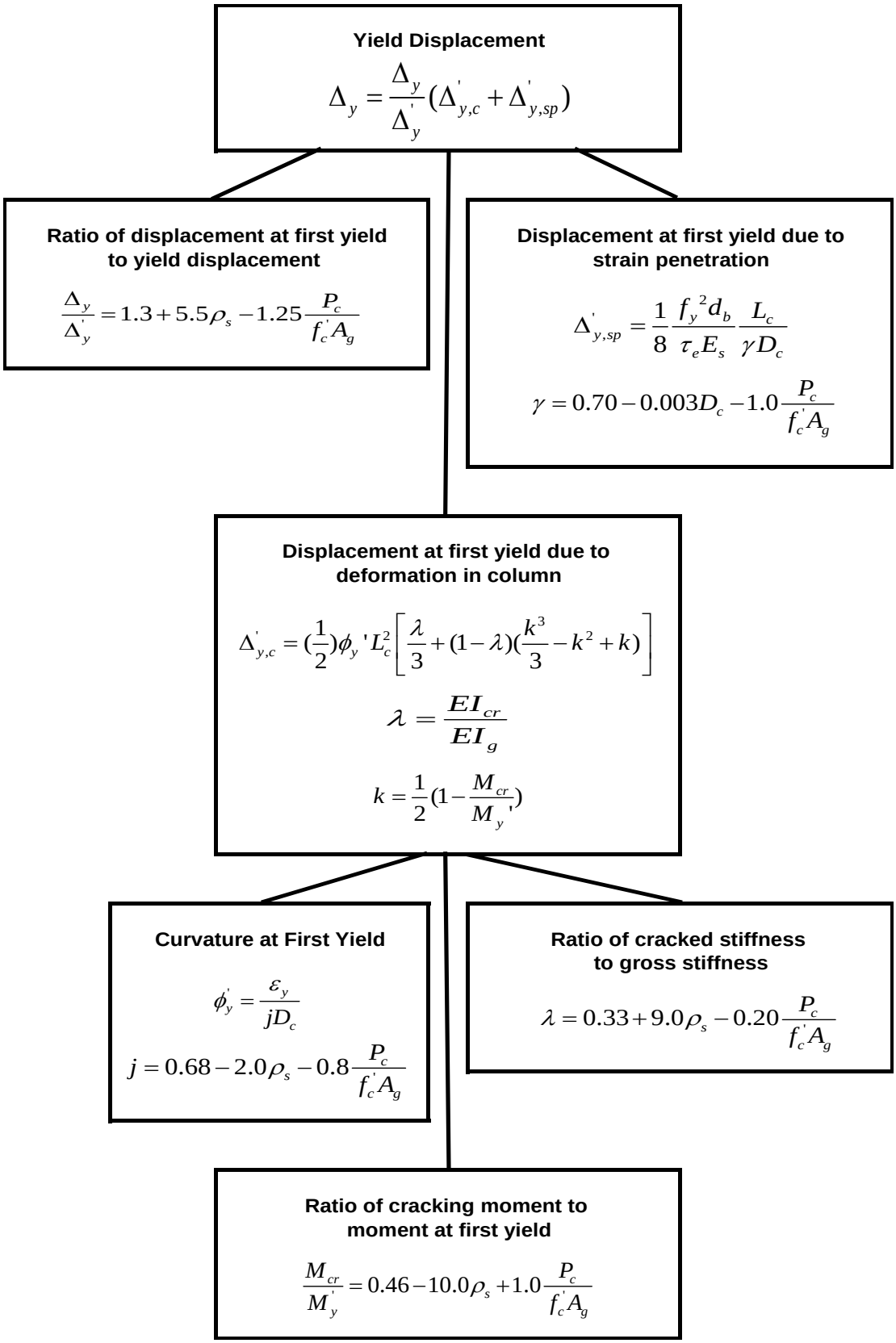

Figure 4.13: Equations for Estimating the Yield Displacement of a CIP Emulation Pier

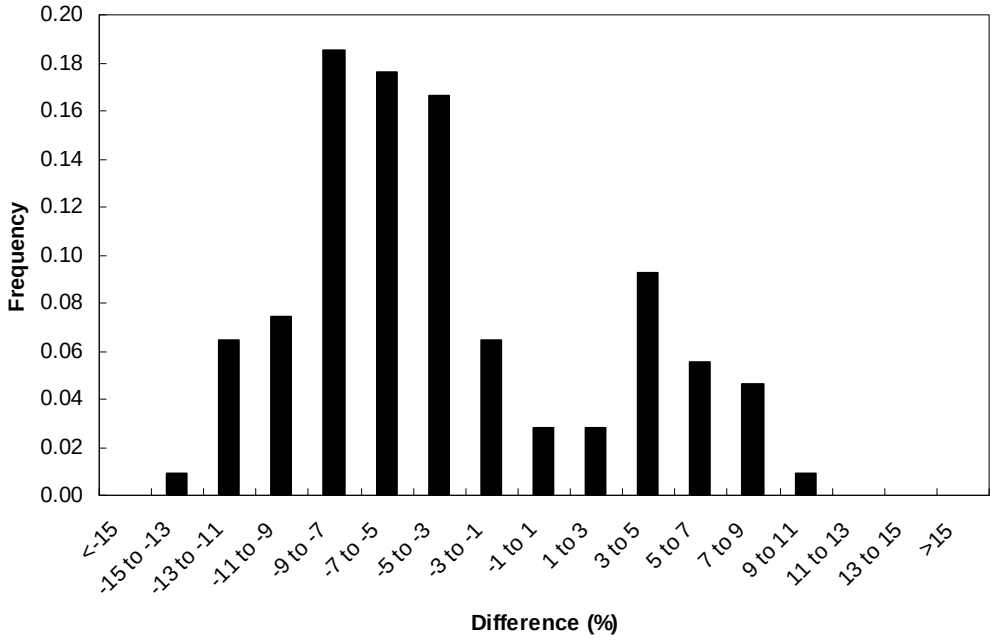

Figure 4.14: Distribution of the Difference of Equation-Based and Nonlinear Analysis Yield Displacement Estimates for CIP Emulation Piers

4.4 EQUATION-BASED METHOD FOR HYBRID PIERS

The yield displacement of a hybrid pier can be estimated by using an approach similar to the one used for the CIP emulation piers. However, there are key differences between the types of piers that must be accounted for. The displacement of a hybrid pier at the yield displacement is attributed to two main sources: flexural deformation of the column and deformation of the interface regions where the columns connect to the footing and cap beam. In a typical hybrid pier, only a portion of the mild steel reinforcement in the column extends across the interface into the footing and cap beam. This causes the columns to have greater moment capacity than the interface regions. Accordingly, when the mild steel reinforcement in the interface reaches ε_y, the reinforcement in the columns will not yield and the column will deform elastically. The displacement of the pier at first yield, is the sum of the displacement at first yield due to deformation of the interface regions ($\Delta'_{y,\text{int}}$) and the displacement due to elastic deformation of the column when the first reinforcing bar in the interface region yields ($\Delta^*_{y,c}$).

$$\Delta_y^{'} = \Delta_{y,\text{int}}^{'} + \Delta_{y,c}^{*} \tag{4.23}$$

The yield displacement can be estimated with Equation (4.24), developed by combining equations (4.1), (4.4), and (4.23).

$$\Delta_y = \frac{\Delta_y}{\Delta_y^{'}}(\Delta_y{}'_{,\text{int}} + \Delta_{y,c}^{*}) \tag{4.24}$$

The development of expressions for $\Delta_{y,\text{int}}^{'}$, $\Delta_{y,c}^{*}$, and $\Delta_y / \Delta_y^{'}$ is discussed in subsequent sections, followed by an examination of the accuracy of the equations.

4.4.1 Displacement at First Yield Due to Deformation of the Interface Regions

The method for computing the deformation of the interface region in hybrid piers is similar to that used for the bar strain penetration in a CIP emulation pier. The columns are assumed to be rigid and to rotate at their ends because of the local deformation. Accordingly,

$$\Delta_{y,\text{int}}^{'} = \theta_{\text{int}} L_c \tag{4.25}$$

where θ_{int} is the rotation due to deformation of the interface region at first yield. Figure 4.15 illustrates the deformation of the interface region. This figure shows that θ_{int} can be related to the elongation of a reinforcing bar at yield ($\Delta_{y,bar}$) and the distance to the neutral axis (ηD_c) by using the following equation.

$$\theta_{\text{int}} = \frac{\Delta_{y,bar}}{\eta D_c} \tag{4.26}$$

Because the reinforcing bars are unbonded in the interface region, $\Delta_{y,bar}$ is given by

$$\Delta_{y,bar} = \frac{f_y}{E_s} L_{unb} \tag{4.27}$$

where L_{unb} is the debonded length of the mild steel reinforcement in the interface region. In this study, L_{unb} was assumed to be equal to one-fourth D_c. Combining equations (4.25), (4.26), and (4.27),

$$\Delta_{y,\text{int}}^{'} = \frac{1}{\eta}\frac{f_y}{E_s} L_{unb} \frac{L_c}{D_c} \tag{4.28}$$

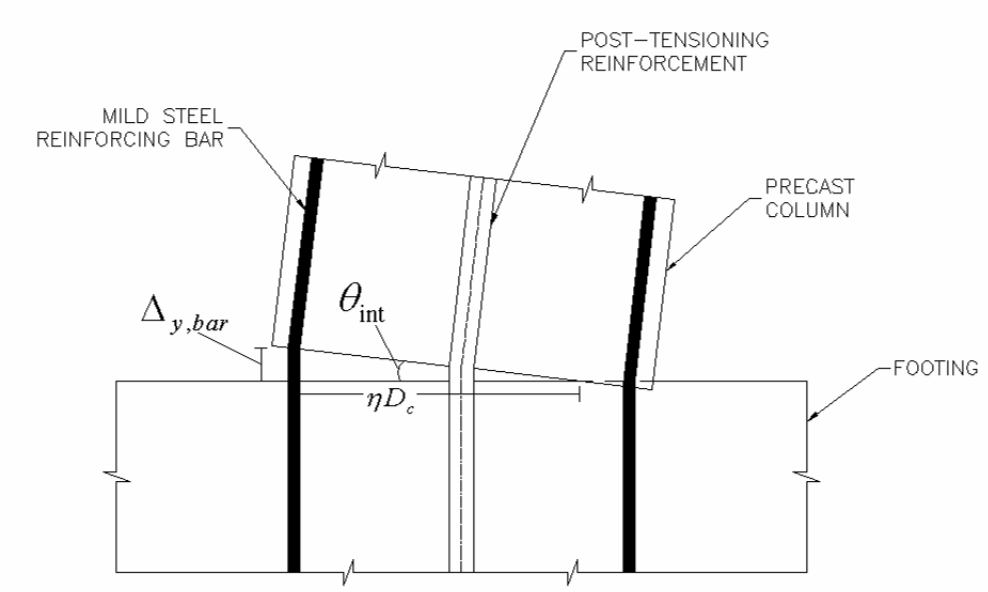

Figure 4.15: Deformation of the Interface Region at First Yield

An empirical equation for η was determined by using the results of nonlinear analyses. Pushover analyses were performed on the 162 hybrid calibration piers presented in Section 4.2, and the rotation of the interface region when the first reinforcing bar reached ε_y was recorded. These values represented θ_{int} and were used to determine values of η with Equation (4.29).

$$\eta = \frac{f_y}{E_s} L_{unb} \frac{L_c}{\Delta_{y,\text{int}}^{'} D_c} \tag{4.29}$$

The values obtained for η from the nonlinear analyses are shown in Figure 4.16. The values of η depend on ρ_s and the normalized axial load in the column. For the hybrid piers, the contributions of both the weight of the superstructure and the initial vertical prestress should be considered when the normalized axial load is determined. Accordingly, the normalized axial load is equal to $\frac{P_c}{f_c^{'} A_g} + \rho_p \frac{f_{p0}}{f_c^{'}}$, where f_{p0} is the stress in the post-tensioning tendons of the undeformed pier. The following equation was determined for η to best fit the results from the nonlinear analyses:

$$\eta = 0.57 - 1.50\rho_s - 0.80\left(\frac{P_c}{f_c^{'} A_g} + \rho_p \frac{f_{p0}}{f_c^{'}}\right) \tag{4.30}$$

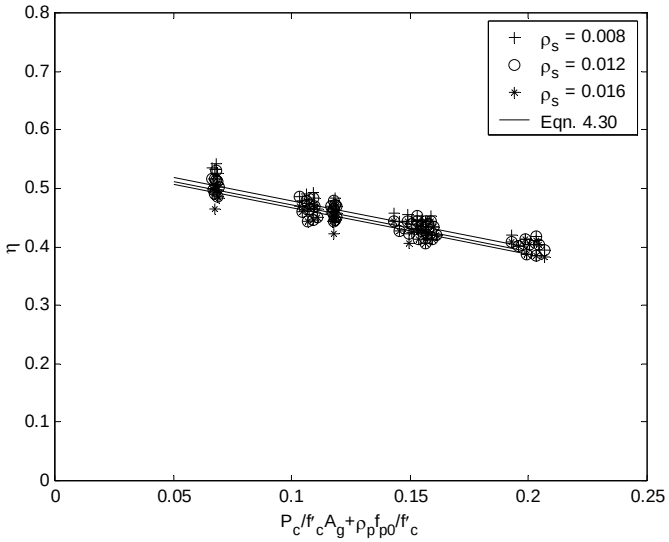

Figure 4.16: Values of η from Nonlinear Analyses

4.4.2 Displacement at First Yield due to Elastic Deformation of the Columns

The elastic flexural displacement of the column ($\Delta^*_{y,c}$) can be calculated with the following equation:

$$\Delta^*_{y,c} = \frac{L_c^3}{12 n_c EI_{eff}} F_y^{'} \tag{4.31}$$

In Equation (4.31), EI_{eff} is the flexural rigidity of the effective column cross-section, which is used to account for cracking in the column. An empirical equation for EI_{eff} was determined to match the results of nonlinear analyses. A more in-depth analysis considering the progression of cracking in the column could be used; however, the cracking behavior of hybrid columns is not well understood, making this an unattractive solution. Pushover analyses of the 162 hybrid calibration piers were performed, and $\Delta_y^{'}$, $F_y^{'}$, and θ_{int} were recorded. Values of $\Delta^*_{y,c}$ were determined by making the interface regions at the ends of the column rigid and performing a pushover analysis to find the displacement that corresponded to $F_y^{'}$. Values of EI_{eff} were then determined by inverting Equation (4.31). These values were normalized by dividing by the flexural rigidity of the

uncracked section (EI_g). For simplicity, the effect of the reinforcing steel on the flexural rigidity of the uncracked section was ignored.

$$EI_g = E_c I_g \tag{4.32}$$

Values of $\frac{EI_{eff}}{EI_g}$ are plotted in Figure 4.17. The following empirical equation was developed to best fit the data:

$$\frac{EI_{eff}}{EI_g} = 0.32 + 14.0\rho_s + 1.50\left(\frac{P_c}{f_c^{'} A_g} + \rho_p \frac{f_{p0}}{f_c^{'}}\right) \tag{4.33}$$

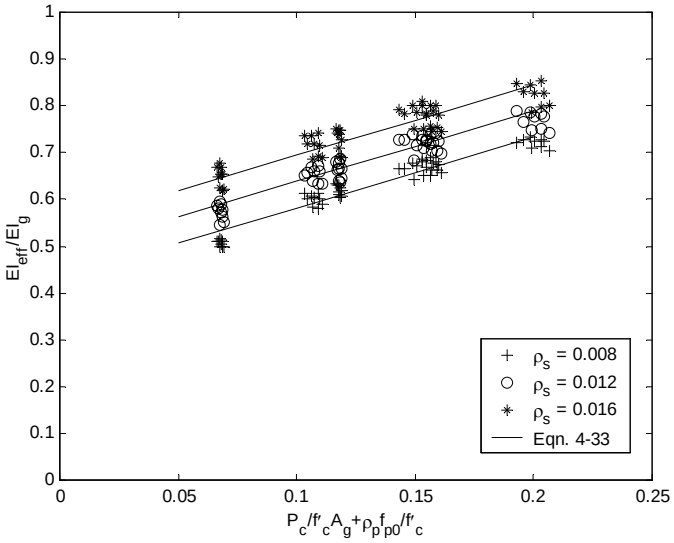

Figure 4.17: Values of $\frac{EI_{eff}}{EI_g}$ from Nonlinear Analyses

The force on the pier at first yield ($F_y^{'}$) was determined from the moment capacity of the interface region when the first mild steel reinforcing bar yields ($M_y^{'}$). The forces on the interface region due to the mild steel reinforcement, post-tensioning steel, gravity load, and compression in the concrete are shown in Figure 4.18. The distribution of the mild steel reinforcement throughout the circular cross-section requires that the contribution of each bar to the moment capacity of the interface region be considered separately. This was simplified by assuming that a portion of the total mild steel reinforcement (αA_s) is located at the extreme tension bar and assumed to yield. The

value of α is determined so that this configuration results in an equivalent moment to the actual distribution of reinforcement. Applying moment equilibrium to the forces on the interface shown in Figure 4.18 results in the following equation for $M_y^{'}$:

$$M_y^{'} = \alpha A_s f_y(\varphi D_c) + A_p f_{p0}(\varphi D_c - \frac{D_c}{2}) + P_c(\varphi D_c - \frac{D_c}{2}) \tag{4.34}$$

where A_s is the area of mild steel reinforcement, A_p is the area of post-tensioning reinforcement, and φD_c is the distance from the result compressive force in the concrete to the extreme reinforcing bar at first yield in the interface region. Simplifying this equation,

$$M_y^{'} = \left[\alpha\varphi\frac{\pi f_y}{4}\rho_s + (\varphi - \frac{1}{2})\frac{\pi f_c^{'}}{4}(\frac{P_c}{f_c^{'}A_g} + \rho_p\frac{f_{p0}}{f_c^{'}})\right]D_c^{\,3} \tag{4.35}$$

Equation (4.36) can be used to relate $M_y^{'}$ and $F_y^{'}$:

$$F_y^{'} = \frac{2n_c M_y^{'}}{L_c} \tag{4.36}$$

Combining equations (4.35) and (4.36),

$$F_y^{'} = \left[\alpha\varphi\frac{\pi f_y}{4}\rho_s + (\varphi - \frac{1}{2})\frac{\pi f_c^{'}}{4}(\frac{P_c}{f_c^{'}A_g} + \rho_p\frac{f_{p0}}{f_c^{'}})\right]\frac{2n_c D_c^{\,3}}{L_c} \tag{4.37}$$

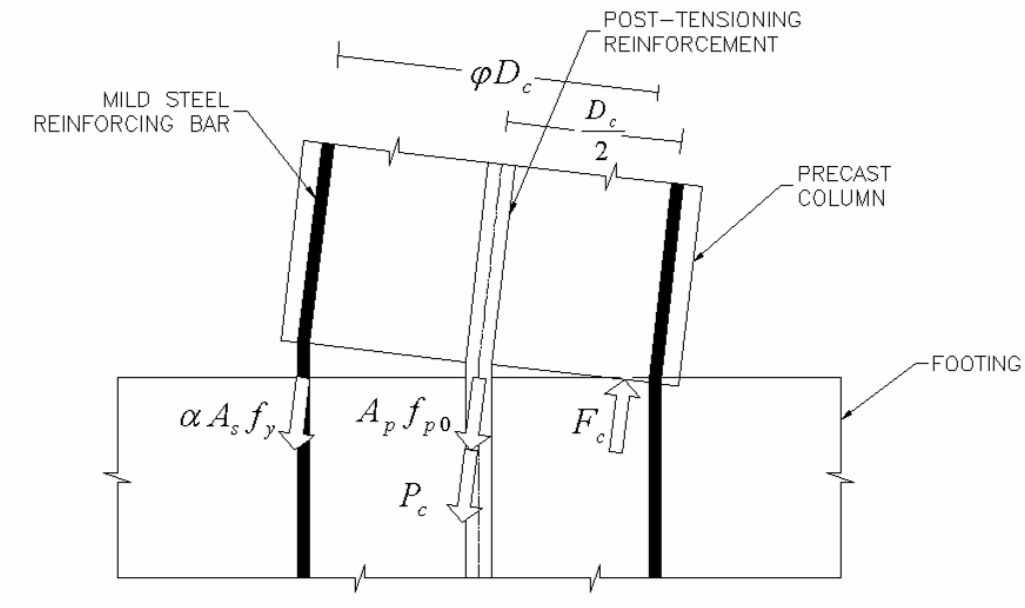

Figure 4.18: Forces Acting on the Interface Region at First Yield

Values for α and φ were determined so that Equation (4.37) would accurately reproduce the results of nonlinear analyses. Pushover analyses were performed on the 162 hybrid calibration piers, and $F_y^{'}$ was determined. The values of α and φ determined so that Equation (4.37) would accurately predict $F_y^{'}$ were 0.33 and 0.76, respectively. The ratio of $F_y^{'}$ determined with Equation (4.37) to $F_y^{'}$ determined from nonlinear analyses was computed and had a mean of 0.99 with a COV of 3.3 percent.

4.4.3 Ratio of Yield Displacement to Displacement at First Yield

The ratio of nominal yield displacement to displacement at first yield ($\Delta_y / \Delta_y^{'}$) was determined by using the same method as that for the CIP emulation piers, except that the 162 hybrid calibration piers were considered. The following equation for $\Delta_y / \Delta_y^{'}$ was determined to best fit the nonlinear analysis results, which are shown in Figure 4.19.

$$\frac{\Delta_y}{\Delta_y^{'}} = 1.42 + 5.00\rho_s - 0.60\left(\frac{P_c}{f_c^{'} A_g} + \rho_p \frac{f_{p0}}{f_c^{'}}\right) \tag{4.38}$$

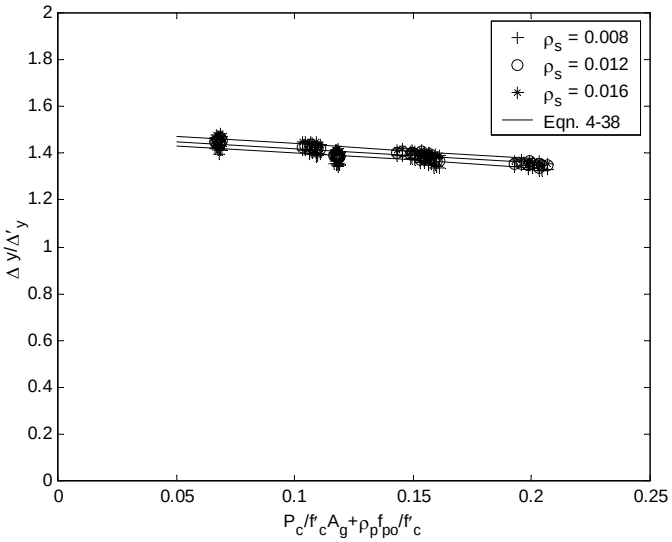

Figure 4.19: Values of $\frac{\Delta_y}{\Delta_y^{'}}$ for Hybrid Piers from Nonlinear Analyses

4.4.4 Accuracy of the Equation-Based Estimates for Hybrid Piers

The yield displacement of a hybrid pier can be estimated by using the equations presented in this section. Figure 4.20 provides a summary of the equations. The accuracy of the equation-based method for estimating the yield displacement of a hybrid pier was determined by comparing the estimates from the equations with estimates from the nonlinear analysis method for the 162 hybrid calibration piers. The ratio of Δ_y determined with the equation-based method to Δ_y determined with the nonlinear analysis method (Section 4.1) was computed for each pier and had a mean of 1.00 with a coefficient of variance of 3.4 percent. The distribution of differences of the equation-based values to the nonlinear analysis values for the calibration piers is shown in Figure 4.21. Over 93 percent of the piers considered had a difference of between -6 percent and +6 percent, verifying that the equation-based method accurately estimates Δ_y for hybrid piers.

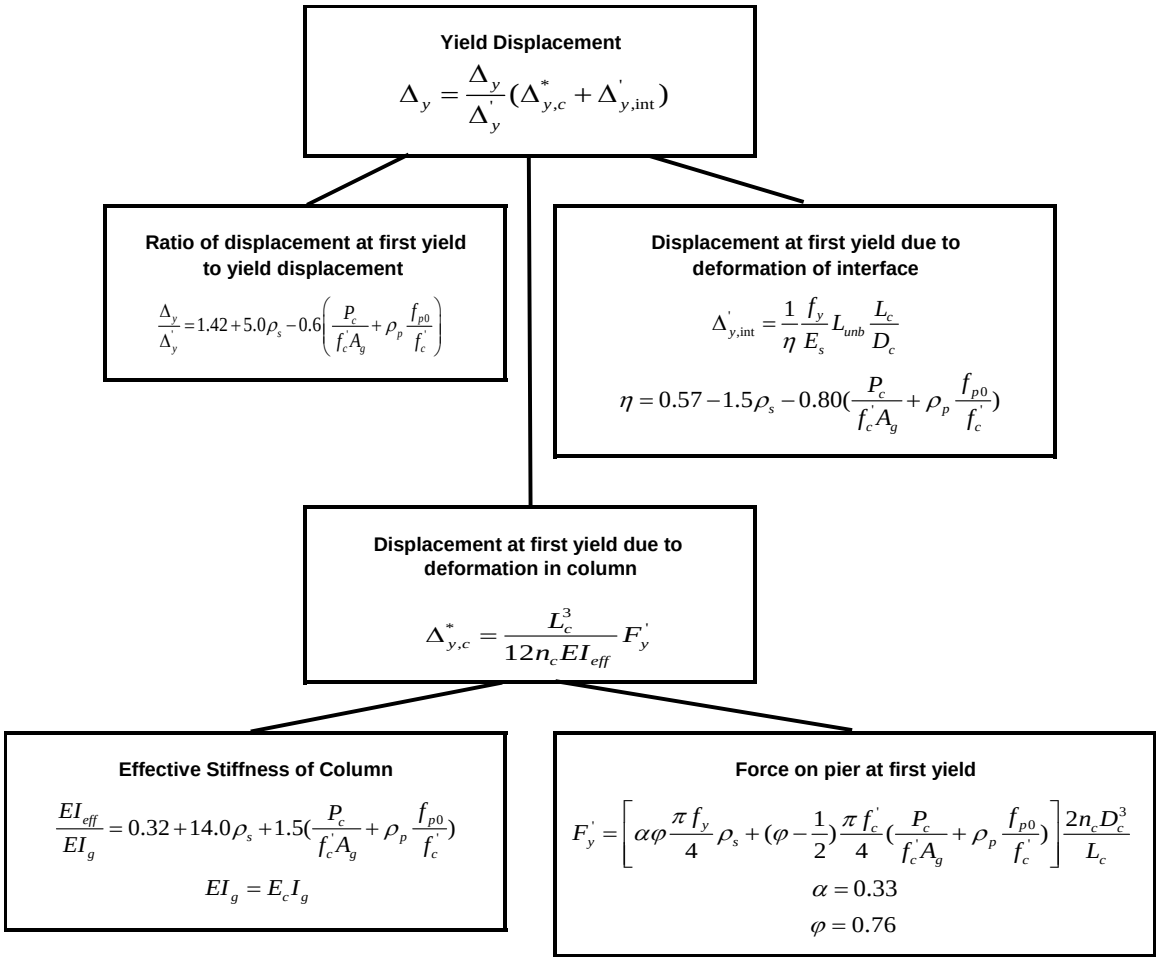

Figure 4.20: Summary of Equations for Estimating the Yield Displacement of a Hybrid Pier

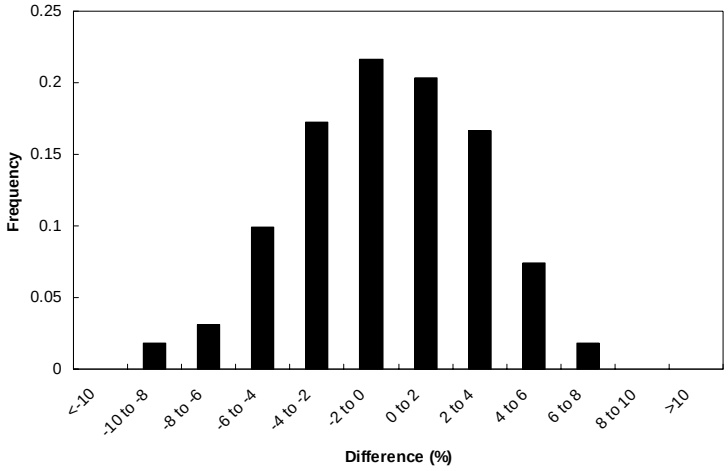

Figure 4.21: Difference of Equation-Based and Nonlinear Analysis Yield Displacement Estimates for Hybrid Piers

CHAPTER 5
METHODS FOR ESTIMATING EQUIVALENT VISCOUS DAMPING

To implement the direct displacement-based design (DDBD) procedures presented in Chapter 3, it was necessary to estimate the viscous damping of the equivalent linear system. The viscous damping is expressed as a fraction of the critical value and is commonly referred to as the equivalent viscous damping (ξ_{eq}). An estimate of ξ_{eq} can be determined by equating the amount of energy dissipated by the nonlinear, hysteretic response of the pier and the equivalent linear system. This relationship is complicated because of the complex post-yield behavior of the piers and the highly variable dynamic deformation history of a pier during an earthquake. The deformation history of the pier is important because, for any non-periodic history, the energy dissipated per cycle is not constant, and consequently, ξ_{eq} varies with time. Several methods for estimating ξ_{eq} are included in this chapter.

The first section of this chapter presents a theoretical derivation of the relationship between ξ_{eq} and the energy dissipated by an inelastic pier. The second section presents a method for estimating ξ_{eq} with nonlinear analysis that can be used for both CIP emulation and hybrid piers. An equation-based method for estimating ξ_{eq} is presented in the third section. The equation-based method was calibrated so that the equations and nonlinear analysis would predict similar values. The equation-based method can be applied to both CIP emulation and hybrid piers. The final section of this chapter presents empirical equations for estimating ξ_{eq}. The empirical equations are simple and do not require that the amount of reinforcement in the pier be known, but these empirical equations produce less accurate estimates for ξ_{eq} than the nonlinear analysis and equation-based methods.

In the development that follows, the only energy dissipation considered is that associated with the nonlinear behavior of the structural system. Radiation damping is ignored because it depends on soil conditions, which vary from site to site and were not

considered in this study. Viscous damping is neglected, because it is not expected to be significant in a bridge pier without any non-structural elements. Therefore, at any given site, the total energy dissipation will be greater than the value obtained with the methods described here, and the peak displacement will be smaller. Accordingly, the method is conservative.

5.1 THEORETICAL BACKGROUND FOR EQUIVALENT VISCOUS DAMPING

The equivalent viscous damping (ξ_{eq}) can be determined so that it represents the energy dissipated by a structure during an earthquake (Gulkan and Sozen 1974; Chopra 2001). The primary source of damping in a pier is dissipation of energy from plastic deformation of the reinforcing steel and concrete. One method commonly used to determine ξ_{eq} is to equate the amount of energy dissipated by the pier and by the equivalent linear system for equivalent displacement cycles. In this research, ξ_{eq} was determined for a displacement cycle equal to the maximum displacement (Δ_{max}) expected in a design-level earthquake, which in the DDBD procedure is equal to the target displacement (Δ_t).

The amount of energy dissipated by the equivalent linear system can be determined by using structural dynamics. If the cap beam of the pier is assumed to be rigid and the foundations fixed, the pier behaves as a single-degree-of-freedom (SDOF) oscillator. Accordingly, the equivalent linear system used to represent the pier is also an SDOF oscillator. The forces on the equivalent linear system during seismic excitation are shown in Figure 5.1 and result in Equation (5.1),

$$m_p \ddot{u}(t) + c_{eq} \dot{u}(t) + K_{eq} u(t) = -m_p a_g(t) \tag{5.1}$$

where m_p is the mass on the pier, K_{eq} is the stiffness of the equivalent linear system, c_{eq} is the equivalent viscous damping coefficient, and $a_g(t)$ is the acceleration of the ground with respect to time. In Equation (5.1), $u(t)$, $\dot{u}(t)$, and $\ddot{u}(t)$ are respectively the relative displacement, relative velocity, and relative acceleration response of the equivalent linear system with respect to the ground as varied with time.

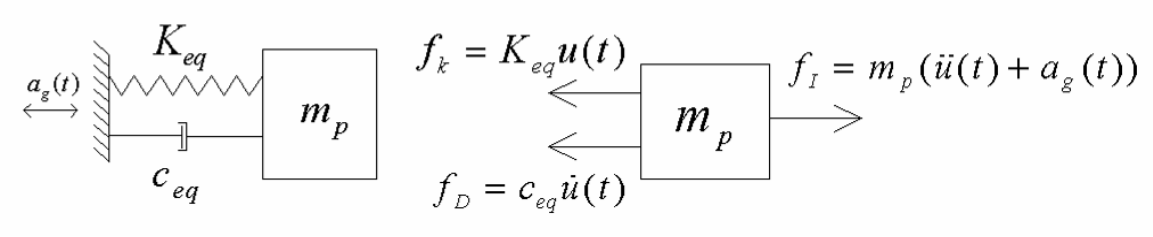

Figure 5.1: Force Action on Equivalent Linear System during Seismic Excitation

The energy dissipated by the equivalent linear system (E_{eq}) can be determined by integrating the work performed by the damping force (f_D) over a complete displacement cycle.

$$E_{eq} = \oint f_D du \tag{5.2}$$

The damping force can be determined from the properties of the linear system as follows:

$$f_D = c_{eq}\dot{u}(t) = \frac{2K_{eq}\xi_{eq}}{\omega_n}\dot{u}(t) \tag{5.3}$$

where ω_n is the natural frequency of vibration of the equivalent linear system. Introducing this expression into Equation (5.2) and expressing the integral in terms of time results in

$$E_{eq} = \frac{2K_{eq}\xi_{eq}}{\omega_n}\int_0^{2\pi/\omega_n} \dot{u}(t)^2\, dt \tag{5.4}$$

This formulation is complex because $\dot{u}(t)$ is influenced by the inertial force acting on the system as a result of the ground acceleration ($a_g(t)$). Because $a_g(t)$ is unique for each ground motion acceleration record, $\dot{u}(t)$ can only be determined numerically and is only applicable for that particular ground motion. To develop a more general and simplified solution, $a_g(t)$ is assumed to be sinusoidal with a forcing frequency equal to the natural frequency (ω_n) of the pier and a peak value of a_o:

$$a_g(t) = a_o \sin(\omega_n t) \tag{5.5}$$

The steady state displacement ($u(t)$) and velocity ($\dot{u}(t)$) responses of the equivalent linear system are

$$u(t) = \Delta_t \sin(\omega_n t - \frac{\pi}{2}) \tag{5.6}$$

$$\dot{u}(t) = \Delta_t \omega_n \cos(\omega_n t - \frac{\pi}{2}) \tag{5.7}$$

Substituting Equation (5.7) into Equation (5.4) and integrating results in the following:

$$E_{eq} = 2\pi \xi_{eq} K_{eq} \Delta_t^2 \tag{5.8}$$

The energy dissipated by the equivalent linear system can be equated to the hysteretic energy dissipated by the pier (E_{hyst}), resulting in the following expression for ξ_{eq} :

$$\xi_{eq} = \frac{E_{hyst}}{2\pi F_t \Delta_t} \tag{5.9}$$

where F_t is the lateral force on the pier at Δ_t . The hysteretic energy dissipated by the pier (E_{hyst}) can be determined to be the plastic work done by the pier. The response of both the pier and equivalent linear systems are shown in Figure 5.2. The area entrapped by the load-deflection curve of the pier (A_{loop}) is the plastic work done by the pier during a displacement cycle and is equal to E_{hyst} :

$$A_{loop} = E_{hyst} \tag{5.10}$$

The area of the rectangle connecting the points of maximum response (A_{rect}) can be expressed as

$$A_{rect} = 4F_t \Delta_t \tag{5.11}$$

Combining equations (5.9), (5.10), and (5.11) results in a final expression for ξ_{eq} :

$$\xi_{eq} = \frac{2}{\pi} \frac{A_{loop}}{A_{rect}} \tag{5.12}$$

Equation (5.12) shows that ξ_{eq} can be calculated directly from the nonlinear load-deflection response of the pier when it is subjected to a complete displacement cycle to $\pm\Delta_t$.

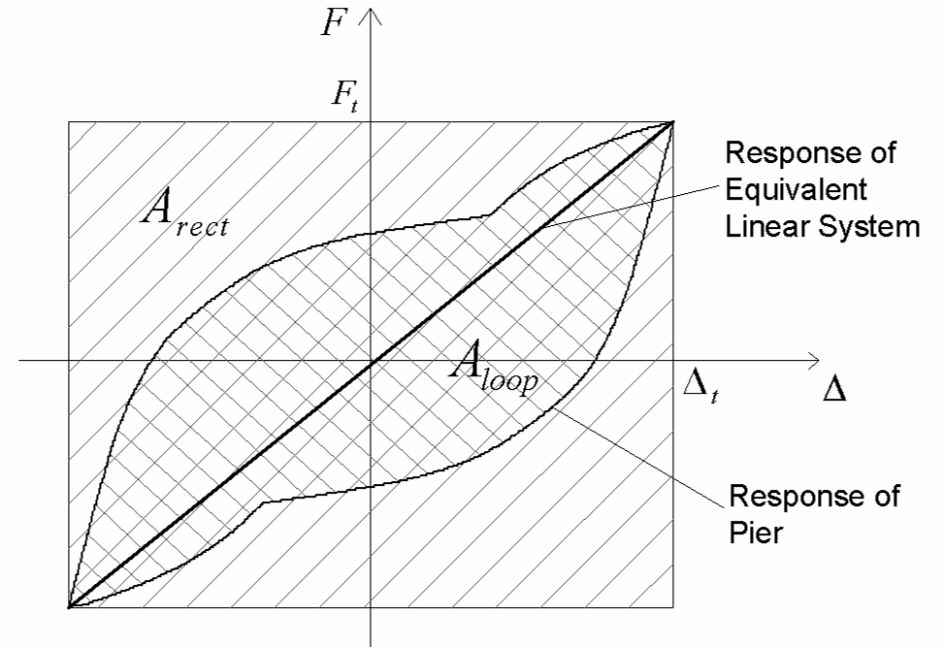

Figure 5.2: Force-Displacement Relationship of Pier and Equivalent Linear System

The derivation for ξ_{eq} assumed that the ground acceleration was sinusoidal with a driving frequency equal to the natural frequency of the equivalent system. The actual ground acceleration during an earthquake will be much less uniform. The difference between the assumed sinusoidal ground acceleration used in this derivation and actual earthquake ground acceleration records introduces error in the equivalent viscous damping estimates.

For structures with a well-defined load-displacement relationship, such as that of a linear elastic-perfectly plastic oscillator (shown in Figure 5.3), determining ξ_{eq} is straightforward. Calculating the amount of area enclosed by the curve and applying Equation (5.12) yields

$$\xi_{eq} = \frac{2}{\pi}\left(1 - \frac{1}{\mu_\Delta}\right) \tag{5.13}$$

where μ_Δ is the displacement ductility. The load-displacement behavior of the precast pier systems, however, is much more complex and affected by characteristics of the pier. Methods for estimating ξ_{eq} have been developed and are presented in the following sections.

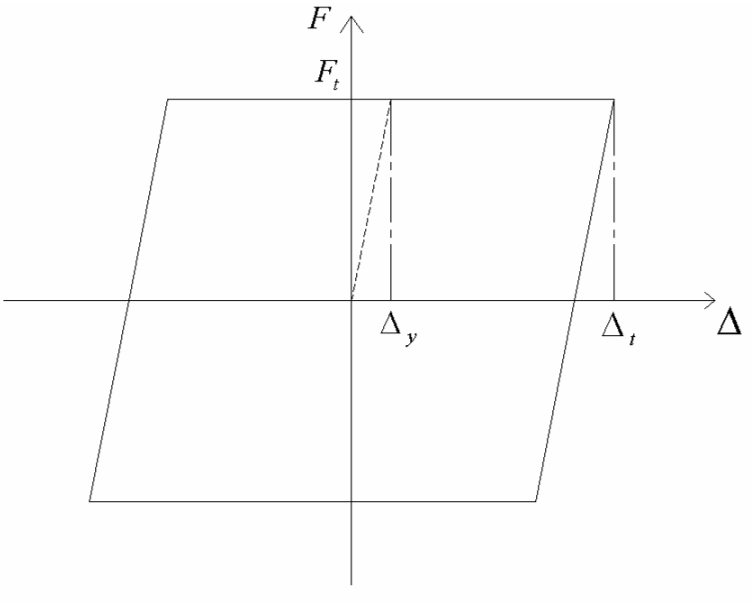

Figure 5.3: Load-Deflection Behavior of a Linear Elastic-Perfectly Plastic Oscillator

5.2 NONLINEAR ANALYSIS METHOD

The nonlinear analysis method for estimating ξ_{eq} consists of performing a push-pull analysis, as described in Appendix A, to the target displacement (Δ_t) specified in the DDBD procedure. Numerical integration is used to determine A_{loop} from the load-displacement relationship. The force at the target displacement (F_t) and Δ_t are used to calculate A_{rect} according to Equation (5.11). Equation (5.12) is then used to estimate ξ_{eq}. The procedure is identical for CIP emulation and hybrid piers. Although the procedure is straightforward conceptually, it requires nonlinear analysis of the pier, which can be time consuming.

5.3 EQUATION-BASED METHOD

An equation-based method for estimating ξ_{eq} is presented in this section.

5.3.1 Shapes of Typical Hysteretic Loops

In order to estimate ξ_{eq} with Equation (5.12), equations must be developed to represent the load-deflection relationship of the precast pier systems so that A_{loop} and A_{rect} can be calculated. This is difficult because the load-deflection behavior changes

significantly depending on the amount of mild steel reinforcement in the pier (ρ_s), the amount of normalized axial force in the pier columns due to the weight of the superstructure ($P_c / f_c' A_g$), and the presence of vertical post-tensioning in the hybrid piers. Figure 5.4 shows load-displacement relationships for the CIP emulation piers with various combinations of ρ_s and $P_c / f_c' A_g$ for a typical hybrid pier.

Several conclusions can be drawn from the plots in Figure 5.4. First, the behavior of the CIP emulation pier with high ρ_s and low $P_c / f_c' A_g$ differs significantly from that of the CIP emulation pier with low ρ_s and high $P_c / f_c' A_g$. Whereas the load-deflection relationship of the CIP emulation pier with large ρ_s is rather broad in shape, the relationship of the pier with high $P_c / f_c' A_g$ is slender because of the re-centering force caused by the weight. The broad load-deflection relationship is expected to exhibit greater ξ_{eq} than the slender relationship. It can also be seen from these plots that the load-deflection relationship of the hybrid pier is similar to that of a CIP emulation pier with high $P_c / f_c' A_g$.

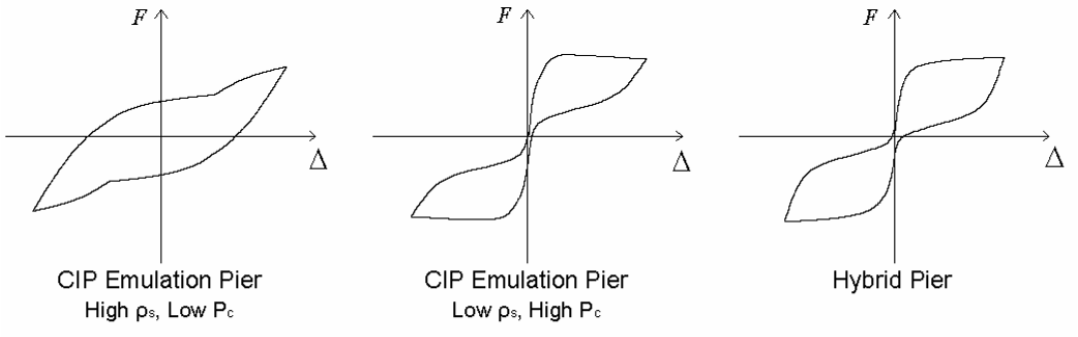

Figure 5.4: Load-Deflection Relationship for Select Precast Piers

Consequently, the shape of the load-deflection relationship of the precast piers depends mainly on two key parameters: ρ_s and the normalized axial load in the columns. The normalized axial load in the columns is $P_c / f_c' A_g$ for CIP emulation piers and $\frac{P_c}{f_c' A_g} + \rho_p \frac{f_{p0}}{f_c'}$ for hybrid piers because of additional axial load on the columns from the

vertical prestressing. This is a simplification because the axial force in the column changes as the pier displaces as a result of increases in the tendon force from tendon elongation. For small amounts of displacement (drifts of less than 2 percent) this effect is minimal. The effects of ρ_s and the normalized axial load on the hysteretic behavior of a pier are determined separately. They can then be combined to form an expression for determining ξ_{eq} of a pier with any arbitrary combination of the two.

The load-displacement relationship of a typical pier with mild steel reinforcement alone (no axial load or post-tensioning) is shown in Figure 5.5. Although ρ_s directly affects the magnitude of the force, its influence on the general shape of the curve is small. If the shape does not change, then the ratio of A_{loop} to A_{rect} is relatively constant, and ξ_{eq}, calculated with Equation (5.12), is relatively insensitive to ρ_s.

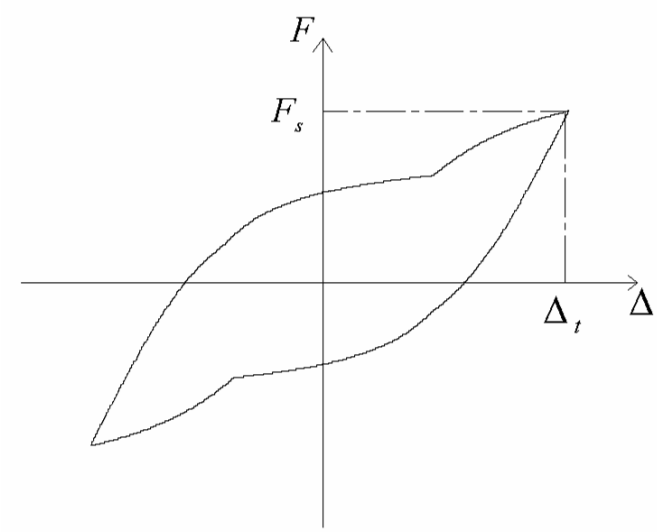

Figure 5.5: Load-Displacement Relationship of Pier with Mild Steel Reinforcement Alone

The load-deflection relationship developed by Takeda et al. (1970), shown in Figure 5.6, was used to represent the response of piers with mild steel reinforcement alone. This relationship was chosen over the linear elastic-perfectly plastic relationship, shown in Figure 5.3, because it better represents the shape of the nonlinear analysis results. The reason the linear elastic-perfectly plastic model does not fit the behavior well is that the reinforcing bars near the neutral axis of the column do not yield. The unloading

slope of the Takeda relationship was chosen to be dependent on $\sqrt{\mu_\Delta}$, following the precedent set by previous researchers for reinforced concrete structures (Gulkan and Sozen 1974; Kowalsky et al. 1995). Through geometric consideration of the load-displacement response, shown in Figure 5.6, it can be determined that

$$\frac{A_{loop}}{A_{rect}} = \frac{1}{2}\left(1 - \frac{1}{\sqrt{\mu_\Delta}}\right) \tag{5.14}$$

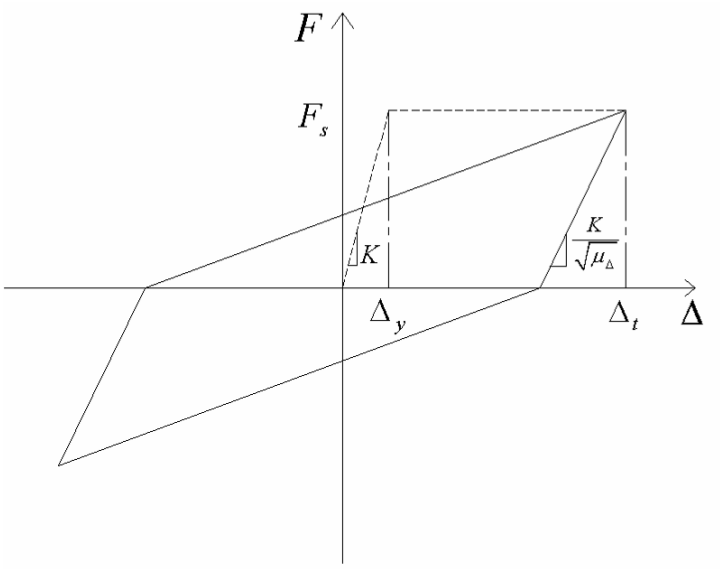

Figure 5.6: Takeda Load-Displacement Relationship

The load-deflection relationship for a pier with axial load alone (no mild steel reinforcement) can be illustrated in its simplest form by considering the behavior of a rigid block rocking about its corner. This system is shown in Figure 5.7a. If the block is prismatic, has self-weight (W), and carries an axial load (P), the lateral force (F) required to displace the top of the block as a function of drift ($\frac{\Delta}{L_c}$) can be shown by statics to be

$$F = \frac{1}{2}\frac{W+P}{\frac{L_c}{D_c} + \tan\frac{\Delta}{L_c}}\left[1 - \frac{2P+W}{P+W}\frac{L_c}{D_c}\tan\frac{\Delta}{L_c}\right] \tag{5.15}$$

The force-displacement relationship of a rigid block with typical dimensions is shown in Figure 5.7b. The monotonic curve is nearly linear and, for small displacements, it is similar to a rigid-plastic response. Unloading re-traces the loading curve, and there is no hysteresis.

A more realistic system, which includes initial loading that is elastic rather than rigid and some subsequent crushing of the concrete at the toe of the columns, was simulated with the nonlinear model of the pier. The response from the nonlinear model without mild steel reinforcement is shown in Figure 5.7c. The loading curve has an initial elastic rising region, followed by a falling region that resembles the curve for the rigid block. The unloading curve follows a slightly different path that leads to a small amount of hysteresis. For the displacements shown, the behavior is nearly bilinear elastic.

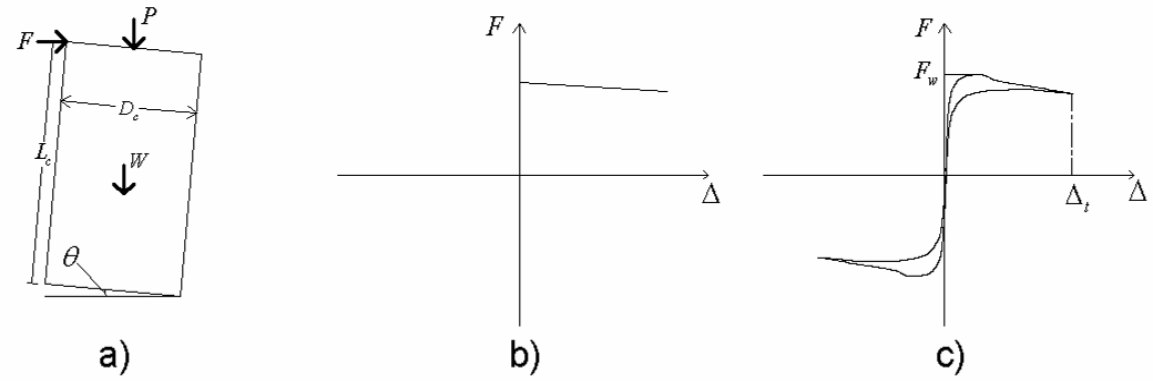

Figure 5.7: Load-Displacement Relationship with Axial Load Alone: (a) Rigid Rocking Block, (b) Response of Rigid Block, (c) Response of Pier

In this study, the load-deflection relationship of the pier with axial load alone was approximated by the bilinear elastic relationship shown in Figure 5.8. Because of P-delta effects and increasing force in the post-tensioning tendon, the true behavior will differ slightly from that exhibited by this idealized model; however, these effects are minimal at small drifts and were neglected in this study. Because of the model chosen, the energy dissipation of the pier with axial load alone was assumed to equal zero.

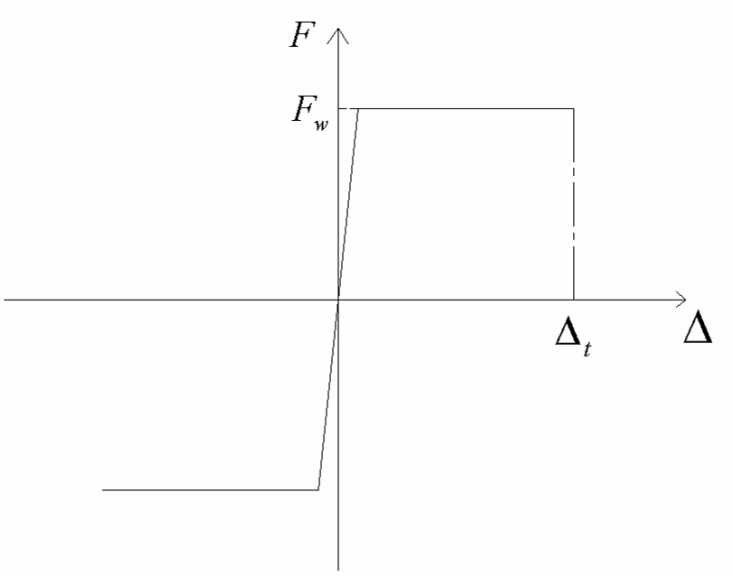

Figure 5.8: Bilinear Elastic Load-Displacement Relationship

5.3.2 Superposition of Hysteretic Loops

The load-displacement relationship of a pier is assumed to be the superposition of the load-deflection relationships for the pier with mild steel reinforcement alone and for the pier with axial load alone. Although superposition does not apply to nonlinear relationships, it was verified with nonlinear analysis to be sufficiently accurate in this instance. The shape of the combined load-deflection relationship depends on the force capacity of the pier with mild steel alone (F_s) and the force capacity of the pier with axial load alone (F_w). Figure 5.9 shows load-displacement relationships for large F_s relative to F_w and vice versa. Piers with large ρ_s relative to $P_c / f_c' A_g$ will have large F_s relative to F_w, and the method of superimposing load-deflection curves is shown to accurately predict the shape of the load-displacement curve of actual piers. Again, by using geometry it can be determined from Figure 5.9 that

$$\frac{A_{loop}}{A_{rect}} = \frac{1}{2}\frac{F_s}{F_s + F_w}\left(1 - \frac{1}{\sqrt{\mu_\Delta}}\right) \tag{5.16}$$

Combining equations (5.12) and (5.16) results in Equation (5.17) for expressing the ξ_{eq} of a precast pier:

$$\xi_{eq} = \frac{1}{\pi}\frac{F_s}{F_s + F_w}\left(1 - \frac{1}{\sqrt{\mu_\Delta}}\right) \tag{5.17}$$

Because of the assumptions used in developing Equation (5.17), such as the assumed load-deflection relationships and the use of superposition, the equation above is not exact. An equation that is more representative of the true damping can be obtained by retaining the form of Equation (5.17) but adjusting the numerical coefficients to achieve the best fit with results from nonlinear analysis (Section 5.2). The form of the equation is chosen to be

$$\xi_{eq} = C_1 + C_2\frac{F_s}{F_s + F_w}\left(1 - \frac{1}{\sqrt{\mu_\Delta}}\right) \tag{5.18}$$

The development of expressions for F_s and F_w is presented in sections 5.3.3 and 5.3.4. The numerical coefficients, C_1 and C_2, are determined in Section 5.3.5.

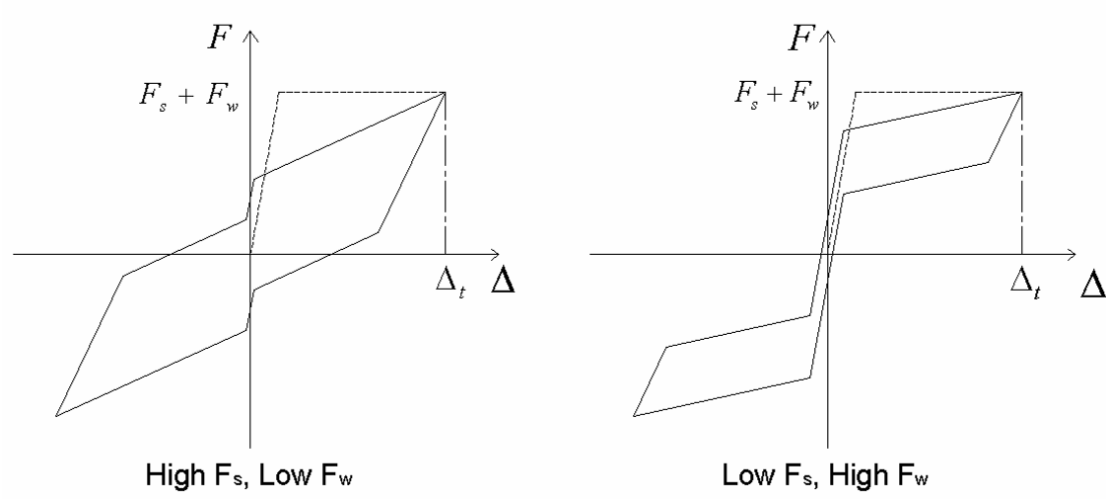

Figure 5.9: Idealized Load-Deflection Relationships for Precast Piers

5.3.3 The Force Capacity of a Pier with Mild Steel Reinforcement Alone

The force capacity of the pier with mild steel reinforcement alone (F_s) is determined from the moment capacity of the pier columns with mild steel reinforcement alone (M_s). If the cap beam of the pier is assumed to be rigid and the foundations assumed to be fully fixed, then from equilibrium

$$F_s = \frac{2M_s n_c}{L_c} \tag{5.19}$$

The internal forces on the column consist of forces in the reinforcing bars and compression in the concrete. Figure 5.10 illustrates the internal forces and can be used to determine M_s. In Figure 5.10, the reinforcing bars are not represented separately but are represented by a combined force $A_s f_y$. The location of the force from the compressive force in the concrete (κD_c) is determined so that the moment caused by the combined force is equal to the sum of the moments that would be caused by the individual bars. Summing moments in Figure 5.10 about the centroid of the concrete compression stress block results in

$$M_s = A_s f_y \kappa D_c \tag{5.20}$$

which can be expressed in non-dimensional terms as

$$M_s = \kappa \frac{\pi f_y}{4} D_c^3 \rho_s \tag{5.21}$$

Combining equations (5.19) and (5.21) produces

$$F_s = \kappa \frac{\pi f_y n_c}{2} \frac{1}{L_c} D_c^3 \rho_s \tag{5.22}$$

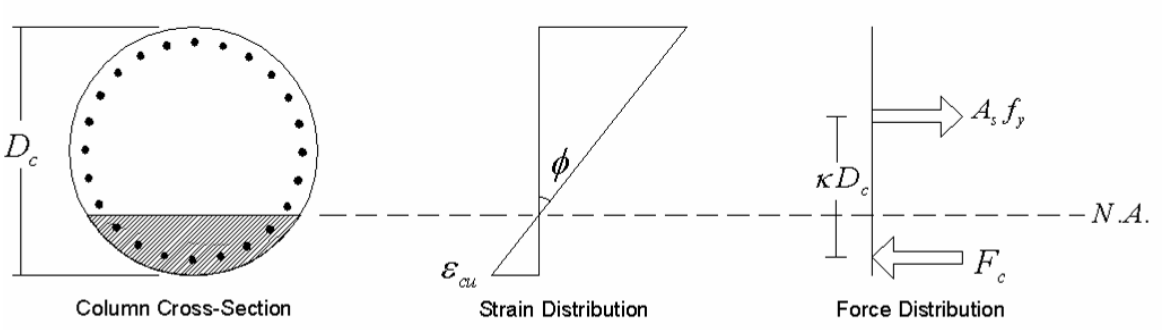

Figure 5.10: Internal Forces on Column Cross-Section

An expression for κ was determined so that Equation (5.22) would approximate values of F_s determined with nonlinear analyses. These values were determined by performing a pushover analysis, as described in Appendix A. The lateral load on the pier required to induce a strain of 0.004 in the extreme compressive fibers of the cross-section

at the top or bottom of the columns was taken to be F_s. Values of F_s were determined for 36 CIP emulation piers consisting of all possible combinations of

- column diameter (D_c): 36 in., 48in., and 60in.
- column aspect ratio (L_c / D_c): 5, 6, and 7
- mild steel reinforcing ratio (ρ_s): 0.005, 0.01, 0.02, and 0.03
- normalized axial dead load ($\frac{P_c}{f_c' A_g}$): 0

and for 27 hybrid piers consisting of all the possible combinations of

- column diameter (D_c): 36 in., 48in., and 60in.
- column aspect ratio (L_c / D_c): 5, 6, and 7
- mild steel reinforcing ratio (ρ_s): 0.008, 0.012, and 0.016
- post-tensioning reinforcing ratio (ρ_p): 0
- normalized axial dead load ($\frac{P_c}{f_c' A_g}$): 0

Equation (5.22) was used to determine values of κ corresponding to the values of F_s from nonlinear analysis. The values of κ are shown in Figure 5.11 below. A line was fitted to these data to minimize the squared difference, resulting in the following expression for κ:

$$\kappa = 0.45 - 2.35\rho_s \tag{5.23}$$

Equation (5.24) for F_s is developed by substituting Equation (5.23) into Equation (5.22):

$$F_s = (0.45 - 2.35\rho_s)\frac{\pi f_y n_c}{2}\frac{1}{L_c} D_c^3 \rho_s \tag{5.24}$$

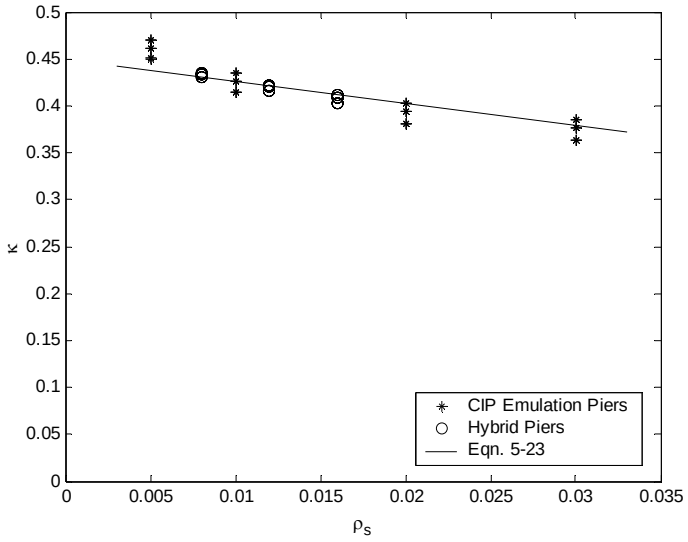

Figure 5.11: Values of κ from Nonlinear Analyses

5.3.4 Force Capacity of the Pier with Axial Load Alone

The force capacity of the pier with axial load alone (F_w) was determined by assuming that the pier behaves as an assembly of rigid blocks. Figure 5.12 shows the assumed deformation of the pier. Some plastification is assumed to occur at the ends of the columns and is represented in the figure. The forces acting on each of the columns of the pier are shown in Figure 5.13. Applying moment equilibrium to the column results in the following expression for F_w:

$$F_w = \psi \frac{n_c(P_c + A_p f_{p0})}{L_c / D_c} \tag{5.25}$$

where ψ is the distance between the vertical forces acting on the column divided by D_c. The weight of the pier columns is ignored in Equation (5.25) because it is small in comparison to P_c. For CIP emulation piers without unbonded post-tensioning (A_p = 0), Equation (5.25) simplifies to

$$F_w = \psi \frac{n_c P_c}{L_c / D_c} \tag{5.26}$$

Equations (5.25) and (5.26) can be expressed in non-dimensional terms as

$$F_w = \psi \frac{n_c \left(\frac{P_c}{f_c' A_g} + \rho_p \frac{f_{p0}}{f_c'} \right) f_c' A_g}{L_c / D_c} \tag{5.27}$$

and

$$F_w = \psi \frac{n_c \left(\frac{P_c}{f_c' A_g} \right) f_c' A_g}{L_c / D_c} \tag{5.28}$$

Equation (5.28) is simplified from Equation (5.27) to represent the absence of additional axial load in the columns resulting from post-tensioning in the CIP emulation piers.

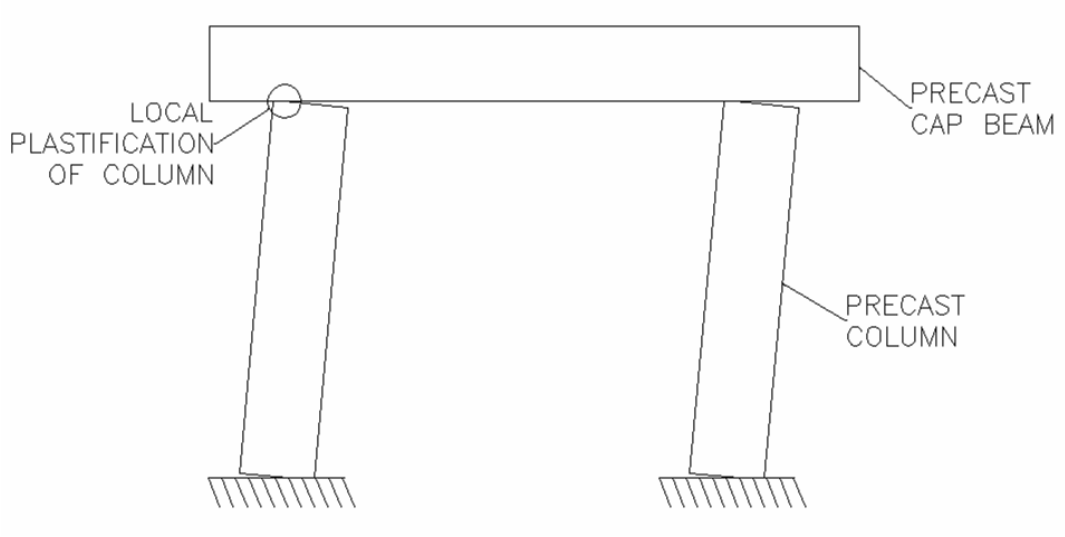

Figure 5.12: Assumed Deformation Behavior of Pier with Axial Load Alone

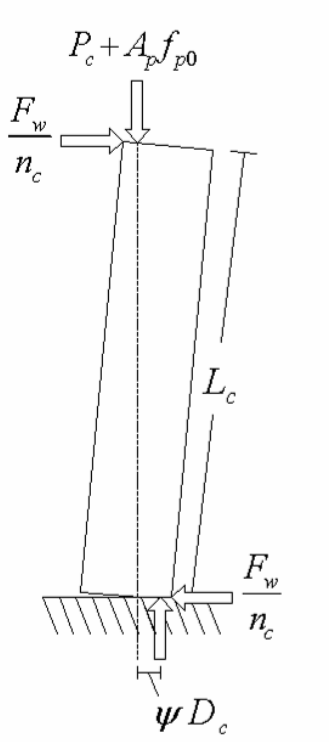

Figure 5.13: Forces on Column of Pier with Axial Load Alone

An expression for ψ was developed so that Equation (5.27) would approximate the results of nonlinear analysis. Pushover analyses of a large number of piers were performed. The largest lateral load recorded during each pushover analysis was assumed to be F_w. The analyses considered a total of 27 CIP emulation piers consisting of all possible combinations of

- column diameter (D_c): 36 in., 48in., and 60in.
- column aspect ratio (L_c / D_c): 5, 6, and 7
- mild steel reinforcing ratio (ρ_s): 0
- normalized axial dead load ($\frac{P_c}{f_c' A_g}$): 0.05, 0.10, and 0.15

and 54 hybrid piers consisting of all possible combinations of

- column diameter (D_c): 36 in., 48in., and 60in.
- column aspect ratio (L_c / D_c): 5, 6, and 7

- mild steel reinforcing ratio (ρ_s): 0
- post-tensioning reinforcing ratio (ρ_p): 0.0005, 0.0016, and 0.0028
- normalized axial dead load ($\frac{P_c}{f_c^{'} A_g}$): 0.05 and 0.10

For a given analysis, Equation (5.27) was inverted to find the value of ψ corresponding to the measured F_w.Figure 5.14 shows the values of ψ obtained from the analyses. A linear function fitted to these data has the following form:

$$\psi = 0.86 - 1.00\left(\frac{P_c}{f_c^{'} A_g} + \rho_p \frac{f_{p0}}{f_c^{'}} \right) \tag{5.29}$$

Combining equations (5.27) and (5.29) results in the following expression for F_w:

$$F_w = \left(0.86 - 1.00\left(\frac{P_c}{f_c^{'} A_g} + \rho_p \frac{f_{p0}}{f_c^{'}} \right) \right) \frac{n_c \left(\frac{P_c}{f_c^{'} A_g} + \rho_p \frac{f_{p0}}{f_c^{'}} \right) f_c^{'} A_g}{L_c / D_c} \tag{5.30}$$

This equation can be used for both CIP emulation piers and hybrid piers. For CIP emulation piers, ρ_p is equal to zero.

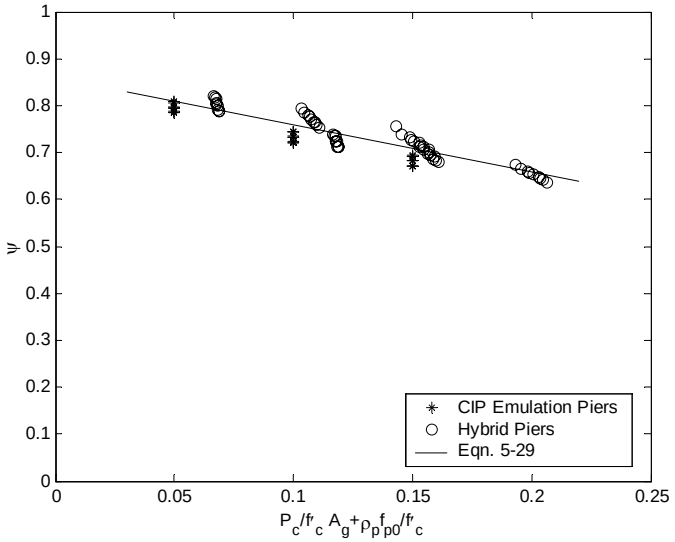

Figure 5.14: Values of ψ from Nonlinear Analyses

5.3.5 Calibration of ξ_{eq}

The results of nonlinear analyses, and the equations developed for F_s and F_w above, were used to determine the constants C_1 and C_2 in Equation (5.18). Push-pull analyses were performed on all 108 CIP emulation piers and 162 hybrid piers used for calibration in Section 4.2. For each pier, five push-pull analyses were conducted to the maximum displacements corresponding to displacement ductilities (μ_Δ) of 1, 2, 3, 4, and 5. The nonlinear analysis method presented in Section 5.2 was used to determine ξ_{eq} for each analysis.

The value of C_1 was determined by averaging ξ_{eq} for each pier when displaced to a maximum displacement corresponding to μ_Δ = 1.0. Theoretically, if a pier is only displaced to the yield displacement, which corresponds to a μ_Δ of 1.0, then ξ_{eq} should be zero because no yielding has occurred and no energy has been dissipated. This is evident in the absence of a coefficient in Equation (5.17), which was derived from theory. However, in this study, the piers do not yield sharply because all of the reinforcing bars do not yield simultaneously, yet a sharp nominal yield displacement point must be defined (Section 4.1) in order to define μ_Δ. As a result, some bars will begin to yield before the pier reaches the nominal yield displacement, and some energy will be dissipated, even at μ_Δ = 1.0. The equivalent viscous damping (ξ_{eq}) corresponding to this energy dissipation before the nominal yield displacement is reached is represented by the constant C_1. From the nonlinear analysis values, it was determined that C_1=0.025.

The value of C_2 was determined so that Equation (5.18) would accurately estimate ξ_{eq} obtained from nonlinear analysis when F_s and F_w were determined with equations (5.24) and (5.30), respectively. This was accomplished by inverting Equation (5.18) and determining the value of C_2 required to achieve ξ_{eq} for each of the piers at all levels of ductility greater than 1.0. The values of C_2 obtained were then averaged, resulting in C_2=0.63.

The flowchart shown in Figure 5.15 summarizes the equations used to estimate ξ_{eq}. The accuracy of these equations was gaged by comparing the estimates they give for ξ_{eq} with the estimates of ξ_{eq} obtained by using the nonlinear analysis method for the 108 CIP emulation piers and 162 hybrid piers presented above. The distribution of differences between the equation-based values ($\xi_{eq,eb}$) and the nonlinear analysis values ($\xi_{eq,nla}$) are shown in Figure 5.16. It can be seen that the equation-based method is inaccurate for low levels of ductility. Nonetheless, it provides accurate estimates of ξ_{eq} for $\mu_{\Delta} \geq 3$, with more than 95 percent of all piers considered having a percentage difference of between -10 percent and +10 percent. The mean value and coefficient of variance (COV) of the ratio of $\frac{\xi_{eq,eb}}{\xi_{eq,nla}}$ for each level of ductility are presented in Table 5.1. The majority of bridge piers will be designed for ductilities of 3.0 or greater, making the equation-based method for estimating ξ_{eq} acceptable for use in the iterative DDBD procedures presented in Section 3.2.1. The values of F_s and F_w can also be determined directly from strength analysis, if desired.

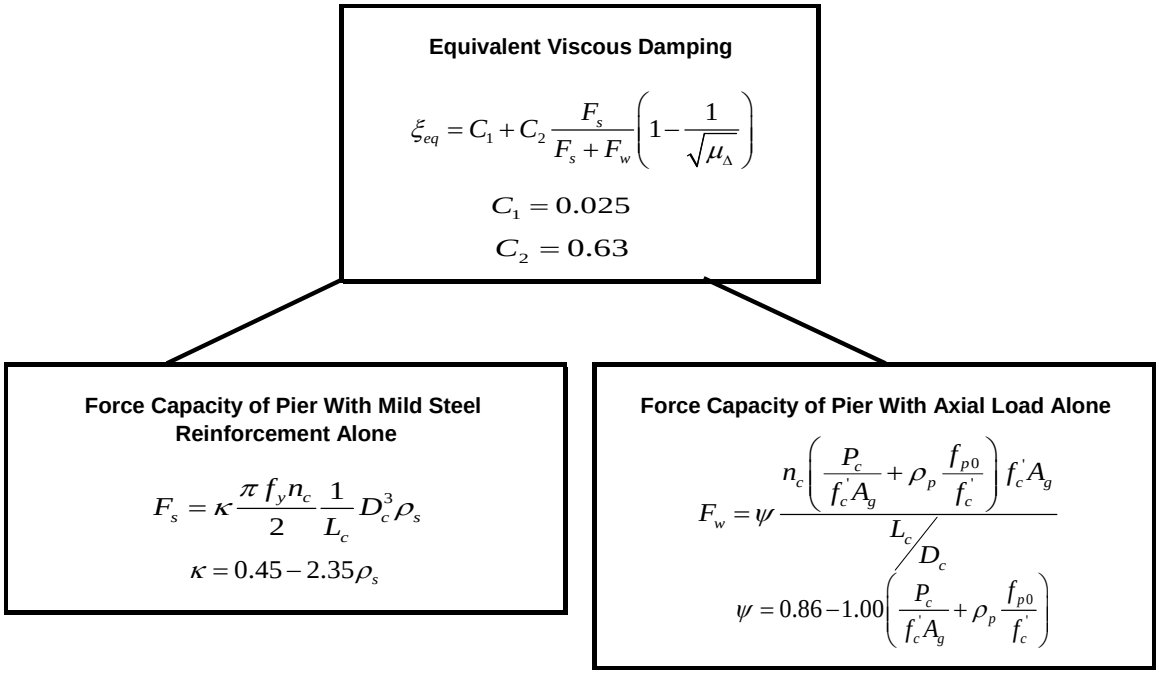

Figure 5.15: Flowchart of Equations for Estimating ξ_{eq}

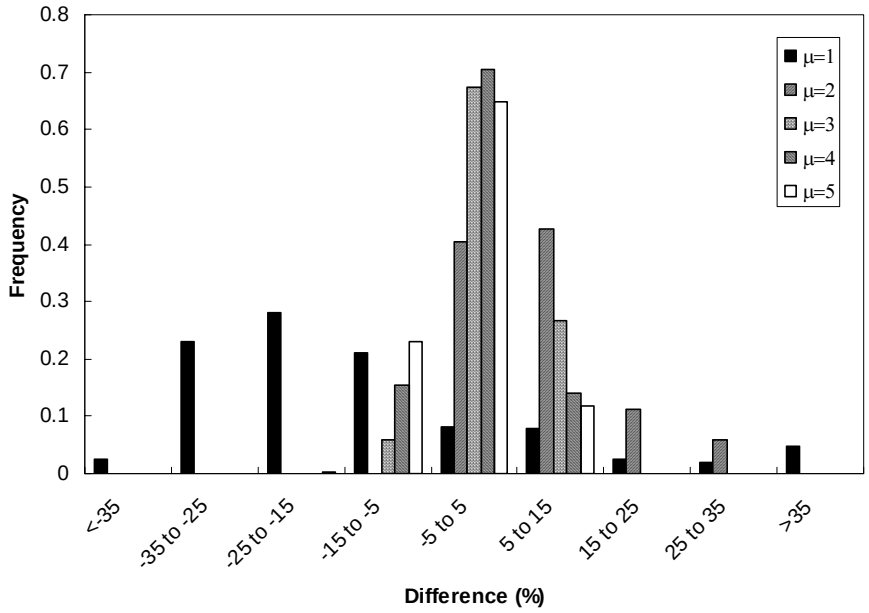

Figure 5.16: Distribution of Difference of Estimates for ξ_{eq}

Table 5.1: Statistical Parameters of $\frac{\xi_{eq,eb}}{\xi_{eq,nla}}$ for Equation-Based Method

Ductility	Mean	COV (%)
1	0.88	21.0
2	1.08	7.0
3	1.02	4.9
4	1.00	4.7
5	0.99	5.2

5.4 EMPIRICAL METHOD

The direct (non-iterative) DDBD procedure presented in Section 3.2.2 requires ξ_{eq} to be estimated without knowing the amount of reinforcement in the pier columns. Both the nonlinear analysis and equation-based methods presented above require knowledge of the amount of reinforcement. To accommodate the non-iterative DDBD procedure, an empirical relationship between ξ_{eq} and the drift at the target displacement (Δ_t / L_c) was developed for both the CIP emulation and hybrid piers.

The values of ξ_{eq} and Δ_t / L_c for the CIP emulation piers used to calibrate the equation-based method are shown in Figure 5.17. There is considerable scatter in the

data; however, a distinct trend appears. Fitting an empirical equation to these data by using a best fit approach results in

$$\xi_{eq} = \begin{cases} 0.15\ln(\dfrac{\Delta_t}{L_c}) + 0.8 & for \quad \dfrac{\Delta_t}{L_c} \geq 0.0055 \\ 0.025 & for \quad \dfrac{\Delta_t}{L_c} \leq 0.0055 \end{cases} \tag{5.31}$$

The piece-wise function is used to prevent negative values of ξ_{eq} and represents the amount of damping before the nominal yield displacement is reached. A better fit to this data could be established by using μ_Δ rather than Δ_t / L_c ; however, this is not possible because μ_Δ requires knowledge of the yield displacement (Δ_y), which is dependent on the amount of reinforcing steel. The difference between the ξ_{eq} values determined with the empirical method ($\xi_{eq,emp}$) and the nonlinear analysis method ($\xi_{eq,nla}$) is shown in Figure 5.18. It can be seen that although the empirical method is quick and easy to use and requires minimal knowledge about the pier, it produces less accurate estimates of ξ_{eq} than the equation-based method, with only 44 percent of piers considered having a difference of between -10 percent and +10 percent. The mean value of $\dfrac{\xi_{eq,emp}}{\xi_{eq,nla}}$ for the CIP emulation piers is 1.05 with a COV of 25.0 percent.

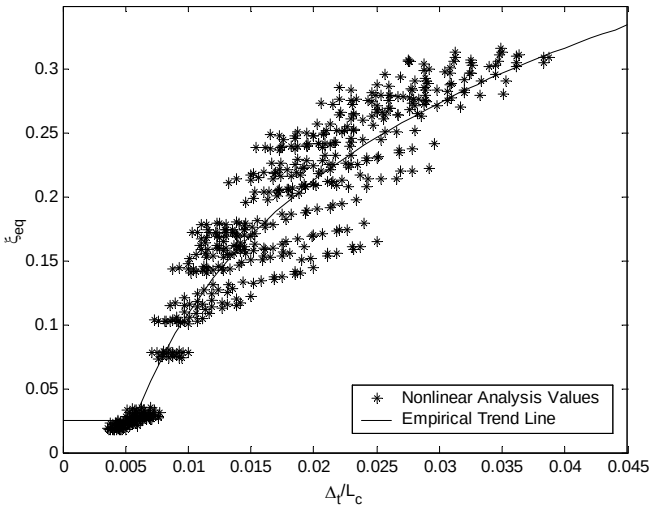

Figure 5.17: Relationship of ξ_{eq} and $\dfrac{\Delta_t}{L_c}$ for CIP Emulation Piers

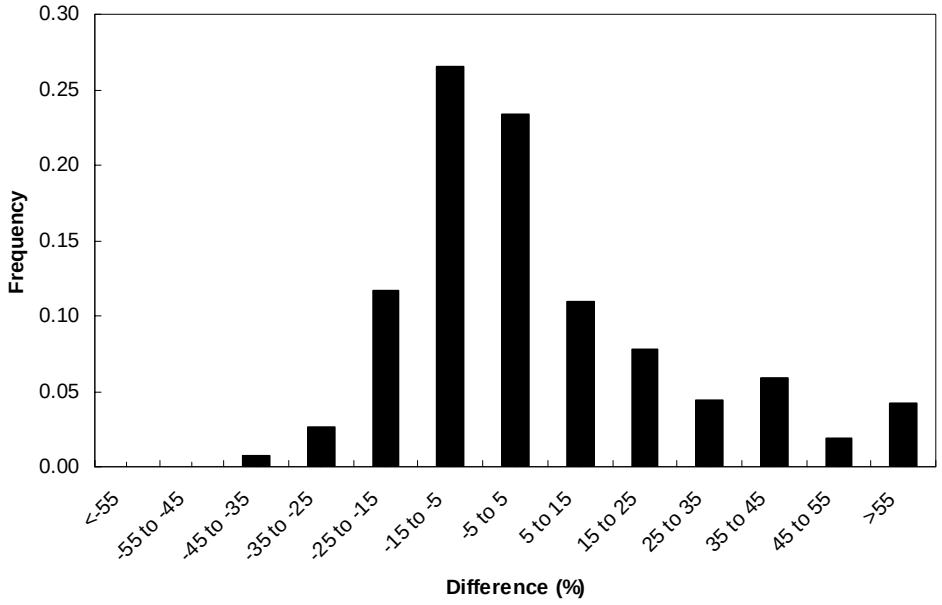

Figure 5.18: Distribution of Difference of ξ_{eq} Calculated with Empirical and Nonlinear Analysis Methods for CIP Emulation Piers

An empirical equation for ξ_{eq} of a hybrid pier was determined in the same fashion. The relation between ξ_{eq} and Δ_t / L_c for the hybrid piers considered above is presented in Figure 5.19. Fitting a curve to this data results in

$$\xi_{eq} = \begin{cases} 0.11\ln(\dfrac{\Delta_t}{L_c}) + 0.67 & for \ \dfrac{\Delta_t}{L_c} \geq 0.0035 \\ 0.025 & for \ \dfrac{\Delta_t}{L_c} \leq 0.0035 \end{cases} \tag{5.32}$$

The distribution of differences between the ξ_{eq} values calculated from the empirical method ($\xi_{eq,emp}$) and the nonlinear analysis method ($\xi_{eq,nla}$) is shown in Figure 5.20. It can be seen that the differences are significant and greater than those for the CIP emulation piers. In this case, only 27 percent of the piers considered have differences of between -10 percent and +10 percent. The mean value of $\dfrac{\xi_{eq,emp}}{\xi_{eq,nla}}$ for hybrid piers is 1.31 with a COV of 32.0 percent.

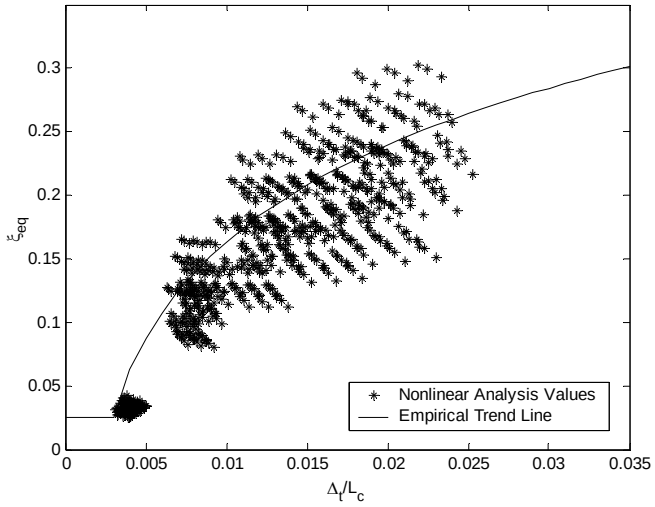

Figure 5.19: Relationship of ξ_{eq} and $\frac{\Delta_t}{L_c}$ for Hybrid Piers

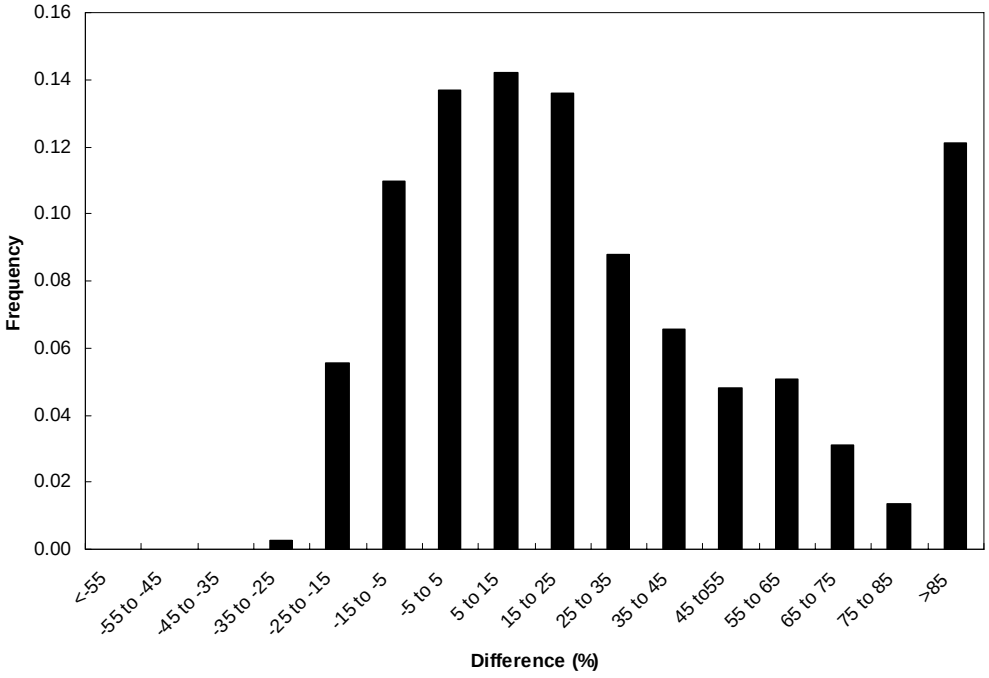

Figure 5.20: Distribution of Differences for ξ_{eq} Calculated with Empirical and Nonlinear Analysis Methods for Hybrid Piers

CHAPTER 6
DAMPING MODIFICATION FACTOR FOR THE DDBD PROCEDURES

The direct displacement-based design (DDBD) procedures presented in Section 3.2 approximate the inelastic behavior of a bridge pier in a design-level earthquake with an equivalent linear system. A damping modification factor (β) is included in the procedures so that the maximum displacement estimated by the equivalent linear system, also referred to as the target displacement (Δ_t), approximates the maximum inelastic displacement of the pier (Δ_{max}). The damping modification factor (β) is defined as the ratio of the effective equivalent viscous damping ($\hat{\xi}_{eq}$) to the equivalent viscous damping measured from the hysteretic behavior of the pier (ξ_{eq}) (Section 5.1). The effective equivalent viscous damping ($\hat{\xi}_{eq}$) is the amount of equivalent viscous damping that will cause the maximum displacements of the equivalent linear system and inelastic pier to coincide. β is defined as follows:

$$\beta = \frac{\hat{\xi}_{eq}}{\xi_{eq}} \tag{6.1}$$

Reasons for needing a modification factor in the design procedures are presented in Section 6.1. Section 6.2 presents the development of β values, followed by the formulation of relationships for β in Section 6.3.

6.1 SOURCES OF ERROR IN THE DDBD PROCEDURES

Error is introduced into the DDBD procedures through the use of an equivalent linear system to represent the behavior of an inelastic pier and the use of a design displacement response spectrum to estimate the response of a pier to a variety of earthquakes.

The equivalent viscous damping (ξ_{eq}) is determined so that the amount of energy dissipated by the equivalent linear system and that dissipated by an inelastic pier during an earthquake are approximately equal. As discussed in Chapter 5, ξ_{eq} is estimated from

the hysteretic behavior of the structure when displaced to the target displacement (Δ_t). These estimates do not result in accurate displacement predictions for two reasons. First, the amplitude of the majority of the displacement cycles during a typical earthquake will be smaller than Δ_t, as shown in Figure 6.1. Accordingly, estimating the equivalent viscous damping from the hysteretic behavior at Δ_t over-predicts the energy dissipation. Quantifying this effect is difficult because it is highly dependent on the characteristics of the ground motion exciting the structure.

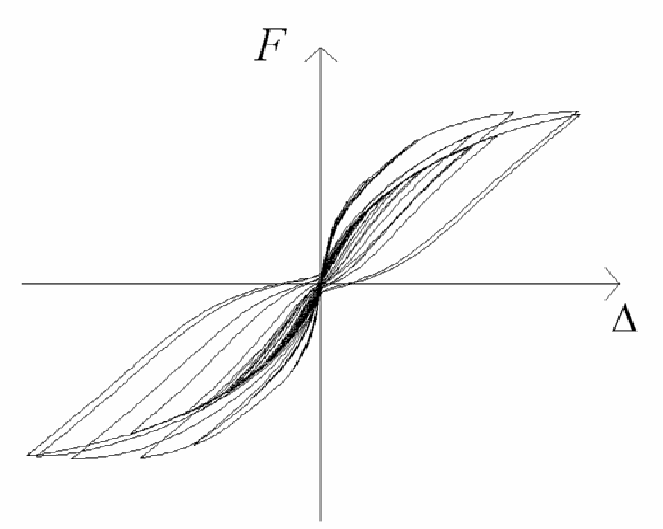

Figure 6.1: Force-Displacement Relationship of a Pier Subjected to Earthquake Excitation

A second source of error is the assumption of a sinusoidal ground acceleration record with a driving frequency equal to the natural frequency of the pier when the equivalent viscous damping is related to the hysteretic behavior of the pier (Section 5.1). The amount of error introduced by this assumption depends on the characteristics of both the pier and ground motion.

The use of a design response spectrum also introduces error into the procedures because the spectrum does not estimate the response of the pier to a particular ground motion but rather the average response expected if the pier were subjected to a variety of design-level earthquakes. In design, the effects of a variety of earthquakes on the performance of the pier must be considered. The need to consider multiple earthquakes makes the issue of determining the response of a pier to a particular ground motion less

important. Consequently, relationships for β were developed by averaging the response of the pier to five design-level earthquakes and using the average response to determine β. The effects of scatter between individual and average maximum displacement values on the performance of a pier are addressed in Chapter 8.

6.2 DEVELOPMENT OF B VALUES USED IN CALIBRATION

The relationships for β used in this study were determined empirically from the results of nonlinear time-history analyses for a large number of piers subjected to a variety of ground motions. The values of β obtained for the piers on the basis of the average response of the dynamic analyses for the five ground motions considered are denoted as β_{da}. The empirical relationships for β to be used in the design procedures were obtained by fitting equations to the β_{da} values. Separate relationships for β were developed for CIP emulation and hybrid piers because the piers will behave differently during an earthquake.

6.2.1 Piers Considered in Calibration

The piers used to generate β_{da} values were selected to encompass a wide range of typical pier characteristics. A total of 108 CIP emulation piers were considered, consisting of all combinations of the following variables:

- column diameter (D_c): 36 in., 48 in., and 60 in.
- column aspect ratio (L_c / D_c): 5, 6, and 7
- mild steel reinforcing ratio (ρ_s): 0.005, 0.01, 0.02, and 0.03
- normalized axial dead load ($\frac{P_c}{f_c' A_g}$): 0.05, 0.10, and 0.15.

A total of 162 hybrid piers were considered, consisting of all combinations of the following variables:

- column diameter (D_c): 36 in., 48 in., and 60 in.
- column aspect ratio (L_c / D_c): 5, 6, and 7
- mild steel reinforcing ratio (ρ_s): 0.008, 0.012, and 0.016

- post-tensioning reinforcing ratio (ρ_p): 0.0005, 0.0016, and 0.0028
- normalized axial dead load ($\frac{P_c}{f_c' A_g}$): 0.05 and 0.10.

Only the two smaller normalized axial dead load levels were considered for the hybrid piers. This was done both to limit the number of piers that needed to be considered and to avoid the high axial load that would have resulted from the combination of post-tensioning and high axial dead load.

Each pier was subjected to the five ground-motion acceleration records shown in Appendix F. The maximum displacements (Δ_{max}) from the five dynamic analyses were averaged for each pier. The average maximum displacement ($\overline{\Delta}_{max}$) was used to determine β_{da}. This approach resulted in a total of 108 β_{da} values for the CIP emulation piers and 162 β_{da} values for the hybrid piers.

6.2.2 Procedure for Developing β_{da} Values

The procedure used to determine the value of β_{da} for each pier considered is summarized by the flowchart in Figure 6.2.

Step #1: Determine the Average Maximum Displacement of the Pier

The average maximum displacement of the pier ($\overline{\Delta}_{max}$) was determined by subjecting the pier to the five ground motion acceleration records and taking the average of the maximum displacements (Δ_{max}). Dynamic time-history analysis, conducted with the models described in Appendix A, was used to estimate the Δ_{max} of the pier subjected to a ground-motion acceleration record.

Step #2: Determine the Force at the Average Maximum Displacement

A static pushover analysis, as described in Appendix A, was performed to $\overline{\Delta}_{max}$ to determine $\overline{F}_{max}$, the lateral force on the pier at $\overline{\Delta}_{max}$. A pushover analysis was used to determine $\overline{F}_{max}$ instead of measuring it directly from the dynamic analyses to eliminate

any strength degradation associated with cyclic loading, which is dependent on the characteristics of the ground motion considered.

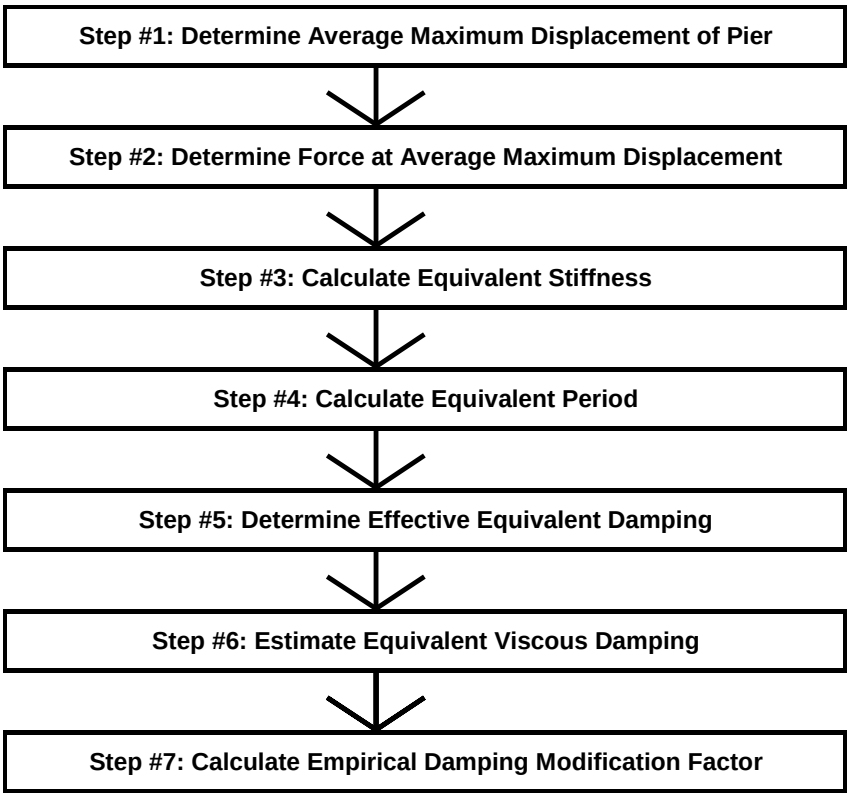

Figure 6.2: Procedure for Determining β_{da} Values

Step #3: Calculate the Equivalent Stiffness

The stiffness of the equivalent linear system (K_{eq}) was determined by using Equation (6.2).

$$K_{eq} = \frac{\bar{F}_{\max}}{\bar{\Delta}_{\max}} \tag{6.2}$$

Step #4: Calculate the Equivalent Period

The equivalent period of vibration (T_{eq}) was determined by using Equation (6.3)

$$T_{eq} = 2\pi\sqrt{\frac{m_p}{K_{eq}}} \tag{6.3}$$

where m_p is the mass of the superstructure and pier.

Step #5: Determine the Effective Equivalent Damping

The design displacement response spectrum with 5 percent viscous damping, represented by Equation (6.4), can be used to relate T_{eq} and the expected spectral displacement ($S_{d-5\%}$).

$$S_{d-5\%} = \frac{1.2}{4\pi^2} ASgT_{eq}^{4/3} \leq \frac{2.5}{4\pi^2} AgT_{eq}^2 \tag{6.4}$$

In Equation (6.4), A is the acceleration coefficient and S is the soil coefficient, as defined in the AASHTO specifications (AASHTO 2002; AASHTO 2004).

For the T_{eq} value calculated in Step #4, the spectral displacement ($S_{d-5\%}$) determined with Equation (6.4) is not necessarily equal to the value of $\bar{\Delta}_{\max}$ determined in Step #1. This difference occurs because $\hat{\xi}_{eq}$ is not necessarily equal to 5 percent. Instead, the value of $\hat{\xi}_{eq}$ is determined so that the displacement response spectrum, modified for the new level of damping, will predict $\bar{\Delta}_{\max}$ for the corresponding T_{eq}, as shown in Figure 6.3.

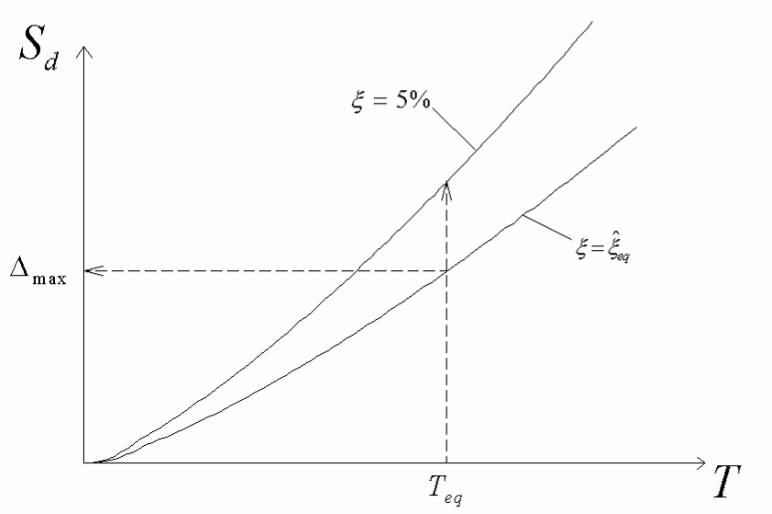

Figure 6.3: Relationship for Determining Effective Equivalent Viscous Damping

A EUROCODE 8 provision, presented in Equation (6.5) (EUROCODE 1994), was used to relate spectral displacements for various levels of viscous damping.

$$S_{d-\hat{\xi}_{eq}} = \sqrt{\frac{7}{2+100\hat{\xi}_{eq}}} S_{d-5\%} \tag{6.5}$$

To verify this equation, displacement response spectra were generated for the five ground motions considered in this study for a wide range of damping values (ξ). For each ground motion and level of damping considered, the ratio of $\frac{S_{d-\xi}}{S_{d-5\%}}$ was calculated and averaged over a range of periods of vibration from 0 to 2 seconds. Figure 6.4a shows the relationship between $\frac{S_{d-\xi}}{S_{d-5\%}}$ and ξ for the five ground motions. The average relationship, developed by averaging $\frac{S_{d-\xi}}{S_{d-5\%}}$ from the five ground motions at every level of damping, is shown in Figure 6.4b with the relationship specified by EUROCODE 8 (Equation (6.5)). The relationships are sufficiently similar to support the use of the EUROCODE 8 provision.

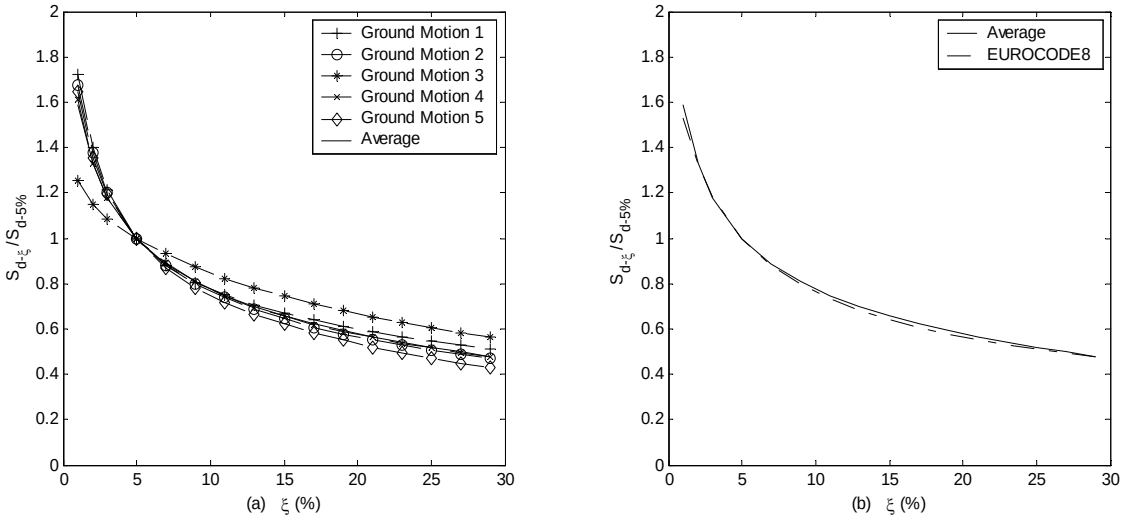

Figure 6.4: Effect of Damping on Spectral Displacement: (a) Individual Ground Motions, (b) Average Values

The value of $\hat{\xi}_{eq}$ that caused T_{eq} to correspond to $\bar{\Delta}_{\max}$ was then determined by solving Equation (6.6) numerically:

$$\bar{\Delta}_{\max} = \sqrt{\frac{7}{2+100\hat{\xi}_{eq}}}\frac{1.2}{4\pi^2}ASgT_{eq}^{4/3} \le \sqrt{\frac{7}{2+100\hat{\xi}_{eq}}}\frac{2.5}{4\pi^2}AgT_{eq}^2 \quad (6.6)$$

Step #6: Estimate the Equivalent Viscous Damping from the Hysteretic Behavior

The equivalent viscous damping (ξ_{eq}) was determined from the hysteretic behavior of the pier by using the nonlinear analysis method presented in Section 5.2.

Step #7: Calculate the Empirical Modification Factor

Equation (6.7) was then used to calculate β_{da}:

$$\beta_{da} = \frac{\hat{\xi}_{eq}}{\xi_{eq}} \quad (6.7)$$

6.3 RELATIONSHIPS BETWEEN β AND μ_Δ

The values of β_{da} calculated for the CIP emulation and hybrid piers with the procedure presented in Section 6.2.2 are shown in Figure 6.5. The values are plotted against the displacement ductility (μ_Δ), which is a measure of inelastic displacement demand on the pier:

$$\mu_\Delta = \frac{\bar{\Delta}_{\max}}{\Delta_y} \quad (6.8)$$

In Equation (6.8), Δ_y is the yield displacement of the pier determined with the nonlinear analysis method presented in Section 4.1.

Values of β_{da} corresponding to μ_Δ of less than 1.25 were removed because in this range the piers behave nearly elastically. Accordingly, the damping values are extremely small, allowing small errors in the damping value estimates to magnify into large errors in the β_{da} values.

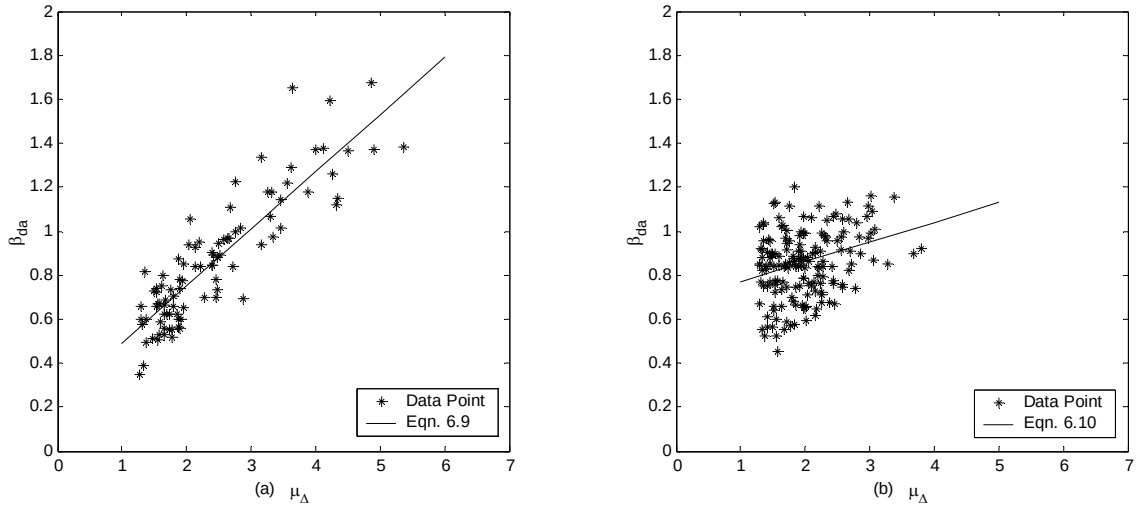

Figure 6.5: β_{da} Values: (a) CIP Emulation Piers, (b) Hybrid Piers

The trend in the values of β_{da} suggests the use of a linear relationship to represent β. To minimize the squared difference with the β_{da} values, the relationship for β was determined to be

$$\beta = 0.26 + 0.23\mu_\Delta \tag{6.9}$$

for the CIP emulation piers and

$$\beta = 0.55 + 0.12\mu_\Delta \tag{6.10}$$

for the hybrid piers. The ratio, β_{da}/β, was calculated for each data point to evaluate the quality of fit obtained using the linear relationships for β. The distribution of β_{da}/β versus μ_Δ is shown in Figure 6.6 for the CIP emulation and hybrid piers. These distributions show that, although considerable scatter exists in the values, the β relationships can be used throughout the range of μ_Δ considered to obtain reasonable results. The ratio β_{da}/β had a mean value of 0.99 with a coefficient of variation (COV) of 16.0 percent for the CIP emulation piers and a mean value of 1.02 with a COV of 17.1 percent for the hybrid piers.

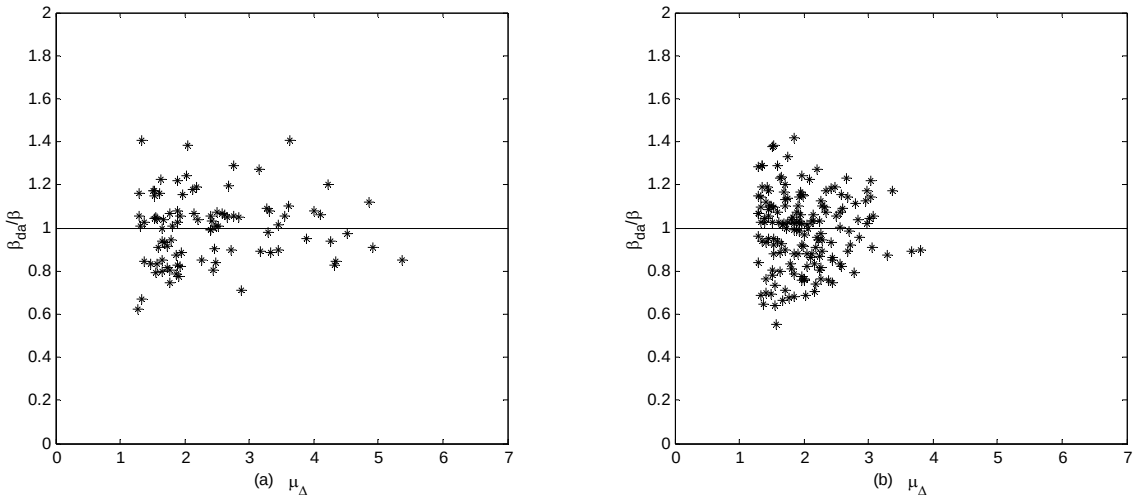

Figure 6.6: Distribution of β_{da}/β for $\beta - \mu_\Delta$ Relationships: (a) CIP Emulation Piers, (b) Hybrid Piers

The COVs of the β_{da}/β ratios are relatively large. However, the scatter in the maximum displacement of the linear system is less than the scatter in β_{da} values, as will be shown in Chapter 8.

6.4 RELATIONSHIP BETWEEN B AND DRIFT RATIO

One additional difficulty arises when the direct (non-iterative) DDBD procedure (Section 3.2.2) is used because μ_Δ is not determined in the procedure, preventing the use of Equation (6.9) or (6.10) to determine β. This difficulty can be alleviated by relating β directly to the drift ratio ($\frac{\overline{\Delta}_{\max}}{L_c}$), as shown in Figure 6.7 for the CIP emulation and hybrid piers.

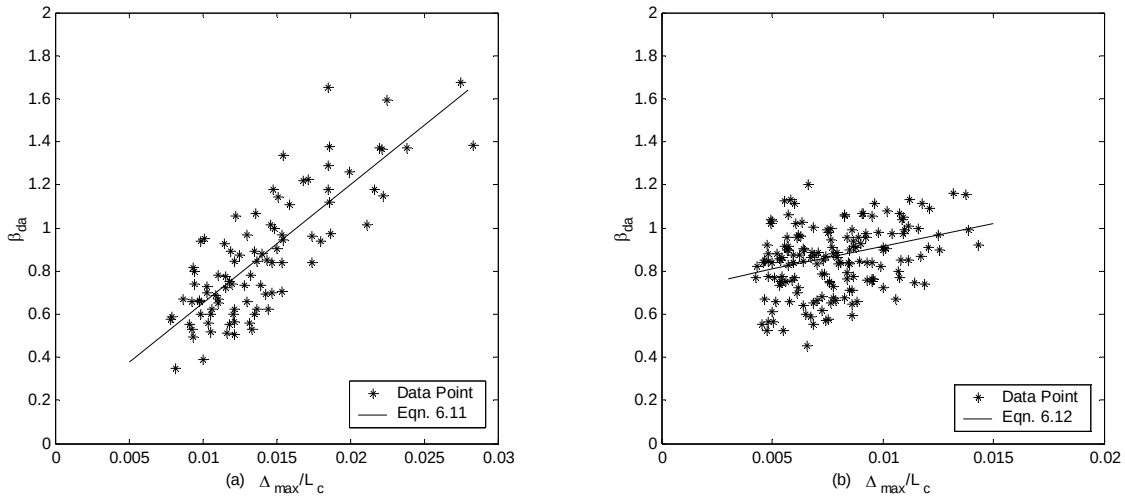

Figure 6.7: Relationship of β_{da} and $\frac{\overline{\Delta}_{\max}}{L_c}$: (a) CIP Emulation Piers, (b) Hybrid Piers

Fitting linear relationships to the β_{da} values to minimize the sum of the squared difference results in

$$\beta = 0.14 + 48.5\frac{\overline{\Delta}_{\max}}{L_c} \tag{6.11}$$

for CIP emulation piers and

$$\beta = 0.57 + 29.0\frac{\overline{\Delta}_{\max}}{L_c} \tag{6.12}$$

for hybrid piers.

The distribution of the ratio β_{da}/β is shown in Figure 6.8 for the CIP emulation and hybrid piers. The ratio β_{da}/β had a mean value of 1.00 with a COV of 20.0 percent for the CIP emulation piers and a mean value of 1.02 with a COV of 17.0 percent for the hybrid piers. Because the behavior of a pier can vary significantly for a given drift level (i.e., a slender column might remain elastic at a certain level of drift whereas a stocky column would experience a significant amount of inelastic deformation to reach the same drift level), equations (6.11) and (6.12) are only applicable within the range of column aspect ratios (L_c/D_c) considered in the calibration.

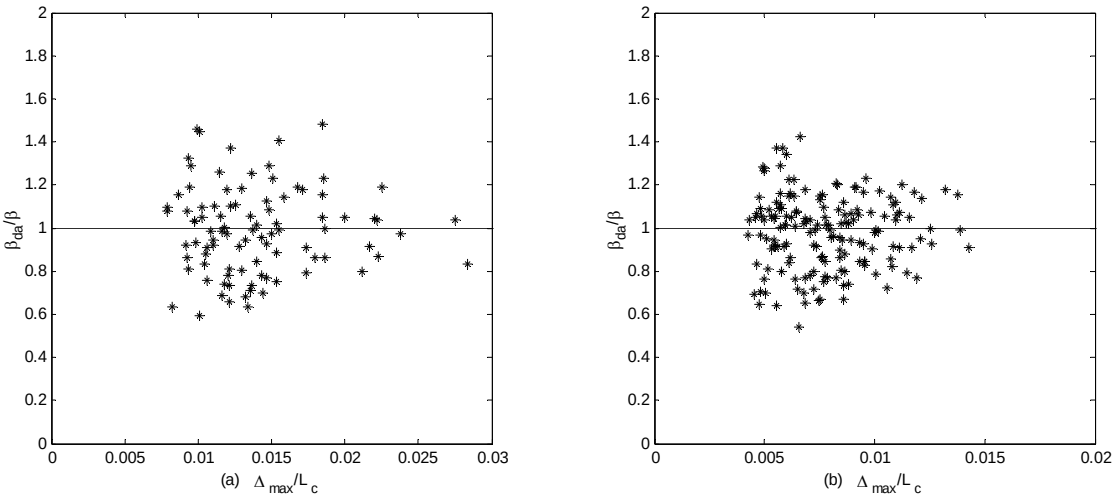

Figure 6.8: Distribution of β_{da}/β for β-Drift Relationships: (a) CIP Emulation Piers, (b) Hybrid Piers

CHAPTER 7
METHODS FOR DETERMINING PIER STRENGTH

The equivalent lateral force design (ELFD) and direct displacement-based design (DDBD) procedures presented in chapters 2 and 3 require a method for determining the amount of reinforcing steel required to provide a pier with sufficient strength. Methods for estimating the amount of reinforcing steel required to provide a force resisting capacity (F_{cap}) greater than the design force (F_d) for both CIP emulation and hybrid piers are presented in this chapter. A method for estimating F_{cap} that uses nonlinear analysis is presented in Section 7.3, followed by a sectional analysis method for estimating F_{cap} in Section 7.4.

7.1 RESISTANCE FACTORS

Estimates of F_{cap} obtained with either the nonlinear analysis or sectional analysis method are multiplied by a resistance factor to account for variations in material properties, workmanship, and other factors. The AASHTO specifications (AASHTO 2002; AASHTO 2004) state that the resistance factor for reinforced concrete members subjected to compression and flexure (ϕ_{cf}), such as bridge columns, in seismic applications should be

$$\phi_{cf} = \begin{cases} 0.9 - 2\dfrac{P_c}{f_c' A_g} & for \quad \dfrac{P_c}{f_c' A_g} \le 0.20 \\ 0.5 & for \quad \dfrac{P_c}{f_c' A_g} > 0.20 \end{cases} \tag{7.1}$$

where $\dfrac{P_c}{f_c' A_g}$ is the normalized axial load in the columns due to the weight of the superstructure and columns. The AASHTO specifications do not stipulate resistance factors for hybrid piers. Equation (7.1) was used to determine ϕ_{cf} for hybrid piers in this research because the quality of the precast columns used in both types of piers is expected to be equal. If the capacity of the pier is controlled by flexural yielding of the

columns, which is commonly the desired failure mechanism in bridges, F_{cap} of the pier must be large enough such that Equation (7.2) is satisfied.

$$\phi_{cf} F_{cap} \geq F_d \tag{7.2}$$

The force resisting capacity (F_{cap}) is determined by using one of the methods in sections 7.3 and 7.4 and substituting it into Equation (7.2). If the inequality is not met, the amount of reinforcing steel is increased and F_{cap} is recalculated. If $\phi_{cf} F_{cap}$ is significantly larger than F_d , the pier has an excessive amount of reinforcement, resulting in an uneconomical design, and the amount of reinforcing steel is decreased until $\phi_{cf} F_{cap}$ is approximately equal to F_d .

7.2 DEFINITION OF CAPACITY

One complication arises because the ELFD and DDBD procedures use different definitions for the deformation of the pier at which F_{cap} should be determined. The ELFD procedure defines F_{cap} as the force resisted by the pier when the extreme compression concrete reaches a strain of 0.004, referred to in this chapter as the critical-strain-capacity definition. The DDBD procedure defines F_{cap} as the force resisted by the pier at a particular target displacement, referred to as the target-displacement-capacity definition in this chapter.

The nonlinear analysis method presented in Section 7.3 can be modified to determine F_{cap} on the basis of either definition. The sectional analysis method for determining the F_{cap} of CIP emulation piers uses the critical-strain-capacity definition, making it more suitable for the ELFD procedure. The sectional analysis method for determining the F_{cap} of hybrid piers uses the target-displacement-capacity definition, making it more suitable for the DDBD procedure.

However, it will be shown that because the precast pier systems do not exhibit significant post-yield stiffness, the values of F_{cap} based on both the critical-strain and target-displacement definitions are similar for the range of displacements expected in a design-level earthquake. This fact allows the sectional analysis methods to be used for

either type of pier in both ELFD and DDBD procedures without introducing significant error.

7.3 NONLINEAR ANALYSIS METHOD

A nonlinear pushover analysis can be used to determine F_{cap}. A nonlinear finite-element model of the pier is created, as described in Appendix A, and a static pushover analysis to the target displacement (Δ_t) is performed. The lateral force on the pier at Δ_t is F_{cap} based on the target-displacement-capacity definition. The strain in the extreme compressive fiber of the columns is also monitored and the force on the pier corresponding to a peak strain of 0.004 is F_{cap} based on the critical-strain-capacity definition. This method can be used for both CIP emulation and hybrid piers. The only differences between CIP emulation and hybrid piers are those associated with the development of the nonlinear model and the location where strains are measured, as discussed in Chapter 4.

7.4 SECTIONAL ANALYSIS METHOD

Sectional analysis methods for determining the F_{cap} of both CIP emulation and hybrid pier systems are presented below. The sectional analysis methods do not require any nonlinear modeling, making them more practical to use in certain situations. Both CIP emulation and hybrid piers are typically designed so that the columns will yield in flexure before any other component of the pier fails. Accordingly, the F_{cap} of the pier depends on the moment capacity of the columns (M_{cap}). If the cap beam is assumed to be rigid and the foundations are assumed to be fixed,

$$F_{cap} = \frac{2}{L_c} \sum_{n_c} M_{cap} \tag{7.3}$$

where $\sum_{n_c} M_{cap}$ is the sum of the moment capacity for each column in the pier, n_c is the number of columns in the pier, and L_c is the clear height of the columns. Equation (7.3) assumes that the moment capacities at the top and bottom of each column are equivalent.

The additional axial load in the columns (ΔP) due to overturning of the pier caused by the lateral load should be considered when M_{cap} is determined. Statics and symmetry can be used to determine ΔP in the exterior columns of a pier with three columns or less given the design force (F_d) acting on the pier. If the cap beam and foundations of the pier are assumed to be rigid and the columns both yield, Equation (7.4) can be used to determine F_d for two- and three-column piers.

$$\Delta P = \frac{F_d L_c}{2 d_c} \tag{7.4}$$

In Equation (7.4), d_c is the center-to-center spacing of the exterior pier columns. The lateral load (F_d) will increase the axial compression in one column and decrease it in the other. The moment capacity (M_{cap}) should then be determined for each column. In design, both columns should contain the same amount of reinforcement because of the load reversals associated with seismic loading.

The procedures for determining M_{cap} differ between the CIP emulation and hybrid columns because of differences in the detailing of the connection regions and the presence of post-tensioning in hybrid piers. Methods for determining the M_{cap} for both types of piers are presented in the following sections, along with evaluations of the estimates for F_{cap} obtained from sectional analysis. Example calculations for determining the F_{cap} of both the CIP emulation and hybrid piers using sectional analysis are presented in Appendix E.

7.4.1 CIP Emulation Piers

The moment capacity (M_{cap}) of the columns in a CIP emulation pier can be determined from analysis of the column cross-section by enforcing strain compatibility and internal force equilibrium. This approach is commonly used for the design of reinforced concrete members and is included in the AASHTO specifications (AASHTO 2002; AASHTO 2004).

The strain distribution through the cross-section is assumed to be linear, as shown in Figure 7.1. The ultimate compressive strain in the concrete (ε_{cu}) is specified to be

0.004. The distance from the extreme compressive face of the column to the neutral axis (c) is estimated. The forces in the mild steel reinforcing bars ($F_{ms,i}$) can be determined from the strain distribution and the constitutive model for steel, which is taken to be elastic-perfectly plastic.

The force in the concrete (F_c) is determined by using an equivalent uniform stress distribution (Mattock et al. 1961) to represent the stress in the concrete. The equivalent stress distribution has a magnitude of $0.85 f_c^{'}$ with a depth of

$$a = c\beta_1 \tag{7.5}$$

where:

$$\beta_1 = \begin{cases} 0.85 & for \quad f_c^{'} \le 4ksi \\ 0.85 - 0.05(f_c^{'} - 4) \ge 0.65 & for \quad f_c^{'} > 4ksi \end{cases} \tag{7.6}$$

and c is the depth of the neutral axis. The resultant force in the concrete (F_c) can be determined from the properties of the equivalent stress block and the geometry of the circular column as discussed by MacGregor (1997).

The axial loads on the column due to the weight of the superstructure (P_c) and the additional axial load due to overturning (ΔP) are assumed to act along the centroid of the column. The internal forces acting on the cross-section are shown in Figure 7.1.

The depth of the neutral axis (c) is varied until the internal forces acting on the cross-section are in axial equilibrium. After equilibrium is obtained, M_{cap} is determined by summing the moments caused by the internal forces.

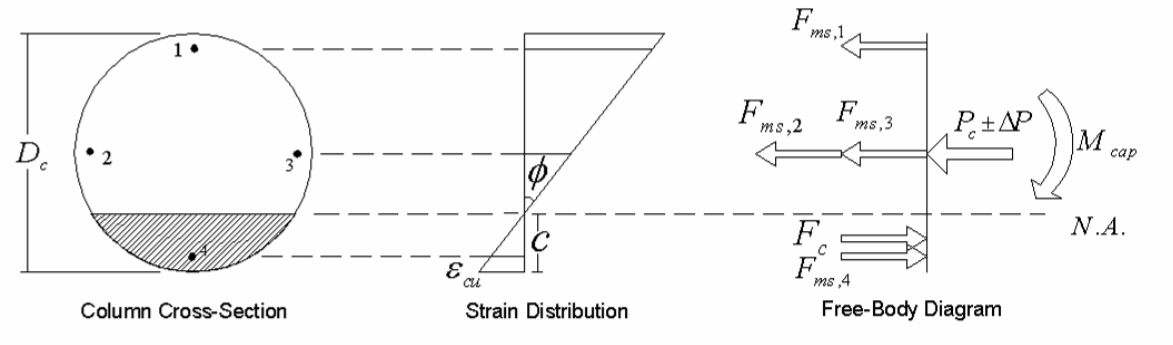

Figure 7.1: Strain Distribution and Free-Body Diagram of CIP Emulation Column Cross-Section

To determine whether the sectional analysis method can be used for the equivalent lateral force design of CIP emulation piers, values of F_{cap} calculated with the sectional analysis method ($F_{cap,sa}$) were compared to values of F_{cap} determined with the nonlinear analysis method ($F_{cap,nla}$)incorporating the critical-strain-capacity definition (Section 7.2). The values were compared for 108 CIP emulation piers that used all combinations of

- column diameter (D_c): 36 in., 48 in., and 60 in.
- column aspect ratio (L_c / D_c): 5, 6, and 7
- mild steel reinforcing ratio (ρ_s): 0.005, 0.01, 0.02, and 0.03
- normalized axial dead load ($\frac{P_c}{f_c' A_g}$): 0.05, 0.10, and 0.15.

Figure 7.2 shows the distribution of difference between $F_{cap,sa}$ and $F_{cap,nla}$. The ratio $\frac{F_{cap,sa}}{F_{cap,nla}}$ was determined for each pier and had a mean value of 1.01 with a coefficient of variation (COV) of 2.5 percent. The sectional analysis method provided accurate estimates of F_{cap} for the critical-strain-capacity definition, with 94 percent of all piers considered having a difference of between -4 percent and +4 percent. The calculations can be performed with a spreadsheet, which allows the ELFD procedure to remain simple and does not require nonlinear modeling.

Using the sectional analysis procedure for determining the F_{cap} of a CIP emulation pier in the DDBD procedure is not as simple because the DDBD procedure uses the target-displacement-capacity definition, whereas the sectional analysis method uses the critical-strain-capacity definition. If the piers exhibit significant post-yield stiffness, then the values determined for F_{cap} with the two definitions will not correlate well. However, if the post-yield stiffness of the piers is minimal then the values of F_{cap} will be similar, regardless of the capacity definition. This behavior was investigated by comparing values of $F_{cap,sa}$ to values of $F_{cap,nla}$ based on the target-displacement definition.

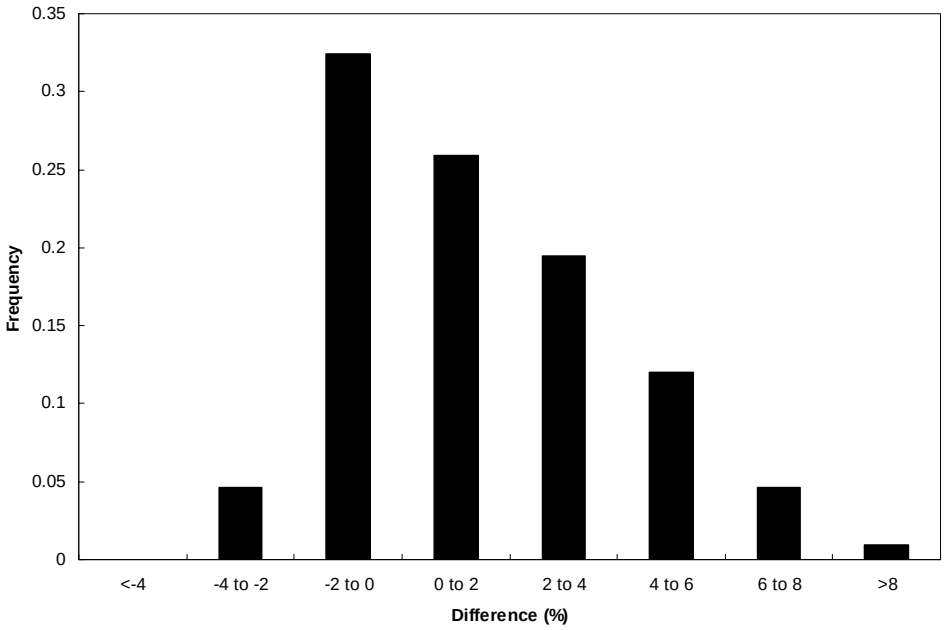

Figure 7.2: Distribution of Differences of F_{cap} Values for CIP Emulation Piers Using Critical-Strain-Capacity Definition

The differences between these values were determined for each of the 108 CIP emulation piers subjected to displacements corresponding to displacement ductilities (μ_Δ) of 1, 2, 3, 4, and 5. The distribution of differences is shown in Figure 7.3. The ratio $\frac{F_{cap,sa}}{F_{cap,nla}}$ was calculated for every pier with $\mu_\Delta \geq 2$ and had a mean value of 1.0 with COV of 5.6 percent. The sectional analysis method consistently over-estimates F_{cap} at $\mu_\Delta = 1$, because the pier has not reached its full capacity. However, at these low levels of μ_Δ, the amount of inelastic deformation in the piers is small, and excessive damage would not be expected even if the columns were slightly under strength. At larger levels of μ_Δ, equal to or greater than 2, it can be seen from Figure 7.3 that the differences are relatively small. Of all the piers examined for $\mu_\Delta \geq 2$, 91.5 percent had a difference of between -10 percent and +10 percent.

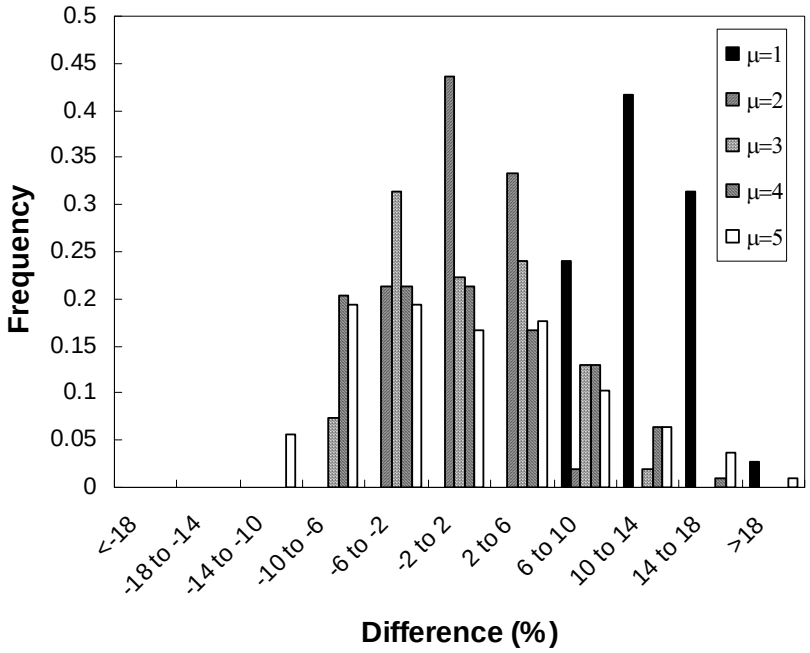

Figure 7.3: Distribution of Differences of F_{cap} Values for CIP Emulation Piers Using the Target-Displacement-Capacity Definition

A better estimate for F_{cap} based on the target-displacement-capacity definition could possibly be obtained from the sectional analysis method by considering the post-yield stiffness of the piers. However, such an estimate would be complicated because the post-yield stiffness is affected by a variety of factors, including the amount of reinforcing steel and the axial load on the pier. Because the differences obtained with the sectional analysis method above were not very large, it was desirable to maintain as much simplicity as possible in the sectional analysis method.

7.4.2 Hybrid Piers

The moment capacity of hybrid pier columns can be determined by considering the column-to-footing and column-to-cap beam interface regions. Only a portion of the mild reinforcing steel runs through the interface, causing that region to have a smaller capacity than the body of the columns.

The moment capacity (M_{cap}) of the interface can be determined by assuming that the column rotates as a rigid body about the footing and cap beam. The angle of rotation (θ) is determined from Δ_t and L_c. The depth of the neutral axis from the extreme compression face of the column (c) is estimated, resulting in the distribution of deformations shown in Figure 7.4.

The forces in the mild steel reinforcing bars ($F_{ms,i}$) can be determined by assuming that the deformation of a bar is evenly distributed along the unbonded length of the bar (L_{unb}) in the interface region. The mild steel bars are assumed to exhibit linear elastic-perfectly plastic stress-stain behavior.

The force in the post-tensioning tendons (F_p) is determined from the stress in the post-tensioning at Δ_t. The initial stress in the post-tensioning tendons (f_{p0}) is determined so that the tendons will not yield before the pier reaches Δ_t. The initial stress (f_{p0}) in the tendons should also not exceed any code-specified initial stress limitations (f_{pi}). The stress in the post-tensioning tendon at Δ_t can then be found by combining f_{p0} and the change in stress caused by deformation of the tendon at Δ_t.

The compressive force in the concrete (F_c) is determined by using the equivalent stress distribution as described for CIP emulation piers above. The calculation of F_c assumes that plane sections remain planar, which is not necessarily accurate for hybrid columns. However, experimental testing of similar hybrid connections in building structures has shown that the assumption that plane sections remain planar is be adequate for calculating flexural capacity (Stanton and Nakaki 2002) The axial loads on the pier ($P_c \pm \Delta P$) are also considered in the same manner as those for CIP emulation piers. The internal forces acting on the interface region are shown in Figure 7.4.

The depth of the neutral axis (c) that results in internal force equilibrium can be determined by using iteration. The moment capacity (M_{cap}) can then be determined by combining the moment contribution from each of the internal forces.

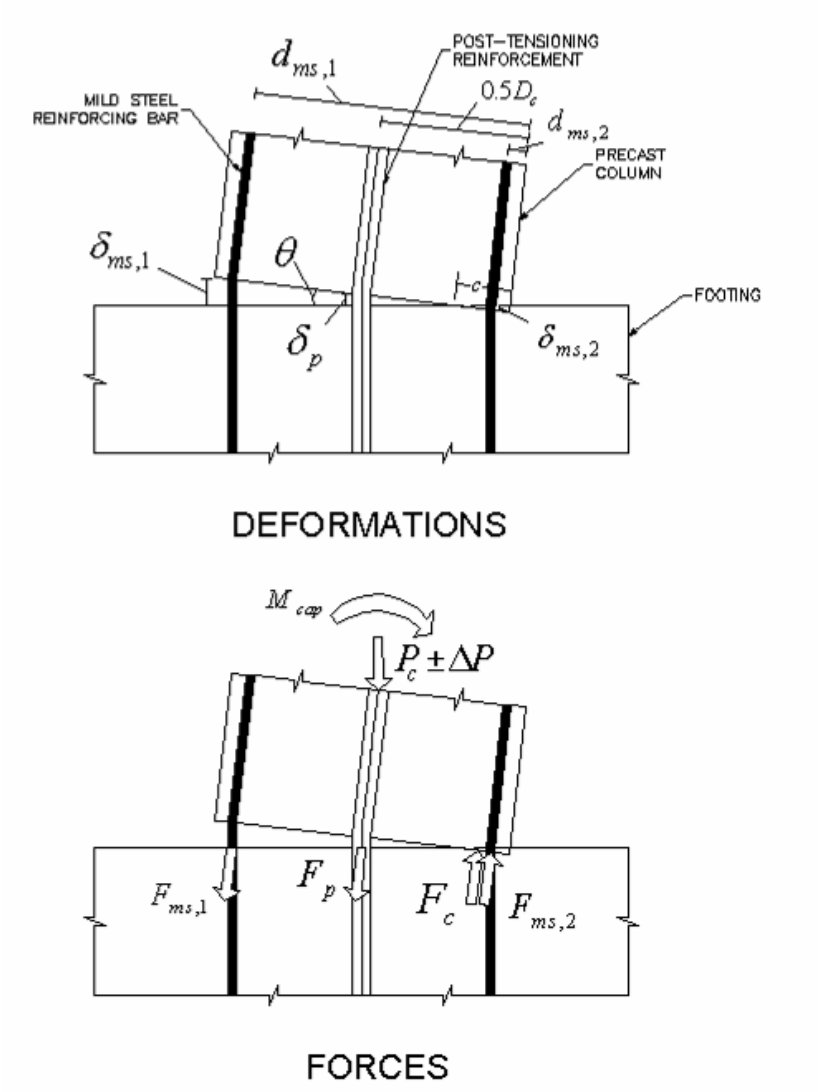

Figure 7.4: Deformation of and Internal Forces Acting on the Interface Region

Because the sectional analysis method for determining the F_{cap} of a hybrid pier is based on the target-displacement-capacity definition, it is best suited for use in the DDBD procedure. The sectional analysis estimates for F_{cap} ($F_{cap,sa}$) were compared to estimates of F_{cap} obtained with the nonlinear analysis method ($F_{cap,nla}$) based on the target-displacement-capacity definition (Section 7.2). The values were compared for 168 hybrid piers consisting of combinations of the following variables:

- column diameter (D_c): 36 in., 48 in., and 60 in.

- column aspect ratio (L_c/D_c): 5, 6, and 7
- mild steel reinforcing ratio (ρ_s): 0.008, 0.012, and 0.016
- post-tensioning reinforcing ratio (ρ_p): 0.0005, 0.0016, 0.0028
- normalized axial dead load ($\frac{P_c}{f_c' A_g}$): 0.05 and 0.10.

The values of $F_{cap,sa}$ and $F_{cap,nla}$ were compared at pier displacements corresponding to a μ_Δ of 1, 2, 3, 4, and 5. The ratio $\frac{F_{cap,sa}}{F_{cap,nla}}$ was calculated for every pier with $\mu_\Delta \geq 2$ and found to have a mean of 0.99 with COV of 2.3 percent. The distribution of differences of $F_{cap,sa}$ to $F_{cap,nla}$ for each level of μ_Δ is shown in Figure 7.5. It can be seen that although the sectional analysis method significantly overestimates F_{cap} for μ_Δ = 1, it provides good estimates for μ_Δ equal to or greater than 2, with 94 percent of all piers examined having a difference of between -6 percent and +6 percent.

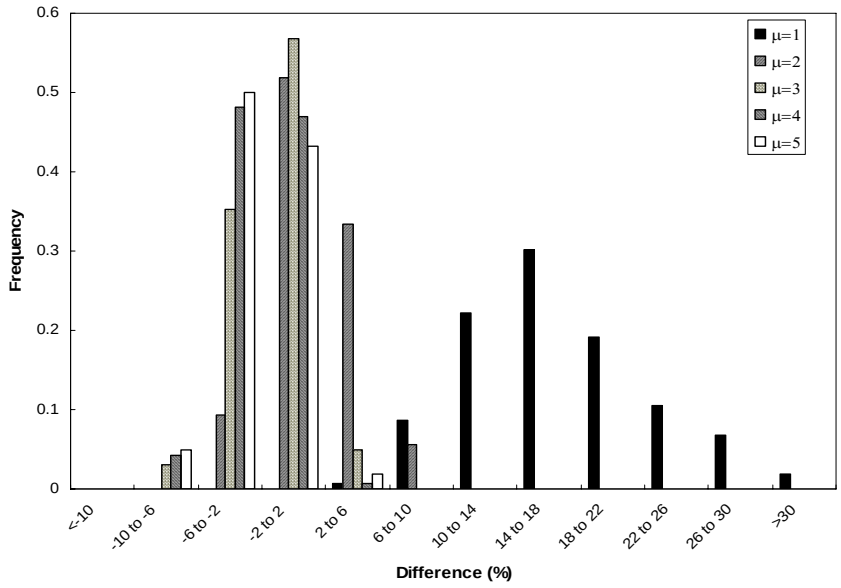

Figure 7.5: Distribution of Difference of F_{cap} Values for the DDBD Procedure for Hybrid Piers

The reason for the disparity at μ_Δ equal to 1 is believed to be because the equivalent uniform stress block used to represent the compressive stress distribution in the concrete is not a good approximation at low levels of deformation at which the stress in the concrete is considerably less than $f_c^{'}$. Although this overestimation could lead to unconservative designs at low levels of ductility, few piers are designed for low levels of ductility, and those that are experience little inelastic deformation. Accordingly, their structural safety will not be jeopardized by being slightly under strength.

The ELFD procedure uses the critical-strain-capacity definition for F_{cap}. This complicates the use of the sectional analysis method for equivalent lateral force design of hybrid piers because the sectional analysis method determines F_{cap} with the target-displacement-capacity definition. However, if the piers do not exhibit significant post-yield stiffness, the values of F_{cap} based on both definitions will be similar, and the sectional analysis method can be used to estimate F_{cap} for the equivalent lateral force design of hybrid piers. To check this assumption, $F_{cap,sa}$ was calculated for target displacements corresponding to pier drifts of 0.5, 1.0, 1.5, and 2.0 percent and compared to estimates of $F_{cap,nla}$ based on the critical-strain-capacity definition. The pier displacements were based on the drift ratio rather than μ_Δ because μ_Δ is not determined in the ELFD procedure. The ratio $\frac{F_{cap,sa}}{F_{cap,nla}}$ was computed for every pier with drift > 1 percent and found to have a mean value of 0.99 with a COV of 1.5 percent. The distribution of differences of the values is shown in Figure 7.6. Over 90 percent of the piers had a difference of between -3 percent and +3 percent for levels of drift greater that 1 percent. This confirms that the sectional analysis method can be used for the equivalent lateral force design of hybrid piers. This research used 2 percent drift when determining the F_{cap} of hybrid piers in the ELFD procedure.

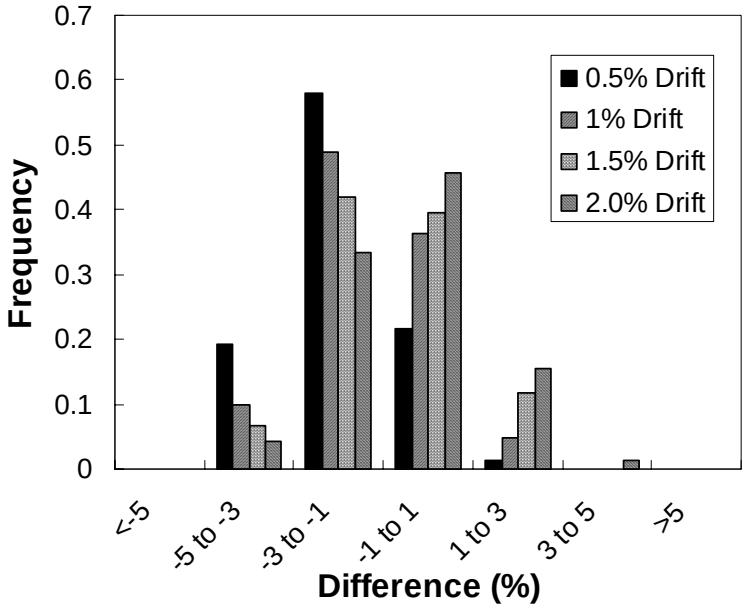

Figure 7.6: Distribution of Difference of F_{cap} Values for the ELFD Procedure for Hybrid Piers

7.5 RECENTERING REQUIREMENTS FOR HYBRID PIERS

An additional requirement in the design of hybrid piers is specifying the proportion of mild steel reinforcement to post-tensioning reinforcement. Greater proportions of mild steel will increase the amount of energy that the pier dissipates, reducing the maximum displacement, while greater amounts of post-tensioning will increase the ability of the pier to re-center after an earthquake, reducing the residual displacement. The designer has the ability to adjust the proportion of mild steel to post-tensioning to achieve the desired pier performance. It is recommended that at least enough post-tensioning be provided to ensure that the pier self-centers after an earthquake.

The recentering ability of a pier is determined by considering the restoring and resisting forces acting on the pier after an earthquake. The mild steel reinforcing bars, which yield when the pier is displaced to Δ_t, provide a resisting force ($F_{ms0,i}$) because they must be forced to yield in order to return to their original length. The force provided by the bars is equal to and opposite of the force in the bars when the pier is displaced to the target displacement. Reinforcing bars near the neutral axis that do not yield are

assumed to provide no resisting force because they will elastically return to their original length.

The restoring forces on the pier are assumed to come from the unbonded post-tensioning (F_{p0}) and the weight of the superstructure on the pier (P_c). The stress in the post-tensioning is assumed to be f_{p0} when recentering is examined. The displacement of the pier is assumed to not exceed the critical limit at which P_c becomes a resisting force rather than a restoring force. The compressive force in the concrete (F_{c0}) is also a restoring force and is determined by using the equivalent stress distribution, as discussed above. The internal forces on the cross-section that affect recentering are shown in Figure 7.7.

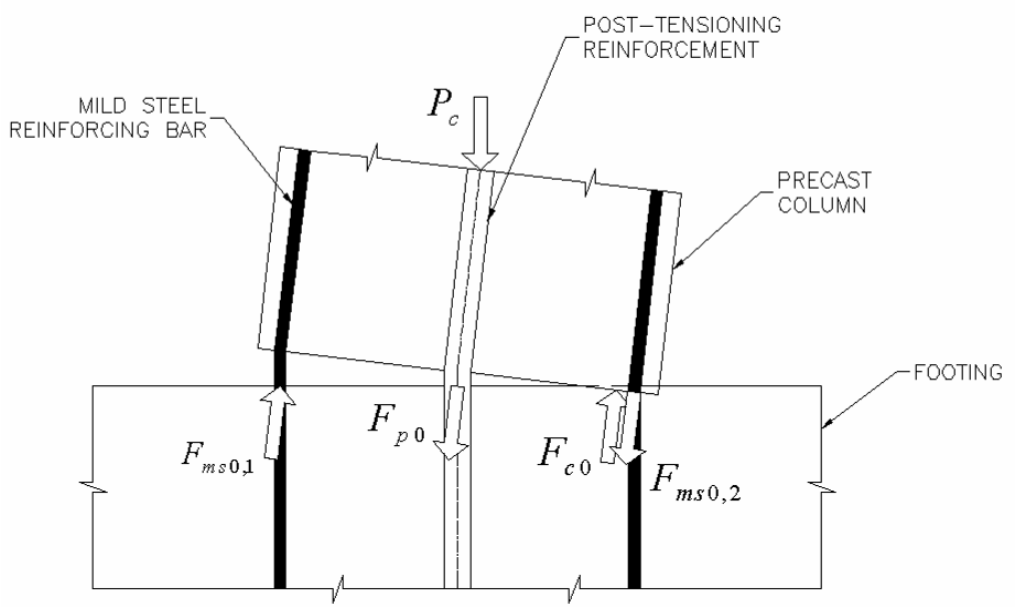

Figure 7.7: Forces on Hybrid Pier Column When Recentering Is Assessed

The depth of the neutral axis (c) is determined by using iteration so that the internal forces are in equilibrium. The moments caused by the resisting and restoring forces about the neutral axis are then determined. If the total restoring moment is greater than the total resisting moment, the column is expected to recenter. A more detailed examination of the recentering properties of hybrid systems is presented by Stanton and Nakaki (2002).

CHAPTER 8
VALIDATION OF THE DDBD DISPLACEMENT ESTIMATES

The accuracy of the displacement estimates from three formulations of the direct displacement-based design (DDBD) procedure (Section 3.2) are investigated in this chapter. The performance of piers designed with the DDBD procedures depends directly on the selected target displacement. If the maximum displacement (Δ_{max}) that occurs during an earthquake is larger than the target displacement (Δ_t) selected in design, the pier will likely experience more damage than intended. The DDBD procedures must be validated to ensure that Δ_{max} is similar in magnitude to Δ_t so that the amplitude of the displacement and, accordingly, the extent of the damage incurred is similar to that intended by the designer.

The following three formulations of the DDBD procedure were considered in the validation study:

- Iterative procedure (Section 3.2.1) with
    - yield displacement determined with the nonlinear analysis method (Section 4.1)
    - equivalent viscous damping ratio determined with the nonlinear analysis method (Section 5.2)
    - pier capacity determined with the nonlinear analysis method (Section 7.3)
- Iterative procedure (Section 3.2.1) with
    - yield displacement determined with the equation-based method (Section 4.3 and Section 4.4)
    - equivalent viscous damping ratio determined with the equation-based method (Section 5.3)
    - pier capacity determined with the sectional analysis method (Section 7.4)
- Direct (Non-iterative) procedure (Section 3.2.2) with
    - equivalent viscous damping ratio determined with the empirical method (Section 5.4)
    - pier capacity determined with the sectional analysis method (Section 7.4).

The use of these three formulations allowed the accuracy of both the iterative (Section 3.2.1) and direct (Section 3.2.2) DDBD procedures to be examined and compared. The effect of using the different methods for determining values needed in design could also be examined.

One way to validate the DDBD procedures is to design a pier for a selected Δ_t. The average maximum displacement ($\overline{\Delta}_{max}$) of the pier is then determined by averaging the results of five nonlinear dynamic analyses (Appendix A) with different ground motions and comparing them to Δ_t. The ground motions are scaled to match the design response spectrum specified by AASHTO (AASHTO 2002; AASHTO 2004), as discussed in Appendix B. Although this procedure is straightforward, it requires nonlinear dynamic analysis, which is time consuming. A less computationally intensive way of evaluating the DDBD procedures would be to determine the target displacement (Δ_t) needed to achieve $\overline{\Delta}_{max}$. The target displacement (Δ_t) required to obtain a given $\overline{\Delta}_{max}$ for a pier can be found by working backwards through the DDBD procedures. The main advantage of this method is that the results of previously performed analyses can be used to perform the validation, eliminating the need for further nonlinear analyses. This approach was used in this study.

The displacement predictions from the DDBD procedures were evaluated on the basis of the ratio $\overline{\Delta}_{max}/\Delta_t$. The data from Section 6.2 were used to determine values of $\overline{\Delta}_{max}/\Delta_t$, eliminating the need for further nonlinear analysis. Using these data provided 108 $\overline{\Delta}_{max}/\Delta_t$ values for CIP emulation piers and 162 $\overline{\Delta}_{max}/\Delta_t$ values for hybrid piers.

8.1 EVALUATION OF THE ITERATIVE PROCEDURE USING NONLINEAR ANALYSIS

The distribution of $\overline{\Delta}_{max}/\Delta_t$ versus displacement ductility (μ_Δ) for the iterative procedure (Section 3.2.1) using nonlinear analysis methods is shown in Figure 8.1 for CIP emulation and hybrid piers. The mean value of $\overline{\Delta}_{max}/\Delta_t$ is 1.01 with a coefficient of variation (COV) of 6.3 percent for CIP emulation piers and 1.01 with a COV of 6.6 percent for hybrid piers. The fact that the ratio $\overline{\Delta}_{max}/\Delta_t$ is near unity at all levels of μ_Δ

for both types of piers shows that the iterative DDBD procedure using nonlinear analysis methods meets the goal of enabling an engineer to design a pier to reach a specific Δ_t. The COV is slightly larger for the hybrid piers. This increase likely occurred because the β relationship used for hybrid piers (Equation 6.10) is not as precise as the β relationship used for CIP emulation piers (Equation 6.9).

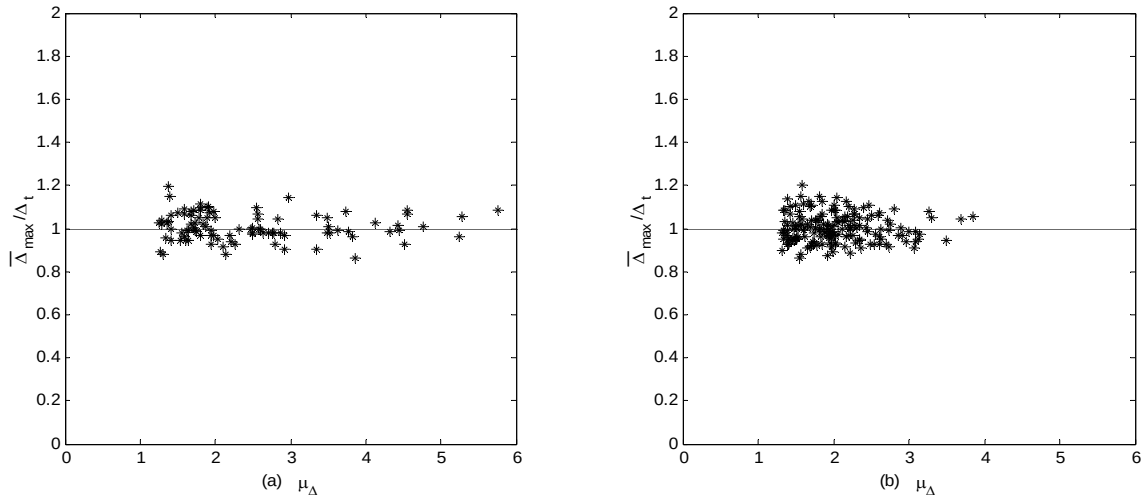

Figure 8.1: Distribution of $\overline{\Delta}_{max}/\Delta_t$ from Iterative Procedure using Nonlinear Analysis Methods: (a) CIP Emulation Piers (b) Hybrid Piers

The ratio Δ_{max}/Δ_t was determined for each pier and ground motion combination considered and is shown Figure 8.2 for CIP emulation and hybrid piers to evaluate the increased variability in results when the response of piers to individual ground motion acceleration records is considered. The mean value of Δ_{max}/Δ_t is 1.01 with a COV of 21.1 percent for CIP emulation piers and 1.04 with a COV of 18.9 percent for hybrid piers. There is a considerably larger amount of scatter in the Δ_{max}/Δ_t values than the $\overline{\Delta}_{max}/\Delta_t$ values, which illustrates the large influence on Δ_{max} of variations in ground motions.

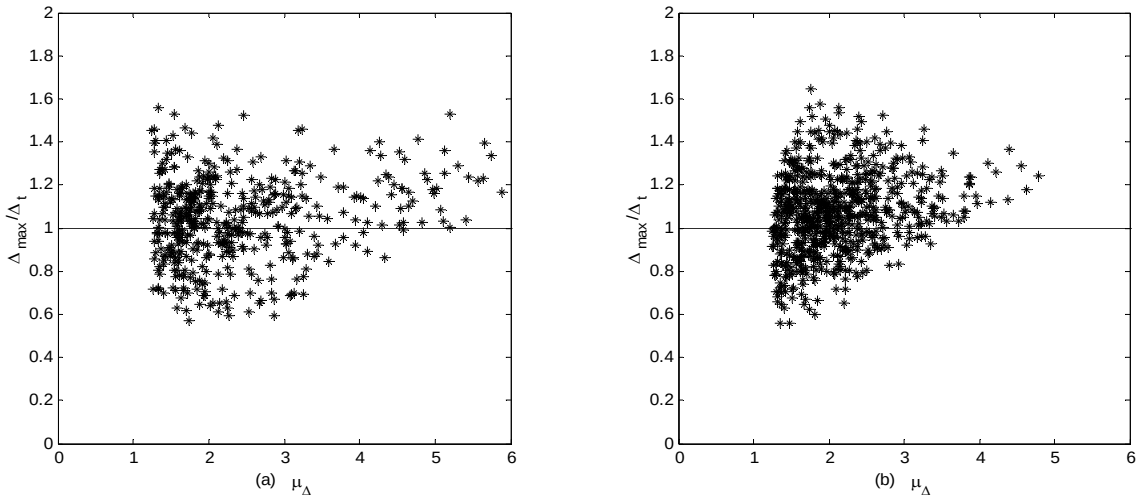

Figure 8.2: Distribution of Δ_{max}/Δ_t : (a) CIP Emulation Piers (b) Hybrid Piers

The DDBD procedure is formulated to ensure that the pier reaches Δ_t during the design earthquake. The fact that the average Δ_{max}/Δ_t in Figure 8.2. is close to 1.0 is a measure of the formulation's success. However, a designer is likely to be more interested in the maximum probable displacement, rather than the average displacement. This could be achieved by designing for a reduced Δ_t, which is selected so that it has a small, user-defined probability of being exceeded. One possibility is to select the reduction factor as the inverse of the mean value plus one standard deviation of the ratio Δ_{max}/Δ_t. This is, coincidentally, 1.23 for both the CIP emulation and hybrid piers. If the target displacement (Δ_t) is divided by this factor, 1.23, the probability of exceeding Δ_t in a design-level earthquake is approximately 15 percent.

8.2 EVALUATION OF ITERATIVE PROCEDURE USING EQUATION-BASED METHODS

The distribution of $\overline{\Delta}_{max}/\Delta_t$ obtained with the iterative procedure (Section 3.2.1) using equation-based methods is shown in Figure 8.3 for CIP emulation and hybrid piers. The ratio $\overline{\Delta}_{max}/\Delta_t$ has a mean value of 1.15 with a COV of 9.3 percent for CIP emulation piers and 1.05 with a COV of 7.8 percent for hybrid piers. Many of the values of $\overline{\Delta}_{max}/\Delta_t$ are slightly greater than unity, which signifies that the iterative procedure using

equation-based methods is slightly unconservative. Piers designed with the procedure will likely have a $\overline{\Delta}_{\max}$ slightly larger than the chosen Δ_t. For CIP emulation piers, the procedure is most unconservative at low levels of μ_Δ, which is acceptable because well-confined bridge piers are rarely designed for low levels of μ_Δ. At larger ductilities the procedure leads to a $\overline{\Delta}_{\max}$ value that is close to Δ_t.

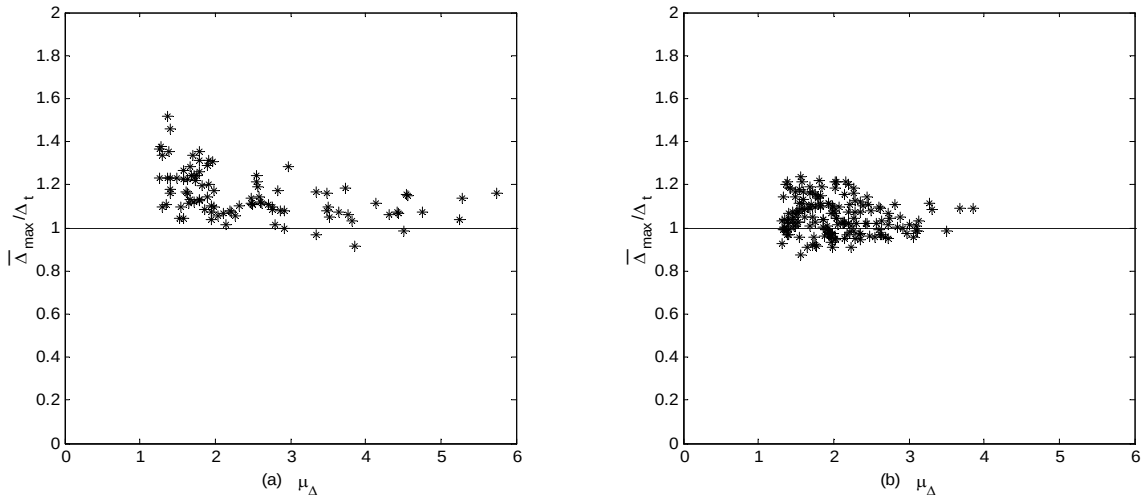

Figure 8.3: Distribution of $\overline{\Delta}_{\max}/\Delta_t$ from Iterative Procedure Using Equation-Based Methods: (a) CIP Emulation Piers (b) Hybrid Piers

It is difficult to ascertain why the iterative procedure using equation-based methods produces slightly unconservative designs because many values, including the yield displacement (Δ_y) and the equivalent viscous damping (ξ_{eq}), are estimated. Some error is involved with each estimate, and the errors can compound in the design procedure. In this situation, it is believed that the yield displacement is under-estimated. The smaller yield displacement estimates lead to larger estimates of μ_Δ, which results in over-estimation of the effective equivalent damping ($\hat{\xi}_{eq}$). Over-estimating $\hat{\xi}_{eq}$ reduces the predicted maximum displacement of the pier, causing the design to be unconservative.

8.3 EVALUATION OF DIRECT PROCEDURE USING EQUATION-BASED METHODS

The distribution of $\overline{\Delta}_{\max}/\Delta_t$ for CIP emulation and hybrid piers designed with the direct procedure (Section 3.2.2) using equation-based methods is shown in Figure 8.4. The $\overline{\Delta}_{\max}/\Delta_t$ values are compared to drift ($\overline{\Delta}_{\max}/L_c$) rather than μ_Δ because μ_Δ is not determined when the direct procedure is used. The mean value of $\overline{\Delta}_{\max}/\Delta_t$ is 1.11 with a COV of 12.1 percent for CIP emulation piers and 1.13 with a COV of 8.4 percent for hybrid piers. The COV values obtained with the direct procedure are larger than those from the iterative procedure (Section 8.1 and 8.2), indicating an increased amount of scatter. This increase in scatter likely occurred because the empirical method (Section 5.4) used to estimate ξ_{eq} in the direct procedure is less accurate than the nonlinear analysis method (Section 5.2) or the equation-based method (Section 5.3) used in the iterative procedures.

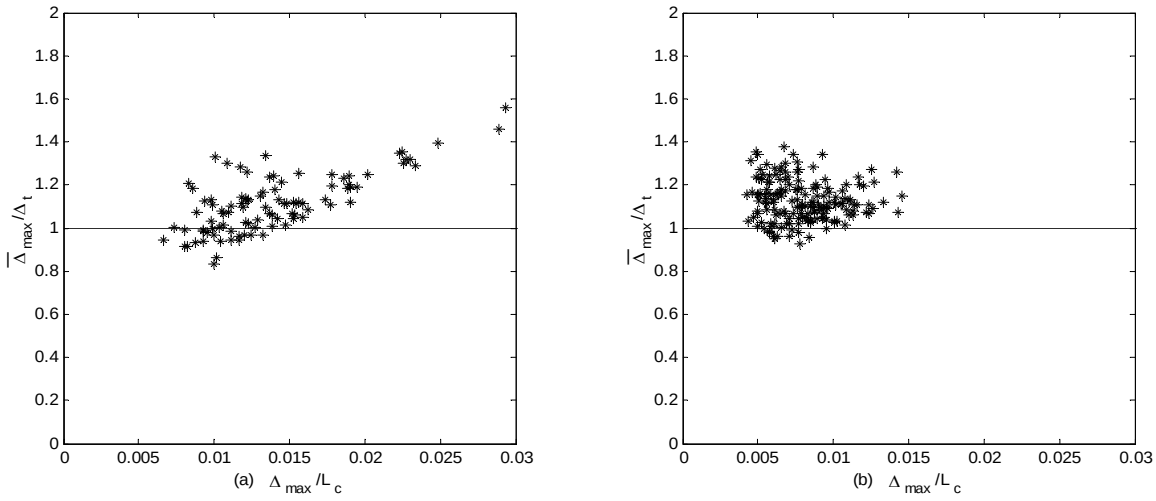

Figure 8.4: Distribution of $\overline{\Delta}_{\max}/\Delta_t$ from Direct Procedure using Equation-Based Methods: (a) CIP Emulation Piers (b) Hybrid Piers

The piers designed with the direct procedure appear to be increasingly unconservative as drift increases. The piers in this region are lightly reinforced, and further investigation would be needed to determine the cause of this trend and its effect on design. It is likely that the direct procedure could be significantly improved by improving the method for estimating ξ_{eq} (Section 5.4).

The direct procedure is inherently less robust than the iterative procedure and should not be used for columns with aspect ratios (L_c/D_c) outside the range of 5 to 7 for which the procedures were calibrated. This is explained by the fact that the damping was implicitly assumed to be independent of L_c/D_c. While this appears to be an acceptable assumption within the range of L_c/D_c considered here, it is possible to envision a slender column that would remain elastic and provide no damping, while the direct procedure would estimate the column to have a large amount of damping.

8.4 RECOMMENDATIONS

The mean value and COV of $\overline{\Delta}_{max}/\Delta_t$ for CIP emulation and hybrid piers determined for the three formulations of the DDBD procedure considered in this chapter are summarized in Table 8.1.

Table 8.1: Statistics for Distribution of $\overline{\Delta}_{max}/\Delta_t$ for Formulations of the DDBD Procedure

	CIP Emulation Piers		Hybrid Piers	
	Average	COV (%)	Average	COV (%)
Iterative Procedure using Nonlinear Analysis Method	1.01	6.3	1.01	6.6
Iterative Procedure using Equation-Based Methods	1.16	9.3	1.05	7.8
Direct Procedure using Equation-Based Methods	1.11	12.1	1.13	8.4

Of the procedures considered, the iterative procedure using nonlinear analysis methods (Section 8.1) produces the most accurate displacement estimates. However, it is also the most time consuming because it requires nonlinear analysis to be performed multiple times in an iterative procedure.

The iterative procedure using equation-based methods (Section 8.2) is easier to apply and also produces accurate displacement predictions, although $\overline{\Delta}_{max}$ tends to be slightly larger than Δ_t. The slight increase in $\overline{\Delta}_{max}$ over Δ_t may lead to slightly larger amounts of damage than anticipated by the designer. The expected increase in the maximum displacement is also well within the scatter of maximum displacements that can be caused by the individual ground motions. The iterative procedure using equation-based methods could be implemented quickly by using a computer spreadsheet program.

The direct procedure using equation-based methods (Section 8.3) is the easiest of the three formulations to apply. The displacement estimates obtained using the procedure, however, have the largest amount of scatter of the three procedures considered, and the range of L_c/D_c for which it can be used is limited. The direct procedure displacement estimates at large levels of drift also warrant further investigation. Improvements could be made to the direct procedure to reduce the scatter in the displacement predictions. The ease with which the direct procedure can be applied make it an attractive preliminary design tool for determining, with little effort, the appropriate column diameter and number of columns required for a pier.

CHAPTER 9
EVALUATION OF THE ELFD PROCEDURE

In this chapter, the equivalent lateral force design (ELFD) procedure is evaluated to ensure that piers designed with it are neither overly conservative nor prone to excessive damage during a design-level earthquake. To evaluate whether the ELFD procedure results in acceptable designs for typical pier configurations, the procedure was applied to design 12 piers comprising all combinations of

- column aspect ratio (L_c/D_c): 5, 6, and 7
- normalized axial dead load ($P_c/f_c^{'}A_g$): 0.05, 0.10, 0.15, and 0.20
- column diameter (D_c): 48 in.

The performance of the piers was evaluated on the basis of the likelihood of damage occurring during a design-level earthquake. The design-level earthquake was defined according to the AASHTO specifications (AASHTO 2002; AASHTO 2004) and corresponds to a peak ground acceleration with a 10 percent probability of exceedance in 50 years. The expected maximum displacement (Δ_{max}) of each pier was determined for the five design-level earthquakes presented in Appendix F using dynamic nonlinear analysis (Appendix A). The five ground motions were considered to account for variation in the response of a pier resulting from variations in the ground-motion acceleration records. Damage models were then used to assess the expected damage resulting from displacing the pier to Δ_{max}.

The performance of the piers was evaluated by using population-based and individual pier-based representations. The population-based representation considered the percentage of piers in a population likely to exceed certain amounts of damage. The individual pier-based representation examined changes to the amount of damage to a pier from varying L_c/D_c and $P_c/f_c^{'}A_g$.

9.1 DAMAGE ESTIMATION METHODS

Pier designs were evaluated for several damage states, including the onset of cover concrete spalling, buckling of the longitudinal reinforcing bars, and fracture of the longitudinal reinforcing bars.

The probability of cover concrete spalling occurring (P_{spall}) was estimated by using an approach developed by Berry and Eberhard (2004). On a the basis of regression analysis of test results of 40 spiral-reinforced circular columns and 62 rectangular columns in the PEER column database (PEER 2005), Berry and Eberhard (2004) determined that the drift at the onset of cover spalling ($\frac{\Delta_{spall,calc}}{L_c}$) can be estimated with Equation (9.1).

$$\frac{\Delta_{spall,calc}}{L_c}(\%) \cong 1.6\left(1-\frac{P_c}{f_c^{'}A_g}\right)\left(1+\frac{1}{10}\frac{L_c}{D_c}\right) \tag{9.1}$$

The ratio of experimental displacement at the onset of spalling to displacement at the onset of spalling calculated with Equation (9.1) ($\frac{\Delta_{spall}}{\Delta_{spall,calc}}$) for the columns in the database had a mean value of 1.07 and a coefficient of variation (COV) of 35.2 percent. The probability of cover spalling (P_{spall}) at the maximum displacement (Δ_{max}) achieved during an earthquake could then be estimated as follows.

$$P_{spall} = \Phi\left(\frac{\frac{\Delta_{max}}{1.07\Delta_{spall,calc}}-1}{0.352}\right) \tag{9.2}$$

where Φ is the cumulative density function for a normal distribution, which relates the standard normal variable and probability of not being exceeded.

Although Equation (9.1) was developed for cast-in-place reinforced concrete columns, the same equation was applied to hybrid columns. It was unclear whether the additional axial load on the hybrid columns due to the vertical prestressing should be included in Equation (9.1), because insufficient experimental test data exist to develop an equation for predicting the occurrence of spalling in hybrid columns. The additional axial load was omitted in spalling calculations in this study.

The probability of longitudinal reinforcing bar buckling (P_{bb}) was also determined from the work of Berry and Eberhard (2004). From regression analyses of tests of 42 spiral-reinforced circular columns and 62 rectangular columns, they proposed that the drift at the onset of bar buckling ($\frac{\Delta_{bb,calc}}{L_c}$) could be estimated with:

$$\frac{\Delta_{bb,calc}}{L_c}(\%) = 3.25\left(1 + k_e\rho_{eff}\frac{d_b}{D_c}\right)\left(1 - \frac{P_c}{f_c^{'}A_g}\right)\left(1 + \frac{1}{10}\frac{L_c}{D_c}\right) \tag{9.3}$$

In Equation (9.3), k_e is 150 for spiral-reinforced columns, d_b is the diameter of the reinforcing bars, and ρ_{eff} is the effective confinement ratio:

$$\rho_{eff} = \frac{\rho_t f_{yt}}{f_c^{'}} \tag{9.4}$$

where ρ_t is the volumetric reinforcing ratio of the transverse reinforcement and f_{yt} is the yield strength of the transverse reinforcement. For the 42 spiral-reinforced circular column tests, the ratio of experimental displacement at the onset of bar buckling to the calculated displacement at the onset of bar buckling ($\frac{\Delta_{bb}}{\Delta_{bb,calc}}$) had a mean of 0.97 and a COV of 24.6 percent. The probability of bar buckling (P_{bb}) at $\Delta_{\max}$ is then:

$$P_{bb} = \Phi\left(\frac{\frac{\Delta_{\max}}{0.97\Delta_{bb,calc}} - 1}{0.246}\right) \tag{9.5}$$

Because of the lack of hybrid column test data, the estimated drift at the onset of bar buckling for a hybrid pier was assumed to be the same as that for a CIP emulation pier. The additional axial load in the columns of hybrid piers due to the vertical prestressing was not included in the calculations of P_{bb} .

The damage relationships presented by Berry and Eberhard (2004) were developed from the experimental results of tests of single columns. In this research, it was assumed that damage in multi-column piers would be similar to that of a single column for a given drift level. Because the cap beam and foundations were assumed to be rigid in this research, the columns were assumed to behave as if they have fixed-end

conditions, which is consistent with the use of the damage estimates proposed by Berry and Eberhard (2004).

Longitudinal reinforcing bar fracture was evaluated by determining the expected maximum strain in the extreme longitudinal bar (ε_{max}) with a static pushover analysis to Δ_{max}. The strain at which longitudinal bars will fracture varies greatly and depends on the bar quality, bar size, and other factors. It is particularly sensitive to load history, in that the probability of bar fracture increases significantly if buckling has occurred in previous cycles. In monotonically loaded specimens, bar fracture typically occurs between tensile strains of 0.05 and 0.12 (MacGregor 1997). This study conservatively assumed that bars would fracture at a strain of 0.05.

9.2 PARAMETERS CONSIDERED IN THE ELFD EVALUATION

The amount of damage incurred by piers designed with the ELFD procedure is affected by the response modification factor (R). The AASHTO specifications (AASHTO 2002; AASHTO 2004) recommend using R factors of 1.5 for "critical" bridges, 3.5 for "essential" bridges, and 5.0 for "other" bridges when columns are designed for flexural forces. A drawback of the ELFD method is that it is not clear how much damage will occur for a pier designed with a given R. The amount of damage expected to occur for a population of piers designed with certain R factors should be determined to ensure that the procedure leads to economical designs with a level of damage that is acceptable.

Because the R value is independent of the characteristics of the pier, it is possible that two piers designed with the same R value will experience different amounts of damage. The variation in amount of damage for a variety of pier characteristics should be determined to ensure that no piers are designed inappropriately.

The following sections present the amount of damage expected for a population of piers designed with the ELFD procedure for three values of R. The variation in the amount of damage for piers with varying L_c/D_c and $P_c/f_c^{'}A_g$ is also presented to assess whether variations in the R factors to account for pier characteristics are required. The expected damage to both the CIP emulation and hybrid piers is examined and compared to determine whether different R values are warranted for the different types of piers.

Because a fixed column diameter (D_c) and number of columns (n_c) were used for all of the piers considered, some of the designs contained amounts of reinforcement outside the range typically used in practice. The amount of reinforcement required in the design of both the CIP emulation and hybrid piers for all three values of R is shown in Table 9.1. In practice, D_c and/or n_c would be altered to produce designs that have more reasonable amounts of reinforcement. No limitations were placed on the amount of reinforcing steel in the primary evaluation for the ELFD procedure to reduce the number of variable pier characteristics that needed to be considered.

Table 9.1: Reinforcing Ratio for Piers Designed with the ELFD Procedure

				CIP Emulation Piers			Hybrid Piers		
				R = 1.5	R = 3.5	R = 5.0	R = 1.5	R = 3.5	R = 5.0
Pier No.	D_c (in)	L_c/D_c	P_c/f'_cA_g	ρ_s	ρ_s	ρ_s	ρ_{eq}	ρ_{eq}	ρ_{eq}
1	48	5	0.05	0.0130	0.0026	0.0004	0.0142	0.0026	0.0004
2	48	5	0.1	0.0361	0.0088	0.0031	0.0528	0.0097	0.0033
3	48	5	0.15	0.0616	0.0164	0.0069	0.1194	0.0210	0.0080
4	48	5	0.2	0.0981	0.0293	0.0143	0.2407	0.0470	0.0198
5	48	6	0.05	0.0170	0.0041	0.0014	0.0191	0.0042	0.0014
6	48	6	0.1	0.0361	0.0088	0.0031	0.0527	0.0097	0.0033
7	48	6	0.15	0.0616	0.0163	0.0069	0.1205	0.0211	0.0080
8	48	6	0.2	0.0981	0.0293	0.0143	0.2499	0.0471	0.0198
9	48	7	0.05	0.0177	0.0043	0.0016	0.0201	0.0044	0.0016
10	48	7	0.1	0.0361	0.0088	0.0032	0.0527	0.0098	0.0033
11	48	7	0.15	0.0616	0.0163	0.0069	0.1220	0.0211	0.0081
12	48	7	0.2	0.0981	0.0292	0.0143	0.2585	0.0471	0.0198

Statistics representing the amount of damage expected to occur in the population are expressed for both the entire population and a subset of the population consisting of piers with reasonable amounts of reinforcement expected to be used in practice. In this study, a reasonable amount of reinforcement was assumed to correspond to a reinforcing ratio of between 0.005 and 0.03. This was done to ensure that the amounts of damage predicted were not skewed by piers with unreasonable amounts of reinforcement that would not be used in practice. The effects of implementing a lower bound on the amount of reinforcement are discussed in Section 9.8.

Sample calculations for designing piers with the ELFD procedure are provided in Appendix C.

9.3 REINFORCEMENT RATIO

The reinforcing ratio required for each pier configuration and R value is shown in Figure 9.1 for the CIP emulation and hybrid piers. An equivalent reinforcing ratio (ρ_{eq}), defined by Equation (9.6), is used for the hybrid piers to allow for comparison.

$$\rho_{eq} = \frac{\rho_s f_y + \rho_p f_{py}}{f_y} \tag{9.6}$$

where ρ_s is the mild steel reinforcing ratio, f_y is the yield strength of the mild steel reinforcement, ρ_p is the reinforcing ratio of the post-tensioning reinforcement, and f_{py} is the yield strength of the post-tensioning reinforcement.

In Figure 9.1, the required reinforcing ratio is significantly larger for small values of R. The design force is increased by a factor of 3.33 when R = 1.5 is used in design as opposed to R = 5.0, but the required amount of reinforcing steel increases by about 11 times on average. The amount of reinforcing steel required increases with $P_c / f_c^{'} A_g$ because of the greater inertial forces created by the larger seismic mass. The aspect ratio (L_c / D_c) has little effect on the required amount of reinforcement. This can be attributed to an offsetting effect, in that increasing the aspect ratio increases the period of vibration reducing the design forces, but at the same time it increases the lever arm of the column moments. The design acceleration response spectrum used in the AASHTO specifications (AASHTO 2002; AASHTO 2004) causes the two effects to compensate for each other exactly, making the amount of reinforcement independent of the aspect ratio, unless the period of vibration (T) of the pier is small and falls in the constant acceleration region of the design acceleration response spectrum. This occurs for piers with small axial loads, explaining the slight variations in the required reinforcing ratio for different L_c / D_c values at low values of $P_c / f_c^{'} A_g$, as shown in Figure 9.1.

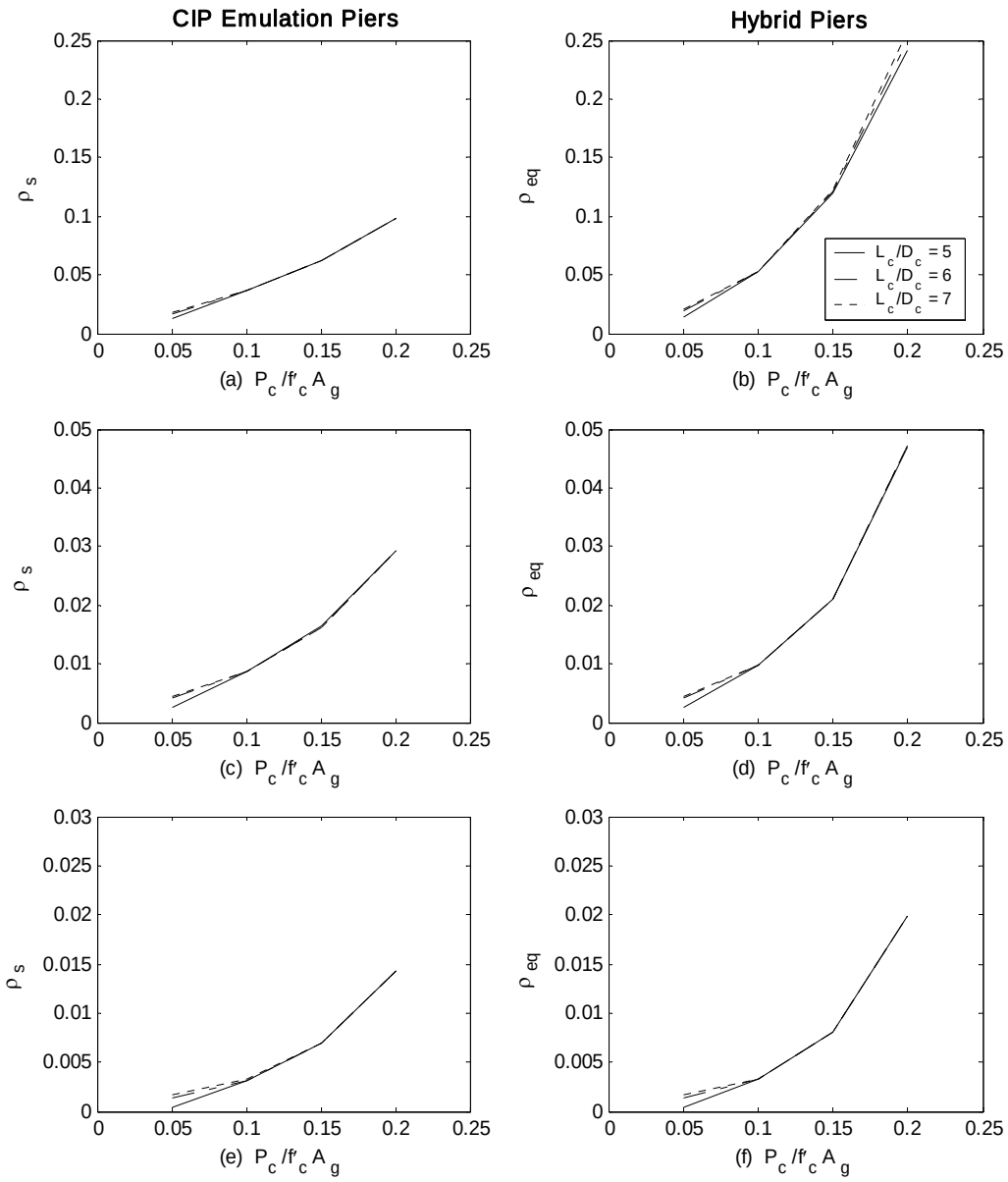

Figure 9.1: Reinforcing Ratio for the ELFD Procedure: (a) and (b) R=1.5, (c) and (d) R=3.5, (e) and (f) R=5.0

The equivalent reinforcing ratio (ρ_{eq}) required for hybrid piers is similar to the required mild steel reinforcing ratio (ρ_s) for lightly reinforced CIP emulation piers. For heavily reinforced piers, the required ρ_{eq} increases disproportionately to ρ_s. This difference is reasonable because the additional post-tensioning reinforcement increases the axial load in the columns, causing the neutral axis of the column to move toward the location of the post-tensioning, and reduces the internal lever arm and the moment

capacity provided by the post-tensioning. Figure 9.2 displays the value of ρ_s and ρ_{eq} required to provide the same amount of force capacity for a variety of piers. From the figure, it can be seen that, for the concrete strength and confinement levels used here, hybrid piers become uneconomical for a ρ_{eq} of greater than approximately 0.03; however, it is unlikely that piers would be designed for reinforcement ratios of larger than 0.03 in practice.

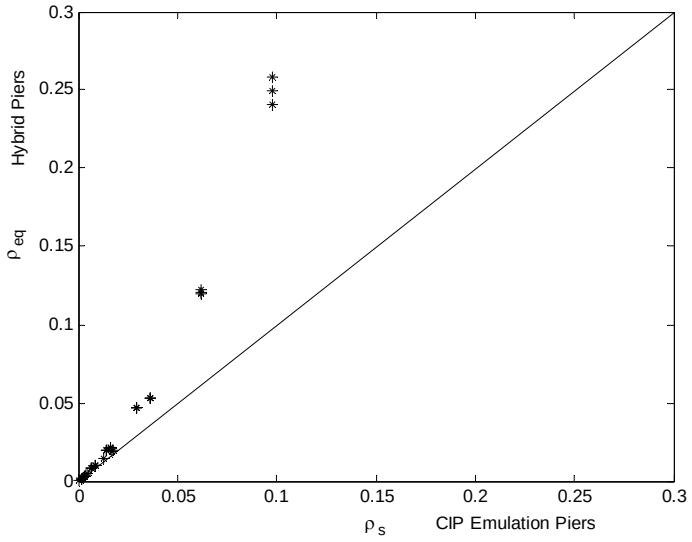

Figure 9.2: Equivalent Reinforcing Ratios for the ELFD Procedure

9.4 MAXIMUM DRIFT

A maximum drift hazard curve for the 12-pier population subjected to five design-level earthquakes is shown in Figure 9.3. The maximum drift hazard curve is similar to a damage hazard curve with maximum drift used as a proxy for damage. The average maximum drift and coefficient of variation (COV) for the CIP emulation and hybrid piers using the three R values are shown in Table 9.2.

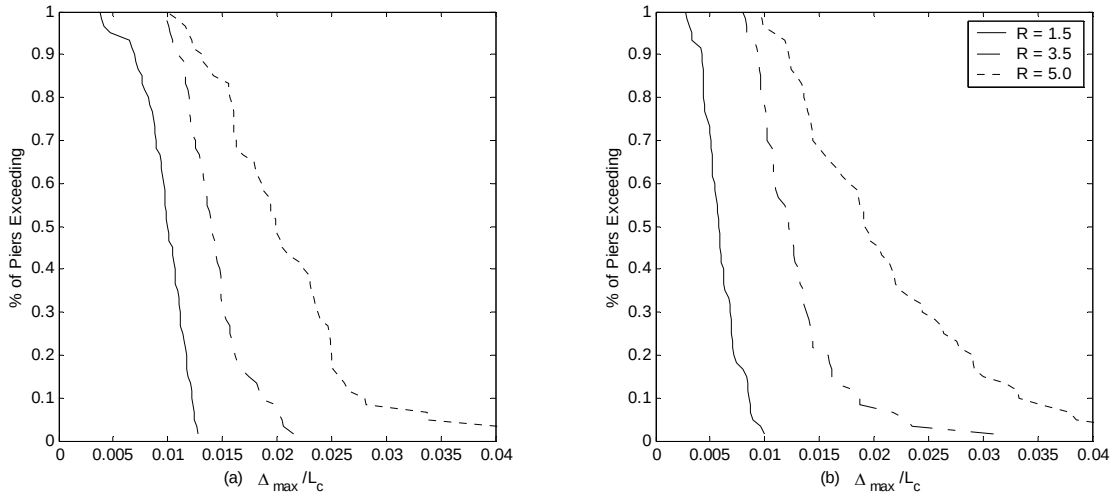

Figure 9.3: Maximum Drift Hazard Curves for the ELFD Procedure: (a) CIP Emulation Piers, (b) Hybrid Piers

Table 9.2: Maximum Drift Statistics for the ELFD Procedure

	All Piers				Piers with Reasonable Reinforcement			
	CIP Emulation		Hybrid		CIP Emulation		Hybrid	
R	Average	COV (%)	Average	COV (%)	Average	COV (%)	Average	COV (%)
1.5	0.0097	22.8	0.0059	28.6	0.0089	22.6	0.0064	30.4
3.5	0.0142	20.0	0.0130	32.6	0.0143	20.0	0.0131	27.8
5	0.0207	32.6	0.0211	41.6	0.0191	23.4	0.0177	38.7

The maximum drift values for both the CIP emulation and hybrid piers are within reasonable limits for all values of R considered. Only 20 percent of the CIP emulation piers and 25 percent of the hybrid piers are expected to have a maximum drift of over 2.5 percent in a design-level earthquake. At R = 1.5, the average maximum drift is significantly larger for the CIP emulation piers than for the hybrid piers, and it is almost equal at R = 3.5 and R = 5.0. The variation of the data, depicted by the COV and slope of the maximum drift hazard curves, is slightly larger for hybrid piers, possibly because of the larger range of reinforcing ratios used in the hybrid pier designs. Removing piers with unreasonable amounts of reinforcement had little effect on the average maximum drift or variation.

The effect of pier characteristics on the average maximum drift for the five ground motions ($\overline{\Delta}_{\max}/L_c$) is shown in Figure 9.4 for the CIP emulation and hybrid piers designed with the three R values. From Figure 9.4, it can be seen that L_c/D_c and

$P_c / f_c' A_g$ have little effect on the average maximum drift; all the curves are nearly horizontal and are closely grouped.

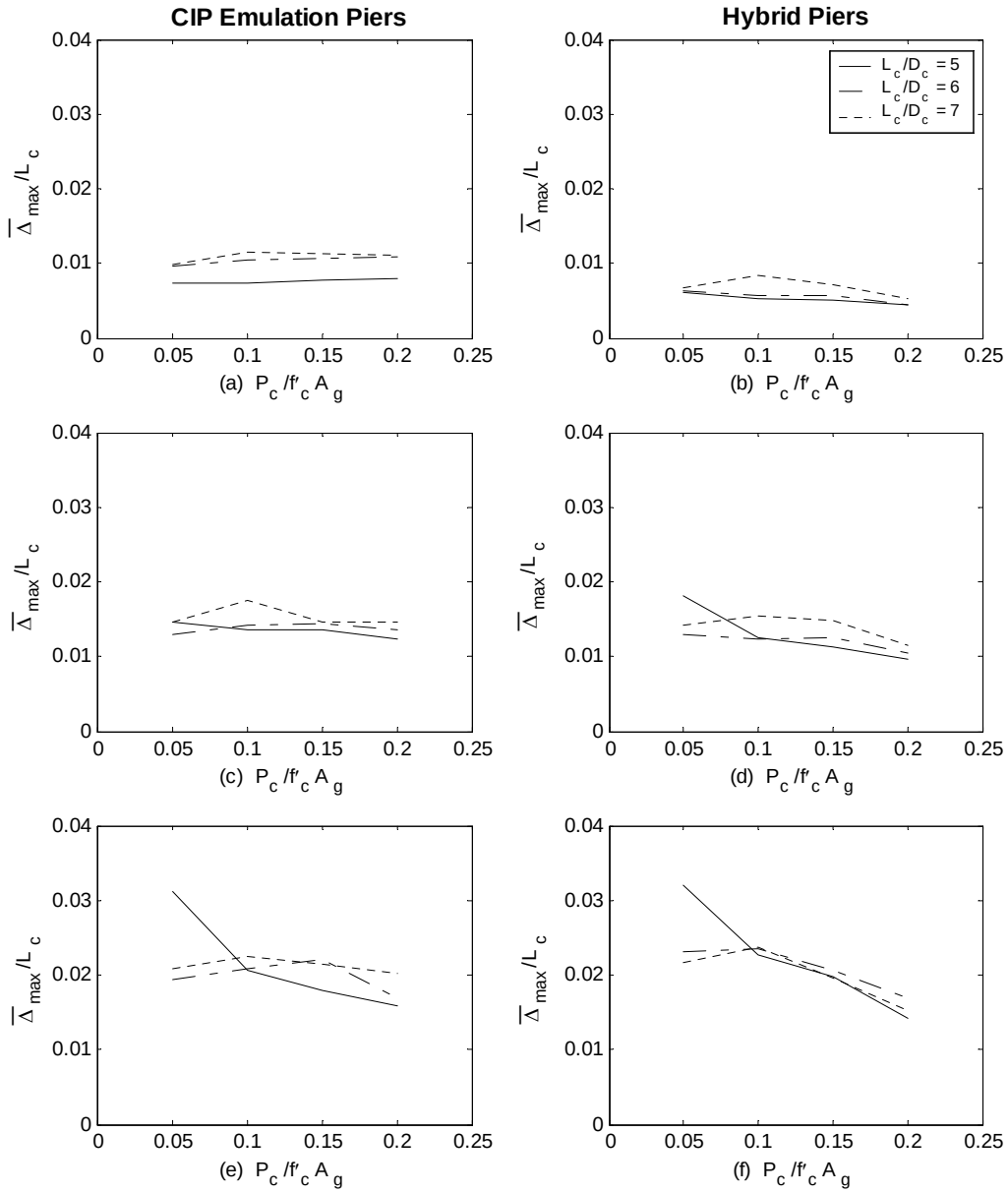

Figure 9.4: Variation in Maximum Drift for the ELFD Procedure: (a) and (b) R=1.5, (c) and (d) R=3.5, (e) and (f) R=5.0

9.5 PROBABILITY OF THE ONSET OF COVER SPALLING

The probability of the onset of concrete cover spalling (P_{spall}) was calculated from the maximum drift for each of the 12 piers subjected to each of the five ground-motion

acceleration records using the equations developed by Berry and Eberhard (2004) (Section 9.1). The probabilities were used to develop the probability of spalling hazard curves shown in Figure 9.5. The statistics for P_{spall} are compiled in Table 9.3.

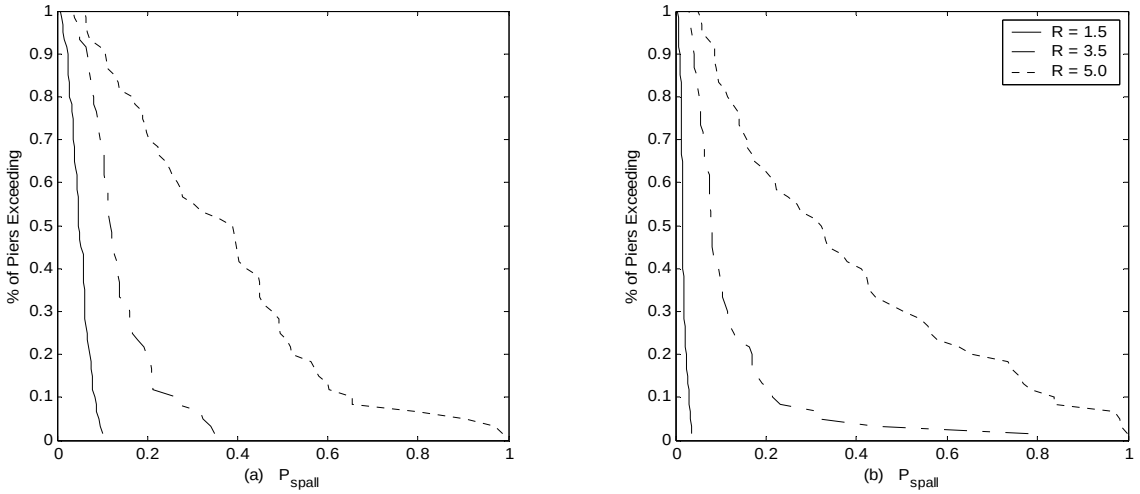

Figure 9.5: Probability of Spalling Hazard Curves for the ELFD Procedure: (a) CIP Emulation Piers, (b) Hybrid Piers

Table 9.3: Probability of Spalling Statistics for the ELFD Procedure

	All Piers				Piers with Reasonable Reinforcement			
	CIP Emulation		Hybrid		CIP Emulation		Hybrid	
R	Average	COV (%)	Average	COV (%)	Average	COV (%)	Average	COV (%)
1.5	0.050	45.6	0.017	42.1	0.0333	43.8	0.0179	49.0
3.5	0.137	54.1	0.116	101.0	0.1473	51.6	0.1159	77.3
5	0.363	62.7	0.374	75.5	0.3467	48.9	0.3010	82.1

The average probability of the onset of spalling appears to be consistent with test and field experience. The CIP emulation piers had an average P_{spall} of 5 percent, 15 percent, and 35 percent for R factors of 1.5, 3.5, and 5.0, respectively. The hybrid piers had an average P_{spall} of 2 percent, 12 percent, and 37 percent for R of 1.5, 3.5, and 5.0, respectively. For R values of 3.5 and 5.0, the average probability of spalling for a CIP emulation and a hybrid pier is approximately the same. Considering only piers with reasonable amounts of reinforcement results in no consistent changes to the average probability of spalling. The variation is decreased slightly in some cases while remaining approximately the same in others.

Although an average P_{spall} of 35 percent may seem large, spalling damage is repairable and unlikely to cause structural failure of the pier. A significant reduction in P_{spall} can be obtained by designing for smaller values of R. For the CIP emulation piers, approximately 70 percent of piers designed for R = 5.0 have a P_{spall} of greater than 20 percent in comparison to only 20 percent of the piers designed for R = 3.5. Decreasing R to 1.5 in design results in none of the piers considered having a probability of spalling of over 20 percent. Trends are similar for hybrid piers. However, as shown in Figure 9.1, the cost of these performance improvements is a significant increase in the amount of required reinforcing steel. In practice, the columns with high reinforcing ratios would have larger column sizes. Determining the most economical R value for design would require information on the costs of constructing piers with varying amounts of reinforcement, repairing spalling damage, and indirect user costs associated with closing bridges for repairs. Such a benefit-cost evaluation lies beyond the scope of this study.

Figure 9.6 shows the probability of the onset of spalling for the same pier population. No significant trends appear in P_{spall} for L_c/D_c or $P_c/f_c'A_g$. The plots in Figure 9.6 do show that significant scatter exists in the P_{spall} values, with significant increases in P_{spall} at low levels of $P_c/f_c'A_g$ in some cases. However, this variation may have more to do with the low levels of reinforcement typically employed at low $P_c/f_c'A_g$ than the low amounts of $P_c/f_c'A_g$ themselves. Section 9.8 explores the effects of low amounts of reinforcing steel on the results.

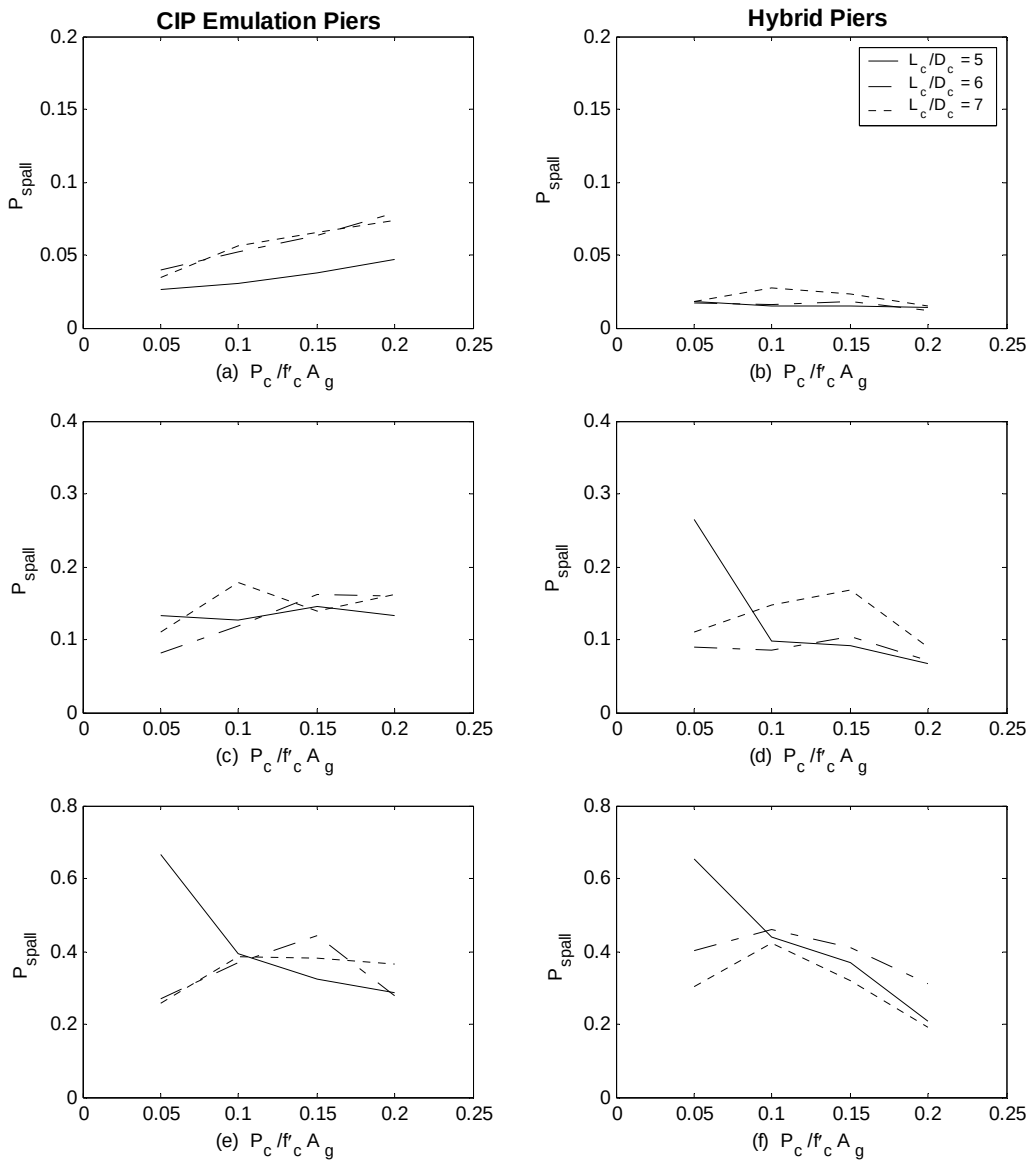

Figure 9.6: Variation in Probability of Spalling for the ELFD Procedure: (a) and (b) R=1.5, (c) and (d) R=3.5, and (e) and (f) R=5.0

9.6 PROBABILITY OF BAR BUCKLING

Buckling of longitudinal reinforcing bars can put a bridge out –of service and require extensive and expensive repairs. The probability of bar buckling (P_{bb}) was calculated for the 12 piers considered in the evaluation study subjected to each of the five ground motions. Probability of bar buckling hazard curves are displayed in Figure 9.7. The statistics for the distribution of P_{bb} are shown in Table 9.4. In this study, all bars

were considered to have a diameter of 1.41 in. Using smaller diameter bars would increase P_{bb}.

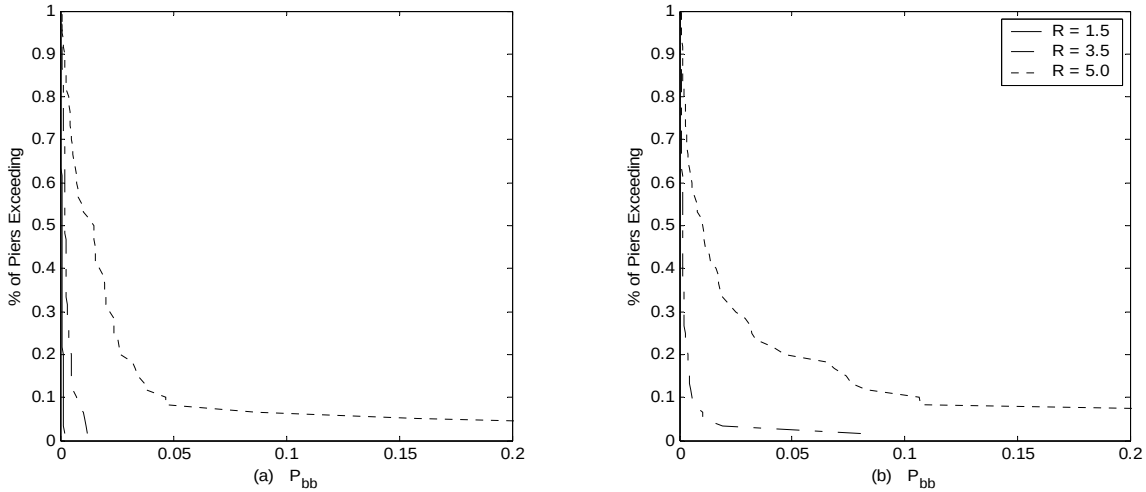

Figure 9.7: Probability of Bar Buckling Hazard Curves for the ELFD Procedure: (a) CIP Emulation Piers, (b) Hybrid Piers

Table 9.4: Probability of Bar Buckling Statistics for the ELFD Procedure

	All Piers				Piers with Reasonable Reinforcement			
	CIP Emulation		Hybrid		CIP Emulation		Hybrid	
R	Average	COV (%)	Average	COV (%)	Average	COV (%)	Average	COV (%)
1.5	0.0008	54.5	0.0002	47.9	0.0005	44.2	0.0002	55.2
3.5	0.0031	84.8	0.0036	290.8	0.0035	81.8	0.0027	134.7
5	0.0282	218.6	0.0440	226.6	0.0153	81.6	0.0245	253.3

The probability of bar buckling hazard curves illustrate the benefits of designing for lower R values. All the piers designed for R = 1.5 and R = 3.5 had probabilities of bar buckling of below 0.5 percent, whereas approximately 20 percent of the piers designed for R = 5.0 had a probability of bar buckling of greater than 3 percent. However, these performance benefits must be balanced with the significant increases in the amount of reinforcement required for piers designed for smaller R values.

The average probability of bar buckling and variation for the subset of the population that contains only piers with reasonable amounts of reinforcement are similar to the values calculated for all piers. Significant reductions were seen in the average probability of bar buckling of piers designed for R=5.0. The variation of damage was drastically reduced in some cases, but no consistent trend emerged.

The same trends for L_c/D_c and $P_c/f_c^{'}A_g$ appear in the P_{bb} results shown in Figure 9.8 as those in the P_{spall} results shown in Figure 9.6.

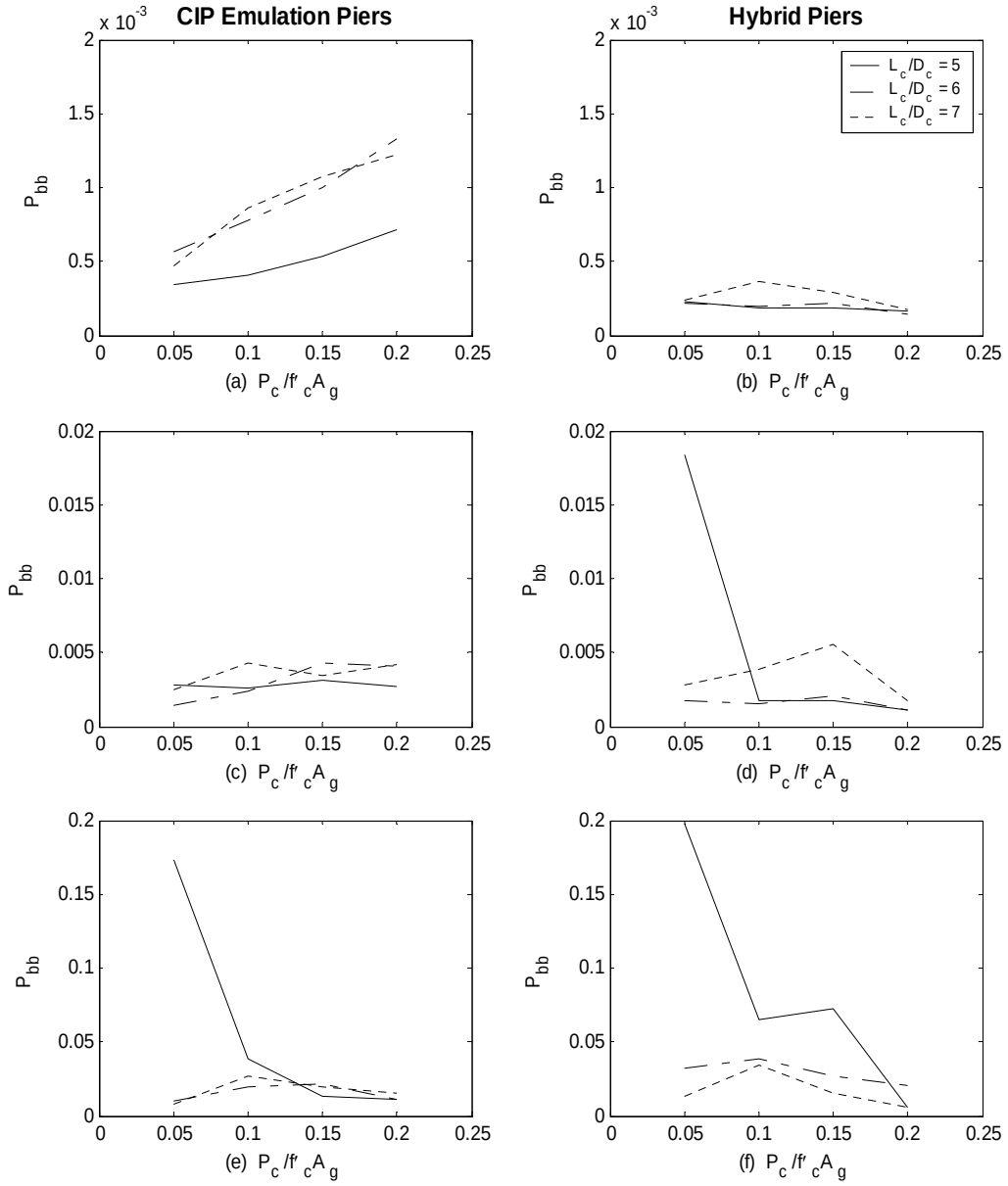

Figure 9.8: Variation in Probability of Bar Buckling for the ELFD Procedure: (a) and (b) R=1.5, (c) and (d) R=3.5, (e) and (f) R=5.0

9.7 MAXIMUM STRAIN IN LONGITUDINAL REINFORCING BARS

The maximum tensile strain in the mild steel reinforcing bars ($\varepsilon_{\max}$) of the pier columns was determined by conducting pushover analyses to each value of $\Delta_{\max}$. The

average value of the maximum strain ($\overline{\varepsilon}_{max}$) for a given pier was determined by averaging the five strains determined for the individual ground motions. The maximum strain (ε_{max}) was computed from a pushover analysis rather than directly from the ground motion analyses to eliminate any strength degradation effects, which depend on the characteristics of the ground motion.

Maximum strain hazard curves are shown in Figure 9.9. The maximum strains expected in a design-level earthquake are consistent with field experience. For the CIP emulation piers, the maximum strain only exceeds the assumed fracture strain of 0.05 in approximately 10 percent of all piers designed for R = 5.0. The maximum strains in the hybrid piers are larger, and over 50 percent of all piers exceed the fracture strain for R = 5.0. However, the strain in the mild steel reinforcement of a hybrid pier depends directly on the length of the mild steel that is debonded in the interface region. Debonding a greater length of the reinforcing bar would reduce the maximum strains. A debonded length equal to one-fourth the column diameter was used in this study. From the results in Figure 9.9, it appears that larger debonded lengths are required for piers designed for larger R values. However, the ELFD procedure does not provide any means for determining the required debonded length to prevent bar fracture.

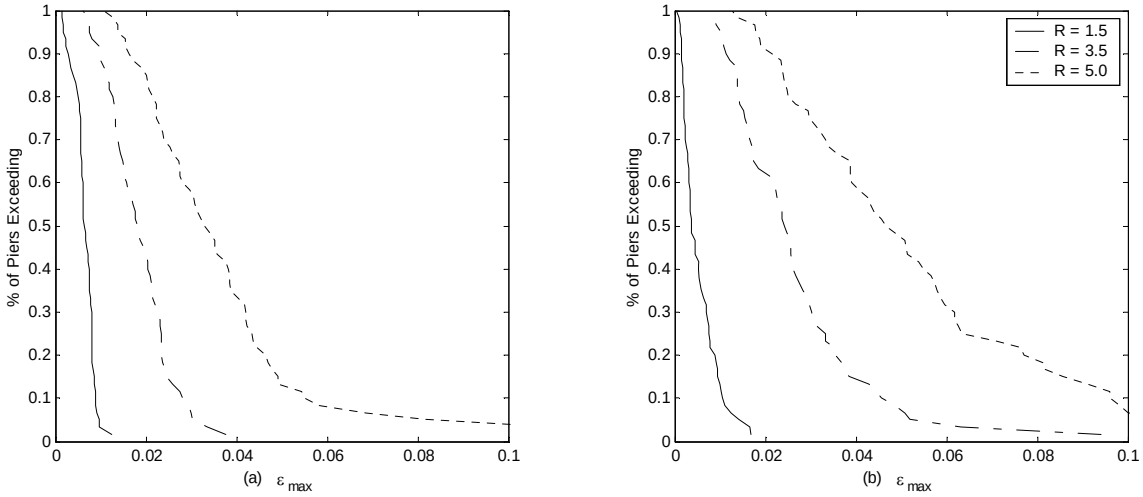

Figure 9.9: Maximum Strain Hazard Curves for the ELFD Procedure: (a) CIP Emulation Piers, (b) Hybrid Piers

Statistics on the distribution of maximum steel strains are displayed in Table 9.5. The statistics for the subset of the population that contains only piers with reasonable

amounts of reinforcement varied from the statistics for all piers in a similar fashion to that exhibited for the probability of bar buckling.

Table 9.5: Maximum Strain Statistics for the ELFD Procedure

	All Piers				Piers with Reasonable Reinforcement			
	CIP Emulation		Hybrid		CIP Emulation		Hybrid	
R	Average	COV (%)	Average	COV (%)	Average	COV (%)	Average	COV (%)
1.5	0.0064	35.8	0.0052	75.3	0.0073	36.4	0.0094	47.7
3.5	0.0183	38.1	0.0263	57.3	0.0171	35.5	0.0259	38.4
5	0.0360	58.3	0.0523	57.2	0.0282	34.2	0.0368	53.7

The effects of L_c/D_c and $P_c/f_c'A_g$ on the maximum strain of mild steel reinforcing bars of piers designed with various R values are shown in Figure 9.10. From the figure it can be seen that the maximum strain decreases with increasing $P_c/f_c'A_g$. This is because the additional axial load on the column increases the initial compressive stresses in the mild steel reinforcement, decreasing the maximum tensile stress obtained at Δ_{max}. No significant trend with L_c/D_c is apparent.

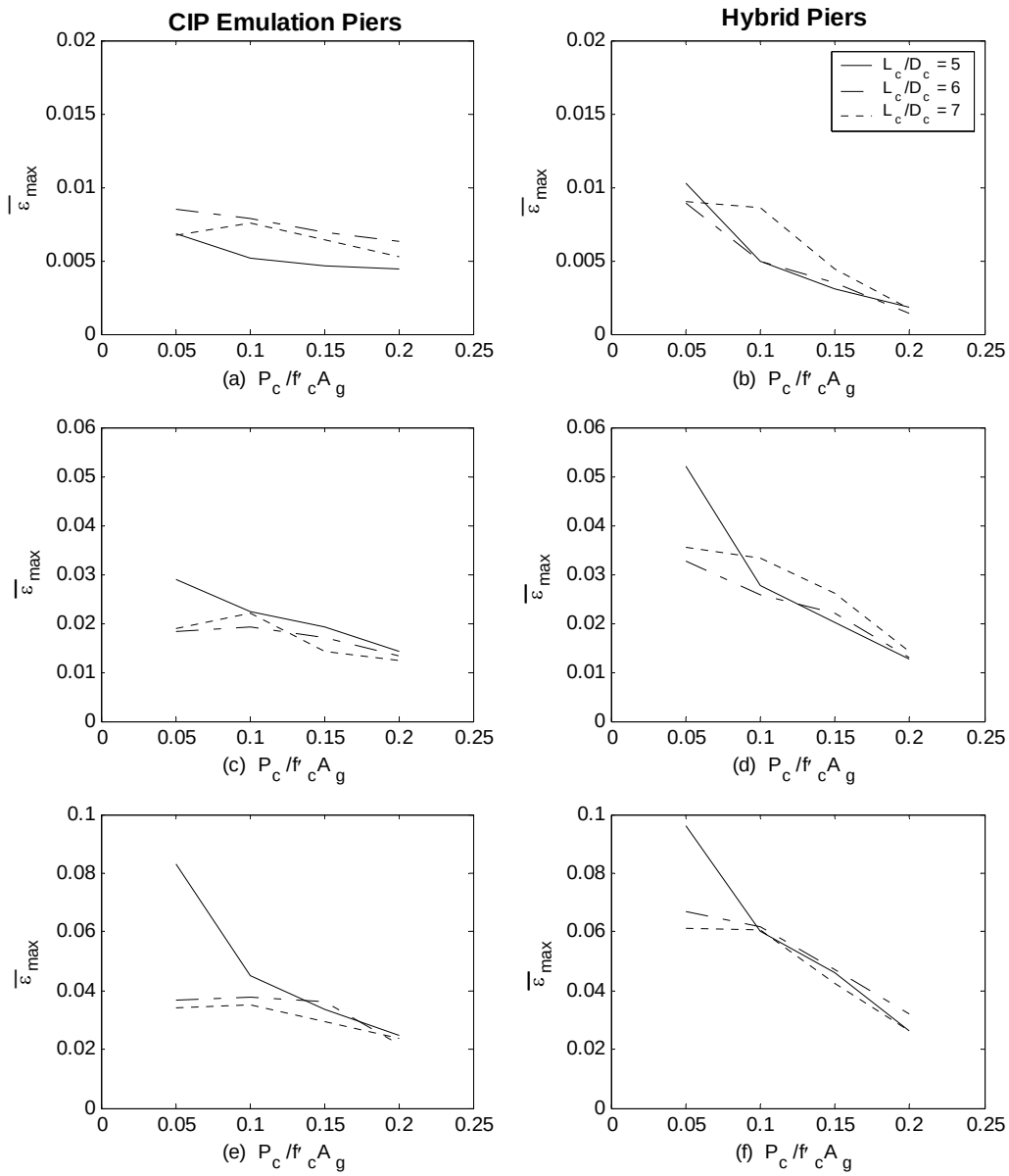

Figure 9.10: Variation in Maximum Strain for the ELFD Procedure: (a) and (b) R=1.5, (c) and (d) R=3.5, (e) and (f) R=5.0

9.8 EFFECT OF MINIMUM REINFORCING STEEL LIMITATIONS

Some of the large probabilities of damage seen in the results of piers designed with the ELFD procedure are believed to result from excessively low reinforcing steel ratios. In practice, the AASHTO specifications (AASHTO 2002; AASHTO 2004) limit the minimum amount of reinforcement that can be used. The effects of low amounts of reinforcement were examined by instituting a minimum ρ_s of 0.005 for the CIP

emulation piers and a minimum ρ_{eq} of 0.005 for the hybrid piers. The limit of 0.005 was selected because the AASHTO specifications (AASHTO 2002; AASHTO 2004) allow a minimum reinforcing ratio of 0.005 to be used if a smaller column with a reinforcing ratio of 0.01 can carry the required design force. It was assumed that smaller columns could carry the design force in all cases, thereby allowing the lower limit of 0.005 to be used.

The minimum reinforcing limit primarily affected piers with low values of $P_c / f_c^{'} A_g$ designed for R = 5.0. The increased amount of reinforcing steel significantly decreased the amount of damage expected for piers where the minimum limit applied. Figure 9.11 shows the probability of spalling and probability of bar buckling of piers designed for R = 5.0 with the minimum reinforcing limit enforced.

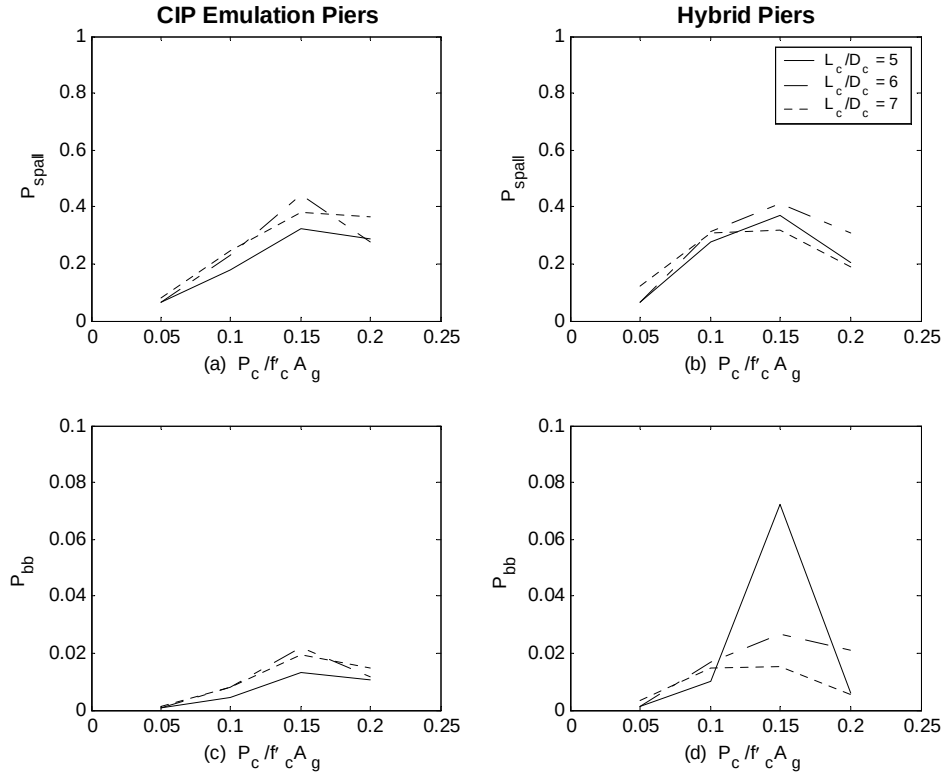

Figure 9.11: Expected Damage for the ELFD Procedure with Minimum Reinforcing Limit: (a) and (b) Probability of Spalling, (c) and (d) Probability of Bar Buckling

The figure shows that the previously high amounts of damage at low $P_c / f_c^{'} A_g$ decreased significantly. Note that the additional reinforcement increases not only the

strength but also the cracked stiffness of the pier. Without further study, it is not possible to say which of the two effects is the more important in reducing the drift and, therefore, the probability of damage.

9.9 SUMMARY OF THE ELFD PROCEDURE EVALUATION

The ELFD procedure produces acceptable designs for both CIP emulation and hybrid piers for the wide range of pier characteristics considered in this evaluation. A minimum reinforcing ratio of 0.005 is recommended to prevent the larger levels of damage associated with lightly reinforced piers. The use of smaller R values results in significant decreases in the amount of damage expected, but the amount of reinforcing steel required is significantly increased.

The probabilities of concrete spalling and bar buckling are similar for both CIP emulation and hybrid piers, supporting the use of the same R values for both types of piers. This conclusion assumes that the equations used to determine probability of spalling and probability of bar buckling are accurate for hybrid piers and that the nonlinear finite element models used in this study accurately depict the behavior of both types of piers. If the hybrid piers are found to experience more or less damage for a given level of drift than that predicted by the model developed by Berry and Eberhard (2004), different R values could be warranted. Improvements to the R factors for hybrid systems are presently limited by the paucity of experimental data.

CHAPTER 10
EVALUATION OF THE DDBD PROCEDURE

The target displacement used in the DDBD procedure can be selected on the basis of a target likelihood of damage in a design-level earthquake. Chapter 8 discussed verification of the correlation between the average maximum inelastic displacement of piers in earthquakes and the selected target displacement. However, the damage that occurs to piers designed for a constant level of damage will vary because of variation in the response of piers to different ground motions and approximations in the DDBD method. This variation in damage will not necessarily be equal to the variation in target displacement values determined in Chapter 8. Therefore, the DDBD procedure needed to be evaluated by designing a variety of piers for a constant likelihood of occurrence of damage and examining the variation in damage expected in a design-level earthquake.

The twelve piers presented in the previous chapter were designed with the DDBD procedure for a constant probability of spalling. The iterative DDBD procedure using nonlinear analysis methods was employed for design because it is the most accurate formulation of the DDBD procedure. To accommodate comparison between the ELFD and DDBD procedures, the piers were designed for three target probabilities of spalling: 5 percent, 15 percent, and 35 percent. The required reinforcing ratios are shown in Table 10.1.

Table 10.1: Reinforcing Ratio for Piers Designed with the DDBD Procedure

				CIP Emulation Piers			Hybrid Piers		
				P_{spall}=5%	P_{spall}=15%	P_{spall}=35%	P_{spall}=5%	P_{spall}=15%	P_{spall}=35%
Pier No.	D_c (in)	L_c/D_c	P_c/f'_cA_g	ρ_s	ρ_s	ρ_s	ρ_{eq}	ρ_{eq}	ρ_{eq}
1	48	5	0.05	0.0058	0.0018	0.0009	0.0056	0.0025	0.0016
2	48	5	0.1	0.0204	0.006	0.0028	0.0169	0.0080	0.0042
3	48	5	0.15	0.0501	0.0131	0.0059	0.0340	0.0154	0.0088
4	48	5	0.2	0.1039	0.0245	0.0106	0.0574	0.0259	0.0145
5	48	6	0.05	0.0072	0.0021	0.001	0.0064	0.0031	0.0016
6	48	6	0.1	0.0258	0.0072	0.0034	0.0193	0.0089	0.0049
7	48	6	0.15	0.0646	0.016	0.0072	0.0388	0.0172	0.0099
8	48	6	0.2	0.1306	0.03	0.013	0.0649	0.0292	0.0168
9	48	7	0.05	0.0086	0.0025	0.0011	0.0071	0.0032	0.0017
10	48	7	0.1	0.0316	0.0085	0.004	0.0212	0.0098	0.0056
11	48	7	0.15	0.0785	0.0189	0.0085	0.0436	0.0194	0.0113
12	48	7	0.2	0.1582	0.0354	0.0154	0.0728	0.0324	0.0186

10.1 REINFORCEMENT RATIO

The required reinforcing ratio for the piers designed for the three target P_{spall} values are shown in Figure 10.1. As was the case for piers designed with the ELFD procedure, the required reinforcing steel ratio increases with $P_c / f_c^{'} A_g$ because of the increased seismic demand from the additional seismic mass. However, unlike the ELFD procedure, the required reinforcing ratio also increases with L_c / D_c. More slender columns, indicated by larger L_c / D_c values, require larger reinforcing ratios than do stockier columns to limit the maximum drift and obtain a constant probability of spalling.

Unlike the ELFD procedure, the DDBD procedure does not require extremely large equivalent reinforcing ratios for heavily reinforced hybrid piers. As shown in Figure 10.2, the ρ_{eq} of a hybrid pier required to obtain the same target displacement as a CIP emulation pier with a given ρ_s decreases for more heavily reinforced piers. This difference was expected because the DDBD procedure accounts for increases to the cracked stiffness of hybrid piers with increased axial load caused by larger amounts of post-tensioning. The increased stiffness reduces the maximum displacement in an earthquake reducing the required amount of reinforcement. This trend makes the DDBD procedure more economical for designing heavily reinforced hybrid piers.

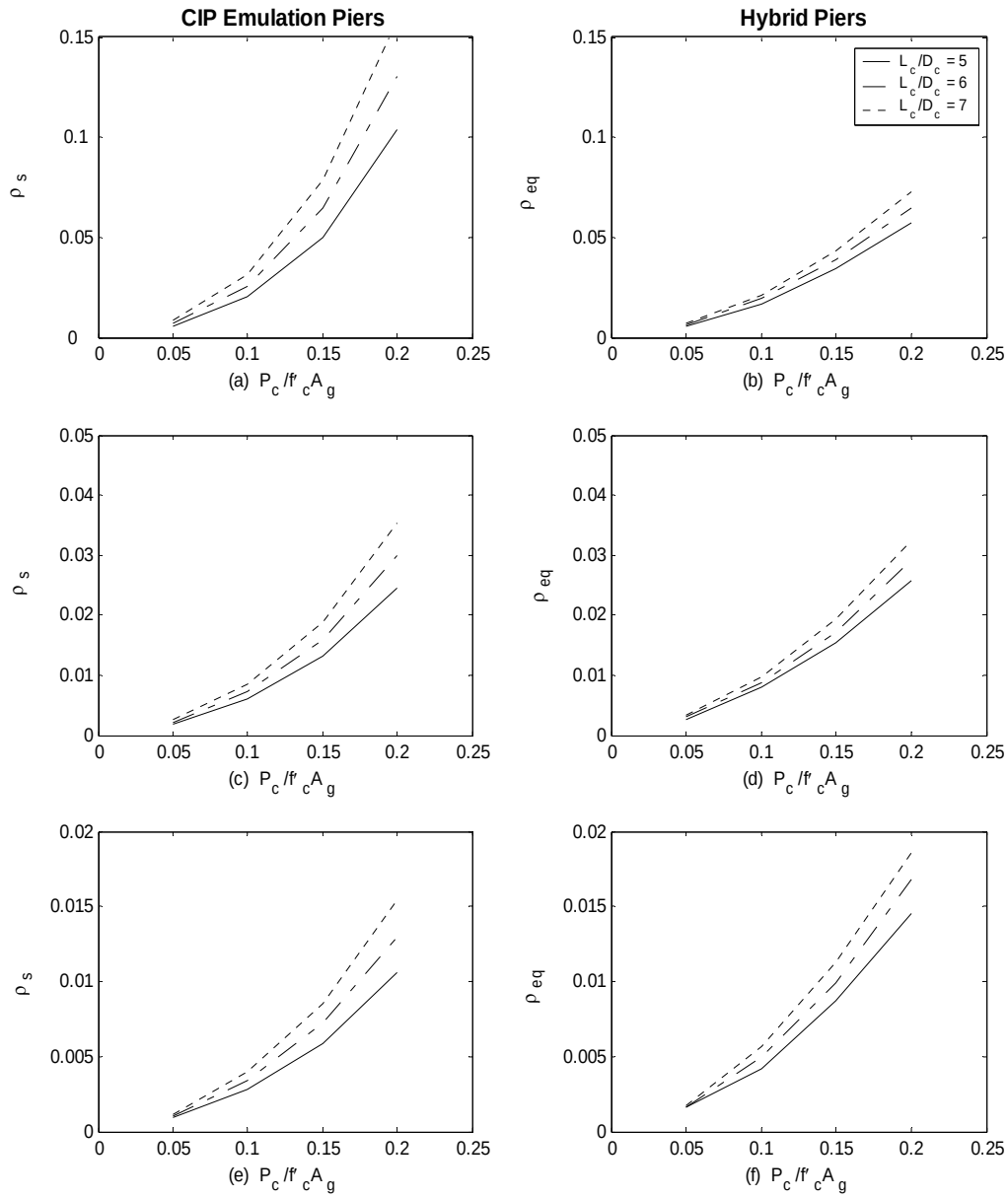

Figure 10.1: Reinforcing Ratio for the DDBD Procedure: (a) and (b) P_{spall} = 5%, (c) and (d) P_{spall} = 15%, (e) and (f) P_{spall} = 35%

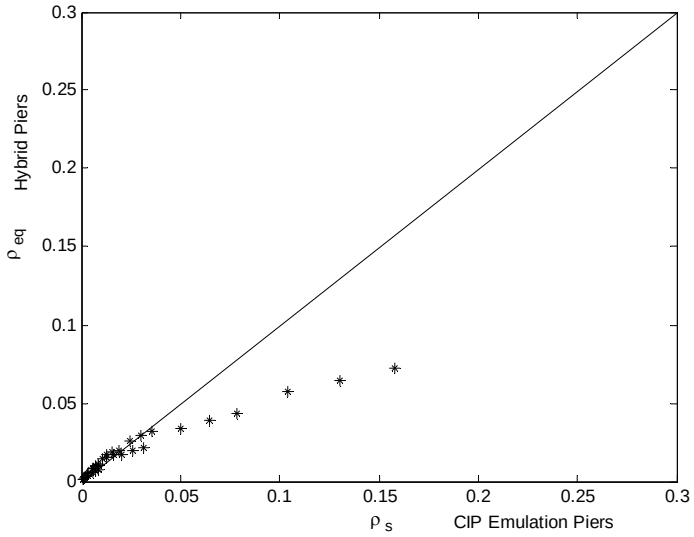

Figure 10.2: Equivalent Reinforcing Ratios for the DDBD Procedure

10.2 MAXIMUM DRIFT

The maximum drift hazard curves for piers designed with the DDBD procedure are shown in Figure 10.3. The expected maximum drift values are consistent with expectations, in that only 10 percent of the piers have a drift of greater than 3 percent in a design-level earthquake. While the variation in maximum drift is slightly smaller than that obtained with the ELFD procedure, there is still a significant amount of scatter in the maximum drift values because of variability in the response of the piers to the various ground motions.

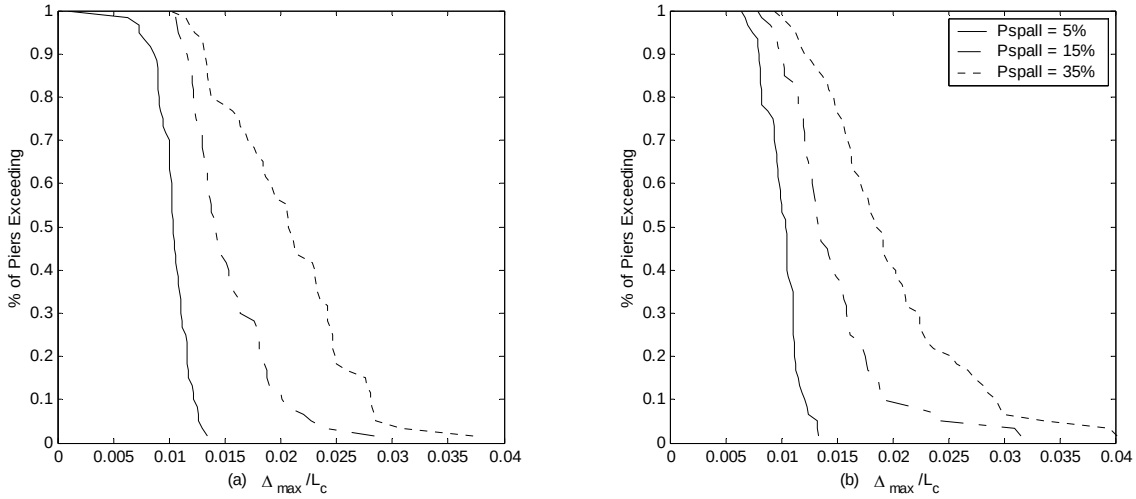

Figure 10.3: Maximum Drift Hazard Curves for the DDBD Procedure: (a) CIP Emulation Piers, (b) Hybrid Piers

The statistics for the distribution of maximum drift are shown in Table 10.2. The statistics for the subset of piers that contain only piers with reasonable amounts of reinforcement are similar to the statistics for all piers in the population.

Table 10.2: Maximum Drift Statistics for the DDBD Procedure

	All Piers				Piers with Resonable Reinforcement			
	CIP Emulation		Hybrid		CIP Emulation		Hybrid	
Target P_{spall}	Average	COV (%)	Average	COV (%)	Average	COV (%)	Average	COV (%)
5%	0.0104	14.2	0.0101	16.1	0.0110	11.6	0.0104	16.9
15%	0.0152	24.3	0.0146	32.2	0.0145	19.8	0.0138	25.9
35%	0.0205	28.0	0.0197	33.9	0.0188	26.0	0.0182	27.0

The average maximum drift values of piers designed with the DDBD procedure are nearly independent of L_c/D_c and $P_c/f_c'A_g$, as indicated by the overlapping, nearly horizontal lines in Figure 10.4. The relation between maximum drift and drift at which cover spalling occurs (Equation 9.1) is not strongly influenced by L_c/D_c and $P_c/f_c'A_g$, resulting in minimal variation in the expected maximum drift for piers designed for a constant probability of spalling. The significant reduction of variability in the average maximum drift values indicates that the DDBD procedure can estimate the average maximum displacement well for a given pier but is not capable of accounting for variations in response for individual ground motion acceleration records. The reduction in variation is much larger for low values of R, which correspond to low target values of damage.

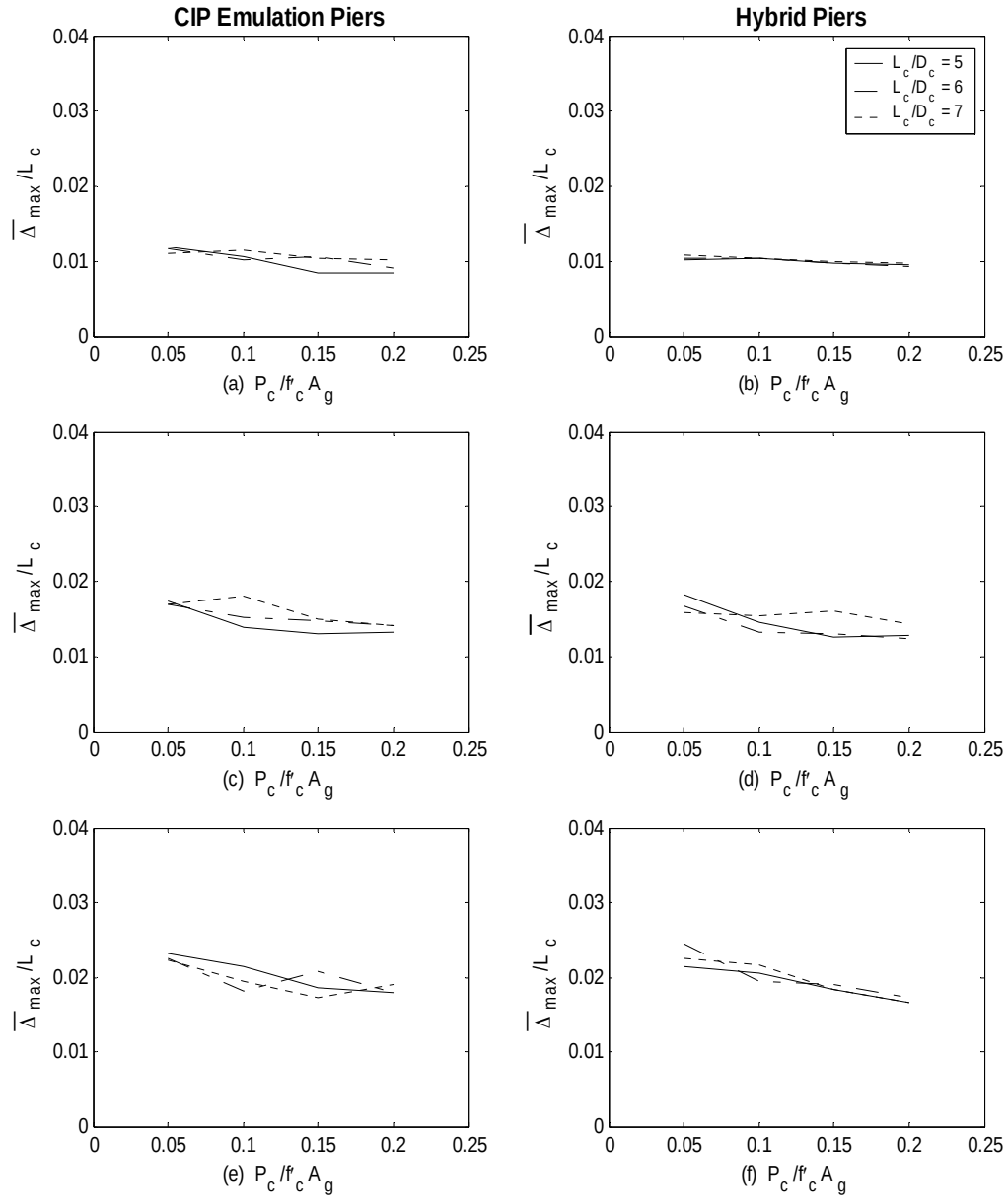

Figure 10.4: Variation in Maximum Drift for the DDBD Procedure: (a) and (b) P_{spall} = 5%, (c) and (d) P_{spall} = 15%, (e) and (f) P_{spall} = 35%

10.3 PROBABILITY OF THE ONSET OF COVER SPALLING

The probability of cover spalling hazard curves for the 12 piers evaluated are shown in Figure 10.5. The distribution of the probability of spalling is also described by the statistics shown in Table 10.3. For the CIP emulation piers, the average probabilities of spalling were 5.6 percent, 16.4 percent, and 36.3 percent for the piers designed with target probabilities of spalling of 5 percent, 15 percent, and 35 percent, respectively. The hybrid piers had average probabilities of 5.3 percent, 15.9 percent, and 32.7 percent for

target values of 5 percent, 15 percent, and 35 percent, respectively. These average values indicate that the DDBD procedure leads to pier designs that have an average probability of spalling within a small range of the target value. The average probability of spalling was similar when calculated for all piers and for the subset that contains only piers with reasonable amounts of reinforcement. The variation in the probability of spalling was slightly less in some instances when only piers with reasonable amounts of reinforcement were considered.

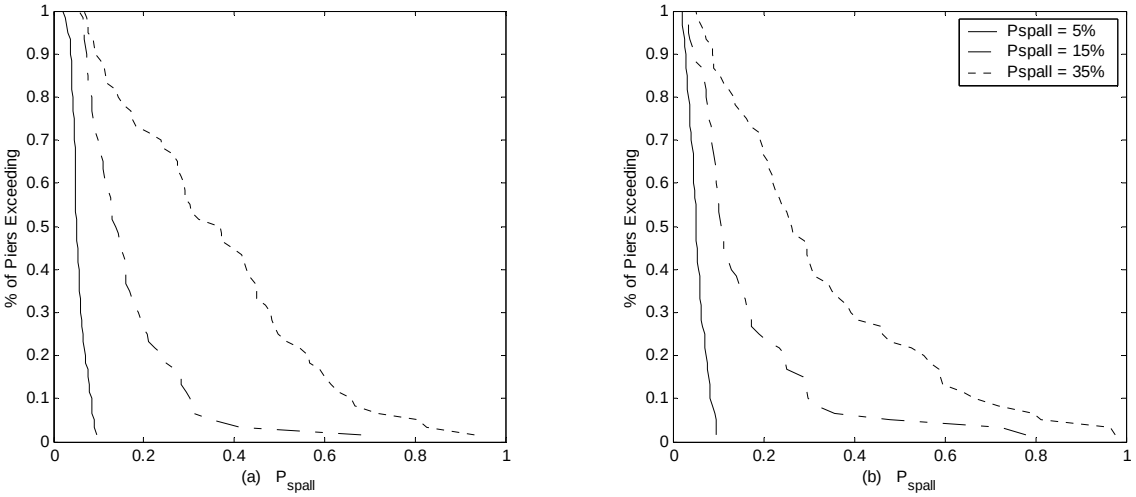

Figure 10.5: Probability of Spalling Hazard Curves for the DDBD Procedure: (a) CIP Emulation Piers, (b) Hybrid Piers

Table 10.3: Probability of Spalling Statistics for the DDBD Procedure

	All Piers				Piers with Resonable Reinforcement			
	CIP Emulation		Hybrid		CIP Emulation		Hybrid	
Target P_{spall}	Average	COV (%)	Average	COV (%)	Average	COV (%)	Average	COV (%)
5%	0.056	30.3	0.053	38.3	0.058	31.0	0.051	39.8
15%	0.164	65.2	0.159	90.9	0.153	49.5	0.141	67.3
35%	0.363	58.9	0.327	70.5	0.344	59.3	0.302	62.6

The variation in the probabilities of spalling is considerable and is larger than that for the maximum drift. This increased variability indicates that the probability of spalling is more sensitive to variations in pier response to individual ground motions than the maximum drift. The COV values for the probability of spalling of piers designed with the DDBD procedure are only slightly less than those obtained with the ELFD procedure. Their lack of improvement is believed to be a result of the fact that the majority of

variation comes from variability in the response of a pier to different ground motions, which neither the ELFD nor DDBD procedures consider directly.

As desired in the DDBD procedure, the probability of spalling is relatively constant regardless of the pier's characteristics. Neither L_c/D_c nor $P_c/f_c^{'}A_g$ significantly affect the probability of spalling as shown in Figure 10,6. The variation in the probability of spalling with L_c/D_c and $P_c/f_c^{'}A_g$ is less than when the piers are designed with the ELFD procedure, as was shown in Figure 9.6. This is of greatest consequence for lightly reinforced piers, which have small values of $P_c/f_c^{'}A_g$. The ELFD procedure produces pier designs that have large P_{spall} values in these situations, whereas the DDBD procedure produces designs that have more uniform P_{spall} values.

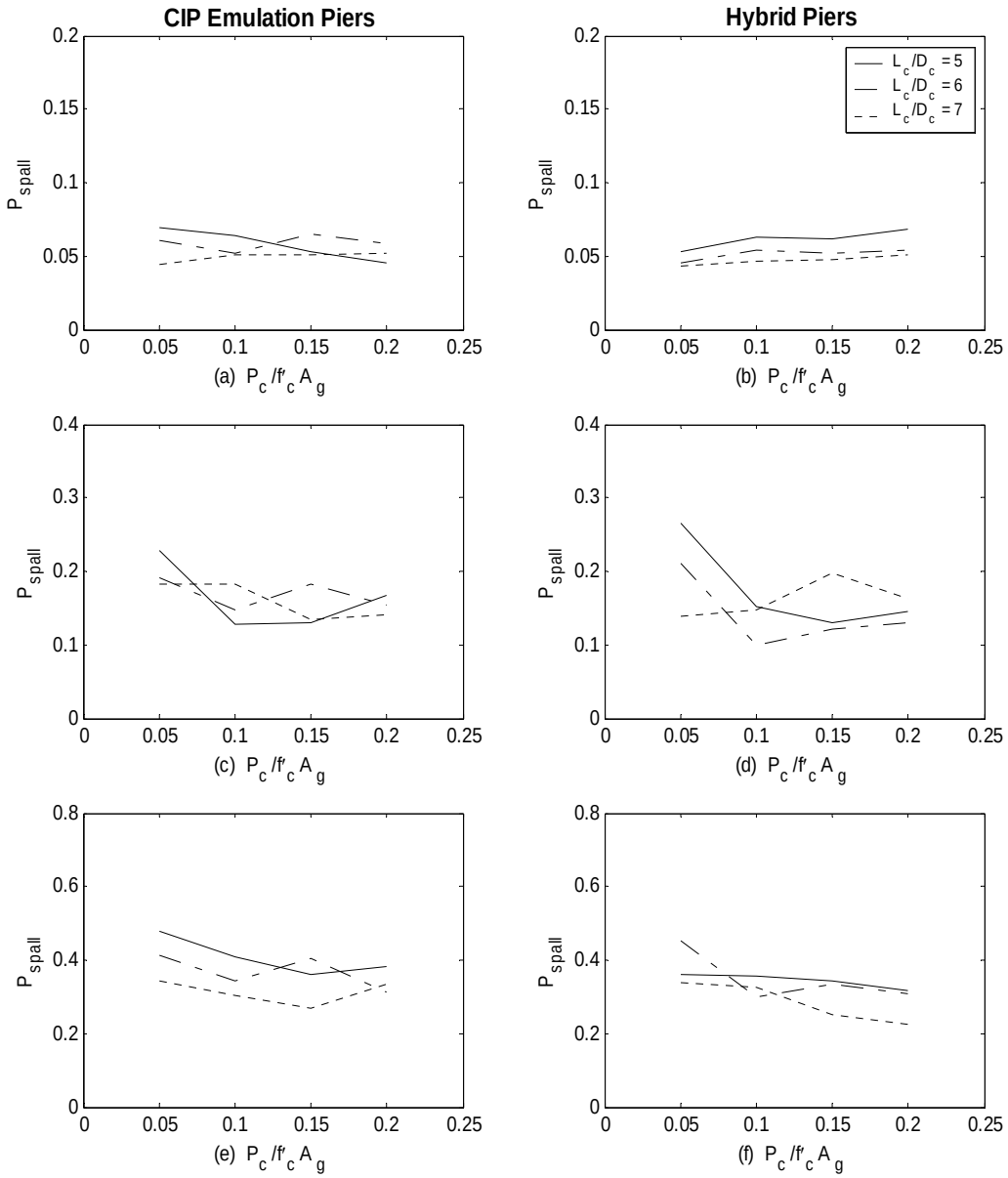

Figure 10.6: Variation in Probability of Spalling for the DDBD Procedure: (a) and (b) P_{spall} = 5%, (c) and (d) P_{spall} = 15%, and (e) and (f) P_{spall} = 35%

10.4 PROBABILITY OF BAR BUCKLING

The curves representing the probability of bar buckling hazard for the piers designed with the DDBD procedures are shown in Figure 10.7. The statistics of the distribution of P_{bb} are shown in Table 10.4. The piers designed for a P_{spall} of 5 percent and 15 percent have a relatively insignificant P_{bb}, whereas the piers designed for a P_{spall} of 35 percent have an average P_{bb} of about 2 percent. When only P_{spall} is considered in

designing the piers, P_{bb} is not always known and depends indirectly on P_{spall}. The average probability of bar buckling and variation changes when only piers with reasonable amounts of reinforcement are considered, in the same manner as those for the ELFD procedure discussed in Section 9.6.

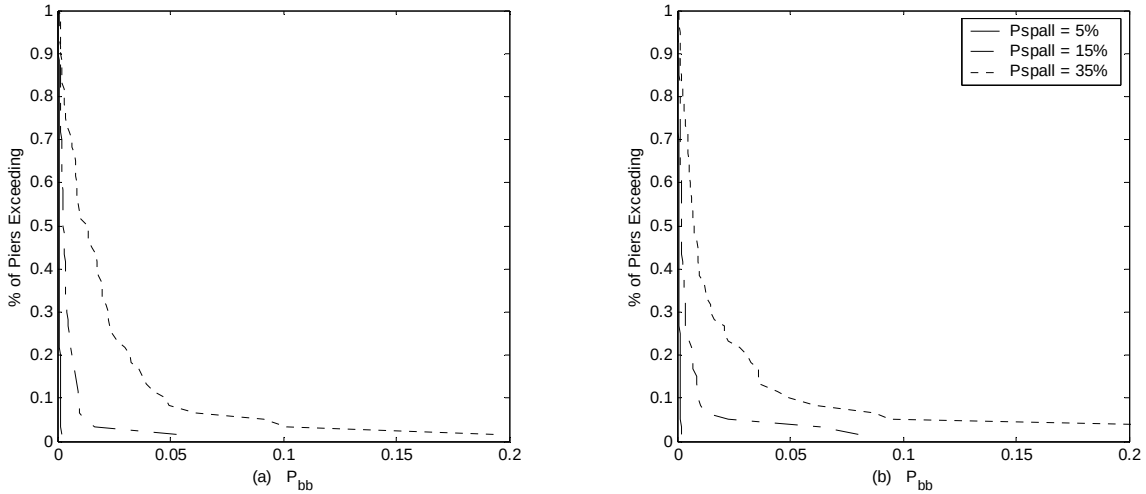

Figure 10.7: Probability of Bar Buckling Hazard Curves for the DDBD Procedure: (a) CIP Emulation Piers, (b) Hybrid Piers

Table 10.4: Probability of Bar Buckling Statistics for the DDBD Procedure

	All Piers				Piers with Resonable Reinforcement			
	CIP Emulation		Hybrid		CIP Emulation		Hybrid	
Target Pspall	Average	COV (%)	Average	COV (%)	Average	COV (%)	Average	COV (%)
5%	0.0009	38.1	0.0008	47.3	0.0009	39.0	0.0008	48.4
15%	0.0046	152.8	0.0057	229.2	0.0036	75.3	0.0035	113.9
35%	0.0211	143.7	0.0240	223.6	0.0175	116.0	0.0140	131.6

A better estimate of P_{bb} can be obtained by designing the piers for target limits on both P_{spall} and P_{bb}. By designing the pier for different limits on both types of damage and then selecting the more conservative design, the designer can ensure that multiple types of failures are not likely to occur. This illustrates another key strength of the DDBD procedure, namely that several limit states can be considered in design, thereby providing the designer more control over the behavior of the pier.

As shown in Figure 10.8, the probability of bar buckling (P_{bb}) is relatively insensitive to L_c/D_c and $P_c/f_c'A_g$, and no clear trends appear. Significant increases in

P_{bb} occur at low $P_c / f_c' A_g$ values in some situations. These increases could likely be eliminated by designing the piers for both P_{spall} and P_{bb}, as discussed above.

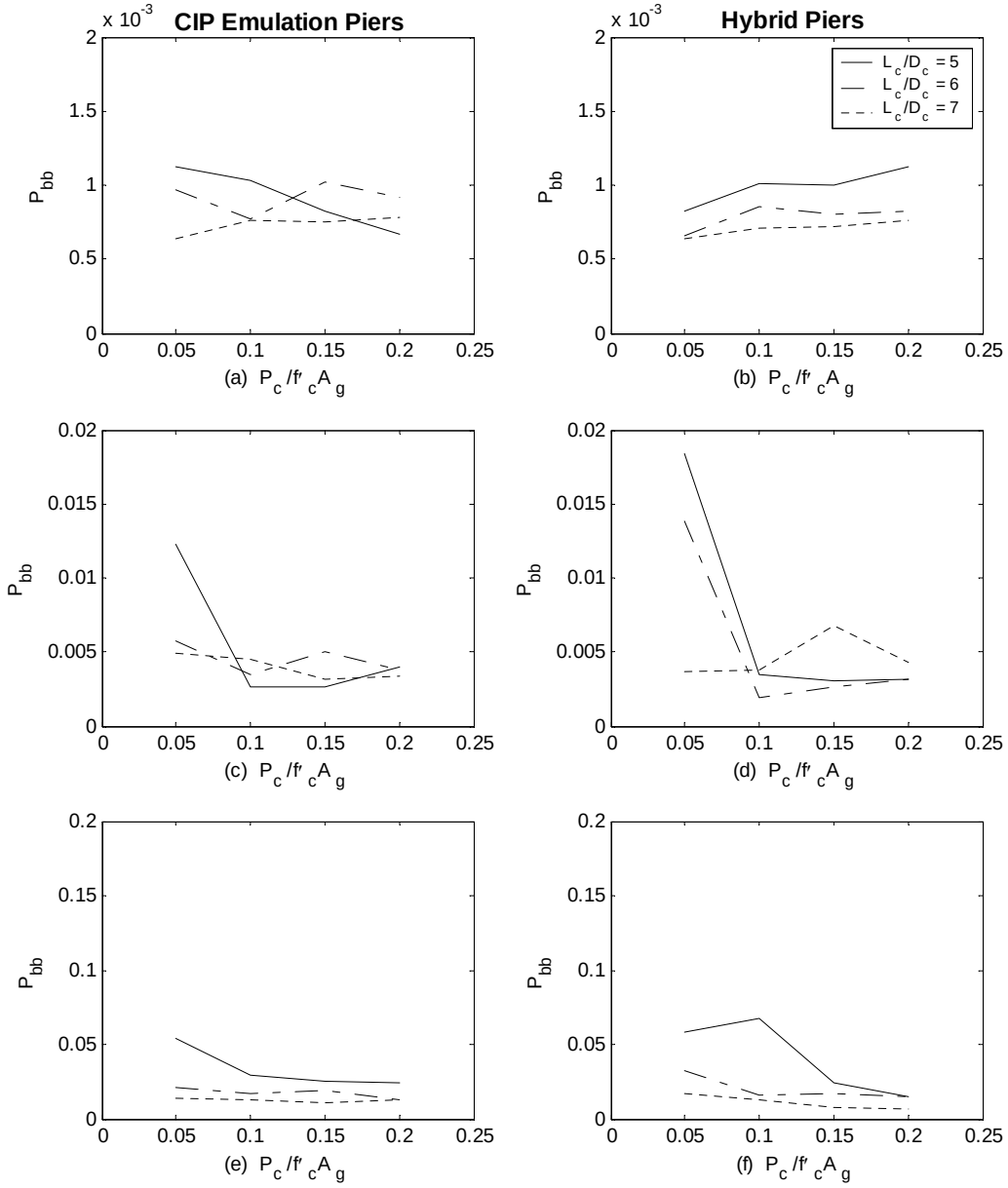

Figure 10.8: Variation in Probability of Bar Buckling for the DDBD Procedure: (a) and (b) P_{spall} = 5%, (c) and (d) P_{spall} = 15%, (e) and (f) P_{spall} = 35%

10.5 MAXIMUM STRAIN IN LONGITUDINAL REINFORCING BARS

The maximum strains in the reinforcing bars for piers designed with the DDBD procedures are similar to those obtained from the ELFD procedures. An advantage of the

DDBD procedure is that the expected maximum strain in the reinforcing steel can be calculated during design by using the target displacement. Limitations on the maximum strain in the reinforcing steel can be enforced, and the amount of reinforcement and reinforcement detailing (i.e., the debonded length of the reinforcing steel) can be determined to ensure that the strain limitations are not exceeded.

10.6 COMPARISON OF CIP EMULATION AND HYBRID PIERS

The DDBD procedure results in pier designs that experience average levels of damage similar to the target damage level for both CIP emulation and hybrid piers. The amount of reinforcement required is similar for both types of piers except at large levels, where the hybrid piers require less reinforcement to obtain a given level of damage. For the 12 piers considered, the hybrid piers exhibited a larger amount of scatter in the probability of damage occurring. This increase in variation likely occurred because the damping modification factor (β) determined in Chapter 6 is less precise for hybrid piers than for CIP emulation piers.

10.7 COMPARISON OF THE ELFD AND DDBD PROCEDURES

The ELFD and DDBD procedures both produce acceptable pier designs that are not expected to experience excessive amounts of damage in a design-level earthquake. The DDBD procedure results in a significantly smaller variation in the amount of damage than the ELFD procedure when the average response of the pier to multiple earthquakes is considered. The COV of the probability of spalling for the 12 piers designed for the largest amount of damage (R = 5, target P_{spall} = 35 percent) illustrates this. Using the ELFD procedure results in a COV of 30.0 percent for CIP emulation piers and 33.0 percent for hybrid piers, while the DDBD has a COV of only 15.8 percent for CIP emulation piers and 17.3 percent for hybrid piers.

Despite the reduced variation in average values obtained by using the DDBD procedure, the variation in the probability of damage occurring to a pier is controlled by variations in the response of the piers to different ground motion acceleration records. Given the same populations of piers, the COVs of piers designed with the ELFD procedure are 62.7 percent for CIP emulation piers and 75.5 percent for hybrid piers. The COVs for CIP emulation and hybrid piers designed with the DDBD procedure are only

slightly better at 58.9 percent for CIP emulation piers and 70.5 percent for hybrid piers. Accordingly, there is little difference in the piers designed with the two procedures when the response of the piers to individual ground motions is considered.

The average amount of reinforcing steel required by the ELFD and DDBD procedures to obtain the same level of damage is similar for both types of piers. Because the amount of damage is directly related to the amount of reinforcement in the pier, it follows that for the ELFD and DDBD procedures to design piers with the same amount of damage, the piers would have to have the same amount of reinforcement. This relation between the amount of reinforcement and damage is believed to cause the average reinforcing values to be approximately equal.

Although the performance of piers designed with the two procedures appears to be similar, there are qualitative arguments that illustrate the differences between the procedures. The ELFD procedure is simple and requires no iteration. The DDBD procedure is more complex and requires iteration. However, in practice, both the ELFD and DDBD procedures can be performed with computer spreadsheet programs, making the required design time for both procedures similar.

The primary advantage of the DDBD procedure is that the expected amount of damage in a design-level earthquake is transparent during design. The ELFD procedure could be given this feature by developing relationships between the response modification factor (R) and the expected amount of damage, as was shown in Chapter 9. However, these relationships are dependent on the characteristics of the ELFD procedure, such as the method chosen for determining the stiffness of the pier, and any changes to the procedure would require the development of new relationships. The DDBD procedure is versatile in that a new relationship between damage and deformation could be implemented with little effort, whereas the ELFD procedure would require an extensive parametric study to develop a relationship between R and the expected amount of damage.

10.8 SUMMARY

The DDBD procedure appears to be an attractive tool for the seismic design of bridge piers because it results in pier designs that, on average, perform as intended. Although the average probabilities of damage for piers designed with the DDBD

procedure have been shown to be similar to the target values, significant variation still exists in the probability of a pier being damaged in a particular design-level earthquake because of significant variations in the response of the pier to different ground motions. This variability cannot be avoided or improved by changes to the design procedure, except by using a design spectrum that lies above the mean for the hazard level being considered.

Although the DDBD procedure cannot ensure that a target damage level will be accurately met in particular pier during a particular earthquake, it is still a valuable tool for designing populations of piers because it provides the designer with a transparent and accurate idea of the average amount of damage experienced by a population of piers.

The DDBD procedure allows the designer to consider different limitations on different types of failures. This ability provides the designer with greater control over the performance of the pier, allowing certain types of failure to be avoided.

The DDBD procedure is accurate for both the CIP emulation and hybrid piers.

CHAPTER 11
SUMMARY AND CONCLUSIONS

11.1 SUMMARY

As traffic congestion in metropolitan areas increases, the costs resulting from disruptions caused by bridge construction also increase. The need for bridge systems that can be constructed rapidly is therefore greater than ever. Assembling bridges out of precast concrete elements is an attractive solution because the elements can be fabricated in advance, away from the bridge site, and then quickly connected on site, thereby minimizing the effects on traffic. Procedures for designing precast concrete bridge pier systems were developed in this study as part of a larger research initiative to develop precast systems that can be used for the rapid construction of highway bridges in seismic regions.

Two types of precast concrete pier systems were considered in this study: a cast-in-place (CIP) emulation pier system and a hybrid pier system. The CIP emulation piers contain only mild steel reinforcement and emulate conventional cast-in-place concrete construction. These piers are expected to behave like conventional cast-in-place piers. The hybrid pier consists of a combination of mild steel reinforcement and vertical unbonded post-tensioning reinforcement. The post-tensioning is designed to remain elastic during an earthquake, so that it provides a restoring force that recenters the pier after an earthquake. The mild steel reinforcement in the hybrid pier is locally unbonded at the top and bottom of the columns to minimize damage to the column.

An equivalent lateral force design (ELFD) procedure (Chapter 2) and a direct displacement-based design (DDBD) procedure (Chapter 3) were developed for determining the amount of reinforcement required to ensure acceptable pier performance in a design-level earthquake. The ELFD procedure is similar to the seismic design provisions currently included in the AASHTO specifications (AASHTO 2002; AASHTO 2004). The inertial force on the pier is determined with elastic dynamic analysis and then reduced by an empirical response modification factor (R) to determine the design force for the pier. The ELFD procedure is simple to apply and requires no iteration; however, it

provides no information on the extent of pier damage to be expected in a design-level earthquake.

The DDBD procedure requires the designer to select a target displacement based on a performance objective. The amount of reinforcement in the pier is determined by representing the inelastic pier with an equivalent linear system and applying elastic dynamic analysis. The intent of the DDBD procedure is to design the pier so that, on average, the maximum displacement during a design level earthquake is equal to the target displacement. The DDBD procedure is more complex than the ELFD procedure, but by selecting the target displacement, the designer has a good idea of how much damage will occur in a design-level earthquake.

To develop the equivalent linear system employed in the DDBD procedure, the yield displacement and equivalent viscous damping of the inelastic pier need to be estimated. Two methods for estimating the yield displacement were presented in Chapter 4. One method determines the yield displacement directly from the nonlinear pushover response of the pier, and the other method uses equations to estimate the yield displacement. The simpler, but more approximate, equation-based method is calibrated to provide yield displacement estimates similar to those from nonlinear analysis.

Methods for estimating the equivalent viscous damping were presented in Chapter 5. A nonlinear analysis method estimates the equivalent viscous damping directly from the area enclosed by a load-deflection cycle of the pier to the target displacement, whereas an equation-based method uses equations to estimate the equivalent viscous damping. A damping modification factor is required in the DDBD procedure because in the basic DDBD method, the damping is computed from load cycles to the peak displacement, whereas in practice, the random nature of ground motions leads to cycles of a variety of amplitudes. Consequently, damping varies throughout the response motion. Chapter 6 discusses empirical determination of the damping modification factor based on the results of a large number of nonlinear, dynamic analyses for both types of pier systems.

The ELFD and DDBD procedures both require a method for determining the amount of reinforcing steel required to provide sufficient capacity to carry the design force on the pier. Methods for determining the required amount of reinforcement on the

basis of the nonlinear response of the pier and sectional analysis were presented in Chapter 7.

Chapter 8 discussed verification of the accuracy of displacement predictions for three formulations of the DDBD procedure. All three formulations were found to provide suitable estimates. Chapters 9 and 10 described evaluation and comparison of the ELFD and DDBD procedures through the design of a series of piers with the two procedures and comparison of the expected damage of the piers during a design-level earthquake.

11.2 CONCLUSIONS

The ELFD and DDBD procedures, as presented in this report, both produce acceptable pier designs for both the CIP emulation and hybrid pier systems. The resulting piers are not expected to experience excessive damage or structural failure in a design-level earthquake.

11.2.1 Evaluation of ELFD Procedure

- The ELFD procedure is a quick and easy method for designing piers.
- The ELFD procedure incorporating the response modification (R) factors suggested by the AASHTO specifications (AASHTO 2002; AASHTO 2004) results in piers with reasonable probabilities of damage in a design-level earthquake.
- The CIP emulation piers have average probabilities of spalling during a design level earthquake of 5 percent, 15 percent, and 35 percent when designed for R =1.5, R = 3.5, and R = 5.0, respectively. The corresponding values for hybrid piers are 2 percent, 12 percent, and 37 percent. Although these probabilities are not small, spalling damage is repairable and is unlikely to cause structural failure of the pier.
- Longitudinal bar buckling has more drastic consequences, but the probabilities of it occurring are extremely low. The CIP emulation and hybrid piers designed for R = 5.0 have average probabilities of bar buckling of only 3.3 percent and 4.4 percent, respectively. The probabilities are below 0.5 percent for R values of 1.5 and 3.5.

- Maximum strains in the mild steel reinforcement are less than the assumed fracture strain of 0.05 in almost all cases for the CIP emulation piers. The hybrid piers have slightly higher maximum strains, but they can be reduced by deliberately debonding a greater length of the reinforcing bars at the top and bottom of the columns.
- The probabilities of damage, as predicted in this study, are similar for the CIP emulation and hybrid piers. This finding justifies the use of the same R values for both types of piers. If future experimental research on hybrid piers allows for better damage estimates, the corresponding R values should be reconsidered.
- Although this research determined the amount of damage likely to occur for piers designed with the three R values included in the AASHTO specifications, the ELFD procedure provides no direct way to estimate *a priori* the damage to be expected if a different value of R is used. Also, if any changes are made to the ELFD procedure, such as the method for estimating the pier stiffness, the relationship between R and the expected amount of damage will have to be determined again.

11.2.2 Evaluation of DDBD Procedure

- The DDBD procedure is slightly more complicated than the ELFD procedure, but it is still simple enough for design office use. It provides the designer with an estimate of the extent of damage likely to occur in a design-level earthquake.
- The three formulations of the DDBD procedure considered in Chapter 8 are all capable of accurately predicting the maximum displacement of the pier. The iterative procedure using nonlinear analysis is the most accurate. While the iterative procedure using equation-based methods and the direct procedure using equation-based methods are not quite as accurate and underpredict the maximum displacement slightly, they do not require nonlinear analysis. This makes them much easier to apply in practice.
- The DDBD procedure can be used to design piers with a constant average probability of damage in a design-level earthquake. While the actual amount of damage can still vary considerably depending on the characteristics of the

particular earthquake, the average amount of damage for a population of piers is close to that selected during design. For the CIP emulation piers, average probabilities of spalling of 5.6 percent, 16.4 percent, and 36.3 percent are obtained for target values of 5.0 percent, 15.0 percent, and 35.0 percent, respectively. For hybrid piers, average probabilities of spalling of 5.8 percent, 15.3 percent, and 34.4 percent are obtained for the same target values.

- Multiple types of damage, such as spalling and bar buckling, and other limit states can be considered in the DDBD procedure. This versatility allows the designer to avoid susceptibility of the pier to any one type of failure. Other types of damage could be incorporated into the DDBD procedure with little effort, provided that a relationship between the deformation of the pier and the expected amount of damage is known.

11.2.3 Comparison of Design Procedures

- Piers designed with the ELFD and DDBD procedures exhibit similar variation in the amount of damage expected during a design-level earthquake.
- Relationships between the response reduction factor (R) and the amount of different types of damage can be developed for use in the ELFD procedure. These relationships would give the designer a clear idea of how much damage to anticipate by designing for a given R; however, any changes to the ELFD procedure would require recalibration of the relationships.
- When piers are designed for a specified damage limit, either through the selection of the target displacement in the DDBD procedure or use of relationships relating R and anticipated damage in the ELFD procedure, the variation in damage to the piers in an earthquake is similar. While the ELFD procedure requires fewer steps, both procedures can easily be implemented in a spreadsheet computer program, making the required design time similar for both procedures. The DDBD is slightly advantageous because it does not require the creation of relationships s

11.2.4 Comparison of the CIP Emulation and Hybrid Piers

- The CIP emulation precast pier system and hybrid precast pier system are both capable of providing lateral force resistance in an earthquake that is sufficient to make any particular form of damage unlikely.
- The amount of reinforcement required to provide sufficient lateral resistance is similar for both types of piers. For the hybrid piers, an equivalent reinforcing ratio is used to define the total amount of reinforcement.
- Hybrid piers are advantageous because they encourage recentering of the pier after an earthquake. However, in many cases the weight of the superstructure acting on the pier would be sufficient to cause CIP emulation piers to recenter anyway.

11.3 RECOMMENDATIONS FOR FUTURE WORK

The following are recommendations for possible future work on the development of precast concrete pier systems for rapid construction in seismic regions and the development of design procedures for bridge piers.

- Methods for connecting the precast concrete elements must still be developed. The connections need to be capable of carrying the full moment capacity of the columns and must be constructed easily. Careful consideration of the transfer of internal forces in the connections is needed. Experimental testing will likely be required to validate connection seismic performance and constructability.
- The design procedures developed in this report were calibrated and evaluated by using nonlinear finite-element pier models. To ensure that the design procedures accurately represent the response of real piers, the nonlinear pier models should be calibrated with experimental test results to ensure that they accurately represent the response of both the CIP emulation and hybrid piers. Sufficient test results currently exist to calibrate the CIP emulation pier, but more experimental testing is required to provide the necessary data for calibrating the hybrid pier model.

- The DDBD procedure developed in this study could be expanded to the design of complete bridges that considers multiple-degree-of-freedom response during an earthquake.
- Better predictions of the amount of damage experienced by hybrid piers could be determined from experimental testing. This would allow a better comparison between CIP emulation and hybrid piers that considered more types of damage than just cover spalling and bar buckling.
- The yield displacement (sections 4.3 and 4.4) and equivalent viscous damping (Section 5.3) values estimated with the equation-based method in this study could be improved by developing relationships that better represent the results of nonlinear analyses than the simplified linear functions employed in this research.
- Further study is required to determine the sources of variability in the expected damage to a pier during various earthquakes.

ACKNOWLEDGMENTS

The research presented in this report was funded by the Washington Department of Transportation (WSDOT) and the Valle Scholarship and Scandinavian Exchange Program at the University of Washington.

Technical support for this project was provided by the Bridges and Structures Office of WSDOT, notably Jugesh Kapur, Jerry Weigel, Mo Sheikhizadeh, and Bijan Khaleghi. Information on the fabrication and construction of precast bridges was also provided by Stephen Seguirant of Concrete Technology Corporation in Tacoma, Washington; Charles Prussack of Central Premix in Spokane, Washington; and a number of members of the Associated General Contractors of Washington.

REFERENCES

AASHTO (1992). *Standard Specifications for Design of Highway Bridges*, 15 ed., American Association of State Highway and Transportation Officials, Washington D.C.

AASHTO (1994). *Load and Resistance Factor Bridge Design Specifications*, 1 ed., American Association of State Highway and Transportation Officials, Washington D.C.

AASHTO (2002). *Standard Specifications for Design of Highway Bridges*, 17 ed., American Association of State Highway and Transportation Officials, Washington D.C.

AASHTO (2004). *Load and Resistance Factor Bridge Design Specifications*, 3 ed., American Association of State Highway and Transportation Officials, Washington D.C.

ATC (1978). *Tentative Provisions for the Development of Seismic Regulations for Buildings*, Applied Technology Council, Report No 3-06, Redwood City, California.

ATC (1981). *Seismic Design Guidelines for Highway Bridges*, Applied Technology Council, Report No. ATC-6, Redwood City, California.

ATC/MCEER (2002). "Comprehensive Specification for the Seismic Design of Bridges," NCHRP Report No 472, National Academy Press, Washington, D.C.

Barkley, T. and Strasburg, G. (2002). "Bridge Rebuilt on the Fast Track," *Public Roads*, V. 66, No. 2, Sept/Oct.

Berry, M. and Eberhard, M. (2004). "Performance Models for the Flexural Damage of Reinforced Concrete Columns," Pacific Earthquake Engineering Research Center, Report No. 2003/18, University of California, Berkeley.

CALTRANS (2004). *Seismic Design Criteria, Version 1.3*, California Department of Transportation, Sacramento, California.

Cheok, G.S. and Lew, H.S., (1991). "Performance of Precast Concrete Beam-to-Column Connections Subject to Cyclic Loading," *PCI Journal*, V. 36, No. 3, May-June, pp. 56-67.

Cheok, G.S. and Lew, H.S., (1993). "Model precast concrete beam-to-column connections subject to cyclic loading," *PCI Journal*, V. 38, No. 4, July-Aug., pp. 80-92.

Chopra A.K., (2001). *Dynamics of Structures: Theory and Applications to Earthquake Engineering*, 2 ed., Prentice Hall, Upper Saddle River, New Jersey.

Chopra, A.K. and Goel, R.K. (2001). "Direct Displacement-Based Design: Use of Inelastic vs. Elastic Design Spectra," *Earthquake Spectra*, V. 17, No. 1, Feb., pp. 47-64.

Endicott, W.A. (2005). “Precast Aids Fast Track Bridge Replacement Again,” *Ascent*, Spring, pp. 32-35.
EUROCODE 8: Design Provisions for Earthquake Resistant Structures- Part 1-1: General Rules- Seismic Actions and General Requirements for Structures (1994). ENV 1998-1-1:1994, CEN- European Committee for Standardization, Brussels.

Gulkan, P. and Sozen, M.A. (1974). “Inelastic Response of Reinforced Concrete Structures to Earthquake Motions,” *ACI Journal*, V. 71, pp. 604-610.

Hamburger, R.O. (2003). “Building Code Provisions for Seismic Resistance,” *Earthquake Engineering Handbook*, ed. Chen, W. and Scawthorn, C., CRC Press, Boca Raton, Florida.

Hieber, D.G., Wacker, J.M., Eberhard, M.O. and Stanton, J.F., (2005a). “State-of-the-Art Report on Precast Concrete Systems for Rapid Construction of Bridges,” Washington State Department of Transportation Technical Report WA-RD 594.1, Olympia, Washington, March.

Hieber, D.G., Wacker, J.M., Eberhard, M.O. and Stanton, J.F., (2005b). “Precast Concrete Pier Systems for Rapid Construction of Bridges in Seismic Regions,” Washington State Department of Transportation Technical Report WA-RD 611.1, Olympia, Washington, Under Review.

Jacobsen, L.S. (1930). “Steady Forced Vibration as Influenced by Damping,” ASME Tansactione, APM-52-15, V. 52, No. 1, pp. 169-181.

Jennings, P.C. (1968) “Equivalent Viscous Damping for Yielding Structures,” *ASCE Journal of the Engineering Mechanics Division*, V. 94, No. EM1, pp. 103-116.

Jones, K. and Vogel, J. (2001). “New Precast Bent Cap System: Saving Texas Time and Money,” *TR News*, No. 212, Feb., pp. 40-41.

Kowalsky M.L., Priestley, M.J. N., and MacRae, G.A. (1995). “Displacement-based Design of RC Bridge Columns in Seismic Regions,” *Earthquake Engineering and Structural Dynamics*, V. 24, pp. 1623-1643.

Lehman, D.E. and Moehle, J.P. (2000). “Performance-Based Seismic Design of Well-Confined Concrete Columns”, PEER Research Report 1998/01, Pacific Earthquake Engineering Research Center.

MacGregor, J.G. (1997). *Reinforced Concrete: Mechanics and Design*, Prentice Hall, Upper Saddle River, New Jersey.

Mattock, A.H., Kriz, L.B., and Hognestad, E. (1961). “Rectangular Concrete Stress Distribution in Ultimate Strength Design,” *ACI Journal, Proceedings,* V. 57, No. 8, Feb., pp. 875-928.

Miranda, E. and Ruiz-Garcia, J. (2002). “Evaluation of approximate methods to estimate maximum inelastic displacement demands,” *Earthquake Engineering and Structural Dynamics*, V. 31, pp. 239-560.

PEER (2005). “PEER Structural Performance Database,” Pacific Earthquake Engineering Research Center, http://nisee.berkeley.edu/spd/.

Priestley, M. J. N., Seible, F., and Calvi, G. M., (1996). *Seismic Design and Retrofit of Bridges*, John Wiley & Sons, New York, NY.

Rosenblueth, E. and Herrera, I. (1964). “On a kind of hysteretic damping,” *ASCE Journal of the Engineering Mechanics Division*, V. 90, No. EM4, pp. 37-48.

Shibata A. and Sozen M.A. (1976). “Substitute-Structure Method for Seismic Design in R/C,” *ASCE Journal of the Structural Division*, V. 102, ST1, pp.1-18.

Stanton, J.F. and Nakaki, S.D. (2002), “Design guidelines for precast concrete seismic structural systems,” PRESSS Report No. 01/03-09, UW Report No. SM 02-02, Department of Civil Engineering, University of Washington, Seattle, January.

Stone, W.C., Cheok, G.S., and Stanton, J.F., (1995). “Performance of hybrid moment-resisting precast beam-column concrete connections subjected to cyclic loading,” *ACI Structural Journal*, V. 91, No. 2, Mar.-Apr., pp. 229-249.

Takeda, T., Sozen M.A., and Nielsen, N.N., (1970). “Reinforced Concrete Response to Simulated Earthquakes,” *Proceedings, ASCE,* V. 96, ST 12, Dec., pp. 2557- 2573.

Wacker, J.M. (2005). “Design of Precast Concrete Bridge Piers for Rapid Bridge Construction in Seismic Regions,” M.S.C.E. Thesis, Department of Civil and Environmental Engineering, University of Washington, 226pp.

APPENDIX A
NONLINEAR MODELING OF PRECAST PIER SYSTEMS

Two-dimensional, nonlinear finite element models were developed to estimate the response of CIP emulation and hybrid precast piers during an earthquake. This appendix discusses the prototype pier chosen for modeling, the formulation of nonlinear finite-element models for the piers, and the different analyses performed on the pier models.

A.1 PROTOTYPE PIER

A pier of the State Route 18 bridge over State Route 516 in King County, Washington, was selected as the prototype pier for this study. This pier was designed by WSDOT in 1996 and chosen because it is uniform and similar to other piers designed by WSDOT during the same time period. CIP emulation and hybrid piers developed with the dimensions of the prototype are shown in Figure A.1. The column diameter (D_c), column height (L_c), mild steel reinforcing ratio (ρ_s) of the column, post-tensioning reinforcing ratio (ρ_p) in hybrid piers, and the gravity load on the pier due to the weight of the superstructure (P_c) were varied in the model. The remaining characteristics of the pier remained constant.

The cross-sections of the pier columns are shown in Figure A.2. Because the amount of mild steel reinforcement was a variable, the size and number of mild steel reinforcing bars was not constant. To eliminate this complication, all columns were assumed to have 24 mild steel reinforcing bars, each with a diameter of 1.41 in. The area of each bar (A_{bar}) was then

$$A_{bar} = \frac{1}{24}\rho_s A_g \tag{A.1}$$

where A_g is the cross-sectional area of the column. This resulted in fictitious bars with diameters and areas that did not physically correspond to one another. This approach was verified to produce results similar to those produced by using a variable number of real

bars. Transverse reinforcement consisting of #6 spiral reinforcement at a 3-in. pitch was used for all models.

Because of the modeling assumptions, presented later in this appendix, the models were not very sensitive to the characteristics of the pier that were not varied. This made the selection of the prototype less critical.

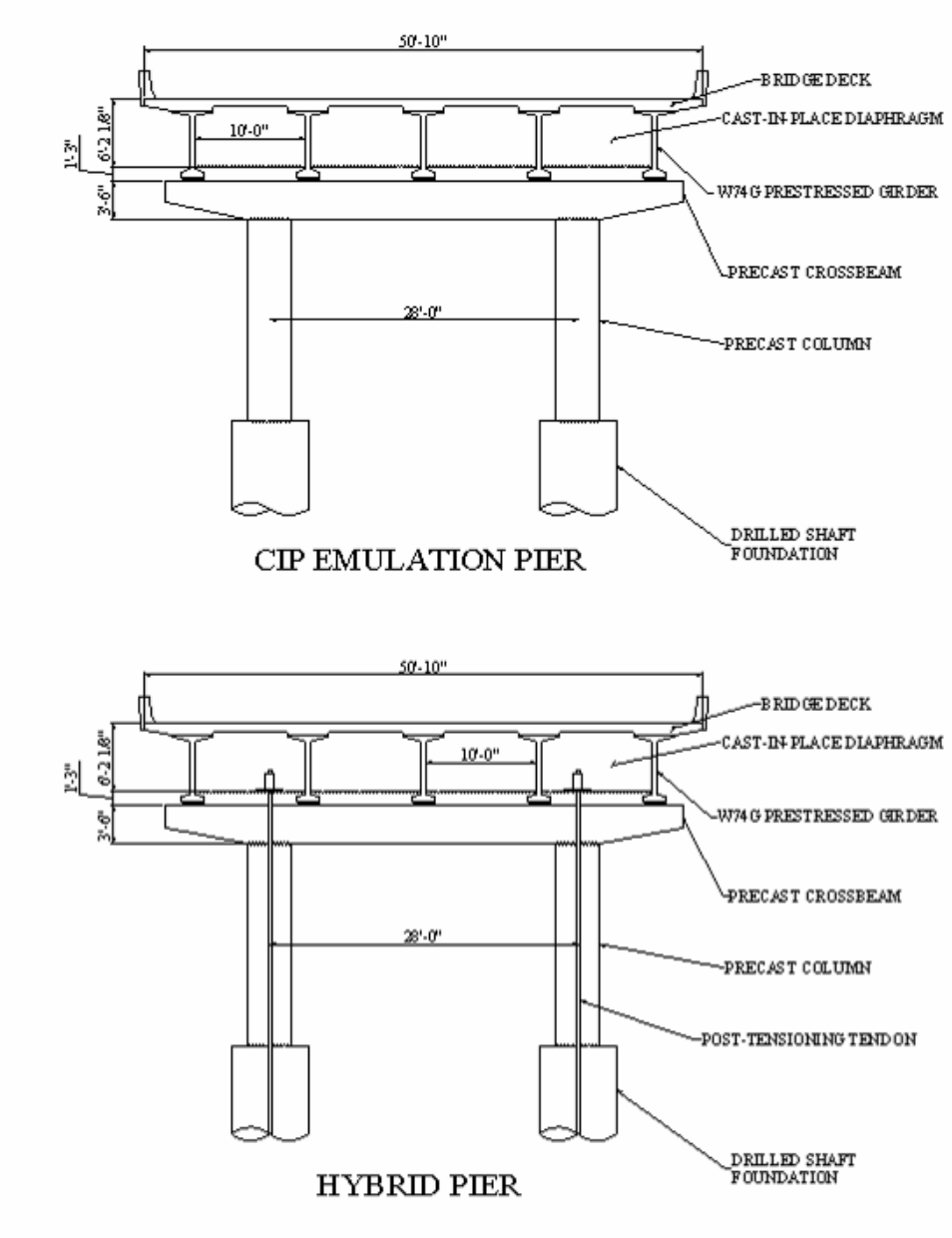

Figure A.1: Elevation View of the Prototype Pier

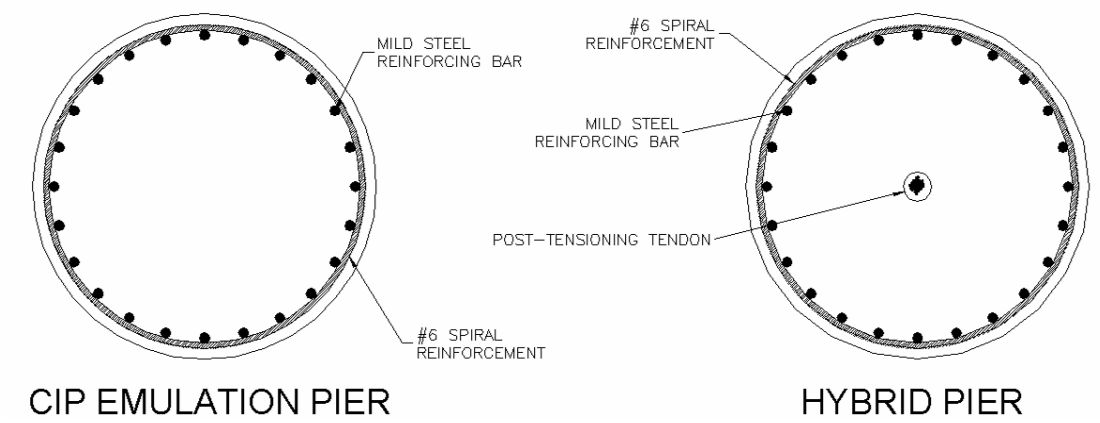

Figure A.2: Cross-Section of the Columns of the Prototype Pier

A.2 NONLINEAR FINITE ELEMENT MODEL OF PIER

The piers were modeled and analyzed with the Open System for Earthquake Engineering Simulation (OpenSEES) program developed by the Pacific Earthquake Engineering Research Center (PEER) (Mazzoni et al. 2005). OpenSEES was developed specifically to simulate the response of structures to earthquakes. It was selected for this study because of its ease of availability, growing popularity among academic researchers, and ability to handle parametric analyses.

Schematics of the models used to represent the pier systems are shown in Figure A.3. The models are composed of elements representing the two distinct portions of the pier: the columns and the cap beam. Rotational springs are included in the models to represent the behavior of the column-to-footing and column-to-cap beam connections. Additional elements are included in the hybrid pier model to represent the unbonded post-tensioning. The elements representing the columns and cap beam are identical for the two types of piers. The rotational springs representing the behavior of the connection regions vary significantly between the models. This mimics real-life, where the only differences between the types of piers are the connections of the precast components and the presence of unbonded post-tensioning in hybrid piers.

Shared properties of the models for both precast pier systems are discussed in Section A.2.1. The rotational springs representing the behavior of the connections and other characteristics specific to the model of one pier system are presented in sections A.2.2 and A.2.3. The computer script used to model and analyze the piers in

OpenSEES, along with an executable OpenSEES program, is described by Wacker (2005).

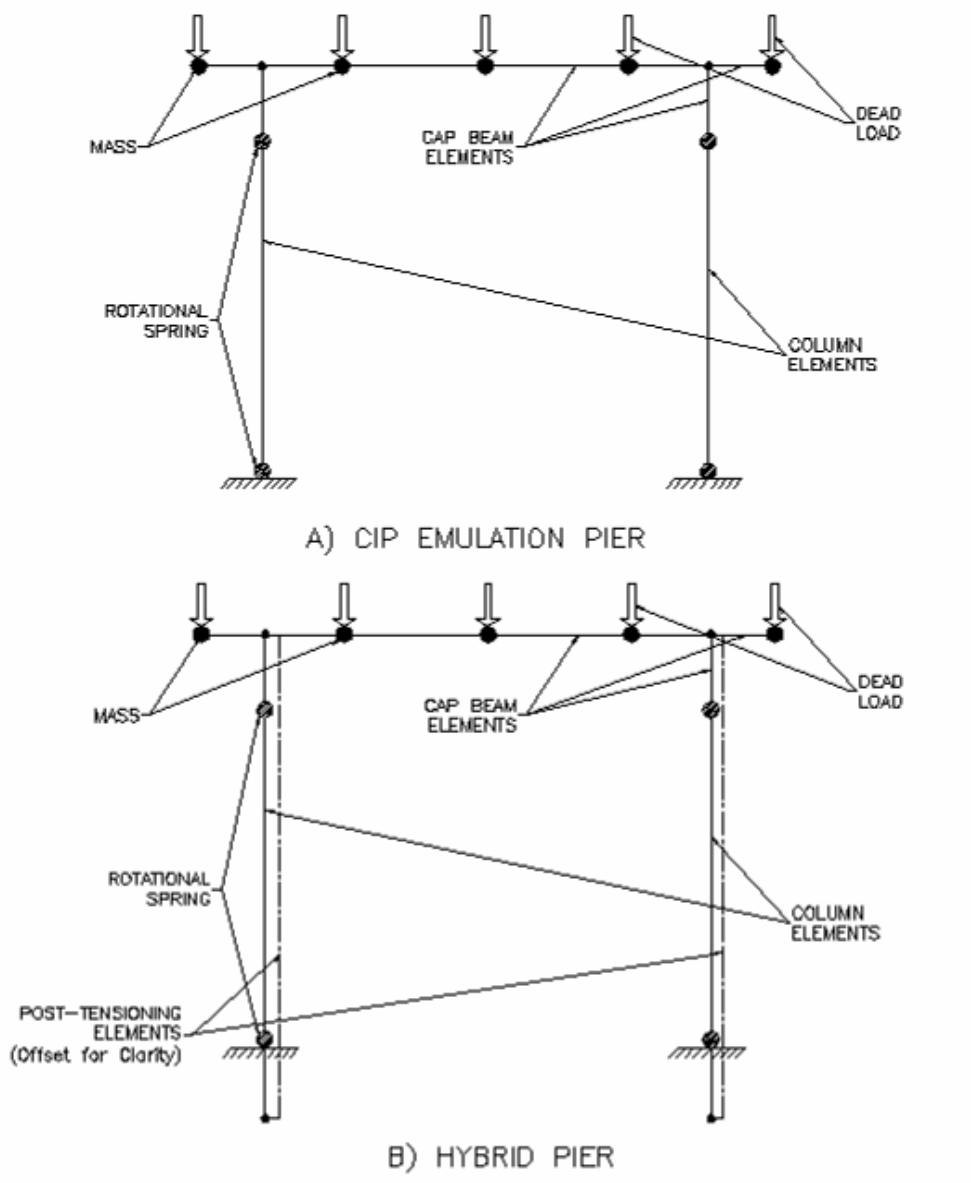

Figure A.3: Schematics of Pier Models

A.2.1 Shared Elements and Characteristics

Column Elements

Each column was represented by one fiber force-based beam-column element (Spacone et al. 1996). The element was intended to capture the nonlinear, hysteretic

behavior of the precast concrete columns by accounting for nonlinearity along the length of the column. The distribution of plasticity was determined by using five integration points spaced along the column according to the Gauss-Lobatto quadrature rule. The number of integration points used can have a significant effect on the behavior of the model. The decision to use five integration points was made arbitrarily to match the work of other researchers (personal communication, R. Tyler Ranf, August 2004).

The strength and stiffness of the column were defined at each integration point with a fiber model of the column cross-section. The fiber model is shown in Figure A.4. The cross-section of the column was discretized into 20 angular divisions. The core (inside the transverse reinforcement) and cover (outside the transverse reinforcement) regions of the column were divided into ten and five radial divisions, respectively. Fibers with different uniaxial stress-strain relationships were used to represent the cover concrete, core concrete, and mild steel reinforcement. The stress-strain relationships of these materials are discussed below.

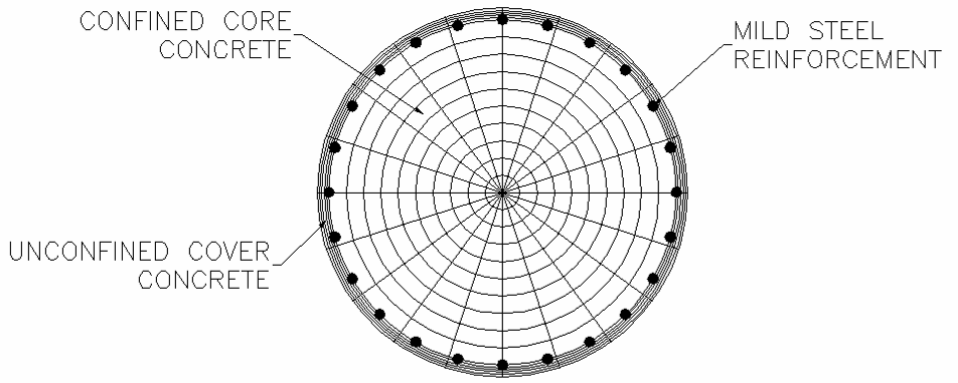

Figure A.4: Fiber Model for Representing the Column Cross-Section

The stress-strain relationship of the unconfined cover concrete was represented with a default material model in OpenSEES, *Concrete02* (Mazzoni *et al*. 2005). Figure A.5 shows the hysteretic stress-strain behavior of the material. The compressive portion of the relationship was adapted from the model proposed by Kent and Park (1971). The portion of the curve before the peak compressive stress ($f_c^{'}$) consists of a parabola with zero slope at $f_c^{'}$. After reaching $f_c^{'}$, the stress decreases linearly with strain until it reaches zero at the ultimate unconfined strain of the concrete (ε_{sh}). The initial slope of

the parabola (m_0) can be determined from $f_c^{'}$ and the strain at the peak compressive stress (ε_{c0}) by using Equation A.2.

$$m_0 = \frac{2 f_c^{'}}{\varepsilon_{c0}} \tag{A.2}$$

For unconfined concrete, m_0 is similar to the elastic modulus of concrete (E_c). The cyclic behavior of the material model consisted of linear unloading and reloading according to the work of Karsan and Jirsa (1969). The tension portion of the relationship was linear to the ultimate tensile strength of concrete ($f_t^{'}$), followed by linear tension softening to zero stress. Both portions of the tensile relationship had slopes equal to E_c . The material properties listed below for unconfined concrete were used in all analyses:

- compressive strength of unconfined concrete ($f_c^{'}$): 5 ksi
- strain at $f_c^{'}$ in unconfined concrete (ε_{c0}): 0.002
- ultimate strain in unconfined concrete (ε_{sh}): 0.005
- ultimate tensile strength of unconfined concrete ($f_t^{'}$): 530 psi.

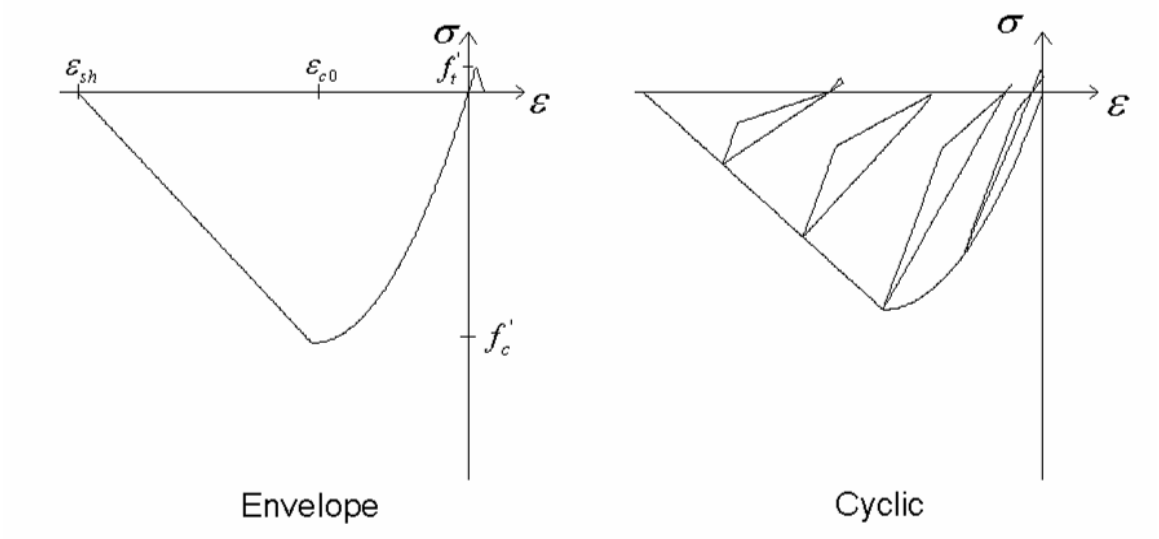

Figure A.5: Stress-Strain Relationship of Unconfined Cover Concrete

The confined concrete was not represented with the same material model as the unconfined concrete. Because of the effects of confinement, using a parabola to represent the confined concrete results in m_0 being significantly less than E_c . This causes the pier

models to significantly overestimate elastic deformations. To avoid this problem, the stress-strain relationship of the confined core concrete was represented with a custom material model developed by Nilanjan Mitra at the University of Washington. The stress-strain relationship for the confined concrete is shown in Figure A.6.

The compressive region of the relationship was represented with the curve developed by Popovics (1973). This curve allows E_c to be specified as m_0. The concrete was assumed to fail at the ultimate confined compressive strain (ε_{cu}), resulting in a sudden drop to zero strength (personal communication, N. Mitra, October 2005). The effects of confinement on the material properties of the core concrete were determined by using the confinement model proposed by Mander et al. (1988). The material model assumed that the core concrete is not capable of carrying tensile stresses. The material properties of the confined core concrete for a 48-in.-diameter column are listed below:

- compressive strength of confined concrete ($f_{cc}^{'}$): 7.30 ksi
- strain at $f_{cc}^{'}$ in confined concrete (ε_{cc}): 0.0065
- ultimate strength of confined concrete ($f_{cu}^{'}$): 6.15 ksi
- ultimate strain of confined concrete (ε_{cu}): 0.0220.

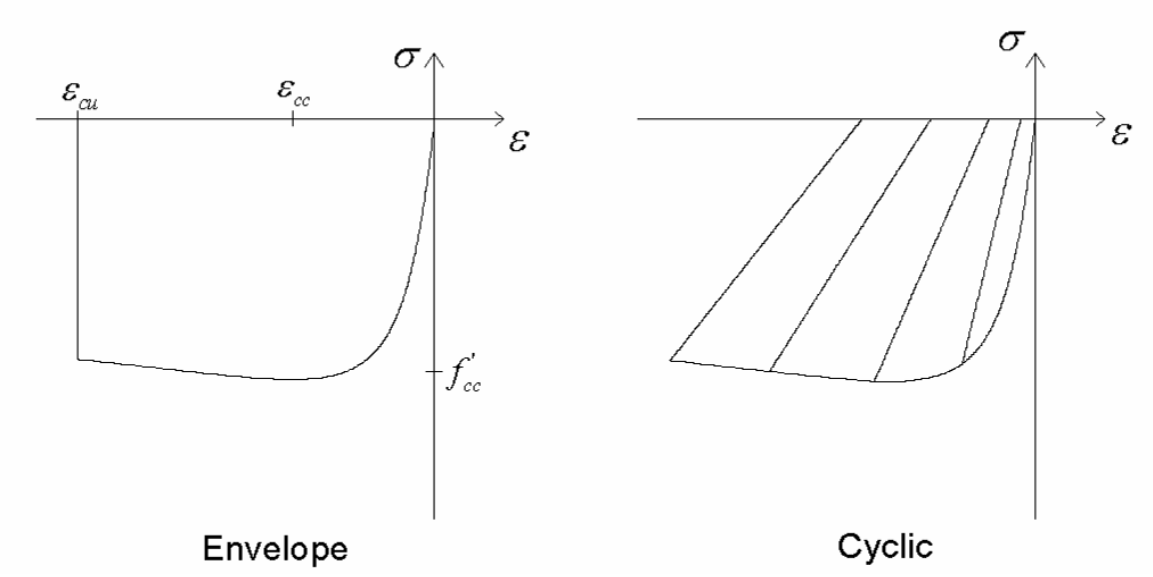

Figure A.6: Stress-Strain Relationship of Confined Concrete

The mild steel reinforcement was represented by the stress-strain relationship shown in Figure A.7 developed by Menegotto and Pinto (1973). This relationship is a default material model in OpenSEES, *steel02* (Mazzoni *et al.* 2005). Isotropic strain hardening of the reinforcement was not considered. The same material properties were used for the mild steel reinforcement in all analyses and are listed below:

- elastic modulus of mild steel reinforcement (E_s): 29,000 ksi
- yield strength of mild steel reinforcement (f_y): 60 ksi
- ultimate strength of mild steel reinforcement (f_{su}): 90 ksi
- ultimate strain in mild steel reinforcement (ε_{su}): 0.12.

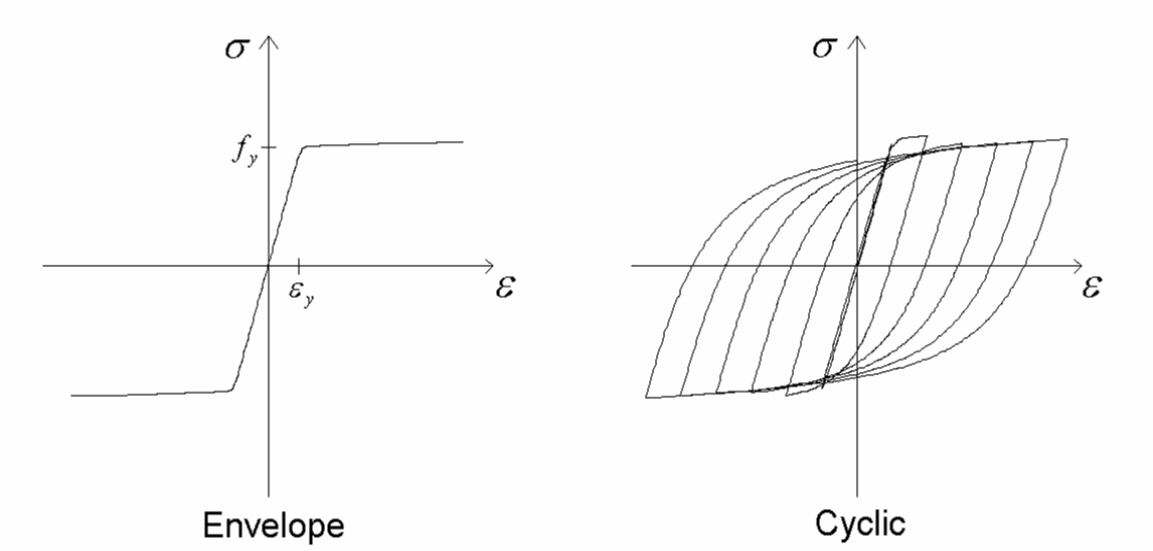

Figure A.7: Stress-Strain Relationship of Mild Steel Reinforcement

Cap Beam

The cap beam of the pier was represented by elastic beam-column elements. The cap beam was modeled with elastic elements because capacity design is used for bridge piers to ensure that the cap beam does not yield during an earthquake. Two elements were used to represent the distance between the top of the columns and the elastic neutral axis of the cap beam. The remainder of the elements represented the span of the cap beam and the overhangs. All of the elements were given very large axial and bending stiffness so that they would perform as rigid beams. A parallel study has shown that cap beams with dimensions similar to the prototype pier behave as essentially rigid beams (Hieber 2005).

Gravity Loads and Mass

Gravity load on the pier due to the weight of the superstructure was applied to the cap beam in the model at the locations of the girders in the prototype. The gravity load was assumed to be distributed evenly among all the girders. The amount of mass corresponding to the gravity load was applied to the model in the same location as the gravity load. The mass was assumed to act only in the horizontal direction.

Foundations

The foundations of all columns were modeled as fixed. This is a simplification because real-life foundations are flexible and can have a significant effect on pier behavior. However, the effect of flexible foundations on the pier models was beyond the scope of this work.

Geometric Effects

Increases to the moment demand on the columns due to second order P-delta effects were considered in all analyses.

Damping

The only type of damping the models considered was hysteretic damping caused by energy dissipation when the pier is deformed inelastically. Viscous damping was neglected because it is likely to be small in bridge piers with no nonstructural elements and difficulties were encountered when viscous damping was implemented in OpenSEES. Radiation damping from soil-structure interaction was ignored because foundation effects were not considered in this study.

A.2.2 Elements Specific to the CIP Emulation System

The effects of strain penetration of the embedded column reinforcing bars on the behavior of the column-to-footing and column-to-cap beam connections in the CIP emulation system were represented in the model using nonlinear rotational springs at the top and bottom of each column. The overall effect of the springs was an increase in the

deflection of the pier for a given amount of load, which is analogous to the effect that strain penetration is expected to have on the pier. Zero-length fiber elements were used to represent the springs. The moment-rotation relationship of the springs was determined by using a fiber model similar to the one used to represent the precast columns. For a given amount of rotation, the deformation in each fiber was determined by assuming the location of the neutral axis. The stress in each fiber was determined by using uniaxial stress-deformation relationships specified for the materials of the spring. The location of the neutral axis was iterated until axial force equilibrium was obtained, and the moment on the cross-section was then calculated. The development of stress-deformation relationships is discussed below.

The tensile stress-deformation relationship for the embedded steel bars was determined by using the Lehman bond-slip model (Lehman and Moehle 2000). The Lehman bond-slip model assumes a uniform bond stress along the length of the embedded bar. The elastic bond strength (τ_e) is assumed to be $0.012\sqrt{1000 f_c'}$, and the inelastic bond strength (τ_i) is assumed to be $0.006\sqrt{1000 f_c'}$, where τ_e, τ_i, and f_c' are in ksi. The deformation of the bar is determined by integrating the strain in the bar along the embedded length. When the bar stress (f_s) is less than the yield stress, the elongation due to strain penetration (δ_{sp}) is

$$\delta_{sp} = \frac{1}{8}\frac{f_s^2 d_b}{\tau_e E_s} \tag{A.3}$$

where d_b is the diameter of the mild steel reinforcing bars. For bar stresses greater than the yield stress, δ_{sp} becomes

$$\delta_{sp} = \frac{1}{8}\frac{d_b}{\tau_i}\left[(f_s - f_y)^2\left(\frac{\varepsilon_{su} - \varepsilon_y}{f_{su} - f_y}\right) + \frac{2 f_y (f_s - f_y)}{E_s}\right] + \frac{1}{8}\frac{f_y^2 d_b}{\tau_e E_s} \tag{A.4}$$

The tensile stress-deformation relationship for the 1.41-in.-diameter reinforcing bars considered in this study is shown in Figure A.8 along with a trilinear curve used to approximate the relationship. The stress-deformation relationship of the reinforcing bars in compression assumed that the strains in the bar were distributed evenly over an effective length. An effective length of one-half the column diameter was used in this

study. The stress-deformation relationship of the reinforcing bars, as shown in Figure A.9, was implemented in OpenSEES by using a *hysteretic* material model (Mazzoni *et al.* 2005).

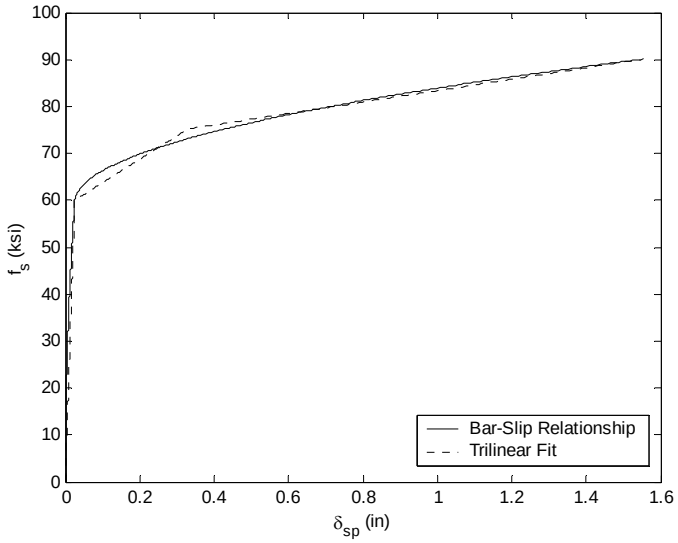

Figure A.8: Stress-Deformation Relationship of Mild Steel due to Strain Penetration

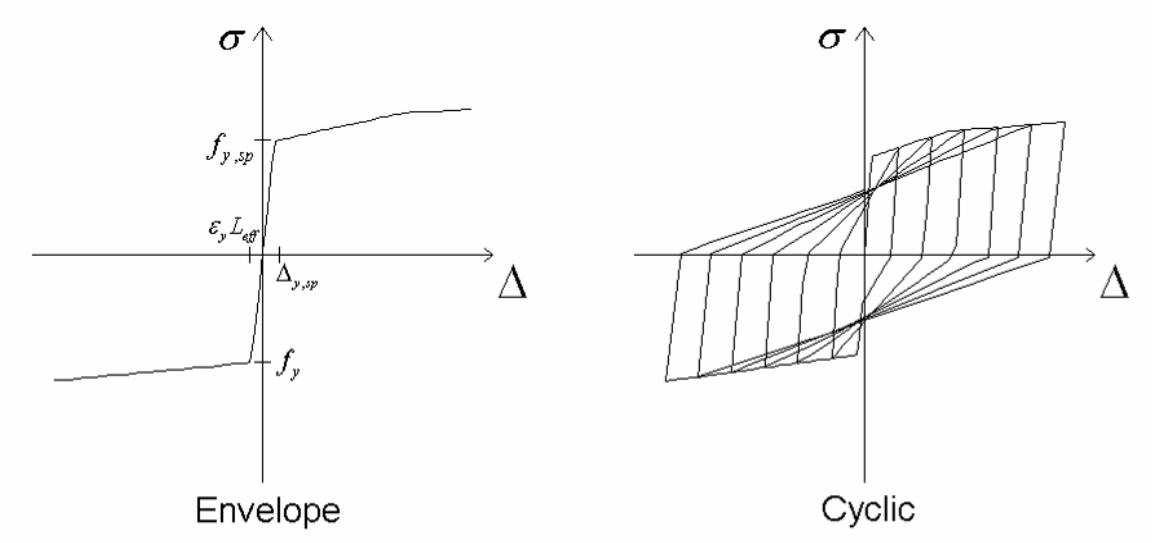

Figure A.9: Stress-Deformation Relationship of Embedded Mild Steel Reinforcement

The stress-deformation relationship of the concrete was adapted from the stress-strain relationship used to represent the core concrete in the columns. The effective depth over which strains in the concrete fibers were assumed to act was one-half the column

diameter. Using this effective length to determine the stress-deformation relationships has been shown to result in deformation estimates that correspond to experimental data for reinforced concrete columns (personal communication, R. Tyler Ranf and Michael Berry, August 2004). The concrete was assumed to be ultra-confined, with ε_{cu} 100 times larger than that for the core concrete in the column. This increased confinement was provided because compressive failure of the concrete in the footing or cap beam of the pier is unlikely to occur before compressive failure of concrete in the column. All concrete fibers in the zero-length element were assumed to be confined.

A.2.3 Elements Specific to the Hybrid System

The effect of debonding the mild steel reinforcement at the column-to-footing and column-to-cap beam interfaces was represented in the hybrid pier model with nonlinear rotational springs. Using the same approach as that for the CIP emulation piers, the nonlinear rotational springs were represented with zero-length fiber elements. The stress-deformation relationship of the mild steel reinforcement was determined from the stress-strain relationship by assuming that the strains distribute uniformly over the portion of the bar that is intentionally debonded in the interface region. The debonded length was assumed to be one-fourth the column diameter in this research. The same stress-deformation relationship was used for the concrete as that used for the CIP emulation pier models (Section A.2.2).

The vertical, unbonded post-tensioning tendons were represented in the model by elastic beam-column elements with negligible bending stiffness. The elements were attached to the pier at locations that represented the post-tensioning anchors in a pier. The bottom anchorage was assumed to be in the middle of the footing and the top anchorage was assumed to be in the middle of the cap beam. An additional rigid link was added to the model to account for the distance from the bottom of the column to the center of the footing. OpenSEES does not support axial element loads. Therefore, the initial prestressing in the post-tensioning tendons was represented in the model with a fictitious change in temperature. The temperature of the elements representing the tendons was reduced causing them to contract until the induced stress was equal to the initial prestress. The material properties of the post-tensioning tendon are listed below:

- elastic modulus of post-tensioning reinforcement (E_p): 28,500 ksi
- yield strength of post-tensioning reinforcement (f_{py}): 243 ksi
- ultimate strength of post-tensioning reinforcement (f_{pu}): 270 ksi.

A.3 TYPES OF ANALYSES

A.3.1 Static

The static analyses consisted of both pushover and push-pull analyses. A pushover analysis consists of displacing the top of the pier horizontally to a specified target displacement through a series of small displacement increments. The horizontal load on the pier that is needed to reach the displacement is determined at every increment. A pushover analysis is typically represented by plotting the horizontal displacement of the pier (Δ) against the horizontal force required to reach the displacement (F), as shown in Figure A.10 for a typical reinforced concrete pier.

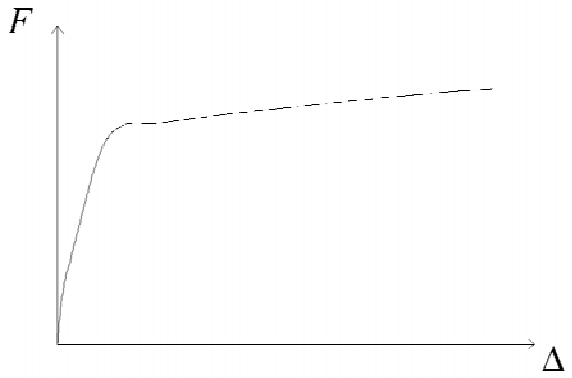

Figure A.10: Pushover Analysis Results of a Typical Reinforced Concrete Pier

A push-pull analysis is an extension of a pushover analysis. After the pier has been displaced to the target displacement, it is brought back to the initial configuration and displaced to the target displacement in the opposite direction before returning to the initial position. This results in a complete displacement cycle, as shown in Figure A.11 for a typical reinforced concrete pier. Several important quantities, including the yield displacement, hysteretic damping, and force at the target displacement, can be determined from these analyses.

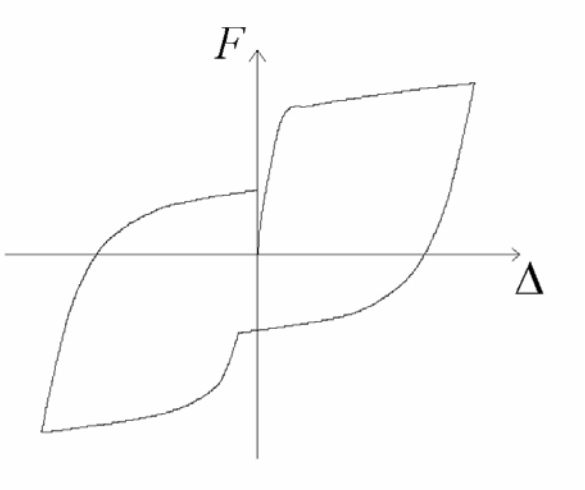

Figure A.11: Push-Pull Analysis Results of a Typical Reinforced Concrete Pier

A.3.2 Dynamic

The dynamic analyses performed in this study consisted of simulating the behavior of the pier during an earthquake. The primary value of interest in the seismic analyses was the lateral displacement of the pier. The response of a typical reinforced concrete pier is shown in Figure A.12. In this study, the response of the pier to ground motion acceleration records from five different earthquakes was considered because the characteristics of the ground motion can have a significant effect on the response of the pier. The development of the five ground motion acceleration records used in this study is discussed in Appendix B.

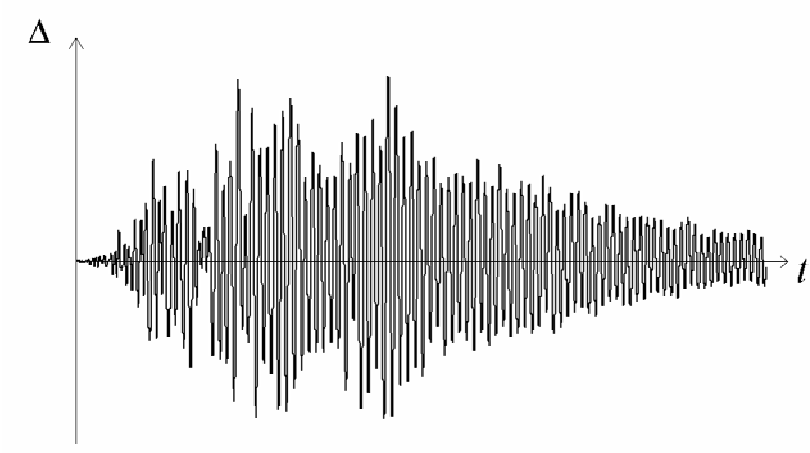

Figure A.12: Ground Motion Analysis Results of a Typical Reinforced Concrete Pier

A.4 REFERENCES

Hieber, D.G. (2005). "Precast Concrete Pier Systems for Rapid Construction of Bridges in Seismic Regions," M.S.C.E. Thesis, Department of Civil and Environmental Engineering, University of Washington, 336pp.

Karsan, I.D. and J.O. Jirsa (1969), "Behavior of Concrete Under Compressive Loading," *ASCE Journal of the Structural Division*, Vol. 95, No. ST12, December, pp. 2543-2563.

Kent, D.C. and Park, R. (1971). "Flexural Members with Confined Concrete," *ASCE Journal of Structural Engineering*, V. 97, ST7, July, pp. 1969-1990.

Lehman, D.E. and Moehle, J.P. (2000). "Performance-Based Seismic Design of Well-Confined Concrete Columns", PEER Research Report 1998/01, Pacific Earthquake Engineering Research Center.

Mander J.B., Priestley, M.J.N, and Park, R. (1988). "Theoretical Stress-Strain Model for Confined Concrete," *ASCE Journal of Structural Engineering*, V. 114, No. 8, pp1804-1826.

Mazzoni, S., McKenna, F., and Fenves, G.L. (2005). "Open System for Earthquake Engineering Simulation User Manual: Version 1.6.0," Pacific Earthquake Engineering Research Center, Univ. of Calif., Berkeley. (http://opensees.berkeley.edu)

Menegotto, M. and Pinto, P. (1973). "Method of Analysis for Cyclically Loaded Reinforced Concrete Plane Frames including Changes in Geometry and Nonelastic Behavior of Elements under Combined Normal Force and Bending," *IABSE Symposium on the Resistance and Ultimate Deformability of Structures Acted Upon by Well-defined Repeated Loads*, Lisbon.

Popovics, S. (1973). "A Numerical Approach to the Complete Stress-Strain Curves for Concrete," *Cement and Concrete Research*, V. 3, No. 5, pp. 583-599.

Spacone, Enricho, Filippou, Filip C, and Taucer, Fabio F. (1996). "Fibre Beam-Column Model for Non-linear Analysis of R/C Frames: Part I Formulation," *Earthquake Engineering and Structural Dynamics*, V. 25, pp. 711-725.

Wacker, J.M. (2005). "Design of Precast Concrete Bridge Piers for Rapid Bridge Construction in Seismic Regions," M.S.C.E. Thesis, Department of Civil and Environmental Engineering, University of Washington, 226pp.

APPENDIX B
DEVELOPMENT OF GROUND MOTION ACCELERATION RECORDS

The ground motion acceleration recorded at a site is dependent on several properties of the earthquake, including the type, magnitude, and distance from the site. The geotechnical characteristics of the region and site also affect the amount of shaking. Ground motion acceleration records are commonly characterized by a shaking intensity, such as the peak ground acceleration. Kramer (1996) provided an in-depth examination of the relationship between an earthquake and the shaking intensity at a particular site.

The results of the earthquake simulations performed in this study were used to develop and calibrate bridge pier design procedures. Accordingly, the ground motion acceleration records used in this study had to represent a magnitude of shaking, specified by a shaking intensity, unlikely to occur during the service life of a typical bridge. This was accomplished by using a shaking intensity with a certain probability of being exceeded in a given time period. The AASHTO specifications (AASHTO 2002; AASHTO 2004) require bridges to be designed for a shaking intensity with a 10 percent probability of exceedance in 50 years. Earthquakes that produce this level of shaking are referred to as design-level earthquakes. The same probability of exceedance was used in this study so that the design procedures developed would result in designs similar to those produced using the AASHTO specifications.

The probability of exceedance for a particular shaking intensity is dependent on many factors, including the number of potential earthquake sources in the vicinity of the site, the potential magnitude of these sources, and the probability of the sources producing earthquakes in a given time period. This causes the shaking intensity associated with a fixed probability of exceedance to change with location. Seismic hazard maps of shaking intensity are used to assure that bridges in different locations are designed for shaking intensities with similar probabilities of being exceeded. This results in bridges in high seismic areas being designed for larger shaking intensities than bridges in areas of low seismicity.

The structural demands induced in a bridge pier by a ground motion are dependent on the shaking intensity, characteristics of the ground motion, and characteristics of the bridge pier. To account for this, the demand on the pier is typically specified with design response spectra, which are discussed in Section B.1. This is followed by a discussion of the process used to select and scale five ground motion acceleration records for use in this study in Section B.2.

B.1 DESIGN RESPONSE SPECTRA

A response spectrum depicts the maximum value of a certain quantity experienced by single-degree-of-freedom oscillators with a fixed amount of damping subjected to a ground motion acceleration record. Response spectra are typically generated for values such as acceleration, velocity, and displacement. One of the benefits of response spectra is that they portray the demand on structures with a wide range of characteristics, represented by the period of the vibration (T). A drawback of response spectra is that they only consider the response of the structure to one particular ground motion. The frequency content of the ground motion acceleration record has a strong effect on the response spectrum, resulting in a jagged shape. The jagged shape can result in significant changes in demand because of minimal changes to T. In areas of high seismicity, an infinite number of different ground motions could occur, each creating a different demand on the structure because of their individual frequency contents.

Design response spectra are used to consider the effects of different ground motions, which have shaking intensities with approximately the same probability of exceedance, on the demand on a structure. The result is then smoothed to eliminate any jaggedness due to the particular frequency contents of the ground motion acceleration records used to create the design spectra. The concept of response spectra and design response spectra was discussed by Chopra (2001).

The design acceleration response spectrum included in the AASHTO specifications (AASHTO 2002; AASHTO 2004) is shown in Figure B.1. The design acceleration response (S_a) spectrum for 5 percent viscous damping is defined by

$$S_a = \frac{1.2ASg}{T^{2/3}} \leq 2.5Ag \qquad \text{(B.1)}$$

In Equation (B.1), A is the acceleration coefficient, which is the peak ground acceleration, in units of g, with a 10 percent probability of exceedance in 50 years at the site, and S is the site coefficient, which accounts for amplification of shaking due to the soil properties at the bridge location. The following values were used in this study (AASHTO 2002; AASHTO 2004).

- A = 0.30 to represent the Puget Sound region
- S = 1.2 to represent soil properties in a variety of locations

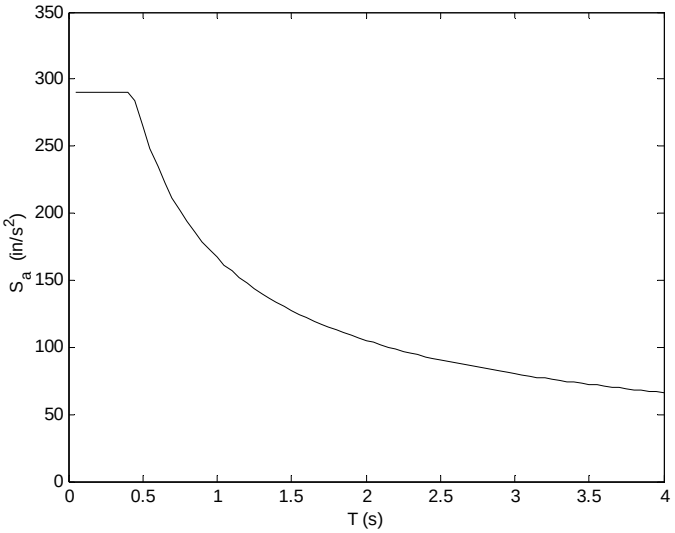

Figure B.1: Design Acceleration Response Spectra

The direct displacement-based design (DDBD) procedure presented in Chapter 3 of this report requires a design displacement response spectrum. The AASHTO specifications (AASHTO 2002; AASHTO 2004) do not include a design displacement response spectrum. The spectral displacement (S_d) can be approximated from the spectral acceleration (S_a) for low levels of damping by

$$S_d \cong \frac{S_a}{4\pi^2} T^2 \tag{B.2}$$

In this research, Equation (B.2) was assumed to be an equality allowing the design displacement response spectrum to be defined as

$$S_d = \frac{1.2}{4\pi^2} ASgT^{4/3} \leq \frac{2.5}{4\pi^2} AgT^2 \tag{B.3}$$

The design displacement response spectrum developed with Equation (B.3) is shown in Figure B.2.

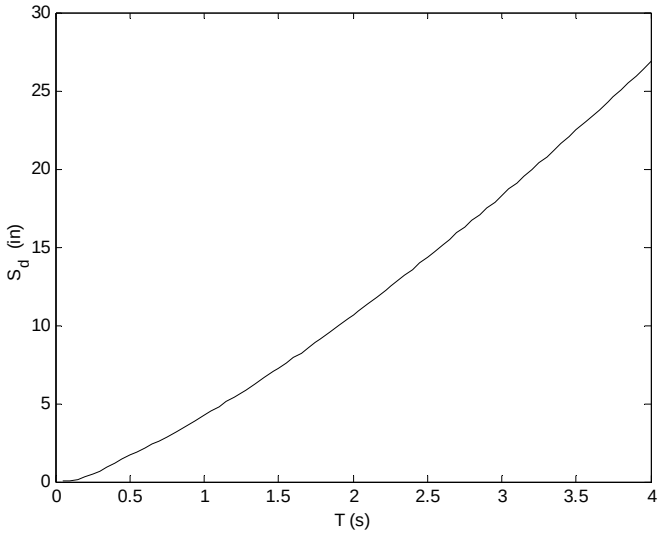

Figure B.2: Design Displacement Response Spectra

B.2 SELECTION AND SCALING OF GROUND MOTION ACCELERATION RECORDS

Ground motion acceleration records for use in this study were determined by scaling historical ground motion records so that the acceleration response spectrum of the ground motion matched the design acceleration response spectrum defined in the previous section. The historical ground motion records were selected from a suite of records originally developed for the SAC Steel Project (Somerville et al. 1997). The potential records were limited to those developed for the Seattle area so that the ground motion records would be representative of those likely to be caused by earthquakes in the Puget Sound region. The SAC suite for the Seattle area consisted of 16 pairs of fault normal and fault parallel ground motion acceleration records. Because a two-dimensional model of the pier was used in this study, the effects of the two ground motion components on the pier were considered separately, resulting in a total suite of 32 ground motion records.

The following procedure was used to select the five ground motions used in this study from the 32 in the SAC suite. The acceleration response spectrum for each ground motion was developed by using the linear acceleration method (Chopra 2001). The ground motion record was then scaled to minimize the sum of the squared difference

between the acceleration response spectrum and the design acceleration response spectrum over a range of T from 0.05 to 2.05 seconds. This range was chosen because it encompasses the range of bridge pier periods encountered in this study. The 32 ground motions were ranked on the basis of the sum of the squared difference, and the five ground motions with the smallest values were chosen subject to the following additional constraints:

- Only one record (fault normal or fault parallel) from an earthquake was selected.
- Large scale factors, over 2.5, were rejected.
- Records with atypical features (such as large pulses) were rejected.

The ground motion acceleration record, acceleration response spectrum, and displacement response spectrum for each of the five selected ground motions are presented in Appendix F. The average acceleration response spectrum for the five ground motions is shown in Figure B.3. The average acceleration spectrum correlates well with the design acceleration response spectrum, verifying the adequacy of the ground motion records selected.

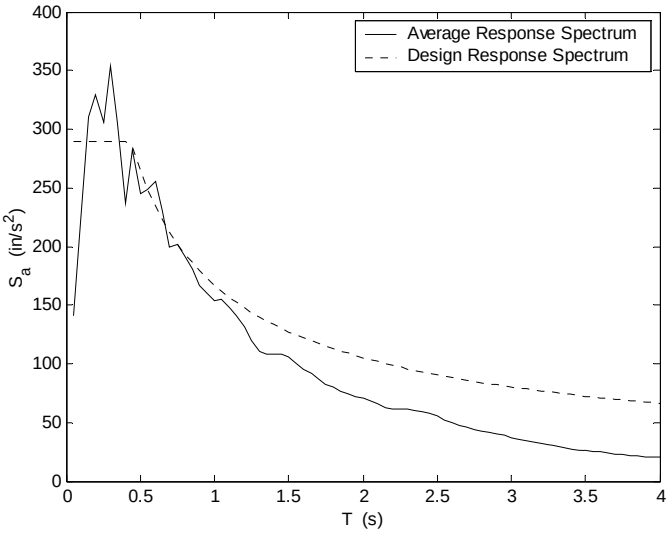

Figure B.3: Average Acceleration Response Spectrum

The average displacement response spectrum and the design displacement response spectrum, shown in Figure B.4, also correlate well for periods of less than 1.0 seconds. For larger periods, the average displacement response spectrum reflects the constant displacement behavior of flexible structures (Chopra 2001). The formulation of

the AASHTO design response spectrum neglects the presence of the constant displacement region.

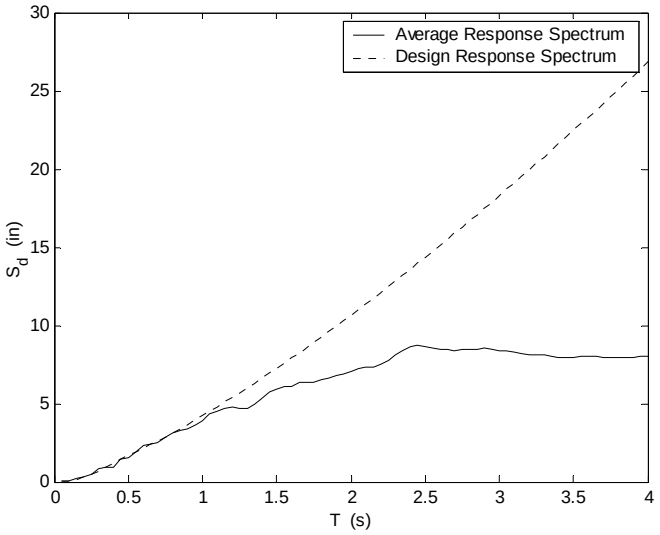

Figure B.4: Average Displacement Response Spectrum

B.3 REFERENCES

AASHTO (2002). *Standard Specifications for Design of Highway Bridges*, 17 ed., American Association of State Highway and Transportation Officials, Washington D.C.

AASHTO (2004). *Load and Resistance Factor Bridge Design Specifications*, 3 ed., American Association of State Highway and Transportation Officials, Washington D.C.

Chopra A.K., (2001). *Dynamics of Structures: Theory and Applications to Earthquake Engineering*, 2 ed., Prentice Hall, Upper Saddle River, New Jersey.

Kramer, S.L. (1996). *Geotechnical Earthquake Engineering*, Prentice Hall, Upper Saddle River, New Jersey.

Somerville, P., Smith, N., Punyamurthula, S., and Sun, J. (1997). *Development of Ground Motion Time Histories for Phase 2 of the FEMA/SAC Steel Project*, Applied Technology Council, Report No. SAC/BD-97/04, Redwood City, California.

APPENDIX C
EQUIVALENT LATERAL FORCE DESIGN EXAMPLE CALCULATIONS

Example calculations for the equivalent lateral force design (ELFD) procedure in Section 2.2 are presented in this appendix. The procedure is used to design the reinforcement of a two-column pier with a column diameter (D_c) of 48 in. and height (L_c) of 288 in. The axial dead load on the columns (P_c) due to the weight of the superstructure and cap beam is 1000 kips per column. The center-to-center spacing of the columns (d_c) is 336 in. The pier is assumed to be part of an "essential" structure as defined by the AASHTO specifications (AASHTO 2002; AASHTO 2004). The ELFD procedure is used to design the pier with the CIP emulation precast system (Section 0) and the hybrid precast system (Section 0).

The following material properties were used in the example calculations:

- compressive strength of concrete ($f_c^{'}$): 5 ksi
- elastic modulus of concrete (E_c): 4720 ksi
- yield strength of mild steel reinforcement (f_y): 60 ksi
- elastic modulus of mild steel (E_s): 29000 ksi
- yield strength of post-tensioning tendons (f_{py}): 243 ksi
- maximum initial stress in post-tensioning tendons (f_{pi}): 216 ksi
- elastic modulus of post-tensioning tendons (E_p): 28500 ksi.

C.1 CIP EMULATION PIER SYSTEM

Step #1: Define Pier Properties

The following pier properties are defined:

- $L_c = 288\,in$
- $n_c = 2$

- $P_c = 1000\,k$
- $D_c = 48\,in$

Step #2: Estimate the Stiffness of the Pier

The gross moment of inertia of a column (I_g) is determined by using Equation (2.1):

$$I_g = \frac{\pi D_c^{\,4}}{64} = \frac{\pi (48\,in)^4}{64} = 260576\,in^4$$

The cracked moment of inertia (I_{cr}) of a column is then

$$I_{cr} = \frac{1}{2} I_g = \frac{260576\,in^4}{2} = 130288\,in^4$$

Equation (2.2) can be used to determine the stiffness of the pier (K_p):

$$K_p = \frac{12 n_c E_c I_{cr}}{L_c^{\,3}} = \frac{12(2)(4720\,ksi)(130288\,in^4)}{(288in)^3} = 617.8\frac{k}{in}$$

Step #3: Calculate the Elastic Period

The seismic mass (m_p), neglecting the self-weight of the columns, acting on the pier is

$$m_p = \frac{n_c P_c}{g} = \frac{2(1000\,k)}{386.4\frac{in}{s^2}} = 5.176\frac{k - s^2}{in}$$

The natural period of vibration (T_n) can be estimated by using Equation (2.3):

$$T_n = 2\pi\sqrt{\frac{m_p}{K_p}} = 2\pi\sqrt{\frac{5.176\frac{k - s^2}{in}}{617.8\frac{k}{in}}} = 0.575\,s$$

Step #4: Estimate the Design Spectral Acceleration

The design spectral acceleration (S_a) can be determined by using Equation (2.4):

$$S_a = \frac{1.2ASg}{T_n^{2/3}} < 2.5Ag = \frac{1.2(0.3)(1.2)(386.4\frac{k-s^2}{in})}{(0.575s)^{2/3}} = 241.4\frac{in}{s^2}$$

where A is the acceleration coefficient and S is the soil coefficient as defined by the AASHTO specifications (AASHTO 2002; AASHTO 2004).

Step #5: Calculate the Equivalent Lateral Force

Equation (2.6) can be used to determine the equivalent lateral force (F_{eq}) acting on the pier:

$$F_{eq} = S_a m_p = 241.4\frac{in}{s^2}(5.176\frac{k-s^2}{in}) = 1249k$$

Step #6: Calculate the Design Force for the Pier

The response modification factor (R) for an "essential" bridge is 3.5 (AASHTO 2002; AASHTO 2004). The design force (F_d) for the pier is then determined by using Equation (2.7):

$$F_d = \frac{F_{eq}}{R} = \frac{1249k}{3.5} = 357.0k$$

Step #7: Design the Flexural Reinforcement of the Columns

The mild steel reinforcing ratio (ρ_s) required for the pier to have sufficient capacity (F_{cap}) to resist the force demand (F_d) is determined by using the sectional analysis method presented in Section 7.4. A mild steel reinforcing ratio (ρ_s) of 0.0196 is required.

C.2 HYBRID PIER SYSTEM

The ELFD procedure for designing a hybrid pier is identical to the procedure for a CIP emulation pier with the exception of determining the flexural reinforcement required to provide the required force capacity. Accordingly, the first six steps of the procedure are identical to those presented in Section C.1. Step # 7 is replaced with the following:

Step #7: Design the Flexural Reinforcement of the Columns

The mild steel reinforcing ratio (ρ_s) and post-tensioning reinforcing ratio (ρ_p) required to meet the design force (F_d) on the pier are determined by using the sectional analysis method presented in Section 7.4. The proportion of mild steel reinforcement to post-tensioning reinforcement must be specified. For this example, it was decided to provide an equal amount of internal force capacity with the mild steel reinforcement and the post-tensioning tendons. Accordingly,

$$\rho_p = \rho_s \frac{f_y}{f_{py}}$$

For lightly reinforced columns, this condition causes the amount of moment capacity contributed by the mild steel and post-tensioning reinforcement to be approximately equal, ensuring recentering of the pier after an earthquake.

A mild steel reinforcing ratio (ρ_s) of 0.0123 and post-tensioning reinforcement ratio (ρ_p) of 0.0030 are required to provide sufficient capacity.

C.3 REFERENCES

AASHTO (2002). *Standard Specifications for Design of Highway Bridges*, 17 ed., American Association of State Highway and Transportation Officials, Washington D.C.

AASHTO (2004). *Load and Resistance Factor Bridge Design Specifications*, 3 ed., American Association of State Highway and Transportation Officials, Washington D.C.

APPENDIX D
DIRECT DISPLACEMENT-BASED DESIGN EXAMPLE CALCULATIONS

Example calculations for the direct displacement-based design (DDBD) procedures discussed in Section 3.2 are presented in this appendix. The procedures are used to design the reinforcement of a two-column pier ($n_c = 2$) with a column diameter (D_c) of 48 in. and clear column height (L_c) of 288 in. The axial load per column (P_c) due to the weight of the superstructure and cap beam is 1000 kips. The center-to-center spacing of the columns (d_c) is 336 in. The following three formulations of the DDBD procedure are considered. These are the same formulations considered in Chapter 8.

- Section D.1: Iterative procedure (Section 3.2.1) with
    - yield displacement determined with the nonlinear analysis method (Section 4.1)
    - equivalent viscous damping ratio determined with the nonlinear analysis method (Section 5.2)
    - pier capacity determined with the nonlinear analysis method (Section 7.3)
- Section D.2: Iterative procedure (Section 3.2.1) with
    - yield displacement determined with the equation-based method (Section 4.3 and Section 4.4)
    - equivalent viscous damping ratio determined with the equation-based method (Section 5.3)
    - pier capacity determined with the sectional analysis method (Section 7.4)
- Section D.3: Direct (Non-iterative) procedure (Section 3.2.2) with
    - equivalent viscous damping ratio determined with the empirical method (Section 5.4)
    - pier capacity determined with the sectional analysis method (Section 7.4).

Each procedure is used to design the pier as a CIP emulation system and a hybrid system.

The following material properties were used in the example calculations:

- compressive strength of concrete ($f_c^{'}$): 5 ksi
- elastic modulus of concrete (E_c): 4720 ksi
- yield strength of mild steel reinforcement (f_y): 60 ksi
- elastic modulus of mild steel (E_s): 29000 ksi
- yield strength of post-tensioning tendons (f_{py}): 243 ksi
- maximum initial stress in post-tensioning tendons (f_{pi}): 216 ksi
- elastic modulus of post-tensioning tendons (E_p): 28500 ksi.

D.1 ITERATIVE PROCEDURE USING THE NONLINEAR ANALYSIS METHODS

D.1.1 CIP Emulation Pier

Step #1: Define Pier Properties

The following pier properties are defined:

- $L_c = 288 in$
- $n_c = 2$
- $P_c = 1000 k$
- $D_c = 48 in$

Step #2: Estimate the Reinforcing Ratio(s) for the Column

The mild steel reinforcing ratio (ρ_s) is estimated to be 0.01. Iteration will be used to determine the best value.

Step #3: Select the Target Displacement

For this example, the target displacement (Δ_t) is selected to correspond to 1.5 percent drift of the pier.

$$\Delta_t = 0.015 L_c = 0.015(288 in) = 4.32 in$$

Step #4: Estimate the Equivalent Viscous Damping

The equivalent viscous damping (ξ_{eq}) is estimated by using the nonlinear analysis method presented in Section 5.2. A nonlinear model of the pier is constructed, and a push-pull analysis to Δ_t is performed. Equation (5.12) is used to determine ξ_{eq} from the push-pull analysis results.

$$\xi_{eq} = 0.1570$$

Step #5: Modify the Equivalent Viscous Damping

The displacement ductility (μ_Δ) of the pier is calculated from Δ_t, and the yield displacement (Δ_y) is determined by using the nonlinear analysis method presented in Section 4.1.

$$\mu_\Delta = \frac{\Delta_t}{\Delta_y} = \frac{4.32in}{1.47in} = 2.94$$

The damping modification factor (β) presented in Equation (6.9) is used to determine the effective equivalent damping ($\hat{\xi}_{eq}$) from Equation (3.1):

$$\hat{\xi}_{eq} = \beta\xi_{eq} = (0.26 + 0.23\mu_\Delta)\xi_{eq} = (0.26 + 0.23(2.94))(0.1570) = 0.1469$$

Step #6: Develop and Modify the Design Displacement Response Spectrum

The design displacement response spectrum is represented by using Equation (3.2).

$$\begin{aligned} S_{d-5\%} &= \frac{1.2}{4\pi^2} ASgT^{4/3} \le \frac{2.5}{4\pi^2} AgT^2 \\ &= \frac{1.2}{4\pi^2}(0.3)(1.2)(386.4\,in/s^2)T^{4/3} \le \frac{2.5}{4\pi^2}(0.3)(386.4\,in/s^2)T^2 \\ &= 4.228T^{4/3} \le 7.341T^2 \end{aligned}$$

where $S_{d-5\%}$ is the design spectral displacement for 5 percent viscous damping, A is the acceleration coefficient taken to be 0.3, S is the site coefficient taken as 1.2, and T is the period of vibration of the pier. Modifying the design displacement response spectrum for $\hat{\xi}_{eq}$ using Equation (3.3),

$$S_{d-\hat{\xi}_{eq}} = \sqrt{\frac{7}{2+100\hat{\xi}_{eq}}} S_{d-5\%}$$

$$= \sqrt{\frac{7}{2+100(0.1469)}} \left(4.228T^{4/3} \le 7.341T^2\right)$$

$$= 2.738T^{4/3} \le 4.754T^2$$

Step #7: Estimate the Equivalent Period

The equivalent period (T_{eq}) can be determined by substituting Δ_t into the design displacement response spectrum. The equation

$$4.32in = 2.738T^{4/3} \le 4.754T^2$$

can be solved numerically:

$$T_{eq} = 1.408s$$

Step #8: Calculate the Equivalent Stiffness

The equivalent stiffness (K_{eq}) is determined by using Equation (3.5):

$$K_{eq} = 4\pi^2 \frac{m_p}{T_{eq}^{\ 2}} = 4\pi^2 \frac{5.176\frac{k-s^2}{in}}{(1.408s)^2} = 103.1\frac{k}{in}$$

where m_p is the total seismic mass acting on the pier from the superstructure and cap beam. The mass of the pier columns is neglected.

Step #9: Calculate the Force at the Target Displacement

The force at the target displacement (F_t), which is the design force (F_d), can be found with Equation (3.6):

$$F_t = K_{eq}\Delta t = 103.1\frac{k}{in}(4.32in) = 445.4k$$

Step #10: Determine the Required Reinforcing Ratio(s)

The nonlinear analysis method, presented in Section 7.3, is used to determine the mild steel reinforcement ratio (ρ_s) required to provide sufficient strength capacity. Nonlinear analysis determines that ρ_s = 0.0080 is required.

Step #11: Perform Iteration

The value of ρ_s determined in Step #10 differs from the value of ρ_s assumed in Step #2, requiring the design procedure to be iterated until the values converge. After several iterations, the required mild steel reinforcing ratio (ρ_s) is determined to be 0.0087.

D.1.2 Hybrid Pier

The only changes to the iterative DDBD procedure using nonlinear analysis methods for the two types of piers is the equation used to determine the damping modification factor (β) and the nonlinear model used to determine values in design.

The proportion of mild steel to post-tensioning steel used to reinforce the hybrid columns must be determined. In this example, the amount of the different reinforcing materials is specified according to

$$\rho_p = \rho_s \frac{f_y}{f_{py}}$$

which results in the post-tensioning and mild steel providing approximately the same amount of moment capacity for lightly reinforced piers. This assures that the pier will recenter even without the presence of gravity loads.

Step #1: Define the Pier Properties

The following pier properties are defined:

- $L_c = 288 in$
- $n_c = 2$
- $P_c = 1000 k$
- $D_c = 48 in$

Step #2: Estimate the Reinforcing Ratio(s) for the Column

The mild steel reinforcing ratio (ρ_s) and the post-tensioning reinforcing ratio (ρ_p) are estimated to be 0.01 and 0.0025, respectively.

Step #3: Select the Target Displacement

For this example, the target displacement (Δ_t) is selected to correspond to 1.5 percent drift of the pier.

$$\Delta_t = 0.015L_c = 0.015(288in) = 4.32in$$

Step #4: Estimate the Equivalent Viscous Damping

The equivalent viscous damping (ξ_{eq}) is determined by using Equation (5.12) from the results of a push-pull analysis as described in Section 5.2.

$$\xi_{eq} = 0.1475$$

Step #5: Modify the Equivalent Viscous Damping

The displacement ductility (μ_Δ) of the pier is calculated from Δ_t and the yield displacement (Δ_y) determined by using the nonlinear analysis method presented in Section 4.1.

$$\mu_\Delta = \frac{\Delta_t}{\Delta_y} = \frac{4.32in}{1.21in} = 3.57$$

The damping modification factor (β) presented in Equation (6.10) is used to determine the effective equivalent viscous damping ($\hat{\xi}_{eq}$) from Equation (3.1):

$$\hat{\xi}_{eq} = \beta\xi_{eq} = (0.55 + 0.12\mu_\Delta)\xi_{eq} = (0.55 + 0.12(3.57))(0.1475) = 0.1443$$

Step #6: Develop and Modify the Design Displacement Response Spectrum

The design displacement response spectrum can be represented by using Equation (3.2).

$$S_{d-5\%} = \frac{1.2}{4\pi^2} ASgT^{4/3} \le \frac{2.5}{4\pi^2} AgT^2 = 4.228T^{4/3} \le 7.341T^2$$

Modifying this expression for $\hat{\xi}_{eq}$ using Equation (3.3),

$$S_{d-\hat{\xi}_{eq}} = \sqrt{\frac{7}{2+100\hat{\xi}_{eq}}} S_{d-5\%}$$

$$= \sqrt{\frac{7}{2+100(0.1443)}} \left(4.228T^{4/3} \le 7.341T^2\right)$$

$$= 2.756T^{4/3} \le 4.791T^2$$

Step #7: Estimate the Equivalent Period

The equivalent period (T_{eq}) can be determined by substituting Δ_t into the design displacement response spectrum. The equation

$$4.32in = 2.756T^{4/3} \le 4.791T^2$$

can be solved numerically:

$$T_{eq} = 1.401s$$

Step #8: Calculate the Equivalent Stiffness

The equivalent stiffness (K_{eq}) can be determined by using Equation (3.5).

$$K_{eq} = 4\pi^2 \frac{m_p}{T_{eq}^{\ 2}} = 4\pi^2 \frac{5.176\frac{k-s^2}{in}}{(1.401s)^2} = 104.1\frac{k}{in}$$

Step #9: Calculate the Force at the Target Displacement

The force at the target displacement (F_t), which is the design force (F_d) for the pier, can be determined by using Equation (3.6).

$$F_t = K_{eq}\Delta t = 104.1\frac{k}{in}(4.32in) = 449.8k$$

Step #10: Determine the Required Reinforcing Ratio(s)

The nonlinear analysis method, presented in Section 7.3, is used to determine the reinforcing ratios needed to provide sufficient force capacity. Sufficient capacity can be obtained by using ρ_s of 0.0050 and ρ_p of 0.0012.

Step #11: Perform Iteration

The values for ρ_s and ρ_p determined in Step #10 are significantly different from those estimated in Step #2. Therefore, the design procedure should be iterated. After several iterations, the required reinforcing ratios are determined to be ρ_s of 0.0055 and ρ_p of 0.0014.

D.2 ITERATIVE PROCEDURE USING EQUATION-BASED METHODS

D.2.1 CIP Emulation Pier

Step #1: Define Pier Properties

The following pier properties are defined:

- $L_c = 288in$
- $n_c = 2$
- $P_c = 1000k$
- $D_c = 48in$

Step #2: Estimate the Reinforcing Ratio(s) for the Column

The mild steel reinforcing ratio (ρ_s) is estimated to be 0.01. The optimal value of ρ_s will be determined with iteration.

Step #3: Select the Target Displacement

The target displacement (Δ_t) is selected to correspond to 1.5 percent drift of the pier.

$$\Delta_t = 0.015L_c = 0.015(288in) = 4.32in$$

Step #4: Estimate the Equivalent Viscous Damping

The equivalent viscous damping (ξ_{eq}) is estimated with the equation-based method presented in Section 5.3. This method requires the displacement ductility (μ_Δ) of the pier when displaced to Δ_t to be known.

$$\mu_\Delta = \frac{\Delta_t}{\Delta_y}$$

An estimate of the yield displacement (Δ_y) of the pier is determined by using the equation-based method presented in Section 4.3.

The yield displacement (Δ_y) of a CIP emulation pier can be estimated using Equation (4.5):

$$\Delta_y = \frac{\Delta_y}{\Delta_y^{'}}(\Delta_{y,c}^{'} + \Delta_{y,sp}^{'})$$

where $\Delta_{y,c}^{'}$ is the displacement at first yield due to deformation of the column, $\Delta_{y,sp}^{'}$ is the displacement at first yield due to strain penetration, and $\frac{\Delta_y}{\Delta_y^{'}}$ is the ratio of yield displacement to displacement at first yield, which can be determined by using Equation (4.22):

$$\frac{\Delta_y}{\Delta_y^{'}} = 1.3 + 5.5\rho_s - 1.25\frac{P_c}{f_c^{'}A_g} = 1.3 + 5.5(0.01) - 1.25(0.11) = 1.218$$

Equation (4.8) is used to determine $\Delta_{y,c}^{'}$:

$$\Delta_{y,c}^{'} = (\frac{1}{2})\phi_y{}' L_c^2\left[\frac{\lambda}{3} + (1-\lambda)(\frac{k^3}{3} - k^2 + k)\right]$$

where λ is the ratio of cracked flexural rigidity to gross flexural rigidity determined by using Equation (4.14), k is determined with equations (4.10) and (4.13), and $\phi_y^{'}$ is the curvature of the column at first yield estimated with equations (4.11) and (4.12).

$$\lambda = \frac{EI_{cr}}{EI_g} = 0.33 + 9.0\rho_s - 0.20\frac{P_c}{f_c^{'}A_g} = 0.33 + 9.0(0.01) - 0.20(0.11) = 0.398$$

$$k = \frac{1}{2}(1 - \frac{M_{cr}}{M_y^{'}}) = \frac{1}{2}\left(1 - (0.46 - 10.0\rho_s + 1.0\frac{P_c}{f_c^{'}A_g})\right)$$

$$= \frac{1}{2}(1 - (0.46 - 10.0(0.01) + 1.0(0.11))) = 0.265$$

$$\phi_y^{'} = \frac{\varepsilon_y}{\left(0.68 - 2.0\rho_s - 0.8\frac{P}{f_c^{'}A_g}\right)D_c} = \frac{0.00207}{\left(0.68 - 2.0(0.01) - 0.8(0.11)\right)(48in)} = 0.0000754\frac{rad}{in}$$

Substituting these values for λ, k, and $\phi_y^{'}$ into the equation for $\Delta_{y,c}^{'}$,

$$\Delta_{y,c}^{'} = (\frac{1}{2})(0.0000754\frac{rad}{in})(288in)^2\left[\frac{0.398}{3} + (1 - 0.398)(\frac{0.265^3}{3} - 0.265^2 + 0.265)\right] = 0.793in$$

Equation (4.19) is used to estimate $\Delta_{y,sp}^{'}$:

$$\Delta_{y,sp}^{'} = \frac{1}{8}\frac{f_y^{'2}d_b}{\tau_e E_c}\frac{L_c}{\gamma D_c}$$

where γ can be determined by using Equation (4.21):

$$\gamma = 0.70 - \frac{3D_c}{1000} - 1.0\frac{P_c}{f_c^{'}A_g} = 0.70 - \frac{3(48in)}{1000} - 1.0(0.11) = 0.446$$

and τ_e is

$$\tau_e = 0.012\sqrt{1000\,f_c^{'}} = 0.012\sqrt{1000(5ksi)} = 0.849ksi$$

resulting in

$$\Delta_{y,sp}^{'} = \frac{1}{8}\frac{f_y^{'2}d_b}{\tau_e E_s}\frac{L_c}{\gamma D_c} = \frac{1}{8}\frac{(60ksi)^2(1.41in)}{(0.849ksi)(29000ksi)}\frac{288in}{(0.446)(48in)} = 0.347in$$

The yield displacement (Δ_y) is then

$$\Delta_y = \frac{\Delta_y}{\Delta_y^{'}}(\Delta_{y,c}^{'} + \Delta_{y,sp}^{'}) = 1.218(0.793in + 0.347in) = 1.389in$$

The displacement ductility (μ_Δ) of the pier at Δ_t is then

$$\mu_\Delta = \frac{\Delta_t}{\Delta_y} = \frac{4.32in}{1.389in} = 3.11$$

Equation (5.18) can be used to estimate ξ_{eq} with this value of μ_Δ:

$$\xi_{eq} = C_1 + C_2 \frac{F_s}{F_s + F_w}\left(1 - \frac{1}{\sqrt{\mu_\Delta}}\right)$$

where C_1 is 0.025, C_2 is 0.63, F_s is the force resisting capacity of the pier with mild steel reinforcement alone determined with Equation (5.24), and F_w is the force resisting capacity of the pier with axial load alone determined with Equation (5.30).

$$F_s = (0.45 - 2.35\rho_s)\frac{\pi f_y n_c}{2}\frac{1}{L_c}D_c^3\rho_s$$

$$= (0.45 - 2.35(0.01))\frac{\pi(60ksi)(2)}{2}\frac{(48in)^3(0.01)}{288in} = 308.7k$$

$$F_w = \left(0.86 - 1.0\left(\frac{P_c}{f_c^{'}A_g} + \rho_p\frac{f_{p0}}{f_c^{'}}\right)\right)\frac{n_c\left(\frac{P_c}{f_c^{'}A_g} + \rho_p\frac{f_{p0}}{f_c^{'}}\right)f_c^{'}A_g}{L_c/D_c}$$

$$= (0.86 - 1(0.11 + 0))\frac{2(0.11 + 0)(5ksi)(1810in^2)}{6} = 248.9k$$

The equivalent viscous damping (ζ_{eq}) is then

$$\xi_{eq} = 0.025 + 0.63\frac{308.7k}{308.7k + 248.9k}\left(1 - \frac{1}{\sqrt{3.11}}\right) = 0.1760$$

Step #5: Modify the Equivalent Viscous Damping

The damping modification factor (β) can be calculated with Equation (6.9).

$$\beta = 0.26 + 0.23\mu_\Delta = 0.26 + 0.23(3.11) = 0.975$$

The effective equivalent viscous damping ($\hat{\xi}_{eq}$) can then be determined by using Equation (3.1):

$$\hat{\xi}_{eq} = \beta\xi_{eq} = 0.975(0.1760) = 0.1717$$

Step #6: Develop and Modify the Design Displacement Response Spectrum

The design displacement response spectrum can be represented with Equation (3.2).

$$S_{d-5\%} = \frac{1.2}{4\pi^2} ASgT^{4/3} \le \frac{2.5}{4\pi^2} AgT^2 = 4.228T^{4/3} \le 7.341T^2$$

Modifying this expression for the amount of effective equivalent viscous damping by using Equation (3.3),

$$\begin{aligned} S_{d-\hat{\xi}_{eq}} &= \sqrt{\frac{7}{2+100\hat{\xi}_{eq}}} S_{d-5\%} \\ &= \sqrt{\frac{7}{2+100(0.1717)}} \left(4.228T^{4/3} \le 7.341T^2\right) \\ &= 2.555T^{4/3} \le 4.437T^2 \end{aligned}$$

Step #7: Estimate the Equivalent Period

The equivalent period (T_{eq}) can be determined by substituting Δ_t into the design displacement response spectrum. The equation

$$4.32in = 2.555T^{4/3} \le 4.437T^2$$

can be solved numerically:

$$T_{eq} = 1.483s$$

Step #8: Calculate the Equivalent Stiffness

The equivalent stiffness (K_{eq}) is determined by using Equation (3.5).

$$K_{eq} = 4\pi^2 \frac{m_p}{T_{eq}^{\ 2}} = 4\pi^2 \frac{5.176\frac{k-s^2}{in}}{(1.483s)^2} = 93.0\frac{k}{in}$$

Step #9: Calculate the Force at the Target Displacement

The force at target displacement (F_t), which is the design force (F_d) for the pier, is determined by using Equation (3.6).

$$F_t = K_{eq}\Delta t = 93.0\frac{k}{in}(4.32in) = 401.6k$$

Step #10: Determine the Required Reinforcing Ratio(s)

The sectional analysis method (Section 7.4) is used to determine the required mild steel reinforcing ratio. Sample calculations for sectional analysis are presented in Appendix E. A mild steel reinforcing ratio (ρ_s) of 0.059 is required to provide the pier with sufficient capacity.

Step #11: Perform Iteration

Because the value of ρ_s calculated in Step #10 differs significantly from the value calculated in Step #2, iteration of the design is required. After several iterations, a ρ_s of 0.069 is determined to be sufficient.

D.2.2 Hybrid Pier

The proportion of mild steel to post-tensioning must be specified when a hybrid pier is designed. In this example, the relationship is expressed as:

$$\rho_p = \rho_s \frac{f_y}{f_{py}}$$

Step #1: Define Pier Properties

The following pier properties are defined:

- $L_c = 288in$
- $n_c = 2$
- $P_c = 1000k$
- $D_c = 48in$

Step #2: Estimate the Reinforcing Ratio(s) for the Column

The mild steel reinforcing ratio (ρ_s) is estimated to be 0.01. The post-tensioning reinforcing ratio (ρ_p) is then

$$\rho_p = \rho_s \frac{f_y}{f_{py}} = 0.01 \frac{60ksi}{243ksi} = 0.0025$$

The initial stress in the post-tensioning tendons should also be estimated. It is recommended that an initial estimate of the maximum allowable initial stress (f_{pi}) be used.

Step #3: Select the Target Displacement

The target displacement (Δ_t) is selected to correspond to 1.5% drift of the pier.

$$\Delta_t = 0.015 L_c = 0.015(288in) = 4.32in$$

Step #4: Estimate the Equivalent Viscous Damping

The equivalent viscous damping (ξ_{eq}) is determined by using the equation-based method presented in Section 5.3. In order to determine ξ_{eq}, the displacement ductility (μ_Δ) should be calculated as

$$\mu_\Delta = \frac{\Delta_t}{\Delta_y}$$

The yield displacement (Δ_y) of the pier is estimated by using the equation-based methods presented in Section 4.4. From Equation (4.24),

$$\Delta_y = \frac{\Delta_y}{\Delta_y^{'}}(\Delta_y{}'_{,\text{int}} + \Delta_{y,c}^{*})$$

where $\Delta_{y,\text{int}}^{'}$ is the displacement at first yield due to deformation of the interface region, $\Delta_{y,c}^{*}$ is the displacement at first yield due to elastic deformation of the column, and $\frac{\Delta_y}{\Delta_y^{'}}$ is the ratio of Δ_y to $\Delta_y^{'}$ and can be determined with Equation (4.38).

$$\frac{\Delta_y}{\Delta_y^{'}} = 1.42 + 5.0\rho_s - 0.6\left(\frac{P_c}{f_c^{'} A_g} + \rho_p \frac{f_{p0}}{f_c^{'}}\right)$$

$$= 1.42 + 5.0(0.01) - 0.6\left(0.11 + 0.0025\frac{216ksi}{5ksi}\right) = 1.339$$

Equation (4.28) can be used to estimate $\Delta_{y,\text{int}}^{'}$:

$$\Delta_{y,\text{int}}^{'} = \frac{1}{\eta}\frac{f_y}{E_s}L_{unb}\frac{L_c}{D_c}$$

where η can be determined by using Equation (4.30):

$$\eta = 0.57 - 1.5\rho_s - 0.80(\frac{P_c}{f_c^{'}A_g} + \rho_p\frac{f_{p0}}{f_c^{'}})$$

$$= 0.57 - 1.5(0.01) - 0.80(0.11 + 0.0025(\frac{216ksi}{5ksi})) = 0.381$$

Accordingly,

$$\Delta_{y,\text{int}}^{'} = \frac{1}{0.381}\frac{60ksi}{29000ksi}(12in)(6) = 0.391in$$

Equation (4.31) can be used to determine $\Delta_{y,c}^{*}$:

$$\Delta_{y,c}^{*} = \frac{L_c^3}{12n_cEI_{eff}}F_y^{'}$$

where $F_y^{'}$ is the force on the pier at first yield determined with Equation (4.37) and EI_{eff} is the effective flexural rigidity determined with Equation (4.33).

$$EI_{eff} = \left(0.32 + 14.0\rho_s + 1.5(\frac{P_c}{f_c^{'}A_g} + \rho_p\frac{f_{p0}}{f_c^{'}})\right)E_cI_g$$

$$= (0.32 + 14.0(0.01) + 1.5(0.11 + 0.0025\frac{216ksi}{5ksi}))(4720ksi)\frac{\pi(48in)^4}{64} = 9.68*10^8in^4$$

$$F_y^{'} = \left[0.25\frac{\pi f_y}{4}\rho_s + 0.26\frac{\pi f_c^{'}}{4}(\frac{P_c}{f_c^{'}A_g} + \rho_p\frac{f_{p0}}{f_c^{'}})\right]\frac{2n_cD_c^3}{L_c}$$

$$= \left[0.25\frac{\pi(60ksi)}{4}(0.01) + 0.26\frac{\pi(5ksi)}{4}(0.11 + 0.0025\frac{216ksi}{5ksi})\right]\frac{2(2)(48in)^3}{288in} = 522.8k$$

Accordingly,

$$\Delta_{y,c}^{*} = \frac{(288in)^3}{12(2)(9.68*10^8in^4)}522.8k = 0.538in$$

The yield displacement (Δ_y) of the hybrid pier can then be estimated as:

$$\Delta_y = 1.339(0.391in + 0.538in) = 1.244in$$

The displacement ductility (μ_Δ) of the pier at Δ_t is then

$$\mu_\Delta = \frac{4.32in}{1.244in} = 3.47$$

The equivalent viscous damping (ξ_{eq}) is then determined by using Equation (5.18):

$$\xi_{eq} = C_1 + C_2 \frac{F_s}{F_s + F_w}\left(1 - \frac{1}{\sqrt{\mu_\Delta}}\right)$$

where C_1 is 0.025, C_2 is 0.63, F_s is the force resisting capacity of the pier with mild steel reinforcement alone determined with Equation (5.24), and F_w is the force resisting capacity of the pier with axial load alone determined with Equation (5.30).

$$F_s = (0.45 - 2.35\rho_s)\frac{\pi f_y n_c}{2}\frac{1}{L_c}D_c^3\rho_s$$

$$= (0.45 - 2.35(0.01))\frac{\pi(60ksi)(2)}{2}\frac{(48in)^3(0.01)}{288in} = 308.7k$$

$$F_w = \left(0.86 - 1.0\left(\frac{P_c}{f_c^{'}A_g} + \rho_p\frac{f_{p0}}{f_c^{'}}\right)\right)\frac{n_c\left(\frac{P_c}{f_c^{'}A_g} + \rho_p\frac{f_{p0}}{f_c^{'}}\right)f_c^{'}A_g}{L_c \diagup D_c}$$

$$= (0.86 - 1(0.11 + 0.0025\frac{216ksi}{5ksi}))\frac{2(0.11 + 0.0025\frac{216ksi}{5ksi})(5ksi)(1810in^2)}{6} = 422.2k$$

The equivalent viscous damping (ζ_{eq}) is then

$$\xi_{eq} = 0.025 + 0.63\frac{308.7k}{308.7k + 422.2k}\left(1 - \frac{1}{\sqrt{3.47}}\right) = 0.1483$$

Step #5: Modify the Equivalent Viscous Damping

`The damping modification factor (β) can be determined with Equation (6.10).

$$\beta = 0.55 + 0.12\mu_\Delta = 0.55 + 0.12(3.47) = 0.9664$$

The effective equivalent viscous damping ($\hat{\xi}_{eq}$) can be found with Equation (3.1):

$$\hat{\xi}_{eq} = \beta\xi_{eq} = 0.9664(0.1483) = 0.1433$$

Step #6: Develop and Modify the Design Displacement Response Spectrum

The design displacement response spectrum can be represented by using Equation (3.2).

$$S_{d-5\%} = \frac{1.2}{4\pi^2} ASgT^{4/3} \le \frac{2.5}{4\pi^2} AgT^2 = 4.228T^{4/3} \le 7.341T^2$$

Modifying this expression for $\hat{\xi}_{eq}$ by using Equation (3.3),

$$\begin{aligned} S_{d-\hat{\xi}_{eq}} &= \sqrt{\frac{7}{2+100\hat{\xi}_{eq}}} S_{d-5\%} \\ &= \sqrt{\frac{7}{2+100(0.1433)}} \left(4.228T^{4/3} \le 7.341T^2\right) \\ &= 2.769T^{4/3} \le 4.806T^2 \end{aligned}$$

Step #7: Estimate the Equivalent Period

The equivalent period (T_{eq}) can be determined by substituting Δ_t into the design displacement response spectrum. The equation

$$4.32in = 2.769T^{4/3} \le 4.806T^2$$

can be solved numerically:

$$T_{eq} = 1.396s$$

Step #8: Calculate the Equivalent Stiffness

The equivalent stiffness (K_{eq}) can be determined by using Equation (3.5).

$$K_{eq} = 4\pi^2 \frac{m_p}{T_{eq}^2} = 4\pi^2 \frac{5.176\frac{k-s^2}{in}}{(1.396s)^2} = 104.9\frac{k}{in}$$

Step #9: Calculate the Force at the Target Displacement

The force at the target displacement (F_t), which is the design force (F_d) for the pier, can be determined with Equation (3.6).

$$F_t = K_{eq}\Delta t = 104.9\frac{k}{in}(4.32in) = 453.1k$$

Step #10: Determine the Required Reinforcing Ratio(s)

The sectional analysis method developed in Section 7.4 is used to determine the required amount of reinforcing steel. Sufficient capacity is provided by a ρ_s of 0.0045 and a ρ_p of 0.0011.

Step #11: Perform Iteration

Because the values of ρ_s and ρ_p calculated in Step #10 differ from the values estimated in Step #2, iteration of the design is required. After several iterations, a ρ_s of 0.0052 and a ρ_p of 0.0013 are determined to provide the pier with sufficient capacity.

D.3 DIRECT (NON-ITERATIVE) EQUATION-BASED APPROACH

D.3.1 CIP Emulation Pier

Step #1: Define Pier Properties

The following pier properties are defined:

- $L_c = 288in$
- $n_c = 2$
- $P_c = 1000k$
- $D_c = 48in$

Step #2: Select the Target Displacement

The target displacement (Δ_t) is selected to correspond to 1.5 percent drift of the pier.

$$\Delta_t = 0.015L_c = 0.015(288in) = 4.32in$$

Step #3: Estimate the Equivalent Viscous Damping

The equivalent viscous damping (ξ_{eq}) is estimated by using the empirical method presented in Section 5.4. Using Equation (5.31),

$$\xi_{eq} = \begin{cases} 0.15\ln(\frac{\Delta_t}{L_c}) + 0.8 & for \frac{\Delta_t}{L_c} \geq 0.0055 \\ 0.025 & for \frac{\Delta_t}{L_c} \leq 0.0055 \end{cases} = 0.15\ln\left(\frac{4.32in}{288in}\right) + 0.8 = 0.1700$$

Step #4: Modify the Equivalent Viscous Damping

The damping modification factor (β) is calculated with Equation (6.11):

$$\beta = 0.14 + 48.5\frac{\Delta_t}{L_c} = 0.14 + 48.5\frac{4.32in}{288in} = 0.8675$$

The effective equivalent viscous damping ($\hat{\xi}_{eq}$) is then determined by using Equation (3.1):

$$\hat{\xi}_{eq} = \beta\xi_{eq} = 0.8675(0.1700) = 0.1475$$

Step #5: Develop and Modify the Design Displacement Response Spectrum

The design displacement response spectrum can be represented with Equation (3.2).

$$S_{d-5\%} = \frac{1.2}{4\pi^2}ASgT^{4/3} \leq \frac{2.5}{4\pi^2}AgT^2 = 4.228T^{4/3} \leq 7.341T^2$$

Modifying this expression for $\hat{\xi}_{eq}$ using Equation (3.3),

$$\begin{aligned} S_{d-\hat{\xi}_{eq}} &= \sqrt{\frac{7}{2+100\hat{\xi}_{eq}}}S_{d-5\%} \\ &= \sqrt{\frac{7}{2+100(0.1475)}}\left(4.228T^{4/3} \leq 7.341T^2\right) \\ &= 2.733T^{4/3} \leq 4.746T^2 \end{aligned}$$

Step #6: Estimate the Equivalent Period

The equivalent period (T_{eq}) can be determined by substituting Δ_t into the design displacement response spectrum. The equation

$$4.32in = 2.733T^{4/3} \le 4.746T^2$$

can be solved numerically, resulting in

$$T_{eq} = 1.410s$$

Step #7: Calculate the Equivalent Stiffness

The equivalent stiffness (K_{eq}) can be determined by using Equation (3.5).

$$K_{eq} = 4\pi^2 \frac{m_p}{T_{eq}^{\ 2}} = 4\pi^2 \frac{5.176\frac{k-s^2}{in}}{(1.410\,s)^2} = 102.8\frac{k}{in}$$

Step #8: Calculate the Force at the Target Displacement

The force at the target displacement (F_t), which is the design force (F_d) for the pier, can be determined by using Equation (3.6):

$$F_t = K_{eq}\Delta t = 102.8\frac{k}{in}(4.32in) = 444.3k$$

Step #9: Determine the Required Reinforcing Ratio(s)

The sectional analysis method (Section 7.4) is used to determine the reinforcing ratio required to provide sufficient capacity. A mild steel reinforcing ratio (ρ_s) of 0.0077 is needed to provide sufficient capacity.

D.3.2 Hybrid Pier

Step #1: Define Pier Properties

The following pier properties are defined:

- $L_c = 288in$
- $n_c = 2$
- $P_c = 1000k$
- $D_c = 48in$

Step #2: Select the Target Displacement

The target displacement (Δ_t) is selected to correspond to 1.5 percent drift of the pier.

$$\Delta_t = 0.015L_c = 0.015(288in) = 4.32in$$

Step #3: Estimate the Equivalent Viscous Damping

The equivalent viscous damping (ξ_{eq}) is estimated by using the empirical method presented in Section 5.4. Utilizing Equation (5.32),

$$\xi_{eq} = \begin{cases} 0.11\ln(\frac{\Delta_t}{L_c}) + 0.67 & for \frac{\Delta_t}{L_c} \geq 0.0035 \\ 0.025 & for \frac{\Delta_t}{L_c} \leq 0.0035 \end{cases} = 0.11\ln\left(\frac{4.32in}{288in}\right) + 0.67 = 0.2080$$

Step #4: Modify the Equivalent Viscous Damping

The damping modification factor (β) is calculated with Equation (6.12):

$$\beta = 0.57 + 29.0\frac{\Delta_t}{L_c} = 0.57 + 29.0\frac{4.32in}{288in} = 1.005$$

The effective equivalent viscous damping ($\hat{\xi}_{eq}$) is then determined with Equation (3.1):

$$\hat{\xi}_{eq} = \beta\xi_{eq} = 1.005(0.2080) = 0.2090$$

Step #5: Develop and Modify the Design Displacement Response Spectrum

The design displacement response spectrum can be represented using Equation (3.2):

$$S_{d-5\%} = \frac{1.2}{4\pi^2}ASgT^{4/3} \leq \frac{2.5}{4\pi^2}AgT^2 = 4.228T^{4/3} \leq 7.341T^2$$

Modifying this expression for the amount of effective equivalent viscous damping using Equation (3.3),

$$S_{dd-\hat{\xi}_{eq}} = \sqrt{\frac{7}{2+100\hat{\xi}_{eq}}} S_{dd-5\%}$$
$$= \sqrt{\frac{7}{2+100(0.2090)}} \left(4.228T^{4/3} \le 7.341T^2\right)$$
$$= 2.337T^{4/3} \le 4.058T^2$$

Step #6: Estimate the Equivalent Period

The equivalent period (T_{eq}) can be determined by substituting Δ_t into the design displacement response spectrum. The equation

$$4.32in = 2.337T^{4/3} \le 4.058T^2$$

can be solved numerically, resulting in

$$T_{eq} = 1.585s$$

Step #7: Calculate the Equivalent Stiffness

The equivalent stiffness (K_{eq}) can be determined by using Equation (3.5):

$$K_{eq} = 4\pi^2 \frac{m_p}{T_{eq}^{\ 2}} = 4\pi^2 \frac{5.176\frac{k-s^2}{in}}{(1.585s)^2} = 81.3\frac{k}{in}$$

Step #8: Calculate the Force at the Target Displacement

The force at the target displacement (F_t), which is the design force (F_d) for the pier, can be determined by using Equation (3.6):

$$F_t = K_{eq}\Delta t = 81.3\frac{k}{in}(4.32in) = 351.3k$$

Step #9: Determine the Required Reinforcing Ratio(s)

The sectional analysis method (Section 7.4) is used to determine the amount of reinforcement required to provide sufficient capacity to exceed F_d. A mild steel reinforcing ratio (ρ_s) of 0.0021 and post-tensioning reinforcing ratio (ρ_p) of 0.0005 are required to provide sufficient capacity.

APPENDIX E
PIER CAPACITY EXAMPLE CALCULATIONS

Example calculations for determining the amount of reinforcement required to provide sufficient force resisting capacity (F_{cap}) for both CIP emulation (Section E.1) and hybrid (Section E.2) piers using the sectional analysis method (Section 7.4) are presented in this appendix. A two-column bent with a column diameter (D_c) of 48 in. is considered for both types of piers. The clear height of the columns (L_c) is 288 in., and the center-to-center spacing of the columns (d_c) is 336.0 in. Each column carries an axial load (P_c) of 1000 kips from the weight of the superstructure. The design force (F_d) for both piers is 300 kips.

The following material properties were used consistently throughout the examples:

- compressive strength of concrete ($f_c^{'}$): 5 ksi
- yield strength of mild steel reinforcement (f_y): 60 ksi
- elastic modulus of mild steel (E_s): 29000 ksi
- yield strength of post-tensioning tendons (f_{py}): 243 ksi
- maximum initial stress in post-tensioning tendons (f_{pi}): 216 ksi
- elastic modulus of post-tensioning tendons (E_{ps}): 28500 ksi.

E.1 CIP EMULATION PIER

The required force resisting capacity (F_{cap}) for the pier can be found by using Equation (7.2):

$$F_{cap} = \frac{F_d}{\phi_{cf}} = \frac{300k}{0.68} = 441.2k$$

where ϕ_{cf} is the resistance factor for a reinforced concrete member in compression, and flexure in seismic applications and can be calculated with Equation (7.1):

$$\phi_{cf} = 0.9 - 2\frac{P_c}{f_c' A_g} = 0.9 - 2\frac{1000k}{5ksi(1810in^2)} = 0.68$$

The sum of the moment capacity (M_{cap}) of the columns ($\sum_{n_c} M_{cap}$) can be determined by using Equation (7.3).

$$\sum_{n_c} M_{cap} = \frac{L_c F_{cap}}{2} = \frac{288in(441.2k)}{2} = 63532.8in - k$$

The columns do not have identical M_{cap} because the axial load in the columns is different as a result of overturning of the pier caused by the lateral load. The additional axial load in the columns due to overturning of the pier can be determined from Equation (7.4):

$$\Delta P = \frac{F_d L_c}{2d_c} = \frac{300k(288in)}{2(336in)} = 128.6k$$

One column should be designed for an axial load of

$$P_c + \Delta P = 1000k + 128.6k = 1128.6k$$

and the other for

$$P_c - \Delta P = 1000k - 128.6k = 871.4k$$

when F_{cap} is determined.

The amount of reinforcement required to provide the columns with sufficient M_{cap} is determined by using iteration. The initial reinforcement estimate is eight reinforcing bars, each with an area (A_{bar}) of 1.56 in.^{2}, as shown in Figure E.1. The initial mild steel reinforcing ratio (ρ_s) is 0.0068.

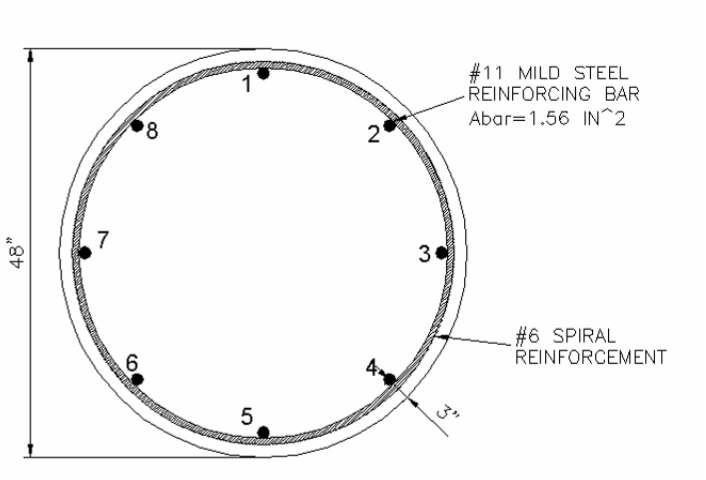

Figure E.1: Cross-Section of CIP Emulation Pier Column

The moment capacity (M_{cap}) of the column with the greater compressive axial load is determined by using the procedure from Section 7.4.1 as shown.

Step #1: Estimate the Depth of the Neutral Axis

The initial estimate for the depth of the neutral axis (c) is taken to be 1/5th the depth of the column diameter:

$$c = 0.20(D_c) = 0.20(48\,in) = 9.6\,in$$

Step #2: Calculate the Net Force in the Mild Steel Reinforcement

The calculations to determine the force in bar number 1, as labeled in Figure E.1, are shown below. The curvature (ϕ) across the cross-section is

$$\phi = \frac{\varepsilon_{cu}}{c} = \frac{0.004}{9.6\,in} = 0.000417\,\frac{rad}{in}$$

where ε_{cu} is the ultimate allowable compressive strain in concrete. The strain in bar 1 ($\varepsilon_{ms,1}$) is

$$\varepsilon_{ms,1} = \phi(d_{ms,i} - c) = 0.000417\,\frac{rad}{in}(45\,in - 9.6\,in) = 0.01475$$

where $d_{ms,i}$ is the distance from bar 1 to the extreme compressive face of the column. The stress in bar 1($f_{ms,1}$) is

$$f_{ms,1} = E_s \varepsilon_{ms,1} = 29000\,ksi(0.01475) = 428\,ksi \geq 60\,ksi$$

$$f_{ms,1} = 60\,ksi$$

The force in bar 1 ($F_{ms,1}$) is

$$F_{ms,1} = A_{bar} f_{ms,1} = 1.56\,in^2(60\,ksi) = 93.6\,k$$

The strain, stress, and force in the other mild steel reinforcing bars are shown in the Table E.1.

Table E.1: Forces in Reinforcing Bars of CIP Emulation Pier for Initial Neutral Axis

i (bar no.)	$\varepsilon_{ms,i}$	$f_{ms,i}$ (ksi)	$F_{ms,i}$ (kips)
1	0.0148	60.0	93.6
2	0.0122	60.0	93.6
3	0.0060	60.0	93.6
4	-0.0002	-5.4	-8.5
5	-0.0028	-60.0	-93.6
6	-0.0002	-5.4	-8.5
7	0.0060	60.0	93.6
8	0.0122	60.0	93.6

Accordingly, the net force in the mild steel reinforcing bars (F_{ms}) is

$$F_{ms} = \sum_{i=1}^{n_{bars}} F_{ms,i} = \sum_{i=1}^{8} F_{ms,i} = 357.5\,k$$

Step #3: Calculate the Compressive Force in Concrete

The compressive force in the concrete (F_c) is

$$\gamma_1 = \cos^{-1}\left(\frac{\frac{D_c}{2} - c\beta_1}{\frac{D_c}{2}}\right) = \cos^{-1}\left(\frac{24\,in - (0.8)9.6\,in}{24\,in}\right) = 0.823$$

$$F_c = -0.85\,f_c^{'} D_c^2\left(\frac{\gamma_1 - \sin\gamma_1\cos\gamma_1}{4}\right)$$

$$= -0.85(5\,ksi)(48\,in)^2\left(\frac{0.823 - (\sin 0.823)(\cos 0.823)}{4}\right) = -794.2\,k$$

Step #4: Enforce the Internal Force Equilibrium

Checking the internal force equilibrium,

$$F_{ms} + F_c + (P_c + \Delta P) = 357.5k - 794.2k + 1128.6k = 691.9k \neq 0$$

Equilibrium is not satisfied, and iteration must be performed on c until the condition is met. By performing iteration, it is found that

$$c = 14.1in$$

The values determined above must be recalculated for the new value of c. The new forces in the mild steel reinforcing bars are shown in Table E.2.

Table E.2: Forces in Reinforcing Bars of CIP Emulation Pier After Iteration

i (bar no.)	$\varepsilon_{ms,i}$	$f_{ms,i}$ (ksi)	$F_{ms,i}$ (kips)
1	0.0088	60.0	93.6
2	0.0070	60.0	93.6
3	0.0028	60.0	93.6
4	-0.0014	-40.7	-63.4
5	-0.0031	-60.0	-93.6
6	-0.0014	-40.7	-63.4
7	0.0028	60.0	93.6
8	0.0070	60.0	93.6

$$F_{ms} = 247.5k$$

For the compressive force in the concrete,

$$\gamma_1 = 0.1012$$

$$F_c = -1376.1k$$

Checking the equilibrium condition reveals that it is now satisfied:

$$F_s + F_c + (P_c + \Delta P) = 247.5k - 1376.1k + 1128.6k = 0$$

Step #5: Calculate the Moment Capacity

The moment contributed by bar 1 ($M_{ms,1}$) about the extreme compression face of the column is

$$M_{ms,1} = F_{ms,1} d_{ms,1} = 93.6k(45in) = 4212in - k$$

The moment contributed by each of the mild steel reinforcing bars is shown in Table E.3.

Table E.3: Moment Contribution from Reinforcing Bars in CIP Emulation Pier

i (bar no.)	$\varepsilon_{ms,i}$	$f_{ms,i}$ (ksi)	$F_{ms,i}$ (kips)	$M_{ms,i}$ (k-in)
1	0.0088	60.0	93.6	4212.0
2	0.0070	60.0	93.6	3636.3
3	0.0028	60.0	93.6	2246.4
4	-0.0014	-40.7	-63.4	-580.4
5	-0.0031	-60.0	-93.6	-280.8
6	-0.0014	-40.7	-63.4	-580.4
7	0.0028	60.0	93.6	2246.4
8	0.0070	60.0	93.6	3636.3

The net moment contribution from the mild steel reinforcement (M_{ms}) is

$$M_{ms} = \sum_{i=1}^{n_{bars}} M_{ms,i} = \sum_{i=1}^{8} M_{ms,i} = 14535.7 in-k$$

The moment contributed by the axial load on the column (M_D) is

$$M_D = (P_c + \Delta P)\frac{D_c}{2} = 1128.6k\frac{48in}{2} = 27086.4 in-k$$

To determine the moment contribution due to the compressive force in the concrete (M_c), the distance from the centroid of the concrete compressive stress to the extreme compression face of the column (d_{Fc}) must first be calculated.

$$d_{Fc} = \frac{D_c}{2} - D_c\left(\frac{1}{3}\frac{\sin^3\gamma}{\gamma - \sin\gamma\cos\gamma}\right) = 24in - 48in\left(\frac{1}{3}\frac{\sin^3(1.012)}{1.012 - \sin(1.012)\cos(1.012)}\right) = 6.60in$$

$$M_c = F_c d_{Fc} = -1376.1k(6.60in) = -9082.3in-k$$

Summing all of the contributing moments to find the total moment capacity,

$$M_{cap} = M_{ms} + M_D + M_c = 14536in-k + 27086in-k - 9082in-k = 32540in-k$$

The moment capacity of the column with the smaller axial load can be found by using the same procedure. For the initial amount of reinforcement, the moment capacity of the column with smaller axial load is 28970 in-k. Accordingly,

$$\sum_{n_c} M_{cap} = 32540in-k + 28970in-k = 61510in-k$$

which is smaller than the demand requiring the amount of reinforcing steel to be increased and the design procedure iterated. It is determined that ρ_s of 0.0076 provides the pier with sufficient capacity to withstand the design force.

E.2 HYBRID PIER

The capacity of the hybrid pier is determined for a target displacement (Δ_t) of 5.76 in., which corresponds to 2 percent drift. The mild steel reinforcing bars have a debonded length (L_{unb}) of 12 in. in the interface regions. The total unbonded length of the post-tensioning tendons (L_{pu}) is 389 in.

Because the hybrid pier is being designed for the same design force (F_d) as the CIP emulation pier and they have the same pier geometry, the required F_{cap} and additional axial load in the columns due to overturning are identical to the values determined for CIP emulation piers in Section E.1. However, the amount of reinforcement needed for the hybrid piers to meet the required $\sum_{n_c} M_{cap}$ has to be determined.

The initial reinforcement of the hybrid pier is assumed to be eight mild steel reinforcing bars, each with A_{bar} = 0.79 in^2, and post-tensioning tendons with a gross area (A_p) of 1.0 in^2. This corresponds to a mild steel reinforcing ratio (ρ_s) of 0.0035 and a post-tensioning reinforcing ratio (ρ_p) of 0.00055. The column cross-section for the hybrid pier is shown in Figure E.2. The moment capacity of the column with greater compressive load is calculated with the following procedure, which is developed from Section 7.4.2.

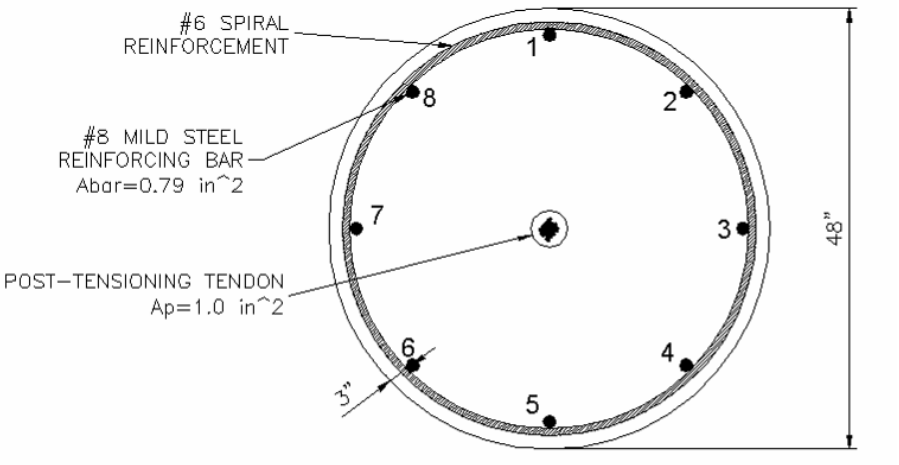

Figure E.2: Cross-Section of Hybrid Pier Column

Step #1: Determine the Column Rotation

The rotation of the column (θ) is

$$\theta = \frac{\Delta_t}{L_c} = \frac{5.76\,in}{288in} = 0.02$$

Step #2: Estimate the Depth of the Neutral Axis

The depth of the neutral axis (c) from the extreme compression face of the column is estimated to be 1/5th of the column diameter:

$$c = 0.20 D_c = 0.20(48\,in) = 9.6\,in$$

Step #3: Calculate the Net Force in the Mild Steel Reinforcing Bars

The calculations to determine the force in bar 1, as labeled in Figure E.2, are shown below. The amount of deformation in the bar ($\delta_{ms,i}$) is

$$\delta_{ms,1} = \theta(d_{ms,1} - c) = 0.02(45in - 9.6in) = 0.708in$$

where $d_{ms,1}$ is the distance from bar 1 to the extreme compressive face of the column. The strain in bar 1 ($\varepsilon_{ms,1}$) is then

$$\varepsilon_{ms,1} = \frac{\delta_{ms,1}}{L_{unb}} = \frac{0.708in}{12in} = 0.059$$

and the corresponding stress ($f_{ms,1}$) is

$$f_{ms,1} = E_s \varepsilon_{ms,1} = 29000\,ksi(0.059) = 1711ksi \geq f_y$$

$$f_{ms,1} = f_y = 60\,ksi$$

The force in bar 1 ($F_{ms,1}$) is then

$$F_{ms,1} = A_{bar} f_{ms,1} = 1.56\,in^2(60\,ksi) = 93.6\,k$$

The deformation, strain, stress, and force in the remaining bars are shown in Table E.4.

Table E.4: Forces in Reinforcing Bars of Hybrid Pier for Initial Neutral Axis Estimate

i (bar no.)	$\delta_{ms,i}$ (in)	$\varepsilon_{ms,i}$	$f_{ms,i}$ (ksi)	$F_{ms,i}$ (kips)
1	0.708	0.059	60.0	47.4
2	0.585	0.049	60.0	47.4
3	0.288	0.024	60.0	47.4
4	-0.009	-0.001	-22.5	-17.7
5	-0.132	-0.011	-60.0	-47.4
6	-0.009	-0.001	-22.5	-17.7
7	0.288	0.024	60.0	47.4
8	0.585	0.049	60.0	47.4

The net force in the mild steel reinforcement (F_{ms}) is

$$F_{ms} = \sum_{i=1}^{n_{bars}} F_{ms,i} = \sum_{i=1}^{8} F_{ms,i} = 195.1k$$

Step #4: Calculate the Force in the Post-tensioning Tendons

The deformation of the post-tensioning tendons (δ_p) when the pier reaches Δ_t is

$$\delta_p = 2\theta\left(\frac{D_c}{2} - c\right) = 2(0.02)(24in - 9.6in) = 0.576in$$

resulting in a change in stress (Δf_p) of

$$\Delta f_p = \frac{\delta_p}{L_{pu}} E_p = \frac{0.576in}{389in} 28500ksi = 42.2ksi$$

The initial stress in the tendon (f_{p0}) is then

$$f_{p0} = \min\begin{Bmatrix} f_{py} - \Delta f_p \\ f_{pi} \end{Bmatrix} = \min\begin{Bmatrix} 243ksi - 42.2ksi \\ 216ksi \end{Bmatrix} = 200.8ksi$$

and the stress at the target displacement (f_p) is

$$f_p = f_{p0} + \Delta f_p = 200.8ksi + 42.2ksi = 243ksi$$

The force in the post-tensioning tendons (F_p) is then

$$F_p = f_p A_p = 243ksi(1.0in^2) = 243k$$

Step #5: Calculate the Compressive Force in the Concrete

The compressive force in the concrete (F_c) is

$$\gamma_1 = \cos^{-1}\left(\frac{\frac{D_c}{2} - c\beta_1}{\frac{D_c}{2}}\right) = \cos^{-1}\left(\frac{24in - (0.8)9.6in}{24in}\right) = 0.823$$

$$F_c = -0.85 f_c^{'} D_c^2 \left(\frac{\gamma_1 - \sin\gamma_1 \cos\gamma_1}{4}\right)$$

$$= -0.85(5ksi)(48in)^2\left(\frac{0.823 - \sin(0.823)\cos(0.823)}{4}\right) = -794.2k$$

Step #6: Enforce the Internal Force Equilibrium

Checking the internal force equilibrium equation

$$F_{ms} + F_p + (P_c + \Delta P) + F_c = 194.5k + 243k + 1128.6k - 794.2k = 771.9k \neq 0$$

The cross-section is not in equilibrium and the depth of the neutral axis (c) must be iterated until equilibrium is achieved. From iteration it is determined that

$$c = 14.7in$$

The values above must be recalculated for the new value of the neutral axis. The new forces in the mild steel reinforcement are shown in Table E.5.

Table E.5: Forces in Reinforcing Bars of Hybrid Pier After Iteration

i (bar no.)	$\delta_{ms,i}$ (in)	$\varepsilon_{ms,i}$	$f_{ms,i}$ (ksi)	$F_{ms,i}$ (kips)
1	0.605	0.050	60	47.4
2	0.482	0.040	60	47.4
3	0.185	0.015	60	47.4
4	-0.112	-0.009	-60	-47.4
5	-0.235	-0.020	-60	-47.4
6	-0.112	-0.009	-60	-47.4
7	0.185	0.015	60	47.4
8	0.482	0.040	60	47.4

$$F_{ms} = 94.8k$$

For the post-tensioning reinforcement,

$$\delta_p = 0.372in$$

$$\Delta f_p = 27.1ksi$$

$$f_{p0} = 215.9\,ksi$$

$$F_p = 243k$$

For the compressive force in the concrete,

$$\gamma_1 = 1.037$$

$$F_c = -1466.4k$$

Applying the equilibrium equation to the new values for the forces,

$$F_{ms} + F_p + (P_c + \Delta P) + F_c = 94.8k + 243k + 1128.6k - 1466.4k = 0$$

Step #7: Calculate the Moment Capacity

The moment contribution from mild steel reinforcing bar 1 ($M_{ms,1}$) about the extreme compression face of the column is

$$M_{ms,1} = F_{ms,1} d_{ms,1} = 47.4k(45in) = 2133in - k$$

The moment contributions of the remaining reinforcing bars are shown in Table E.6.

Table E.6: Moment Contribution from Reinforcing Bars in Hybrid Pier

i (bar no.)	$\delta_{ms,i}$ (in)	$\varepsilon_{ms,i}$	$f_{ms,i}$ (ksi)	$F_{ms,i}$ (kips)	$M_{ms,i}$ ("k)
1	0.605	0.050	60	47.4	2133.0
2	0.482	0.040	60	47.4	1841.5
3	0.185	0.015	60	47.4	1137.6
4	-0.112	-0.009	-60	-47.4	-433.7
5	-0.235	-0.020	-60	-47.4	-142.2
6	-0.112	-0.009	-60	-47.4	-433.7
7	0.185	0.015	60	47.4	1137.6
8	0.482	0.040	60	47.4	1841.5

The net moment contribution of the mild steel reinforcement (M_{ms}) is

$$M_{ms} = \sum_{i=1}^{n_{bars}} M_{ms,i} = \sum_{i=1}^{8} M_{ms,i} = 7081in - k$$

The moment contribution due to the post-tensioning tendons (M_p) is

$$M_p = F_p \frac{D_c}{2} = 243k(24in) = 5832in - k$$

The dead load on the column causes a moment (M_D) of

$$M_D = (P_c + \Delta P)\frac{D_c}{2} = 1128.6k(24in) = 27086in-k$$

Determining the moment contribution from the compressive force in the concrete (M_c),

$$d_{Fc} = \frac{D_c}{2} - D_c\left(\frac{1}{3}\frac{\sin^3\gamma_1}{\gamma_1 - \sin\gamma_1\cos\gamma_1}\right) = 24in - 48in\left(\frac{1}{3}\frac{\sin^3(1.037)}{1.037 - \sin(1.037)\cos(1.037)}\right) = 6.95in$$

$$M_c = F_c d_{Fc} = -1466.5k(6.95in) = -10192in-k$$

The total moment capacity of the pier is then

$$\begin{aligned} M_{cap} &= M_{ms} + M_p + M_D + M_c \\ &= 7081in-k + 5832in-k + 27086in-k - 10192in-k = 29807in-k \end{aligned}$$

The moment capacity of the column with a smaller compressive axial load is found, by using the same procedure, to be 26465 in-k. The sum of the moment capacity of the columns is then

$$\sum_{n_c} M_{cap} = 29807in-k + 26465in-k = 56272in-k$$

This combined moment capacity is less than the required combined demand of 63532.8 in-k determined above. Therefore, the amount of reinforcement must be increased and iteration performed. It is determined that ρ_s of 0.0042 and ρ_p of 0.001 provide the pier with sufficient capacity.

E.3 THE RESTORING PROPERTIES OF THE HYBRID PIER

The restoring properties of the hybrid pier designed in Section E.2 are examined to ensure that the pier will recenter after an earthquake. The recentering ability is examined by using the following procedure adapted from Section 7.5.

Step #1: Determine the Resisting Force in Each Reinforcing Bar

The resisting force in each mild steel reinforcing bar ($F_{ms0,i}$) is shown in Table E.7.

Table E.7: Resisting Force of Reinforcing Bars in Hybrid Pier

i (bar no.)	$F_{ms0,i}$ (kips)
1	-47.4
2	-47.4
3	-47.4
4	47.4
5	47.4
6	47.4
7	-47.4
8	-47.4

The net resisting force in the mild steel reinforcement (F_{ms0}) is

$$F_{ms0} = \sum_{i=1}^{n_{bars}} F_{ms0,i} = \sum_{i=1}^{8} F_{ms0,i} = -94.8k$$

Note that if any of the bars had not reached the yield stress at Δ_t, they would have been assumed to have had no resisting force.

Step #2: Estimate the Depth of the Neutral Axis

The depth of the neutral axis (c_0) is estimated to be 1/5th of the column diameter:

$$c_0 = 0.20D_c = 0.2(48in) = 9.6in$$

Step #3: Calculate the Force in the Post-Tensioning Tendons

The restoring force in the post-tensioning tendons (F_{p0}) is

$$F_{p0} = A_p f_{p0} = 1.0in^2(213.1ksi) = 213.1k$$

Step #4: Determine the Compressive Force in the Concrete

The restoring force from compression in the concrete (F_{c0}) is

$$\gamma_1 = \cos^{-1}\left(\frac{\frac{D_c}{2} - c_0\beta_1}{\frac{D_c}{2}}\right) = \cos^{-1}\left(\frac{24in - (0.8)9.6in}{24in}\right) = 0.823$$

$$F_{c0} = -0.85 f_c^{'} D_c^2 \left(\frac{\gamma_1 - \sin\gamma_1 \cos\gamma_1}{4} \right)$$
$$= -0.85(5\,ksi)(48\,in)^2 \left(\frac{0.823 - (\sin 0.823)(\cos 0.823)}{4} \right) = -794.2\,k$$

Step #5: Enforce the Internal Force Equilibrium

Applying internal force equilibrium,

$$F_{ms0} + F_{p0} + P_c - F_{c0} = -94.8\,k + 215.9\,k + 1000\,k - 794.2\,k = 326.9\,k \neq 0$$

The internal forces are not in equilibrium and c_0 must be iterated to obtain equilibrium. From iteration it is determined that

$$c_0 = 11.2\,in$$

The compressive force in the concrete (F_{c0}) must be recalculated for the new value of c_0:

$$\gamma_1 = 0.935$$

$$F_{c0} = -1118.3k$$

Checking the equilibrium equation,

$$F_{ms0} + F_{p0} + P_c - F_{c0} = -94.8k + 213.1k + 1000k - 1118.3k = 0$$

Step #6: Evaluate the Restoring Properties of the Pier

The restoring properties of the pier are determined from the moments caused by the internal forces on the column cross-section. The moment contributed by mild steel reinforcing bar 1 about the neutral axis is

$$M_{ms0,1} = F_{ms0,1}(d_{ms,1} - c_0) = -47.4\,k(45\,in - 12.2in) = -1554.7\,in - k$$

The moments contributed by the remaining mild steel reinforcing bars are displayed in Table E.8.

Table E.8: Resisting Moment Provided by Reinforcing Bars in Hybrid Pier

i (bar no.)	$F_{ms0,i}$ (kips)	$d_{ms,i}$-c_0 (in)	$M_{ms0,i}$ (k-in)
1	-47.4	32.8	-1554.7
2	-47.4	26.6	-1263.2
3	-47.4	11.8	-559.3
4	47.4	-3.0	-144.5
5	47.4	-9.2	-436.1
6	47.4	-3.0	-144.5
7	-47.4	11.8	-559.3
8	-47.4	26.6	-1263.2

The net moment contribution of the mild steel reinforcement (M_{ms0}) is

$$M_{ms0} = \sum_{i=1}^{n_{bars}} M_{ms,i} = \sum_{i=1}^{8} M_{ms,i} = -5925in-k$$

The moment contribution from the post-tensioning tendons (M_{p0}) is

$$M_{p0} = F_{p0}(\frac{D_c}{2} - c_0) = 213.1k(24in - 12.2in) = 2514.6in-k$$

The moment contribution from the dead load on the pier (M_{D0}) is

$$M_{D0} = P_c(\frac{D_c}{2} - c_0) = 1000k(24in - 12.2in) = 11800in-k$$

The moment contribution from the compressive force in the concrete (M_{c0}) is

$$d_{Fc} = \frac{D_c}{2} - D_c\left(\frac{1}{3}\frac{\sin^3\gamma_1}{\gamma_1 - \sin\gamma_1\cos\gamma_1}\right) = 24in - 48in\left(\frac{1}{3}\frac{\sin^3(0.935)}{0.935 - \sin(0.935)\cos(0.935)}\right) = 5.77in$$

$$M_{c0} = F_{c0}(d_{Fc} - c_0) = -1118.3k(5.77in - 12.2in) = 7191in-k$$

The net restoring moment ($M_{restore}$) is then

$$M_{restore} = M_{p0} + M_{D0} + M_{c0} = 2515in-k + 11800in-k + 7191in-k = 21506in-k$$

and the net resisting moment is

$$M_{resist} = -M_{ms0} = 5925in-k$$

Because the net restoring moment ($M_{restore}$) is larger than the net resisting moment (M_{resist}), the pier is expected to recenter after an earthquake.

APPENDIX F
GROUND MOTION ACCELERATION RECORDS

The acceleration records, acceleration spectra, and displacement spectra for the five ground motions used in the study are presented in the following figures.

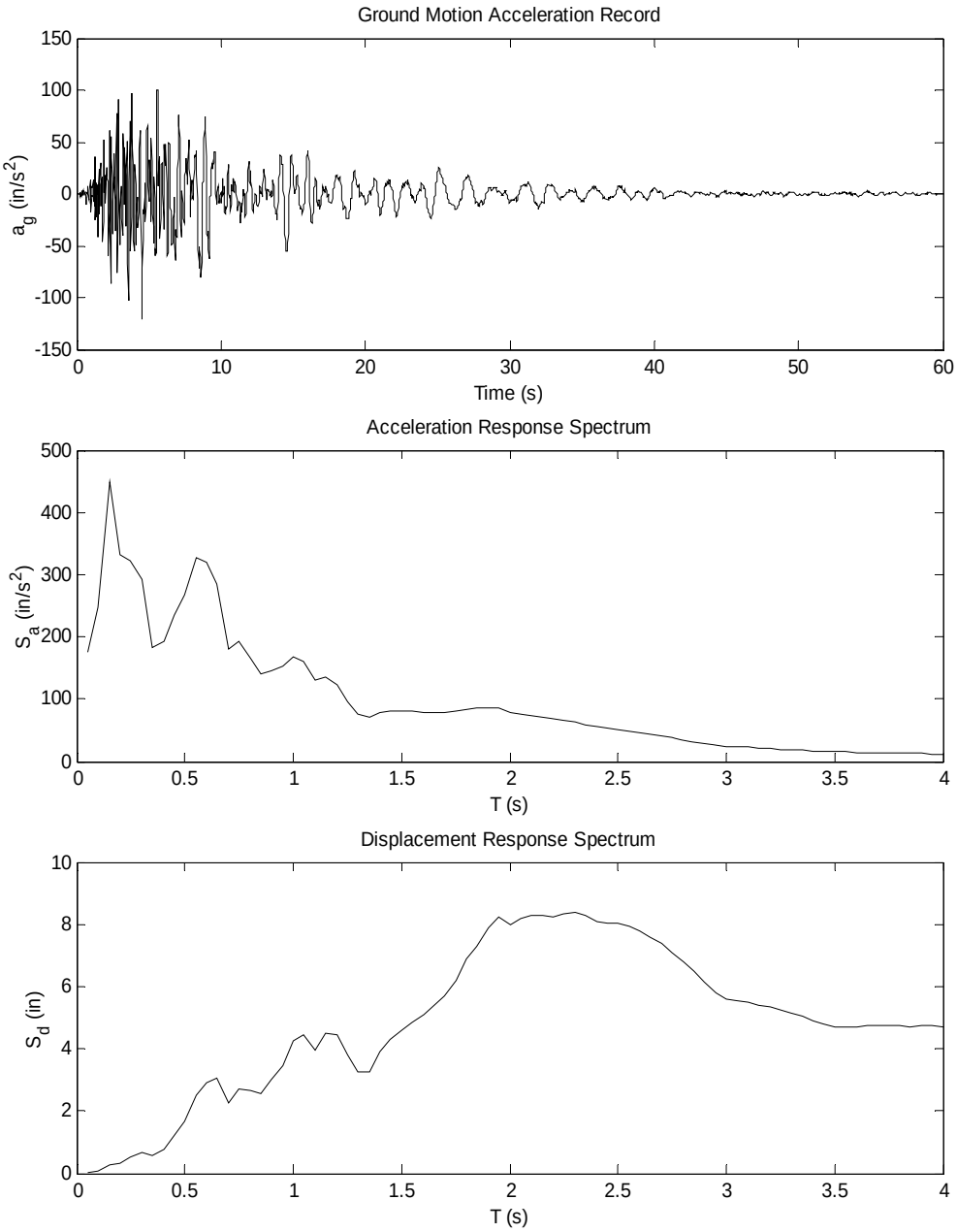

Figure F.1: Ground Motion Record #1

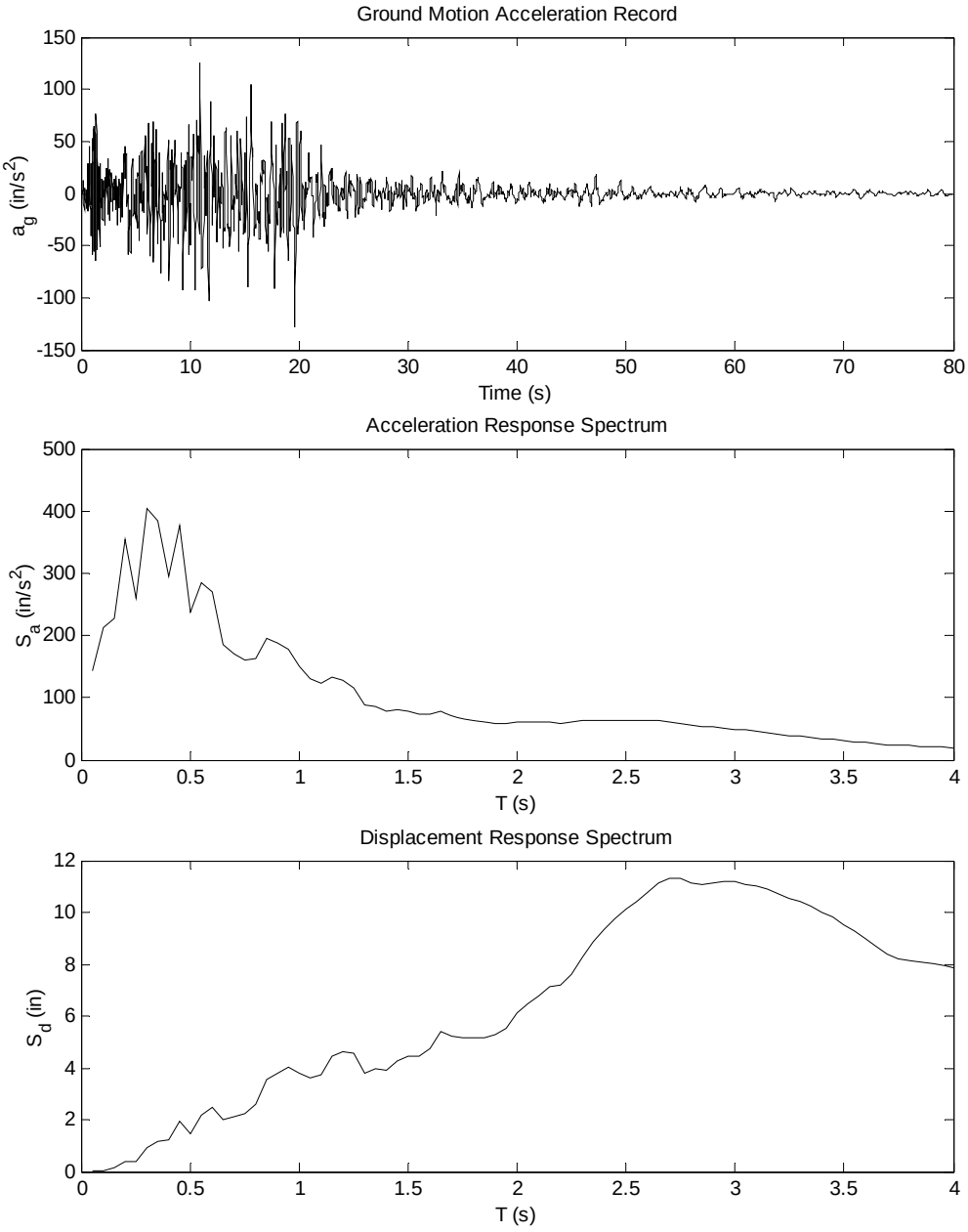

Figure F.2: Ground Motion Record #2

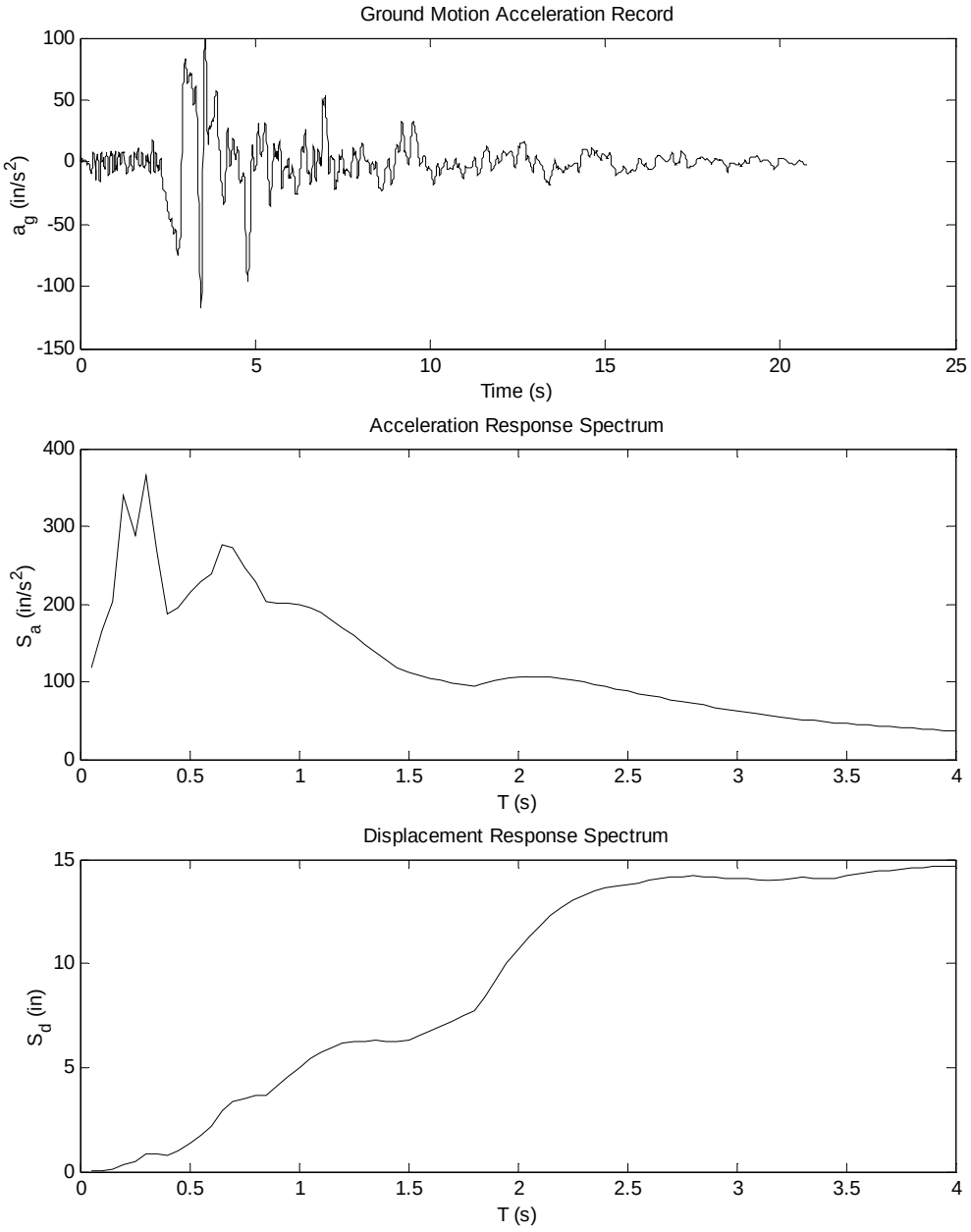

Figure F.3: Ground Motion Record #3

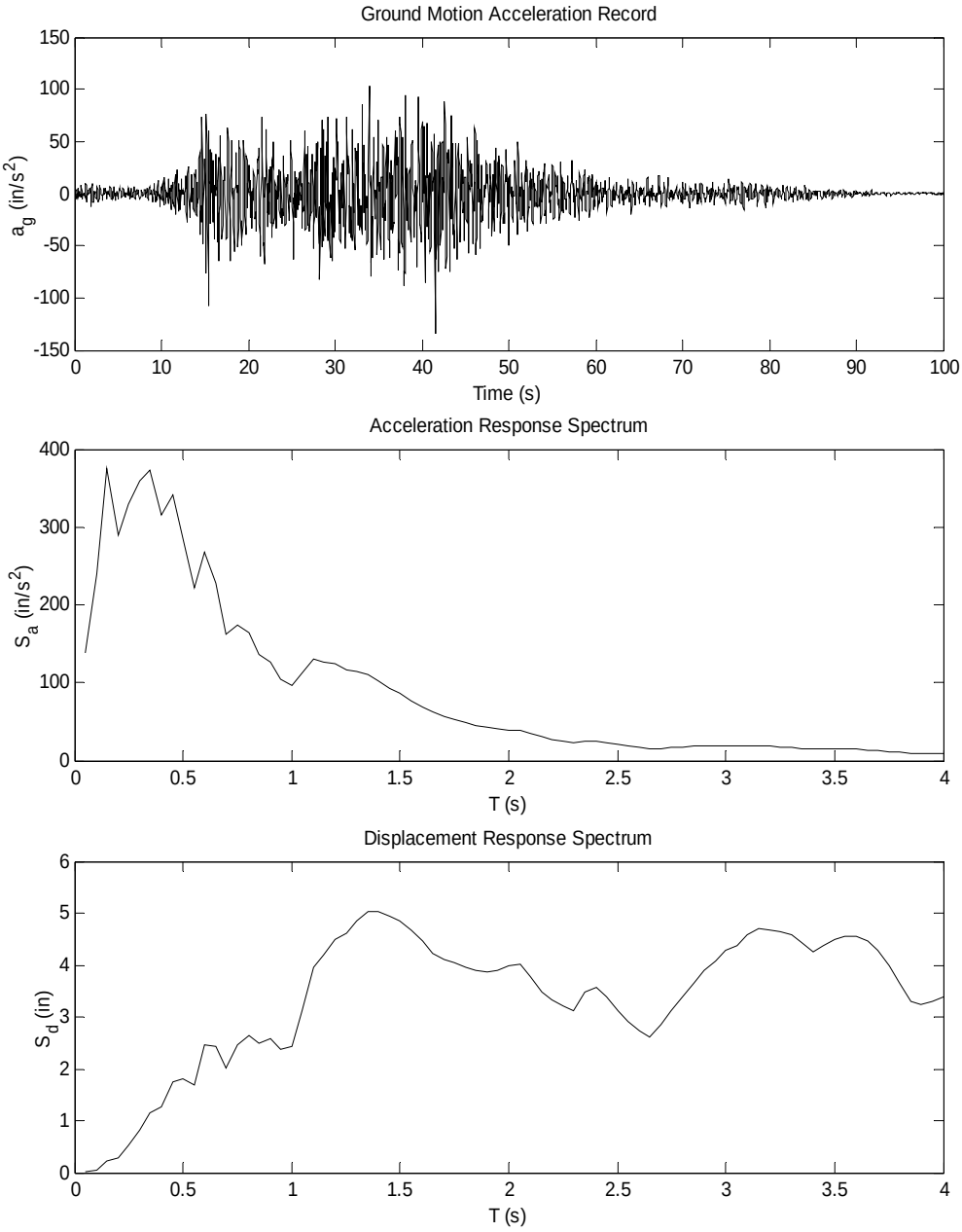

Figure F.4: Ground Motion Record #4

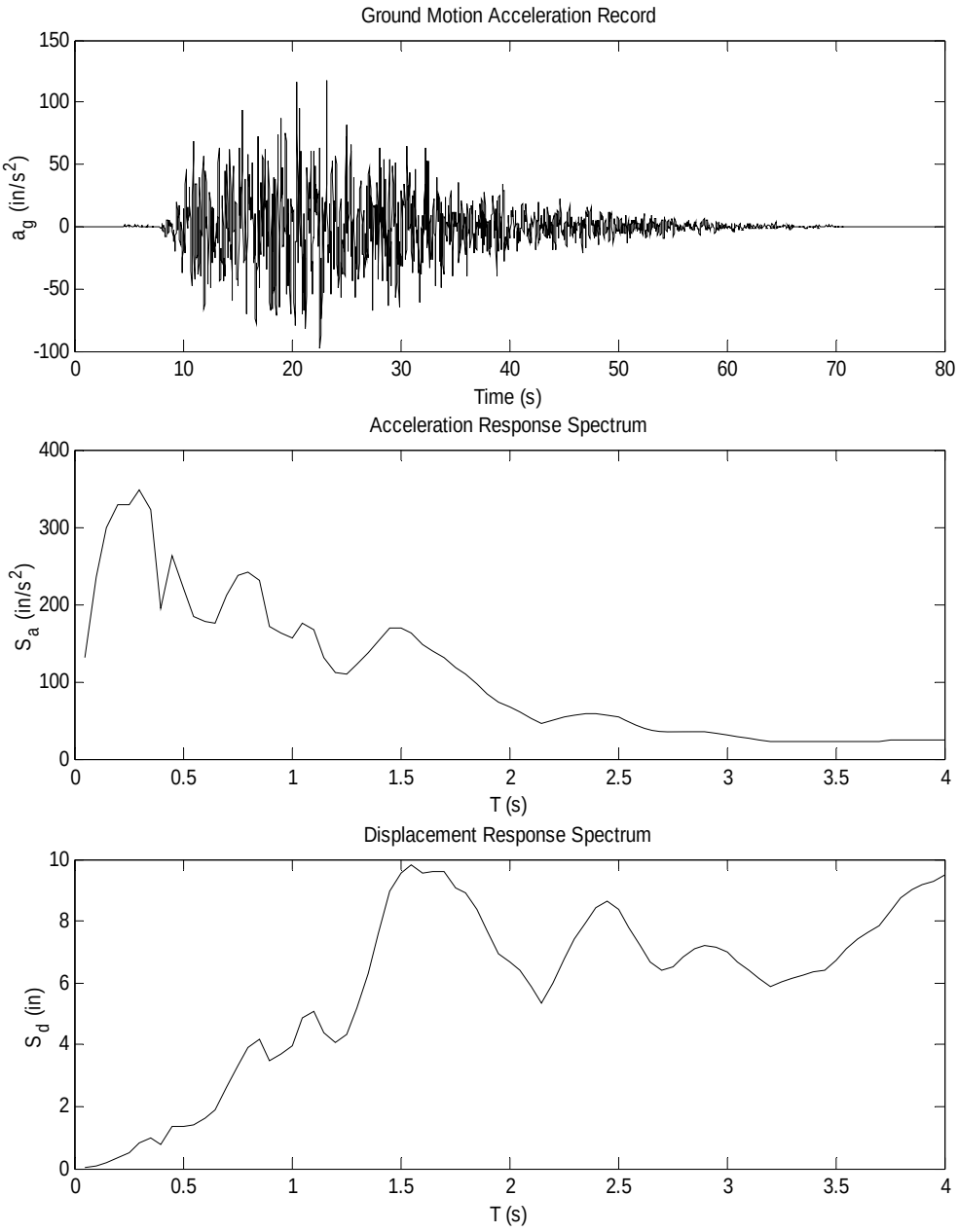

Figure F.5: Ground Motion Record #5